# The Role of Axonal Injury in Glioblastoma Progression

## Zan Florjanic Baronik

A dissertation submitted in partial fulfilment of the requirements for the degree of

**Doctor of Philosophy** 

of

University College London.

Faculty of Medical Sciences, UCL Cancer Institute,
University College London

Supervisors: Simona Parrinello, Ciaran Hill

I, Zan Florjanic Baronik, confirm that the work presented in this thesis is my own. Where information has been derived from other sources, I confirm that this has been indicated in the work.

### **Abstract**

Glioblastoma (GBM) is the most common and most lethal type of primary brain cancer in adults, characterised by poor therapeutic response and significant impact on patient quality of life. While tumour–neuron interactions are increasingly recognised as key drivers of gliomagenesis, the role of axonal injury in shaping tumour progression remains unclear.

Importantly, most insights into GBM biology are derived from late-stage disease, whereas the early phases, where critical determinants of progression likely emerge, remain poorly understood. This thesis addresses this gap by investigating early gliomagenesis using a somatic CRISPR-based mouse model of GBM. A spatiotemporal analysis revealed that early-stage tumours preferentially infiltrate white matter tracts, where they induce progressive axonal degeneration and local neuroinflammation.

Mechanistically, tumour-induced axonal injury was shown to occur via the Wallerian degeneration pathway, dependent on SARM1. Genetic deletion of *Sarm1* preserved axonal integrity and altered tumour phenotype. Tumours which formed in *Sarm1*<sup>-/-</sup> mice exhibited a more diffuse architecture, reduced mesenchymal cell states, and a less inflamed tumour microenvironment. These changes translated into prolonged survival and preserved neurological function.

Abstract 4

Collectively, these findings position axonal degeneration as a key driver of GBM progression, and highlight the tractability and importance of studying early disease as a window into actionable drivers of malignancy. SARM1 may represent a promising therapeutic target for both suppressing tumour progression and preserving neurological function in GBM.

## **Impact Statement**

This thesis uncovers axonal degeneration as an active driver of glioblastoma (GBM) progression, positioning injury-response pathways as tractable therapeutic targets. By showing that blocking the SARM1-dependent Wallerian degeneration pathway preserves axonal integrity, restrains tumour advancement, and maintains neurological function, this work opens new avenues for neuroprotective strategies in oncology.

The burden of GBM at a population level is immense. This is not only due to its lethality but also because of its devastating functional impact on patients. As tumours grow within highly eloquent regions of the brain, they often cause severe motor and cognitive impairments that profoundly affect quality of life. This study highlights that such functional deterioration is not inevitable: by preserving neuronal integrity, disease progression and disability can both be attenuated. These findings challenge the current therapeutic focus on tumour volume alone and argue for incorporating neuroprotective approaches into the clinical management of GBM.

Importantly, this work also demonstrates that early GBM is a targetable phase of this disease. By characterising the early lesion microenvironment and identifying injury as a possible initiator or accelerator of malignancy, this research lays a Abstract 6

foundation for exploring new preventative and diagnostic strategies, opening GBM to the field of cancer interception. In the long term, such insights may support the development of population-level screening programmes or high-risk surveillance approaches, particularly for individuals with prior neurological injury.

Within academia, this work encourages a shift toward studying early-stage disease and tumour–host interactions, laying the groundwork for future research at the intersection of neuroscience, cancer biology, and immunology.

Beyond academia, these insights support the rationale for developing SARM1 inhibitors as part of the therapeutic arsenal against GBM — a direction with translational potential in clinical trials. By reframing axonal degeneration as a modifiable driver of disease, this work may influence public health priorities, clinical trial endpoints, and regulatory standards in neuro-oncology.

# Acknowledgements

This thesis would not have been possible without the support, collaboration, insight, and kindness of many people.

First and foremost, I would like to thank my supervisors, Simona Parrinello and Ciaran Hill, for designing a project that was both intellectually rich and a joy to pursue. Simona – thank you for your guidance, encouragement, and for always challenging me to think more clearly and deeply. Ciaran – thank you for not just your supervisory support but also every bit of career and life advice you have given me along the way.

I am very grateful to my thesis committee – Silvia Marino, Sam Marguerat, and Jemeen Sreedharan – for your thoughtful feedback, encouragement, and the many ways you helped shape this work.

Thank you to everyone in the Parrinello lab, past and present – this PhD was a collaborative effort in every sense. A special thank you to Mel and Holly for your brilliance and care with the animal work and being absolute academic weapons on this project – I learned so much from you both, and I am certainly a much better scientist for it. Thank you to to Wenhao for your computational wisdom and magic that elevated this work. And to Anni for reading this thesis multiple times and enhancing my knowledge of GBM with every study you sent my way.

I'm infinitely grateful to all those who not just contributed to the project but made the lab such a good place to be – Jenda, Saachi, Lucy, Jill, Jasneet, Diya, Stephanie, Rhyla, and everyone else who came through this lab. Thank you for the conversations, the help, the encouragement – and everything in between. Sometimes it really is about the friends we make along the way.

To the wider UCL Cancer Institute community, especially fellow PhD students – thank you. From spontaneous corridor chats to borrowed reagents and shared pints – your generosity and camaraderie made this experience not only productive but deeply enjoyable.

Thank you to the CI Flow Cytometry Platform, especially Yanping and George, for your help and flexibility, and to the CI Single Cell Genomics Facility – Imran and Gordon, your patience and insight keeps the entire building going!

Thank you to all our collaborators, with a special thank you to Ian White, for your help with the electron microscopy, and Ryoichi Sugisawa, for your generous support with the mice; and everyone else who was involved in this project along the way.

To my family – my mum, grandma, and Sandi – thank you for your mostly unwavering belief in me and the moral and material support through all of my long academic endeavours, from staying in a hostel dorm room with me in my first year while I was making plasmids before I knew what plasmids were, to checking in on my experiments and thesis progress. And to my partner Xen – for inspiring me to be a better scientist, medic, person, for teaching me how critical critical thinking can be, for your wisdom, inquisitiveness, and humour, and for listening to and questioning every half-baked theory I throw your way.

These past three years have been more rewarding and fun than I could ever

have imagined a PhD to be – not only because the project itself (which was about as compelling as they get), but because of the people I got to share it with. Thank you all.

## **Abbreviations**

5-ALA 5-aminolevulinic acid.

AC astrocyte.

APC astrocyte progenitor cell.

BBB blood-brain barrier.

BSA Bovine serum albumin.

cADPR cyclic ADP-ribose.

CAR chimeric antigen receptor.

CC corpus callosum.

CLEM correlative light and electron microscopy.

CNS central nervous system.

CSF1R colony stimulating factor 1 receptor.

EGFR epidermal growth factor receptor.

ECM extracellular matrix.

GBM glioblastoma.
GSC glioma stem-like cell.
IDH isocitrate dehydrogenase.
IL interleukin.
MBP myelin basic protein.
MDSC myeloid-derived suppressor cell.
MES mesenchymal.
MRI magnetic resonance imaging.
NAD nicotinamide adenine dinucleotide.
NCC neural crest cell.
NF neurofilament.
NMN nicotinamide mononucleotide.
NMNAT2 nicotinamide mononucleotide adenylyltransferase 2.
NPC neural progenitor cell.
NSC neural stem cell.
OPC oligodendrocyte progenitor cell.
<b>PDGFRB</b> platelet-derived growth factor receptor $\beta$ .

PNS peripheral nervous system.

**ROS** reactive oxygen species.

**SARM1** sterile alpha and TIR motif-containing protein 1.

scRNA-seq single-cell RNA sequencing.

TAM tumour associated microglia/macrophages.

TBI traumatic brain injury.

TME tumour microenvironment.

TMZ Temozolomide.

**TNF**- $\alpha$  tumor necrosis factor- $\alpha$ .

**Treg** regulatory T cell.

TTF tumour treating fields.

**UMAP** Uniform Manifold Approximation and Projection.

WD Wallerian degeneration.

WHO World Health Organisation.

# **Contents**

1	Intr	oductio	on	21
	1.1	Gliobl	lastoma	21
		1.1.1	Clinical landscape of glioblastoma	22
		1.1.2	Biology of glioblastoma	33
	1.2	Axona	al injury	57
		1.2.1	Wallerian degeneration	61
	1.3	Resea	rch Question and Aims	71
2	Mat	erials a	and Methods	72
	2.1	Anima	al work	72
		2.1.1	Animal strains and maintenance	72
		2.1.2	Tumour induction	73
		2.1.3	Animal monitoring	74
		2.1.4	Animal behavioural assessment	75
		2.1.5	Microglial depletion	77
		2.1.6	Tissue collection	78
	2.2	In Vit	<i>ro</i> Work	78
		2.2.1	NSC isolation and culture	78

Contents	1	4	1	
----------	---	---	---	--

	2.2.2	Generation of GSCs	79
	2.2.3	Cell culture media	79
	2.2.4	In Vitro functional assays	79
2.3	Histol	ogy and imaging	80
	2.3.1	Immunofluorescence	80
	2.3.2	Electron microscopy	81
	2.3.3	Image acquisition	82
	2.3.4	Image analysis	82
2.4	Flow	cytometry	84
	2.4.1	Tissue dissociation and staining protocol	84
	2.4.2	Data acquisition and analysis	85
2.5	Transo	criptomic profiling	85
	2.5.1	Single-cell RNA sequencing: Sample preparation and library	
		construction	85
	2.5.2	Single-cell RNA sequencing: data analysis	86
2.6	Statist	ical analysis	87
P1	1:_1		
Eari	y gnot	plastoma lesions preferentially colonise white matter and cause	•
axoı	nal inju	ıry	88
3.1	Introd	luction	88
3.2	Result	S	90
	3.2.1	Time-course analysis of glioblastoma growth reveals preferential	
		early colonisation of white matter	90

Contents 15

		3.2.2	Glioblastoma progression from indolent to rapidly growing	
			disease occurs at the intermediate stage of tumour development	95
		3.2.3	Tumour growth triggers axonal injury and local	
			neuroinflammation	97
	3.3	Concl	usions	103
4	Axo	nal los	ss occurs via a programmed SARM1 dependent degeneration	on
	path	ıway		106
	4.1	Introd	luction	106
	4.2	Result	ts	108
		4.2.1	Axonal injury occurs in the presence of mechanical compression	
			of axons by tumour cells	108
		4.2.2	Sarm1 deletion preserves axonal integrity in tumour regions	110
		4.2.3	Sarm1 <sup>-/-</sup> tumours exhibit a diffuse tumour phenotype but retain	
			intrinsic tumour cell behaviours	115
	4.3	Concl	usions	118
5	Atte	enuatio	n of axonal degeneration leads to development of less advance	ed
	tum	ours ar	nd confers a survival advantage	120
	5.1	Introd	luction	120
	5.2	Result	ts	121
		5.2.1	scRNA-seq reveals that Sarm1-/- tumour cells retain a more	
			neurodevelopmental identity	121
		5.2.2	Sarm1 deletion dampens neuroinflammation and vascular	
			remodelling in the tumour microenvironment	123

Contents	16

		5.2.3 Sarm1 deletion prolongs survival and preserves neurological		
		function	132	
	5.3	Conclusions	136	
6	Disc	ussion and Future Perspectives	140	
	6.1	Introduction	140	
	6.2	Summary of Results and Discussion	140	
	6.3	Future Directions and Conclusion	148	
Αŗ	Appendices 1			
A	Data	availability	151	
В	Exte	nded data tables	152	
C	C Colophon			
Bi	Bibliography 18			

# **List of Figures**

1.1	Transcriptional cellular states in glioblastoma recapitulate normal	
	neurodevelopment.	40
1.2	The molecular pathway of Wallerian degeneration.	64
1.3	Genetic and pharmacological targeting of Wallerian degeneration	68
3.1	Schematic of the npp somatic GBM model	90
3.2	Glioblastoma cells preferentially occupy white matter regions in	
	early disease stages.	92
3.3	Early white matter tropism is preserved in PDX models	94
3.4	Glioblastoma lesion progression from low to high proliferation	
	occurs at the intermediate stage of tumour development	96
3.5	Loss of Thy1-YFP fluorescence reveals axonal loss over disease	
	progression.	98
3.6	Tumour density inversely correlates with axonal integrity at	
	intermediate stages.	100
3.7	Time-course of immune infiltration using flow cytometry reveals	
	progressive increase in immune cell accumulation within the tumour	
	microenvironment as the disease advances.	101

3.8	Reactive astrocytosis and microglial activation correlates with local	
	tumour cell density.	103
4.1	Mechanical compression of axons by tumour cells drives varicosity	
	formation	108
4.2	Sarm1 knockout preserves axonal integrity in tumour-infiltrated	
	regions as measured by immunofluorescence	111
4.3	Correlative light and electron microscopy.	112
4.4	Quantitative EM shows reduced axonal degeneration without altered	
	myelin	113
4.5	Terminal Sarm 1-/- tumours exhibit diffuse morphology and lower	
	cellular density	115
4.6	WT and Sarm1-/- tumour cells display similar proliferation and	
	migration in vitro.	117
5.1	scRNA-seq shows reduced MES-like and increased NPC-like states in	
	tumours generated in Sarm 1 <sup>-/-</sup> animals	122
5.2	scRNA-seq reveals dampened inflammation and reduced angiogenic	
	signatures in tumours generated in Sarm 1 <sup>-/-</sup> animals	125
5.3	scRNA-seq reveals reduced signalling between	
	the microenvironmental and tumour cell compartments in Sarm1-/-	
	tumours	127
5.4	Flow cytometry and immunostaining confirm reduced immune cell	
	infiltration and TAM activation in tumours generated in Sarm1-/-	
	animals	128

5.5	Microglial depletion via CSF1R inhibition reduces tumour size and	
	proliferation.	130
5.6	Vascular architecture analysis shows reduced vascular diameter and	
	branching in tumours generated in Sarm 1 <sup>-/-</sup> animals	132
5.7	Survival analysis and behavioural testing indicate delayed disease	
	progression Sarm1 <sup>-/-</sup> tumours	133
5.8	CRISPR-based Sarm1 knockout model independently validates	
	Sarm 1 <sup>-/-</sup> phenoype	136
6.1	A two-stage model of glioblastoma.	142
6.2	A shift towards studying early disease in the two-stage model of	
	glioblastoma.	143

# **List of Tables**

B.1	Summary of patient-derived glioblastoma lines analysed in Figure 3.3.	. 152
B.2	Processing metrics for single-cell RNA-sequencing experiments	153
В.3	Processing statistics for single-cell RNA sequencing data	154
B.4	Statistical testing of cell type proportions between WT and Sarm1 <sup>-/-</sup>	
	tumours	154
B.5	Gene enrichment analysis of cell type markers in tumour and TME	
	cells from WT and Sarm1 <sup>-/-</sup>	154
B.6	csRNA-seq ligand-receptor analysis outputs for WT tumours	155
B.7	csRNA-seq ligand-receptor analysis outputs for Sarm 1 <sup>-/-</sup> tumours	173

#### Chapter 1

## Introduction

#### 1.1 Glioblastoma

Glioblastoma (GBM) is the most common and the most aggressive malignant primary brain tumour in adults (McKinnon et al. 2021). It is characterised by rapid proliferation, necrosis, angiogenesis, and diffuse infiltration into the surrounding brain parenchyma, features that contribute to its highly invasive and treatment-resistant nature (Torrisi et al. 2022). Despite aggressive multimodal treatment which consists of maximal safe surgical resection, radiotherapy, and chemotherapy with temozolamide (Stupp, Mason et al. 2005), GBM remains incurable, with a median survival of 12–15 months and a 5-year survival of less than 5% (Ostrom et al. 2023). Disease progression is typically swift, and recurrence is considered universal, reflecting the cellular, molecular, and spatial heterogeneity that defines GBM biology and underlies therapeutic failure (Xie et al. 2024). This dismal prognosis is compounded by a range of debilitating symptoms, resulting from both the growing tumour mass and its treatment, and including seizures, physical impairments, and cognitive decline (Bergo et al. 2019).

In this chapter, the clinical landscape of GBM will be outlined, beginning with its classification, epidemiology, presentation, diagnosis, management, and prognosis. Then, the biology of GBM will be explored, highlighting the initiation, cellular states and transcriptomic landscape of the disease, known drivers of progression with additional focus on the tumour microenvironment (TME), and the particular role of injury in this context.

#### 1.1.1 Clinical landscape of glioblastoma

#### 1.1.1.1 WHO classification

The classification of gliomas, including GBM, has undergone extensive development in recent years, reflecting advances in molecular neuro-oncology and a paradigm shift from purely histopathological diagnoses to integrated molecular characterisation. The World Health Organisation (WHO) classification of central nervous system (CNS) tumours, now in its fifth edition (2021) (Louis et al. 2021), incorporates key molecular alterations alongside histological features to define tumour entities.

In the current WHO scheme, GBM is defined as a grade 4 astrocytoma and placed within the group of adult-type diffuse gliomas (Louis et al. 2021). The diagnosis of GBM requires the absence of mutations in the isocitrate dehydrogenase (IDH) genes (referred to as IDH-wildtype) in combination with histopathological features such as necrosis and/or microvascular proliferation. In cases where these histological features are absent, a diagnosis of GBM can still be made if specific molecular hallmarks are present, including a TERT promoter mutation, EGFR amplification, or a chromosome 7 and 10 copy number alteration signature (Louis et al. 2021). These criteria underscore

the importance of molecular diagnostics in identifying high-grade disease, even in histologically ambiguous cases (X. Guo et al. 2023).

The recognition of GBM as an IDH-wildtype, grade 4 astrocytic tumour reflects its distinct clinical behaviour, including rapid progression, poor response to therapy, and limited survival. In contrast, IDH-mutant astrocytomas, even when histologically high-grade, tend to follow a more protracted course and respond more favourably to treatment (Sanson et al. 2009). This separation has therefore refined prognostication within the field of neuro-oncology.

Throughout this thesis, the term GBM will refer exclusively to IDH-wildtype WHO grade 4 astrocytomas, in accordance with the 2021 WHO classification, and mouse models that are representative of the human disease.

#### 1.1.1.2 Epidemiology

GBM accounts for the majority of malignant primary brain tumours in adults, representing approximately 15% of all brain tumours and 50% of all gliomas (Ostrom et al. 2023). The annual incidence of GBM is estimated at 0.59 to 5 per 100,000 persons globally (Grech et al. 2020). The disease predominantly affects older adults, with a median age at diagnosis of approximately 64 years, and shows a higher prevalence in males compared to females, with a male-to-female ratio of roughly 1.6:1 (Colopi et al. 2023). This sex difference may reflect variations in hormonal regulation, immune response, or epigenetic susceptibility, although the underlying mechanisms remain unclear (Colopi et al. 2023).

Unlike many other cancers, few modifiable risk factors for GBM have been identified. The main well-established environmental risk is exposure to ionising

radiation (Braganza, Kitahara et al. 2012), particularly in individuals who have received therapeutic cranial irradiation during childhood (Pearce et al. 2012). There is no consistent evidence linking GBM with mobile phone use, or lifestyle factors such as smoking or alcohol consumption (INTERPHONE 2010) (Braganza, Rajaraman et al. 2014).

While genetic predisposition to GBM is rare, it is significant when it occurs. Inherited cancer syndromes—such as Li-Fraumeni syndrome (Sloan et al. 2020), Turcot syndrome (Dipro et al. 2012), and Lynch syndrome (Vasen et al. 2001), can increase susceptibility to gliomas, including GBM, usually as part of a broader tumour spectrum. Similarly, several phakomatoses, such as neurofibromatosis type 1 and tuberous sclerosis complex, have been associated with glioma development, although these conditions more commonly predispose to low-grade tumours (Smirniotopoulos et al. 1992).

Relevant to this thesis, the role of traumatic brain injury (TBI) in gliomagenesis remains controversial. While large cohort studies have generally not confirmed a definitive association, several case reports have described gliomas arising at the site of prior head trauma (Tyagi et al. 2016; K. Chen et al. 2022; An et al. 2024). A more recent population-based analysis of UK patients has reignited interest in this potential link, suggesting a modest increase in glioma risk following TBI. However, causality remains difficult to ascertain (Simpson Ragdale et al. 2023).

Taken together, GBM is a relatively rare but devastating malignancy with poorly understood aetiology, a strong predilection for older adults, and, as it stands, limited opportunities for prevention. Increased understanding of the biology of the disease including drivers of disease development and progression, have the potential to inform

screening and preventative approaches. Its incidence, age distribution, and resistance to treatment all contribute to its disproportionate impact on global neuro-oncology healthcare burdens (Tebha et al. 2023).

#### 1.1.1.3 Clinical presentation

The clinical presentation of GBM is highly variable and depends largely on the tumour's location, size, rate of growth, and associated peritumoural oedema (Ohmura et al. 2023; Lipková et al. 2022; Sorribes et al. 2019). Symptoms of GBM often develop insidiously. In most patients, the disease presents subacutely over weeks to months, although acute deterioration can occur in cases of haemorrhage or raised intracranial pressure (Sobstyl et al. 2023; Sorribes et al. 2019).

Some presenting symptoms include new-onset seizures, focal neurological deficits, and cognitive or behavioural changes (McKinnon et al. 2021; Armstrong et al. 2015). Seizures are particularly frequent in tumours involving the temporal and cortical regions and are often the initial manifestation, especially in younger patients (Chaichana et al. 2009; Armstrong et al. 2015). Motor, sensory and visual deficits are thought to arise from tumour involvement of respective cortical and subcortical regions, although a clear correlation between symptoms and localisation of the lesion is not always present (Sagberg et al. 2019). Additionally, cognitive dysfunction and personality changes are frequently observed, particularly in tumours affecting the frontal or temporal lobes. These symptoms can include memory loss, impaired executive function, apathy, disinhibition, and mood disturbances, which may be subtle or mistaken for primary psychiatric disorders in the early stages (Parsons et al. 2021; Regli et al. 2023).

Rarely, GBM may present with more atypical features, such as parkinsonism, rapid-onset dementia, or symptoms mimicking stroke, depending on the lesion's anatomical involvement (Cedergren Weber et al. 2023; Sobstyl et al. 2023; Mathur et al. 2014). In some cases, tumours are identified incidentally through neuroimaging performed for unrelated complaints (Kamiguchi et al. 1996).

Clinical presentation of GBM is therefore clearly varied, calling for a high level of clinical suspicion. Symptoms are also very debilitating, highlighting the need for better disease control with the aim of improving patient quality of life during active treatment and beyond (Jakola et al. 2015).

#### 1.1.1.4 Diagnosis

Diagnosis of GBM typically begins with neuroimaging, prompted by symptoms outlined earlier in this section. Magnetic resonance imaging (MRI) with gadolinium contrast is the imaging modality of choice and typically reveals a heterogeneously enhancing mass with central necrosis, a thickened ring of peripheral contrast enhancement, extensive surrounding oedema, and mass effect (McKinnon et al. 2021; Bernstock et al. 2022). These features, although not pathognomonic, are highly suggestive of high-grade glioma. Advanced imaging techniques, including diffusion-weighted MRI, perfusion-weighted MRI, MR spectroscopy, positron emission tomography (PET), etc., can provide further insight into tumour grade, cellularity, and metabolic activity, helping to differentiate GBM from metastases, abscesses, or other mimics (Henssen et al. 2023).

Definitive diagnosis, however, relies on histopathological and molecular analysis of tumour tissue obtained via biopsy or surgical resection (Kanderi et al. 2024).

Histological hallmarks of GBM include cellular pleomorphism, brisk mitotic activity, microvascular proliferation, and necrosis (Aldape et al. 2015). Molecular testing is essential to confirm IDH-wildtype status and to identify additional markers, such as epidermal growth factor receptor (EGFR) amplification, TERT promoter mutations, and gain of chromosome 7 and loss of chromosome 10 alterations that support a diagnosis of GBM even in cases lacking classical histological features (Louis et al. 2021).

The novel approach to GBM diagnosis which relies heavily on molecular characterisation in addition to histological assessment not only improves diagnostic precision but also helps stratify patients for appropriate prognostication and trial eligibility (Iyer et al. 2023).

#### 1.1.1.5 Management

Current standard of care: The management of GBM aims to prolong survival and maintain the patient's quality of life. The current standard of care, established by Stupp et al. in 2005, involves maximal safe surgical resection followed by concurrent radiotherapy and chemotherapy with Temozolomide (TMZ) (Stupp, Mason et al. 2005).

**Surgical resection:** The initial step in GBM treatment is maximal safe resection of the tumour. The extent of resection correlates with improved survival outcomes; however, complete removal is often impeded by the tumour's infiltrative nature and proximity to critical brain structures (T. J. Brown et al. 2016).

**Radiotherapy:** Postoperative radiotherapy typically involves fractionated focal irradiation, delivering a total dose of 60 Gy over six weeks in 2Gy fractions (Fernandes et al. 2017). Radiotherapy aims to eradicate residual tumour cells remaining by

inducing DNA damage, primarily through the generation of double-strand breaks, leading to cell cycle arrest and apoptosis (Khanna et al. 2001). Despite its efficacy, the development of radioresistance remains a significant challenge, often attributed to enhanced DNA repair mechanisms within tumour cells (Ali et al. 2020).

Chemotherapy: TMZ is an oral alkylating agent that has become integral to GBM therapy. It functions adding mutagenic adducts to DNA which causes DNA damage - this is predominanty by generating  $O^6$ -methylguanine which can be repaired by methyl guanine methyl transferase (MGMT), a DNA repair enzyme that removes these methyl groups (Tentori et al. 2009). High MGMT activity can confer resistance to TMZ, as the enzyme repairs the cytotoxic lesions induced by the drug (Kitange et al. 2009). Of note, this is in line with MGMT promoter methylation, which reduces MGMT expression, being a positive prognostic sign in GBM (Everhard et al. 2009; Binabaj et al. 2018).

**Emerging therapies:** Despite the aggressive standard-of-care treatment, GBM remains incurable, in response to which several novel therapeutic approaches have emerged:

Tumour treating fields (TTF)s:: TTFs are a recent therapeutic development and the only new modality to consistently confer a survival advantage across clinical trials. TTFs employ low-intensity, intermediate-frequency alternating electric fields delivered via transducer arrays applied to the scalp. These fields are theorised to disrupt mitotic processes, leading to cell cycle arrest and apoptosis in dividing tumour cells (Rominiyi et al. 2021). Clinical studies have demonstrated that the addition of TTFs to standard therapy can extend median survival by approximately four months (Stupp, Taillibert et al. 2017). However, an efficient and extensive rollout of this

therapy is yet to be achieved, with concerns regarding TTF mechanism of action, cost-effectiveness, and practicality being raised (Bernard-Arnoux et al. 2016).

**Immunotherapy:** As in many other solid tumours, various immunotherapeutic strategies are being explored, including:

Immune checkpoint inhibitors: Agents targeting inhibitory receptors such as PD-1/PD-L1 and CTLA-4 aim to enhance anti-tumour immune responses. While effective in other malignancies, their success in GBM has been limited. This is thought to be multifactorial, with the immunosuppressive microenvironment which is a hallmark of GBM likely to play a key role (Preusser et al. 2015).

Chimeric antigen receptor (CAR) T-Cell Therapy: This approach involves engineering patient-derived T cells to express receptors specific to tumour antigens, thereby directing cytotoxic activity against tumour cells. Early-phase trials have shown feasibility and safety of using chimeric antigen receptor (CAR) T-cells in GBM, with a degree of efficacy, but challenges such as antigen heterogeneity and limited T-cell persistence need to be addressed (Bagley et al. 2018; C. E. Brown et al. 2016; Keu et al. 2017).

Oncolytic virotherapy: This method utilizes genetically modified viruses that selectively infect and lyse tumour cells, with their method of tumour cell killing being both direct, by promoting cell lysis, and indirect, by eliciting anti-tumour immune responses. Several oncolytic viruses are under clinical evaluation for GBM (Hamad et al. 2023; B. Xu et al. 2021).

**Advancements in Surgical Techniques:** Novel advancements in surgical approaches to GBM resection include various surgical adjuncts (intraoperative imaging, neuronavigation, fluorescence-guided surgery, functional mapping of motor

pathways etc.) (Watts et al. 2016). Here, two novel and exciting practices are outlined:

5-aminolevulinic acid (5-ALA) fluorescence-guided surgery: Administration of 5-ALA leads to the accumulation of fluorescent porphyrins in malignant glioma cells, enabling real-time visualisation of tumour tissue during surgery (Stummer et al. 2000). This technique has been shown to enhance the extent of resection and improve progression-free survival (Kiesel et al. 2021). The use of 5-ALA has become a gold standard in tumour resections (Ruichong Ma et al. 2024). However, it is important to note that 5-ALA guided resection suffers from various issues, including variability in fluorescence, intra- and inter-tumoural heterogeneity in tumour cell fluorescence due to variable metabolism, and practical issues with access to appropriate microscopy and equipped surgical theatres and staff (Díez Valle et al. 2019).

Supratotal resection: Another novel surgical approach is supratotal resection, meaning resection extending beyond the gadolinium-enhancing regions to include non-enhancing FLAIR-abnormal regions, which are likely to consist of tumour tissue (Leeuw et al. 2019). This has emerged as a promising approach to maximise tumour resection, with several retrospective studies suggesting that supratotal resection may improve survival, with variable outcomes regarding the impact on neurological deficits (Aziz et al. 2023; Jackson et al. 2020). While encouraging, the evidence remains limited and larger prospective studies are needed before this can be adopted as standard practice, with further patient stratification to limit negative functional outcomes playing a key role. Furthermore, while this approach may prolong survival, so far no data suggest that it has curative potential, with recurrence still being universal.

Despite these advancements, GBM remains a formidable challenge, with

prognosis, described in further detail below, remaining poor.

#### 1.1.1.6 Prognosis

Prognosis for patients with GBM remains poor despite aggressive multimodal treatment. Median overall survival is approximately 15 months, with fewer than 10% of patients surviving beyond five years (Ostrom et al. 2023). Most patients experience clinical deterioration within months of diagnosis, and the disease continues to carry a high global burden in terms of both mortality and disability-adjusted life years (Butenschoen et al. 2019).

The main clinical challenge in improving prognosis is the invariable tumour recurrence. GBM is highly infiltrative, and even after maximal safe resection, residual tumour cells persist in the surrounding brain parenchyma (Vehlow et al. 2013). These cells often evade adjuvant therapies due to factors such as tumour heterogeneity, therapy-induced plasticity, and a highly immunosuppressive microenvironment (Campos et al. 2016). This leads to persistence of minimal residual disease, which gives rise to recurrence, typically within the initial radiation field (H. P. Ellis et al. 2015). Recurrent disease is associated with increased tumour aggression and resistance to further treatment (Campos et al. 2016; Seystahl et al. 2016).

A small proportion of patients survive beyond five years, which is often correlated with favorable histological and molecular characteristics, younger age, and tumour locations that allow for more complete surgical resection (Walid 2008). However, these patients frequently experience significant long-term functional impairments due to both the tumour and its treatment. Common sequelae include cognitive decline, fatigue, seizures, and neurological deficits, all of which can substantially affect quality

of life (Solanki et al. 2017).

While GBM is typically diagnosed at an advanced stage due to its aggressive clinical course, increasing recognition of earlier, more indolent cases has begun to shift this narrative. In a subset of patients, GBMs are discovered incidentally or present with smaller, more diffuse, non-necrotic lesions that lack the overt hallmarks of high-grade disease. These tumours often enter a latent period before undergoing transition into more aggressive and symptomatic forms (Thaler et al. 2012; Stensjøen et al. 2018). This clinical observation challenges the assumption that GBM initiation and early progression are necessarily rapid processes. Instead, it suggests the presence of a prolonged preclinical phase, during which transformed precursor cells remain relatively quiescent until prompted by additional microenvironmental or molecular cues. Such a model aligns with the broader concept of GBM as a two-stage disease — one in which early mutational events must intersect with a permissive niche to initiate full malignant transformation. Understanding this transition represents a critical window for future therapeutic intervention.

Together, these challenges highlight the urgent need for a deeper understanding of GBM biology, which forms the focus of the following chapter.

In summary, GBM is a clinically aggressive and biologically complex disease. Advances in molecular classification have refined diagnosis and prognostication, while improvements in surgical technique, imaging, and adjuvant therapies have modestly extended survival and improved quality of life for some patients. However, despite these efforts, the standard-of-care remains palliative, and the prognosis for most patients is dismal. The universal recurrence of disease, driven by profound intratumoural heterogeneity, infiltrative growth, and therapy resistance, underscores

the limitations of current approaches. Even in the minority of long-term survivors, functional impairments are common, reflecting the lasting impact of both the tumour and its treatment. Together, these challenges highlight the urgent need for a deeper understanding of GBM biology, which forms the focus of the following chapter.

#### 1.1.2 Biology of glioblastoma

#### 1.1.2.1 Glioblastoma initiation

The cellular origins of GBM remain a subject of considerable debate. While it is broadly accepted that GBM arises from cells within the neural lineage, the specific identity of the initiating cell, that is the cell that first acquires tumour-driving mutations and initiates malignant transformation, is not always clear. A growing body of evidence suggests that both neural stem cells (NSCs) and lineage-restricted progenitors are capable of serving as cells of origin, with their relative contributions potentially influenced by context, niche, and genetic insult (Alcantara Llaguno et al. 2016).

NSCs residing in the subventricular zone (SVZ), a site of adult neurogenesis in the human and murine brain, have emerged as a strong candidate population for GBM initiation. Subpopulations of these cells are mitotically active, long-lived, and transcriptionally plastic. These features likely increase their susceptibility to oncogenic transformation (Gil-Perotín et al. 2013). In a foundational study, Zhu et al. (2005) introduced *Trp53* and *Nf1* deletions specifically in GFAP-positive NSCs. The resulting mice developed high-grade astrocytomas predominantly localised to the SVZ and adjacent white matter, providing direct evidence that NSCs can serve as glioma-initiating cells (Y. Zhu et al. 2005). Following on from this work, the same lab

produced another model with *Trp53*, *Nf1*, and additional *Pten* deletions (Kwon et al. 2008) - this model was adopted by Garcia et al., who further confirmed that SVZ NSCs carrying this combination of mutations develop tumours with transcriptomic profiles closely resembling human GBM (Garcia-Diaz et al. 2023; M. Clements et al. 2024). Supporting the translational relevance of these findings, Lee et al. (2018) performed deep sequencing of SVZ tissue from patients with GBM and found that histologically normal SVZ cells harboured driver mutations in genes such as TP53, EGFR, and PDGFR. Importantly, in some patients, these mutations were clonally related to the tumour, suggesting that transformation may begin in the SVZ before the emergence of a radiographically detectable mass (J. H. Lee et al. 2018). Together, these studies position the SVZ as both a cellular and anatomical reservoir of mutation-bearing cells in gliomagenesis.

Beyond stem cells, more committed progenitor populations such as oligodendrocyte progenitor cells (OPCs) have also been shown as capable of acting as cells of origin in GBM. OPCs are distributed widely throughout the adult brain and retain the ability to self-renew and differentiate, making them plausible candidates for transformation (Fernandez-Castaneda et al. 2016). Conditional deletion of *trp53* and *nf1* specifically in OPCs (via NG2-Cre) leads to gliomagenesis in mice, and in some studies, OPCs—but not NSCs—undergo expansion and tumour formation following identical mutational insults, suggesting that the cell of transformation may not always be the cell of initial mutation (Lindberg et al. 2009; Galvao et al. 2014; C. Liu et al. 2011).

Adding further complexity, mature glial cells such as astrocytes have been shown to undergo dedifferentiation in response to various stimuli both *in vitro* and *in vivo*. In

experimental models, introduction of oncogenes or suppression of tumour suppressors (like *p53* and *nf1*) in mature astrocytes or neurons can induce reprogramming into a proliferative, stem-like state capable of driving gliomagenesis (Friedmann-Morvinski et al. 2012). Moreover, injury which triggers reactive astrocytosis can create a window of vulnerability during which more differentiated cells, namely astrocytes, regain stem-like features and acquire oncogenic mutations (Simpson Ragdale et al. 2023; J. P. Magnusson et al. 2014).

Taken together, these findings suggest that GBM may not originate from a single, universally defined cell type, but rather from a spectrum of potential initiating cells across the neural lineage. What appears to unify many of these origin models is the SVZ niche itself, which acts as a reservoir of mutation-bearing cells. This diversity in potential cells of origin may contribute to the profound intra-tumoural and inter-tumoural heterogeneity that defines GBM. Importantly, many of these initiating populations retain or reacquire developmental plasticity. This allows tumour cells to adapt to various microenvironmental cues and therapy-induced stresses, further fueling GBM's heterogeneity and resistance to treatment. The following section will explore how glioma stem-like cells (GSCs) contribute to this dynamic.

#### 1.1.2.2 Glioblastoma Stem Cells

The concept of stem cells within cancers was first identified in haematological malignancies, where a subpopulation of cells was found to sustain disease propagation, self-renew, and differentiate into various tumour cell types (Lapidot et al. 1994). In GBM, this stem-like population is referred to as GSCs, which share these hallmark features: self-renewal, differentiation potential, and the ability to initiate

tumour formation in vivo (S. K. Singh, I. D. Clarke et al. 2003; Lathia et al. 2015; S. K. Singh, Hawkins et al. 2004). The discovery of GSCs revolutionised the understanding of GBM in the early 2000s, as studies revealed that these cells could form neurospheres in culture and differentiate into multiple neuronal, glial, and astrocytic lineages, mimicking the cellular heterogeneity observed in the tumour (Ignatova et al. 2002; R. Chen et al. 2010).

GSCs are commonly identified by their capacity for self-renewal, multilineage differentiation, and, critically, their ability to initiate tumour formation upon orthotopic transplantation into immunocompromised mice (S. K. Singh, Hawkins et al. 2004). In a seminal study, Singh et al. (2003) prospectively isolated CD133-positive cells from brain tumours and demonstrated that these cells could generate tumours in vivo that recapitulated the histological features of the original neoplasm (S. K. Singh, I. D. Clarke et al. 2003). This finding led to the widespread adoption of CD133 as a canonical GSC marker. However, subsequent work revealed that CD133 expression is not universally required for tumourigenicity. For example, Beier et al. (2007) showed that CD133-negative glioma cells could also initiate tumours and even give rise to CD133-positive progeny, highlighting that the GSC population in GBM is not a fixed entity (Beier et al. 2007). Furthermore, CD133 is also expressed in normal ependymal cells as well as NSCs (Pfenninger et al. 2007). Additional markers such as CD44, L1CAM, and SSEA-1 have been proposed based on transcriptomic profiling and functional assays (Son et al. 2009; Krusche et al. 2016), but their expression patterns vary substantially between patient samples and across tumour regions. This variability, coupled with the dynamic nature of marker expression, limits the reliability of any single surface antigen as a definitive identifier of GSCs (J. Lee et al. 2006). As a result, in vivo functional validation—particularly limiting dilution transplantation assays—remains the gold standard for confirming GSC identity (Lathia et al. 2015).

GSCs have been shown to contribute significantly to both tumour initiation and recurrence. Their role in tumourigenesis is exemplified by studies showing that co-implantation of GSCs with differentiated GBM cells enhances tumour formation (Ouchi et al. 2016). In the context of recurrence, GSCs are thought to act as a reservoir for transcriptionally diverse tumour cell states, enabling clonal expansion and adaptation following therapy. GSCs facilitate the process of clonal evolution and expansion through their capacity to reconstitute tumour heterogeneity in response to treatment and microenvironmental cues (Dirkse et al. 2019; Hara et al. 2021). These transcriptional states will be explored further in the next subchapter of this thesis.

In addition to their contribution to tumourigenesis and recurrence, GSCs exhibit robust mechanisms that promote resistance to therapy. A key feature of GSCs is the activation of the NF-kappa B signalling pathway, a major driver of inflammation and cell survival. GSCs, especially in the mesenchymal state, heavily rely on NF-kappa B to resist cell death and promote survival under stress conditions such as radiation and chemotherapy (K. E. Cahill et al. 2015). NF-kappa B activation upregulates anti-apoptotic proteins like Bcl-2 and enhances DNA repair mechanisms, enabling GSCs to survive therapies that induce DNA damage (Koul et al. 2006). This NF-kappa B-driven survival mechanism is particularly important during the proneural-to-mesenchymal transition, where GSCs acquire traits linked to increased therapy resistance (K. P. Bhat et al. 2013).

Furthermore, GSCs exhibit significant genetic instability, which is a hallmark

of their ability to adapt to environmental stresses. Mutations in critical replicative checkpoints, such as those in p53, RB, and NF1, allow GSCs to bypass normal cell cycle regulation and resist apoptotic signals (C. W. Brennan et al. 2013). This genetic instability enables GSCs to rapidly accumulate mutations that may confer resistance to therapies, further complicating treatment efforts. Their enhanced DNA repair capacity also plays a crucial role in therapy resistance. For instance, the upregulation of DNA repair enzymes, such as PARP1, ATR, and ATM, helps GSCs recover from DNA damage induced by radiation or chemotherapy (Bao et al. 2006; C. Peng et al. 2016).

In conclusion, GSCs are central to the initiation, progression, and therapeutic resistance of GBM. Understanding the mechanisms that govern GSC biology—such as their activation of NF-kappa B, their ability to bypass replicative checkpoints, and their enhanced DNA repair capacity—is essential for developing more effective therapies.

#### 1.1.2.3 Cellular states and transcriptomic landscape of glioblastoma

The diversity in cellular states in GBM is not solely a product of different stages of cellular differentiation, extending from stem-like to terminally differentiation GBM cells. GBM cells present a wide range of transcriptomic identities, which pose significant challenges to treatment. Within a single tumour, distinct subpopulations of cells often show divergent responses to therapy, with some persisting as minimal residual disease and driving recurrence (M. Qazi et al. 2017). This inherent variability is a critical barrier to effective treatment and highlights the need for strategies that account for the complex, evolving nature of GBM.

Historically, GBM was classified into four major transcriptional

subtypes—proneural, classical, mesenchymal, and neural—based on genomic data from patient tumours (Verhaak et al. 2010). In this landmark study by Verhaak et al. (2010), the authors performed unsupervised clustering of gene expression profiles from over 200 GBM samples, identifying distinct subtype-specific molecular signatures linked to differing genetic alterations and clinical outcomes. However, the "neural" subtype was later deemed to reflect contamination from non-tumoural tissue, prompting a revised classification that retained only the proneural, classical, and mesenchymal subtypes (Q. Wang et al. 2017).

Crucially, single-cell and multi-region analyses transformed this framework. Sottoriva et al. (2013) performed multi-region sampling and applied clonal evolution models to demonstrate that different tumour regions can harbour distinct transcriptional subtypes, reflecting spatial heterogeneity within the same tumour (Sottoriva et al. 2013). Building on this, Patel et al. (2014) conducted a single-cell transcriptomic analysis of primary GBM samples and showed that individual tumour cells within a single region displayed divergent subtype signatures. This revealed an even greater degree of intra-tumoural heterogeneity than previously recognised (A. P. Patel et al. 2014). Notably, even in tumours broadly classified as "proneural" (a subtype associated with more favourable prognosis), the presence of mesenchymal-like cells has been linked to poorer outcomes, likely due to their enhanced invasiveness and therapy resistance (A. P. Patel et al. 2014).

A central finding from single-cell RNA sequencing (scRNA-seq) studies is that transcriptional heterogeneity in GBM is not random but rather reflects a distorted recapitulation of neural development. Malignant cells organise along a limited number of transcriptional programs that resemble specific neural lineage states. This

observation, first formalised by Neftel et al. (2019) and since confirmed by multiple groups, has led to the classification of four dominant cellular states: neural progenitor cell (NPC)-like, OPC-like, astrocyte (AC)-like, and mesenchymal (MES)-like (Neftel et al. 2019; Couturier, Ayyadhury et al. 2020; Yuan et al. 2018). While the first three are reminiscent of stages in glial development, the MES-like state stands apart, lacking a normal neurodevelopmental counterpart and instead resembling injury-associated or inflammatory phenotypes (L. M. Richards et al. 2021; Q. Wang et al. 2017; Gangoso et al. 2021; Hara et al. 2021) (Figure 1.1).

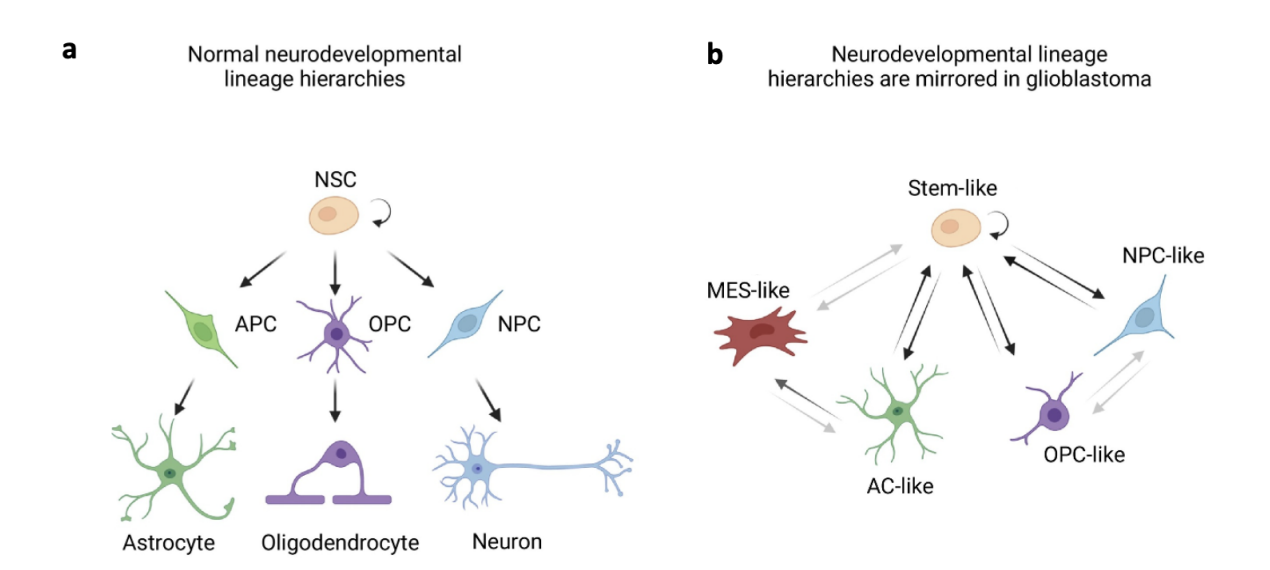


Figure 1.1. Transcriptional cellular states in glioblastoma recapitulate normal neurodevelopment.

a, Normal neurodevelopmental lineage hierarchies, with the NSCs at the top of the hierarchy differentiating into astrocyte progenitor cell (APC), OPC, and NPC) states. These go on to differentiate into astrocytes, oligodendrocytes, and neurons, respectively. b, Neurodevelopmental lineage hierarchies in GBM, with stem-like progenitor cells differentiating into AC-like, NPC-like, and OPC-like cells, as well as a fourth, MES-like state. These cellular states are plastic, with tumour cells moving between them throughout tumour evolution. This figure was adapted from Brooks et al., 2022 (L. J. Brooks, Ragdale et al. 2022)

Importantly, these cellular states are not fixed identities. Rather, GBM cells demonstrate significant plasticity, transitioning between states in response to extrinsic

stimuli such as hypoxia, inflammation, and therapeutic stress (De Silva et al. 2023; L. J. Brooks, M. P. Clements et al. 2021). The proportions of each cellular state within a tumour are shaped by intrinsic genetic drivers. For example, EGFR amplification is thought to bias cells toward the AC-like state, while PDGFRA amplification enriches for OPC-like cells. Furthermore, cell extrinsic, TME factors including immune cell infiltration, proximity to necrosis, and vascular niches also influence transcriptional states (Neftel et al. 2019; Yuan et al. 2018; Q. Wang et al. 2017).

Among these states, the MES-like subpopulation has garnered particular attention, in part due to its clinical significance. MES-like GBM cells are favoured in tumours with *Nf1* deletion and express markers of inflammation, extracellular matrix remodelling, and injury responses, with microenvironmental influences playing a key role in shifting cells towards this state (Q. Wang et al. 2017; L. J. Brooks, Ragdale et al. 2022). This state shares molecular similarities with reactive astrocytes and has been consistently associated with regions enriched in tumour-associated macrophages (TAMs) (K. P. Bhat et al. 2013; Hara et al. 2021; Q. Wang et al. 2017; Couturier, Nadaf et al. 2022). Spatial transcriptomic analyses have shown that MES-like and AC-like states co-localise with immune cell-dense regions, particularly enriched in myeloid populations (Ravi et al. 2022). This is clinically relevant as the presence of MES-like cells correlated with poorer prognosis (S.-J. Yoon et al. 2016).

Furthermore, while the four-state model has become a widely used framework, the continuous evolution of transcriptomic techniques continues to uncover new complexity. A recent study described a neural crest cell (NCC)-like population enriched in early-stage tumours, potentially representing a novel developmental mimicry program that may contribute to gliomagenesis (Hamad et al. 2023).

Taken together, these findings illustrate a tumour that is not only heterogeneous but also plastic, capable of shifting phenotypic identity in response to its environment and therapeutic pressures. This presents a major challenge for targeting GBM, as treatment-resistant subpopulations can persist following therapy. The next subsection will cover how these described processes effect therapeutic resistance in GBM.

# 1.1.2.4 Treatment resistance in glioblastoma: the challenge of cellular diversity and evolution

The failure of current therapeutic strategies in GBM is inextricably linked to the tumour's profound intra-tumoural heterogeneity and phenotypic plasticity. Subpopulations within the tumour can exhibit distinct signalling dependencies, proliferative capacities, and therapy responses, which collectively undermine efforts at durable disease control.

This plasticity allows tumour cells to escape the selective pressure of therapy by dynamically shifting their transcriptional identity. For example, Bhat et al. (2013) demonstrated that ionising radiation induces a proneural-to-mesenchymal transition (PMT) in glioma cells through activation of the NF-kappa B pathway. This transition led to the emergence of a therapy-resistant mesenchymal state, characterised by elevated CD44 and YKL-40 expression, and was associated with worse survival outcomes in patients (K. P. Bhat et al. 2013). Similarly, Hara et al. (2021) showed that exposure to chemoradiotherapy enriches for both mesenchymal-like and stem-like subpopulations in patient-derived xenografts, highlighting the plastic and adaptive responses of glioma cells under treatment pressure (Hara et al. 2021).

Mechanistically, resistance arises through several interconnected processes.

Stommel et al. (2007) provided a seminal demonstration of RTK co-activation in GBM, showing that multiple receptor tyrosine kinases — including EGFR, MET, and PDGFR — can be simultaneously active within different subclones of the same tumour. Using RNA interference to inhibit individual RTKs, they found that single-agent targeting often failed to suppress downstream PI3K signalling unless multiple RTKs were inhibited in parallel (Stommel et al. 2007). This functional redundancy enables tumour cells to bypass the effects of targeted therapies, leading to therapeutic escape. Additionally, EGFR mutations, including EGFRvIII and C-terminal truncations, often exist in non-overlapping subclonal populations (Francis et al. 2014), further complicating efforts to effectively target this pathway in a heterogeneous tumour.

Second, spatial and temporal heterogeneity pose a formidable challenge. Tumour fragments from different brain regions of a single patient may fall into different molecular classifications (Sottoriva et al. 2013), and the dominant subtype at recurrence may differ from that at diagnosis due to clonal selection under treatment. Recurrence is frequently accompanied by an enrichment of mesenchymal-like phenotypes, which are linked to inflammatory signalling, NF1 loss, and resistance to standard therapies (K. P. Bhat et al. 2013; Q. Wang et al. 2017). In contrast, proneural tumours may be more initially responsive but are prone to mesenchymal transition under treatment pressure.

Among the most therapy-resistant populations are GSCs, which exhibit heightened DNA repair capacity, drug efflux, and tumour-initiating potential. These cells, explored in more detail in the section above, often reside in perivascular or hypoxic niches, are enriched at recurrence, and are thought to drive tumour regrowth following treatment (Couturier, Ayyadhury et al. 2020). Their quiescent nature and

plasticity make them particularly difficult to eliminate with cytotoxic agents, and they remain a central target in efforts to overcome therapeutic failure.

Together, these patterns of resistance and clonal adaptation can be contextualised through models of tumour evolution. Historically, two frameworks have been proposed: the stochastic model, in which all tumour cells have the potential to acquire mutations and contribute to progression, and the hierarchical model, in which a dedicated subpopulation of cancer stem cells fuels growth through asymmetric division (Dick 2009). Increasingly, however, a hybrid model of plasticity has been adopted, recognising that differentiated cells may regain stem-like features in response to microenvironmental cues such as hypoxia, inflammation, or therapy (G. R. Bhat et al. 2024). This paradigm shift emphasises the dynamic nature of GBM hierarchies and highlights the importance of targeting state transitions rather than fixed cell types.

In this context, therapeutic interventions may inadvertently act as selective pressures, shaping the tumour's future composition. Monotherapies targeting single drivers such as EGFR or PDGFR have failed to improve survival in clinical trials, partly because they eliminate only the susceptible subset of cells, enriching for resistant clones (W. Wei et al. 2016).

Efforts to overcome resistance have begun to explore multimodal and combinatorial approaches. Future directions must include detailed profiling of recurrent and therapy-adapted GBM, leveraging multiomic and single-cell technologies to map the shifting cellular landscape. Identifying converging dependencies — shared pathways or stress responses across diverse cell states — may improve therapeutic success in GBM.

Taken together, intra-tumoural heterogeneity, dynamic plasticity,

and context-dependent therapy resistance are major drivers of GBM recurrence. Current treatments, predominantly antiproliferative therapies like chemotherapy and radiation, primarily eradicate rapidly dividing cells. However, this approach fails to account for the diverse responses of different tumour subpopulations, particularly the therapy-resistant GSCs, which are often in a quiescent state and can evade the cytotoxic effects of these therapies. While some tumour cells undergo apoptosis in response to treatment, other cells—especially those in protective niches such as perivascular or hypoxic areas—survive, adapt, and repopulate the tumour, driving recurrence. The mesenchymal-like GSC subpopulation, for example, is particularly resistant to standard treatments and can rapidly shift its phenotype in response to microenvironmental stresses like hypoxia or inflammation, further complicating treatment efforts (Hara et al. 2021). Addressing this challenge will require a paradigm shift toward polytherapeutic strategies that target multiple tumour compartments, real-time tracking of tumour evolution to identify emerging resistance mechanisms, and inhibition of the cellular transitions that underpin adaptive resistance. Only by addressing the tumour's cellular diversity and plasticity can we hope to develop more durable therapeutic approaches. The next section will explore the molecular and environmental drivers that fuel this plasticity and shape GBM progression.

# 1.1.2.5 Drivers of glioblastoma

The phenotypic diversity and plasticity of GBM are underpinned by a complex landscape of molecular and environmental drivers that influence tumour growth and progression. These drivers operate at multiple levels, including genomic, epigenomic, transcriptional, and microenvironmental, some of which will be described below.

At the genetic level, GBM is marked by frequent alterations in core signalling pathways that govern proliferation, survival, and genome maintenance. The most commonly altered include:

The *RTK/RAS/PI3K* pathway, frequently activated via amplification or mutation of receptor tyrosine kinases such as *EGFR*, *PDGFRA*, or *MET*, and downstream effectors like *PIK3CA* or *PTEN* loss (H. Zheng et al. 2008; C. W. Brennan et al. 2013).

The **TP53 pathway**, disrupted by mutations in *TP53* itself or by loss of upstream regulators such as *MDM2* and *CDKN2A* (Ying Zhang et al. 2018).

The *RB* pathway, commonly inactivated through deletions or methylation of *CDKN2A/B*, or mutations in *RB1* (Chkheidze et al. 2021; Fueyo et al. 2000).

Together, these mutations enable unchecked cell cycle progression, resistance to apoptosis, and metabolic reprogramming, which are hallmarks of malignant transformation. In addition to these canonical alterations, pathways governing developmental signalling and stress response—including TGF-β, NF-xB, and Notch—are frequently dysregulated in GBM (Pouyan et al. 2025). These pathways contribute to immune evasion, maintenance of stem-like states, and modulation of the tumour microenvironment. For instance, TGF-β signalling promotes tumour cell invasion and immunosuppression, while NF-xB activity is linked to inflammation, therapy resistance, and mesenchymal transition (Golán-Cancela et al. 2024; K. E. Cahill et al. 2015; Koul et al. 2006). Notch signalling plays context-dependent roles in both stemness and differentiation, contributing to intra-tumoural heterogeneity (Bazzoni et al. 2019).

Beyond genetic mutations, epigenetic dysregulation plays a critical role in shaping the GBM landscape. Aberrant DNA methylation, histone modifications, and

chromatin remodelling affect transcriptional programs that define cellular phenotypes and play a critical role in their plasticity (Safa et al. 2015; Nagarajan et al. 2009). GBM often displays focal and heterogeneous epigenetic changes that contribute to tumour plasticity, immune evasion, and resistance to therapy through the modulation of developmental and stress-related gene programs. Transcriptional drivers have been shown to contribute to the establishment and maintenance of specific cellular For instance, expression of SOX2, OLIG2, or STAT3 correlates with the states. neural progenitor-like, oligodendrocyte progenitor-like, or mesenchymal-like states described previously (Filppu et al. 2021; De Silva et al. 2023). These factors not only mark different subpopulations but can also actively reinforce cell state identity or drive transitions between them, particularly under selective pressure such as therapy. Furthermore, recent single-cell studies have shown that early tumour growth can be driven by epigenetic silencing of tumour suppressors such as CDKN2A and activation of oncogenic programs, while progression to higher grades involves genetic amplifications (e.g., PDGFRA, MYCN, CDK4) and loss of interferon signalling through gene deletion (Drucker et al. 2025). These findings support a broader model in which glioma evolution reflects a combinatory effect of both epigenetic and genetic drivers.

Importantly, extrinsic drivers can also impose phenotypic changes on tumour cells. For example, hypoxic niches within the tumour core favour a shift toward the mesenchymal state, mediated by HIF1 $\alpha$  and related factors (M. Dong et al. 2024). Similarly, cytokines released by tumour associated microglia/macrophages (TAM)s can activate transcriptional programs that promote invasion, survival, and immunosuppression. These external cues do not necessarily require genetic alterations to alter tumour behaviour, and may promote reversible, plastic responses that enable

adaptation to TME stress. These GBM-TME interactions will be discussed in more detail in the next section.

#### 1.1.2.6 Glioblastoma-tumour microenvironment interactions

GBM development and progression is constantly influenced by its complex and evolving TME, which comprises a broad array of cellular and molecular components. These include neurons and glial cells, tumour-associated immune cells, stromal and vascular elements, and extracellular matrix (ECM) components. The TME provides dynamic signals that shape glioma cell behaviour, modulating proliferation, migration, cellular identity and resistance to therapy, discussed below (Jang et al. 2025).

Neural Interactions: Neurons are gaining increasing recognition as active players in GBM progression, giving rise to the rapidly evolving field of cancer neuroscience (Winkler et al. 2023). Neurons have been shown to influence GBM growth, plasticity, and invasion through a range of direct and indirect mechanisms.

One of the most striking discoveries in recent years is the ability of GBM cells to form functional synapses with neurons. These neuron-to-glioma synapses have been shown to trigger excitatory currents in tumour cells which in turn depolarise. This has been shown to promote GBM cell proliferation (Venkatesh, Morishita et al. 2019). Furthermore, neuronal hyperactivity can increase functional coupling between tumour cells and neurons, leading to circuit remodelling that promotes glioma integration into existing neural networks. In parallel, neurons secrete activity-dependent growth factors such as neuroligin-3, which have also been identified as signals which stimulate tumour proliferation and invasion (Venkatesh,

Johung et al. 2015).

Neuronal signals also contribute to the spatial dynamics of glioma infiltration. Glioma cells have been shown to exploit axonal tracts and white matter pathways as physical scaffolds for migration, closely resembling normal neuronal migratory patterns (Osswald et al. 2015; Venkataramani et al. 2022; Cuddapah et al. 2014). This behaviour has also been shown to be promoted by GBM-neuronal synaptic connectivity (Venkataramani et al. 2022).

Together, these findings demonstrate that neurons contribute to GBM pathogenesis via both direct synaptic integration and broader neuroglial network effects. The implications of this neuron–tumour crosstalk will be further explored in relation to axonal injury in the next subchapter.

Immune Interactions: GBM is characterised by a profoundly immunosuppressive TME, in which the immune landscape is dominated by TAMs, comprising of both brain-resident microglia and recruited peripheral monocyte-derived macrophages. In the healthy central nervous system (CNS), microglia contribute to tissue homeostasis by performing functions such as synaptic pruning and secretion of neurotrophic factors (Q. Li et al. 2018). However, in the context of GBM, these cells become activated upon sensing damage-associated molecular patterns (DAMPs) released by stressed or dying tumour cells (Donat et al. 2017). In parallel, tumour growth and associated tissue disruption lead to the progressive breakdown of the blood-brain barrier (BBB), allowing bone marrow-derived monocytes to infiltrate the brain and differentiate into macrophages within the tumour microenvironment (A. X. Chen et al. 2021). Expanding on this point, the composition of TAMs is not static but evolves as the disease progresses. In early-stage or in less-infiltrative tumours, TAMs are

primarily microglia-derived. However, as the BBB deteriorates, there is a proportional increase in monocyte-derived macrophages, which come to dominate the immune infiltrate in more advanced or necrotic tumour regions (Buonfiglioli et al. 2021). This shift contributes to spatial and temporal heterogeneity within the tumour immune landscape. Once recruited and activated, TAMs adopt diverse phenotypes that reflect both pro-inflammatory and anti-inflammatory programmes. They can release pro-inflammatory cytokines such as tumor necrosis factor- $\alpha$  (TNF- $\alpha$ ), interleukins (interleukin (IL)-1α, IL-1β, IL-6, IL-12), and complement components like C1q, contributing to oxidative stress, immune cell recruitment, and local inflammation. At the same time, TAMs also express anti-inflammatory mediators including IL-10, TGF-β, and a range of growth and trophic factors, fostering immunosuppression, angiogenesis, and tumour progression (Andersen et al. 2021; Jurga et al. 2020). This dual role of TAMs as both potential anti-tumour agents and tumour-promoting accomplices reflects the high degree of plasticity within the GBM immune TME. Rather than existing as binary "M1/M2" macrophages, TAMs occupy a continuum of activation states, shaped by the local microenvironment and glioma-derived This complexity gives rise to profound inter- and intra-tumoural immune heterogeneity, which presents a formidable barrier to effective immunotherapy (Khan et al. 2023). Moreover, recent studies suggest that TAMs are not merely passive bystanders, but active drivers of tumour evolution. They contribute to the maintenance of mesenchymal-like transcriptional states in glioma cells and may promote therapy resistance through sustained inflammatory signalling (A. X. Chen et al. 2021; Sa et al. 2020). The immune infiltrate in GBM is not limited to TAMs; T cells, particularly CD8+ cytotoxic T lymphocytes, are often present but remain dysfunctional due to the immunosuppressive signals within the TME (Woroniecka et al. 2018). Additionally, other immune populations, such as myeloid-derived suppressor cells (MDSCs) and regulatory T cells (Tregs), further contribute to immune evasion by suppressing anti-tumour immune responses (Raychaudhuri et al. 2011; Ooi et al. 2014). Collectively, these interactions underscore the importance of understanding the immune TME in GBM.

Astrocyte Interactions: Astrocytes are the most abundant glial cell type in the CNS and are increasingly recognised as playing several active roles in GBM. While initially reactive astrocytogliosis acts as a protective response to tissue disruption, this response has also shown to be tumour supportive in various studies. Upon GBM expansion and resulting tissue disruption, astrocytes become activated through signals secreted by tumour cells (such as RANKL) which induces NF-xB signalling and promote GBM cell migration and invasion (J.-K. Kim et al. 2014). In parallel, reactive astrocytes have been shown to secrete cytokines such as IL-6, IL-8, and TGB-β1, many of which can enhance GBM cell proliferation and invasion and correlate with aggressiveness (R. Li et al. 2010; Jiang et al. 2017).

Beyond secreted signals, astrocytes facilitate invasion via ECM remodelling. They secrete enzymes including as MMPs which assisst GBM cell migration through degradation of the surrounding matrix (D. M. Le et al. 2003; Coquerel et al. 2009). Moreover, astrocytes may selectively support the invasive behaviour of GSCs, with co-culture experiments with astrocytes or astrocyte media demonstrating increased invasion of CD133<sup>+</sup> GSCs but not in their CD133<sup>-</sup> counterparts (Rath et al. 2013).

Finally, it is important to note that astrocytes themselves are a heterogeneous population, with regionally distinct subtypes playing different roles in supporting

GBM behaviour (John Lin et al. 2017). Notably, astrocytes in the perivascular niche express markers such as CD44 and tenascin-C, and may contribute to the maintenance of GSC niches (Katz et al. 2012).

Together, these findings highlight the multifaceted roles of astrocytes in shaping the GBM microenvironment, influencing tumour proliferation, invasion, and subtype specification.

Vascular Interactions: GBM is a highly vascularised tumour with profoundly abnormal vasculature (Hara et al. 2021). GBM blood vessels, most of which are newly formed as a result of hypoxia and other molecular drivers, are tortuous, leaky, and poorly structured, contributing to regional hypoxia, oedema, and therapeutic resistance (Guyon et al. 2021). This dysfunctional vasculature results from a combination of excessive pro-angiogenic signalling, particularly via vascular endothelial growth factor (VEGF), and the recruitment of perivascular stromal cells that form a specialised tumour-supportive niche (Sawamiphak et al. 2010).

The hypoxia caused by poor perfusion activates hypoxia-inducible factors (HIFs) in tumour cells, which drive further expression of VEGF, forming a self-reinforcing feedback loop (Apte et al. 2019). Anti-angiogenic therapies aimed at blocking VEGF initially showed promise, but their efficacy has been limited due to adaptive resistance mechanisms, including increased invasiveness, vascular mimicry, alternative angiogenic pathways, and complex relationship with the immune TME (Gerstner et al. 2009; G. Wang et al. 2013).

As discussed previously, GSCs tend to cluster around blood vessels, where they are exposed to signals that maintain their undifferentiated state and support tumour regrowth after treatment (Mosteiro et al. 2022; Hira et al. 2018). Notably, Calabrese et

al. (2007) identified the perivascular niche as a key microenvironmental compartment where endothelial cells promote GSC self-renewal through the secretion of Notch ligands and other stemness-supportive signals (Calabrese et al. 2007). Disruption of this niche may represent a therapeutic opportunity, but targeting it without harming normal neurovascular structures remains a major challenge (M. D. Brooks et al. 2013).

Additionally, the abnormal vasculature contributes to immune exclusion by limiting immune cell infiltration and by establishing gradients of oxygen and nutrients that shape the immune TME (M. Ghosh et al. 2022).

ECM Interactions: The extracellular matrix (ECM) in GBM is not merely a structural scaffold but an active participant in tumour progression. GBM cells dynamically remodel the ECM to create a microenvironment conducive to their survival, invasion, and resistance to therapy (R. Wei et al. 2024).

Key components of the GBM ECM include proteoglycans and glycoproteins such as hyaluronic acid, tenascin-C, and laminins. These molecules interact with cell surface receptors like integrins and CD44, facilitating signaling pathways that promote tumour cell proliferation and migration (Sivasankaran et al. 2009; Bellail et al. 2004). Fibronectin, another prominent ECM component in GBM, has been shown to promote cell adhesion, migration, and survival via integrin-mediated signalling. It also contributes to the stiffening of the ECM and can act as a scaffold for growth factor presentation, reinforcing tumour-supportive signalling loops (Serres et al. 2014; Ohnishi et al. 1998).

GBM cells secrete matrix metalloproteinases (MMPs), which degrade ECM components, enabling tumour infiltration into surrounding brain tissue (Hagemann et al. 2012). Additionally, the altered ECM composition contributes to the formation

of a perivascular niche that supports glioma stem-like cells, further enhancing tumour aggressiveness (S. Xu et al. 2020).

Targeting ECM components and their associated signaling pathways presents a potential therapeutic avenue. Strategies aimed at disrupting ECM-tumour cell interactions or inhibiting ECM remodeling enzymes may impede GBM progression and improve treatment outcomes (Mohiuddin et al. 2021).

Bidirectional Feedback and Phenotypic Plasticity: Importantly, the relationship between GBM cells and their TME is reciprocal. Tumour cells actively reshape their surroundings through secreted factors, proteases, and exosomes. These, in turn, act on stromal and immune cells to reinforce tumour-supportive behaviours. A clear example of this is the ability of GBM cells to induce reactive astrogliosis, converting astrocytes into a more inflammatory or tumour-promoting state (Jang et al. 2025). This ongoing dialogue fuels phenotypic plasticity, enabling glioma cells to shift between transcriptional states in response to environmental cues such as inflammation, therapy, or hypoxia. Such adaptability contributes to treatment failure and recurrence, particularly as resistant subclones are selected under pressure. Among the most potent and complex TME cues is injury. Whether arising from tumour growth or therapeutic insult, injury profoundly alters the tissue landscape, leading to a release of inflammatory signals, disruption of cellular architecture, and reprogramming of cells within the brain parenchyma. The following section explores how these injury-related processes can actively shape GBM progression and influence tumour evolution.

#### 1.1.2.7 The role of injury in glioblastoma progression

GBM can be conceptualised as both a driver and a "consequence" of brain injury. As it expands, GBM inflicts mechanical, metabolic, and inflammatory damage to the surrounding neural tissue—through direct compression, disruption of the vasculature, excitotoxicity, and infiltration. These mechanisms of tumour-induced injury will be explored in greater detail in subsequent chapters of this thesis.

Importantly, the injured brain does not remain passive. Injury-induced responses reshape the TME in ways that can inadvertently support tumour progression. Resident glial cells adopt reactive phenotypes, inflammatory cytokines are released, the BBB is disrupted, and the ECM is remodelled. These responses may be regenerative programs, as shown in context of brain injury, but in the context of GBM, they often lead to enhanced tumour aggression (Addington et al. 2015). GBM appears to hijack injury-response pathways, mimicking and sustaining a reactive environment that favours its own evolution (L. J. Brooks, Ragdale et al. 2022). These include transcriptional programs typically associated with neuroinflammation, reactive gliosis, and regeneration, positioning GBM not just as a passive recipient of environmental changes, but an active manipulator of the injured TME.

Studies exploring the pro-tumourigenic effects of injury have demonstrated that glioma cells in a perilesional injury environment exhibited enhanced proliferation and mesenchymal reprogramming, in part driven by inflammatory and cytokine-mediated signalling (L. M. Richards et al. 2021). This injured niche was shown to promote tumour progression and reduce sensitivity to therapy, highlighting injury as not only a biological consequence of GBM but a critical contributor to its malignant behaviour (Hamed et al. 2025; Watson et al. 2024).

The profound impact of injury on GBM evolution underscores the need to better understand how injury programs are initiated in the context of GBM, how exactly they alter the TME, and through which signals they support aggressive tumour states, which is the focus of this thesis. How these mechanisms intersect with axonal pathology, neuroinflammation, and fibrotic responses, will be explored in the following chapter.

# 1.2 Axonal injury

GBM is a profoundly disruptive disease due to the extensive damage it causes to the surrounding brain tissue. Invasion into the healthy parenchyma, surgical trauma, radiotherapy and neuroinflammation all contribute to the creation of an injured TME. Within this context, axons are particularly vulnerable as they are highly polarised and very metabolically active, making them sensitive to mechanical, metabolic, and inflammatory insults. Damage to axons can lead to alterations in brain function, having a profound effect on patient lives. Furthermore, axonal injury may not merely be a passive consequence of GBM behaviour, but could actively influence tumour progression and therapeutic resistance. Injury-induced changes in the TME, such as neuroinflammation, astrogliosis and fibrosis, may support tumour growth. Therefore, understanding how axons respond to injury, and how these responses shape the biology of GBM, is a critical avenue of investigation. This section outlines the types of axonal insults, the cellular responses they elicit, and the downstream consequences for both neural tissue and tumour progression.

#### 1.2.0.1 Mechanisms of axonal injury: types of axonal insult

Axonal injury can arise from a variety of insults, many of which are highly relevant in the context of GBM. These insults are often multifactorial, with overlapping mechanical, metabolic, excitotoxic, and inflammatory components. Both the tumour itself and its aggressive treatment can therefore initiate and exacerbate axonal injury.

Mechanical injury results from direct structural disruption of axons. In GBM, this may occur through infiltrative tumour growth that physically displaces or transects white matter tracts, through mass effect resulting in increased intracranial pressure,

through impairments in axonal transport, and through surgical manipulation during tumour resection, where axonal bundles are cut or cauterised as part of routine operative procedures (Seano et al. 2019; Mesfin et al. 2017; Travis et al. 2020).

Metabolic injury arises when energetic demands exceed supply. GBM contributes to local hypoxia and nutrient deprivation as it is highly metabolically demanding in part due to its rapid proliferation, abnormal vasculature, and altered metabolic pathways (Agnihotri et al. 2015). This can lead to axonal transport failure and cytoskeletal breakdown, triggering degeneration (Kalogeris et al. 2012).

Excitotoxic injury is driven by excessive glutamate release, a feature commonly observed in glioma-associated tissue (Groot et al. 2011). High extracellular glutamate concentrations overactivate NMDA receptors, triggering calcium overload, oxidative stress, and cytoskeletal damage within axons (Ye et al. 1999; Verma et al. 2022). This mechanism is also observed in other neurological conditions including stroke and epilepsy, but it may be particularly exacerbated by tumour-derived glutamate secretion within the context of GBM (Kaplan-Arabaci et al. 2022; Chapman 2000).

Inflammatory injury involves a cascade of immune-mediated processes which create a toxic environment for axons. In GBM and other brain injuries, breakdown of the blood-brain barrier (BBB) allows infiltration of peripheral immune cells, while resident microglia and astrocytes become reactive. These cells release pro-inflammatory cytokines and reactive oxygen species (ROS), which together result axonal damage (Ramírez-Expósito et al. 2019; Albulescu et al. 2013). This will be discussed in more depth in section 1.2.2.3 - Downstream effects of axonal injury and degeneration.

GBM can hence cause axonal injury through a variety of different mechanisms, highlighting that axonal loss in GBM is rarely results from a single insult. The effects of tumour pressure, metabolic derangement, excitotoxicity, neuroinflammation and therapy-induced injury co-occur and may potentiate one another, creating a complex injured environment. This leads to a number of axonal responses which are discussed below.

#### 1.2.0.2 Axonal responses to injury: degeneration pathways

Axons are highly specialised, polarised extensions of neurons that depend on continuous intracellular transport and metabolic support from the cell body to maintain structure and function. Following injury, axons respond in a range of ways that span from adaptive repair to complete structural degeneration. The precise outcome is determined by factors including the severity of the insult, timing, axon type, and the surrounding cellular environment.

In cases of mild or transient injury, axons can initiate localised repair mechanisms such as cytoskeletal remodelling, membrane resealing, and the local translation of survival-promoting proteins (Hur et al. 2012). If the injury is more severe or sustained, particularly when axonal transport is disrupted, intrinsic degeneration programs are triggered. These are active, regulated processes, not passive decay.

The commonest and well characterised form of axonal degeneration is Wallerian degeneration (WD), which occurs distal to the site of axonal transection or severe transport failure. This process is tightly controlled and mediated by defined molecular players, including nicotinamide mononucleotide adenylyltransferase 2 (NMNAT2) and sterile alpha and TIR motif–containing protein 1 (SARM1), and is explored in

detail in the next section. Traditional WD is triggered by axonal severance, leading to a failure of axonal transport.

Closely related to this is Wallerian-like degeneration, a term used to describe degeneration that mimics many features of WD including cytoskeletal disintegration, mitochondrial swelling, and myelin breakdown, and is also regulated via SARM1 protein activation, but occurs in the absence of axon severance. Wallerian-like degeneration is observed in several pathological contexts, including multiple sclerosis, chemotherapy-induced peripheral neuropathy, neuroinflammatory diseases, as well as within the context of drugs which either directly impair cellular transport and cytoskeleton, or directly activate SARM1 protein (Saggu et al. 2010; Sylaja et al. 2007; Song et al. 2024).

Other degeneration phenotypes include:

Dying-back degeneration, in which axonal breakdown proceeds from the synaptic terminal toward the soma. This has been observed in neurodegenerative diseases and motor neuron disease (Yaron et al. 2016; Dadon-Nachum et al. 2011). It is, however, worth mentioning that dying-back degeneration can arise as a consequence of WD and may result from the lack of retrograde synaptic signalling (Alvarez et al. 2008).

Axon pruning, a developmentally programmed and restricted form of degeneration. This process is usually physiological and critical for normal neural development, but similar pruning-like processes have been co-opted in disease states and can involve caspase activation and synapse loss without neuronal death (L. Luo et al. 2005). It also occurs as a result of NGF deprivation which can arise from reduced synaptic activity (Schuldiner et al. 2015)

Focal degeneration, seen in diseases like multiple sclerosis, where demyelination

and inflammation cause patchy loss of axonal integrity (Nikić et al. 2011; Sorbara et al. 2014).

In reality, these degeneration programs exist on a continuum rather than as distinct outcomes. An axon may initially attempt to recover, only to shift toward degeneration if conditions deteriorate. However, with WD being the most pervasive form, the following section focuses specifically on this pathway: its molecular machinery, relevance in the CNS, and its emerging importance in GBM-associated pathology.

#### 1.2.1 Wallerian degeneration

Wallerian degeneration (WD) is a conserved, actively regulated process of axonal disintegration that occurs distal to the site of injury. Originally observed over a century ago, WD was once thought to be a passive consequence of axon severance. However, recent molecular insights have demonstrated that WD is a cell-autonomous self-destruction program intrinsic to the axon itself (Coleman et al. 2010), the features and molecular mechanism of which will be discussed in the following section of this thesis.

# 1.2.1.1 Morphological features of Wallerian degeneration

WD has several distinct and conserved morphological hallmarks, which have been described across species and model systems. These features arise sequentially in the distal segment of the axon after axonal transport disruption.

A classic early sign of WD is axonal beading, often described as a "beads-on-a-string" appearance (Shen et al. 2013). This reflects focal swellings along the axon, where cytoskeletal breakdown, organelle accumulation, and ionic imbalance

first become visible (Webster 1962). Another hallmark is vacuolisation within the axoplasm (H. Elsayed et al. 2020). Vacuoles form as intracellular organelles swell and membranes destabilise. Among the most striking changes is mitochondrial swelling, a result of calcium overload and loss of membrane potential, which leads to impaired energy metabolism and triggers pro-degenerative cascades (Vial 1958; Webster 1962). These degenerative changes ultimately culminate in the disintegration of the axon, where the axoplasm becomes disrupted, and myelin sheaths begin to unravel (M. Ma, Toby A. Ferguson et al. 2013b).

Histologically, these changes progress in a defined sequence and are distinct from apoptotic or necrotic cell death. Unlike in apoptosis, there is no nuclear condensation or caspase activation in axonal WD; and unlike necrosis, membrane rupture is not an initiating event (Finn et al. 2000). Instead, WD represents a cell-autonomous disassembly process, orchestrated within the axon itself.

The combination of beading, vacuolisation, mitochondrial swelling, and axoplasmic clearing provides a powerful morphological signature for WD, and serves to differentiate it from other degeneration programs such as axon pruning or focal demyelination. These features also make WD detectable by high-resolution imaging, which is relevant to the methodology in this thesis.

In the next section, molecular mechanisms which underly these histological alterations are discussed.

# 1.2.1.2 Wallerian degeneration: a defined molecular pathway

In this thesis, Wallerian degeneration is interchangeable with Sarm1 dependent axonal degeneration pathway. WD occurs when axonal transport is compromised.

Central to this is NMNAT2, a neuron-specific nicotinamide adenine dinucleotide (NAD)<sup>+</sup> synthase that is localised to the Golgi complex and is constitutively transported anterogradely along the axon (Berger et al. 2005). NMNAT2 is packaged into fast axonal transport vesicles, typically derived from Golgi and synaptic precursor trafficking pathways, and moves bidirectionally along microtubules via motor proteins such as kinesins and dyneins (Milde et al. 2013). NMNAT2 catalyses the conversion of nicotinamide mononucleotide (NMN) to NAD<sup>+</sup>, a key metabolite required for axonal maintenance, energetic homeostasis, and resistance to stress (Gilley and Coleman 2010). Following axonal injury, this transport is disrupted, leading to depletion of NAD<sup>+</sup> and accumulation of NMN in the distal stump of the severed axon (Figure 1.2).

This

in NMN/NAD<sup>+</sup> ratio triggers activation of the SARM1, a Toll/interleukin-1 receptor domain–containing NADase (Figley et al. 2021). Mechanistically, NMN and NAD compete for binding to an allosteric pocket in SARM1's ARM domain (Shi et al. 2022). NMN binding disrupts ARM–TIR interactions, allowing TIR domain oligomerisation and activation of its NADase function (Goldner et al. 2017). Once activated, SARM1 initiates a feed-forward degenerative cascade by cleaving NAD<sup>+</sup>, further depleting NAD<sup>+</sup> levels and therefore amplifying SARM1 activation. This results in energy failure within the axon and the initiation of downstream degenerative processes (McGuinness et al. 2024).

One consequence of NAD<sup>+</sup> breakdown is the generation of cyclic ADP-ribose (cADPR), a potent calcium-mobilising molecule. Elevated intracellular calcium levels have been shown to acutely precede axonal fragmentation, with this SARM1-driven calcium influx acting as an executioner or WD (Loreto et al. 2015). Inhibition of

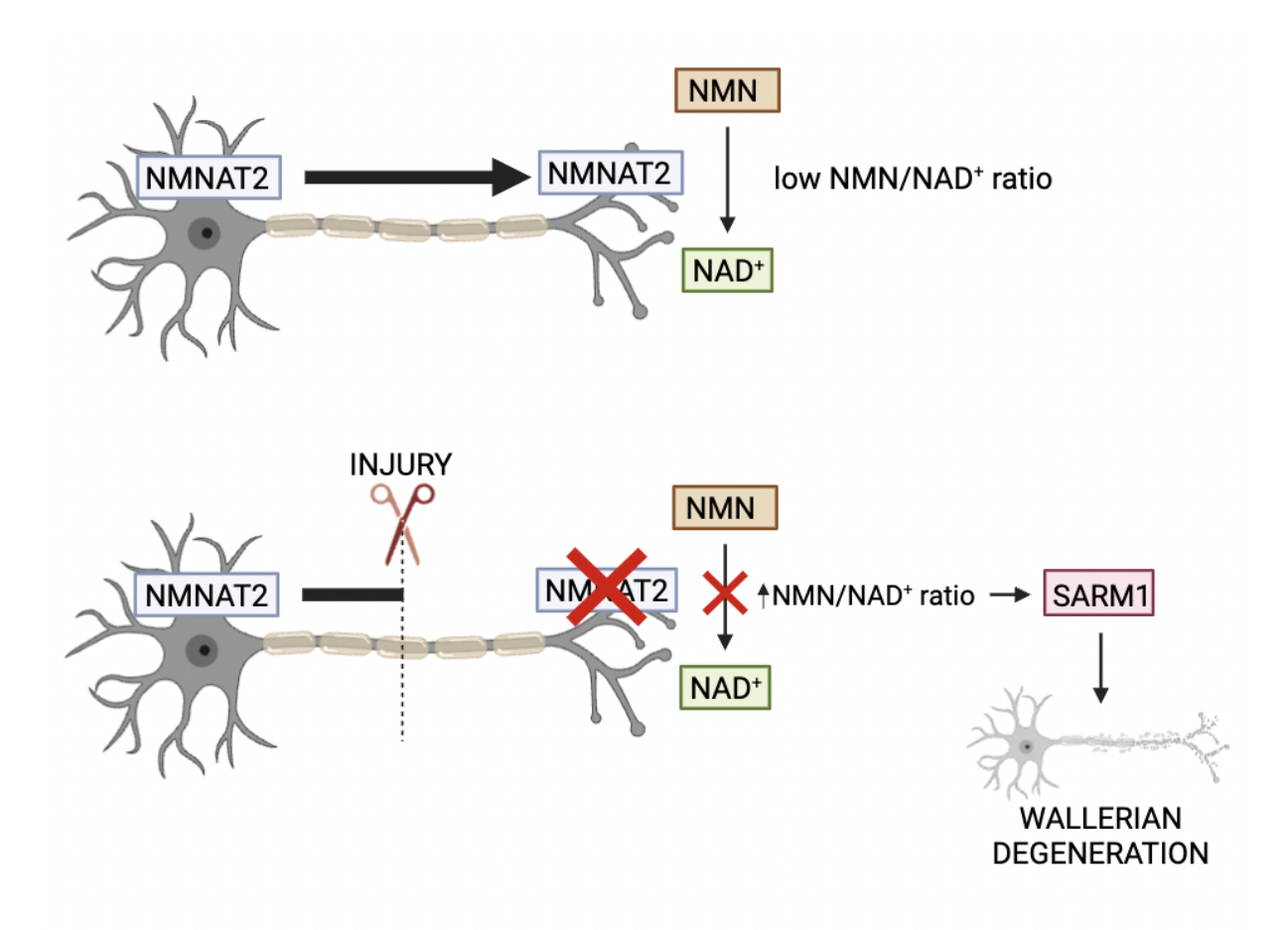


Figure 1.2. The molecular pathway of Wallerian degeneration.

A visual representation of the simplified molecular pathway underlying WD. In a normal axon (above), transport of NMNAT2 is maintained, and the NMN to NAD<sup>+</sup> ratio remains low. When an injury occurs (below), transport of NMNAT2 is blocked, leading to a rise in NMN to NAD<sup>+</sup> ratio, which triggers SARM1 protein. This activated SARM1 protein then orchestrated WD.

cADPR activity can delay this process and suppress WD onset, although this appears to be one of several parallel pathways acting downstream of SARM1 (Essuman et al. 2017).

In addition to this metabolic cascade, early signalling responses triggered by axonal injury also contribute to NMNAT2 destabilisation and may act upstream of the SARM1 axis. Notably, activation of the MAPK signalling pathway, particularly through dual leucine zipper kinases (DLK and LZK), has been shown to mediate rapid NMNAT2 depletion following injury (S. Patel et al. 2015). Inhibition of these kinases

can delay WD onset by preserving NMNAT2 levels and maintaining axonal integrity, providing another potential point of intervention within the pathway.

Moreover, other downstream mechanisms of axonal breakdown continue to be uncovered. Novel players such as Axundead (invertebrate specific) and other conserved regulators identified through invertebrate and vertebrate screens are increasingly recognised as modulators of WD across species (Neukomm et al. 2017). While the full network of execution pathways is still being mapped, the central role of SARM1 and its regulators remains well established.

While new insights into Wallerian degeneration (WD) are still emerging—particularly around its downstream execution mechanisms—the core molecular framework of this self-destructive program is now well defined. The identification of key components such as NMNAT2 and SARM1, and the clarification of their interactions in response to axonal stress, has opened the door to targeted interventions. As a result, both genetic and pharmacological strategies aimed at delaying or halting WD have been developed and will be discussed in the next section.

# 1.2.1.3 Targeting Wallerian degeneration

The molecular dissection of WD has enabled the development of both genetic and pharmacological tools to modulate this process. These interventions not only serve as proof-of-concept for axon-preserving strategies, but also offer models to study the impact of WD on various other biological processes, relevant to the study of GBM, and highlight the potential translational value of studying WD.

One of the earliest genetic models of altered WD is the Wld<sup>S</sup> mouse, which

carries a naturally occurring mutation that delays axonal degeneration following injury. The Wld<sup>S</sup> phenotype arises from the expression of a chimeric fusion protein combining the N-terminal region of Ube4B with the full coding sequence of NMNAT1 (a nuclear isoform of the NAD<sup>+</sup> synthase) (Figure 1.3). This fusion protein exhibits increased stability, meaning it persists longer in the severed axonal stump, effectively substituting the function of NMNAT2 and preserving NAD<sup>+</sup> levels in injured axons (Coleman et al. 2010; Gilley and Coleman 2010; Gilley, Ribchester et al. 2017). Although degeneration still eventually occurs in Wld<sup>S</sup> mice, it is markedly delayed compared to wild-type animals (Gilley, Ribchester et al. 2017).

A more definitive model is the Sarm1<sup>-/-</sup> mouse, in which the master regulator of WD - SARM1 - is genetically inactivated (Figure 1.3). In this model, axons are preserved, in some models indefinitely, after injury, confirming SARM1's central role in driving this degeneration pathway (Gilley, Ribchester et al. 2017). However, if axonal transport is severely impaired, degeneration may still occur through alternative, SARM1-independent mechanisms, such as deprivation of other essential enzymes and factors.

Beyond genetics, several pharmacological approaches have shown promise in preclinical models. One approach involves suppressing the enzyme NAMPT, which generates NMN—the metabolite whose accumulation activates SARM1. Treatment of transected axons with the NAMPT inhibitor FK866 has been shown to delay WD in vitro (Alexandris et al. 2022) (Figure 1.3). However, this strategy has limitations: NAMPT is also needed for NAD biosynthesis, therefore, prolonged inhibition ultimately leads to NAD depletion and, therefore, SARM1 activation (Garten et al. 2015). Other studies have focused on early injury signalling cascades

such as the MAPK pathway. Inhibition of dual leucine zipper kinases prior to axotomy prolongs axonal survival by maintaining NMNAT2 levels and preventing its depletion (S. Patel et al. 2015) - importantly, this has already shown promise in the clinic, with favourable findings from early clinical trial showing reduced neuropathy in certain patient populations (J. Ma et al. 2021). These findings suggest that timely modulation of injury-induced signalling can alter the trajectory of axonal fate. Finally, various SARM1 inhibitors are being developed and are proceeding into early clinical trials stages, which are excitingly not only targeting peripheral neurological disease, but also centrally effecting degeneration, such as multiple sclerosis (Krauss et al. 2019).

Together, these models have transformed WD from a descriptive phenomenon into a targetable biological pathway. By leveraging both genetic and pharmacological tools, researchers are now able to modulate axonal fate with increasing precision, setting the stage for future therapeutic applications in human disease and injury.

#### 1.2.1.4 Downstream effects of axonal injury and degeneration

WD as a pathway of axonal loss is a critical initiator of secondary pathological processes, including neuroinflammation, astrogliosis, and fibrosis. It is important to note, however, that these downstream effects differ markedly between the peripheral nervous system (PNS) and the central nervous system (CNS), with the latter showing more persistent and maladaptive responses. These downstream mechanisms of WD have been studied more extensively within the PNS. However, as this thesis focuses on GBM, a primary malignancy of the CNS, this section places an emphasis on the consequences of axonal injury and degeneration within the CNS.

In the CNS, WD initiates a sustained inflammatory cascade. Axonal and myelin

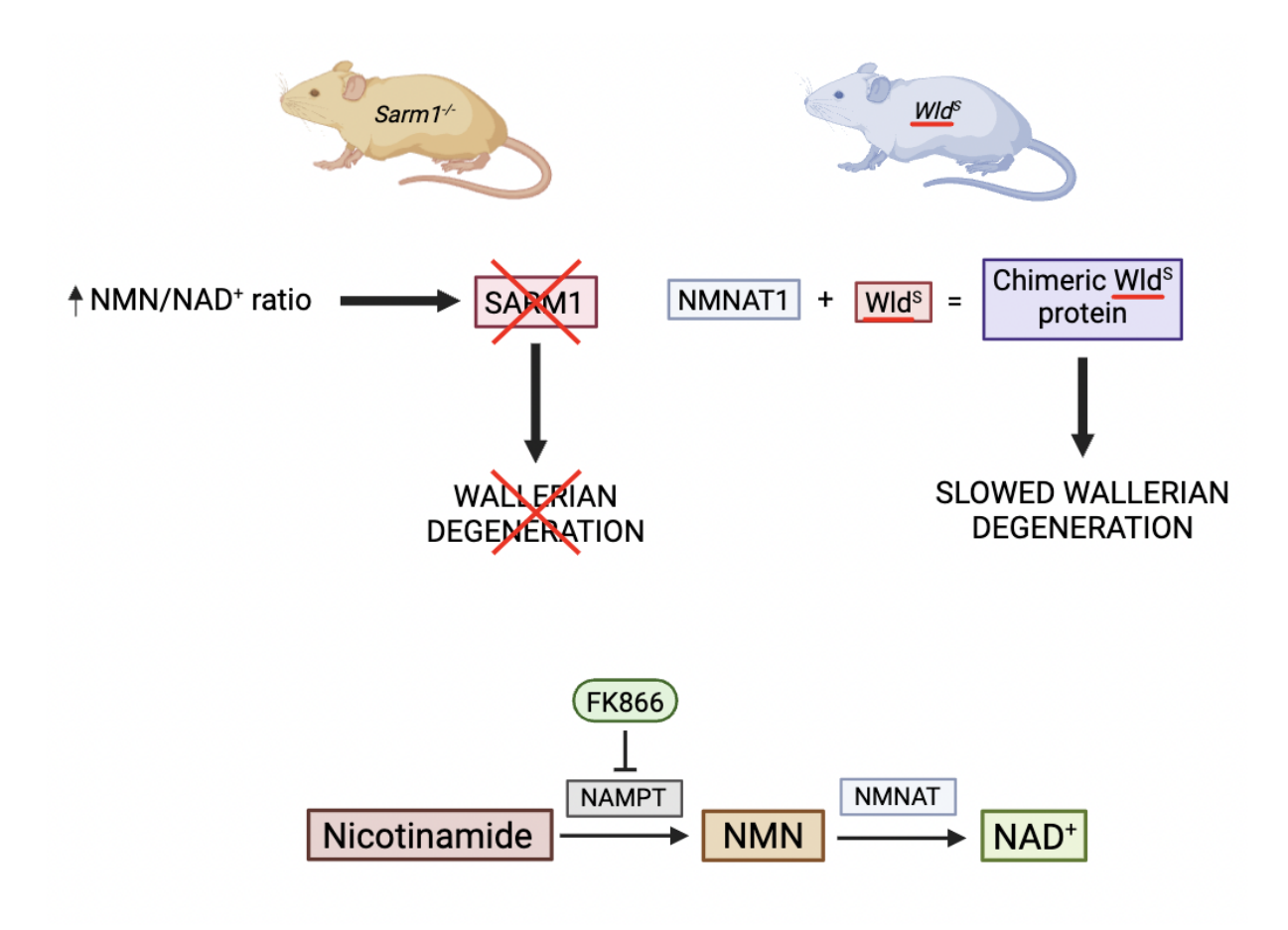


Figure 1.3. Genetic and pharmacological targeting of Wallerian degeneration.

A visual representation of two genetic models of altered WD (above), including Sarm1 knock-out mouse and  $Wld^S$  mouse. Below is a representation of an example of pharmacological WD inhibition, using FK866 as a NAMPT inhibitor which blocks the generation of NMN and thereby maintains a low NMN to NAD<sup>+</sup> ratio.

debris released during degeneration activate resident microglia, as well as peripherally derived macrophages, which adopt a phagocytic and pro-inflammatory phenotype (Reichert et al. 1996; Lafrenaye 2016). These cells release proinflammatory cytokines (such as tumour necrosis factor- $\alpha$  and IL-1 $\beta$ ) and increase oxidative stress (through secretion of reactive oxygen species (ROS) (superoxide radicals(O<sup>2-</sup>), nitric oxide(NO)) (G. Wang et al. 2013; Xiaoming Hu et al. 2012). Unlike the PNS, where Schwann cells and macrophages efficiently clear myelin and support regeneration, the CNS environment lacks robust clearance mechanisms. This inefficiency leads to prolonged

debris accumulation, which maintains an inflammatory niche and inhibits axonal regrowth (Huebner et al. 2009).

Alongside microglia and macrophages, astrocytes play a central role in coordinating the CNS response to axonal degeneration. Upon injury, astrocytes become reactive (a process termed astrogliosis) undergoing morphological and transcriptional changes (Anderson, Ao et al. 2014; Ye Zhang et al. 2010; Burda et al. 2022). These reactive astrocytes upregulate intermediate filaments such as GFAP, proliferate locally, and secrete cytokines, chemokines, and extracellular matrix molecules, influencing inflammatory and fibrotic responses (Giovannoni et al. 2020). In the acute phase, astrogliosis can help restore homeostasis and contain inflammation (Liddelow et al. 2017; Sofroniew 2009). Furthermore, chronic astrocyte reactivity contributes to the formation of the glial scar, which initially limits immune cell infiltration and protects the site of injury from further insult, but was thought to simultaneously create a mechanical and biochemical barrier to axonal regeneration (Yanlu Zhang et al. 2019; Cieri et al. 2023). However, the inhibitory role of the astroglial scar in neuronal regrowth has recently been widely refuted, with new evidence pointing to the contrary, with astrocytic scarring aiding regeneration (Anderson, Burda et al. 2016). These different theories and scientific evidence are likely to be the result of the vast heterogeneity of astrocytic phenotypes upon injury. Furthermore, in the context of GBM, peritumoural astrocytes may interact dynamically with tumour cells and immune populations, further complicating the injury-repair landscape (Henrik Heiland et al. 2019).

In addition to astrocytic reactivity, WD in the CNS promotes the infiltration of perivascular fibroblasts, as well as reprogramming of other cellular states into

fibroblast-like cells, and the formation of a fibrotic scar, rich in collagen and fibronectin (Dorrier et al. 2022; T. Zhou et al. 2019). This fibrotic scar forms in parallel with the glial scar and was, much like the latter, long thought to contribute to the barrier that inhibits axon regrowth. However, this has also been brought into question, with various studies showing little to no inhibition of regrowth in the PNS, which could hold relevance in the CNS setting as well (Risling et al. 1993; Joosten et al. 2000). Recent studies suggest that crosstalk between fibroblasts, astrocytes, and infiltrating immune cells orchestrates this fibrotic response (Ziyu Li et al. 2021). In GBM, where widespread tissue disruption and perivascular infiltration are common, these fibrotic pathways may become pathologically activated, impacting both neuronal repair and tumour behaviour. Recent work exploring the fibrotic response to anti-CSF-1R therapy has, for instance, found that fibrosis accelerates recurrence (Watson et al. 2024), an important concept in line with the exploration of this thesis which highlights the role of TME remodelling in altering tumourigenesis.

Taken together, axonal injury and degeneration can take place in the context of GBM via various mechanisms, both due to the presence of the tumour itself, but also as a consequence of surgical and radiological interventions. WD is a key axonal loss pathway which orchestrates neuroinflammation and scarring, influence the composition and activation states of TAMs, modulating astrocytic reactivity in the peritumoural niche, and reprogramming fibroblast-like cells which leads to fibrotic scarring. These secondary responses may contribute to treatment resistance, tumour recurrence, and the evolution of the TME. Therefore, understanding how WD occurs and how it influences tumour biology can offer varied insight into novel therapeutic targets in this disease.

# 1.3 Research Question and Aims

This thesis explored the following research question:

What role does axonal injury and subsequent Wallerian degeneration play in GBM tumourigenesis?

To test this, the following aims were pursued:

- Characterise the spatiotemporal dynamics of early GBM growth and axonal injury using the "npp" (Nf1<sup>-/-</sup>, Pten<sup>-/-</sup>, p53<sup>-/-</sup>) somatic GBM model.
- Establish the functional contribution of axonal injury to tumour phenotype using the  $Sarm1^{-/-}$  mouse models which are resistant to WD.
- Evaluate whether axonal injury is a tractable pathway for therapeutic intervention in glioblastoma progression.

# Chapter 2

# Materials and Methods

#### 2.1 Animal work

#### 2.1.1 Animal strains and maintenance

All animal procedures were carried out in accordance with the UK Animals (Scientific Procedures) Act of 1986 and were approved by the UCL Animal Welfare and Ethical Review Body (AWERB). Mice were housed in individually ventilated cages within a specific pathogen-free (SPF) facility on a 12-hour light/dark cycle, with ambient temperature maintained at 20–24°C and relative humidity between 45–65%. Animals were provided with environmental enrichment, including nesting materials and cardboard shelters, and had ad libitum access to standard rodent chow and water.

The following strains were used in this study:

C57BL/6NCrl wild-type mice (Charles River) served as the genetic background for the somatic tumour model.

NOD.CB17-Prkdcscid/NCrCrl (NSG) immunodeficient mice (Charles River) were used for patient-derived xenograft (PDX) models.

Sarm1-/- knockout mice (Chr11:78472330-78497754 deletion) were kindly

provided by M. Coleman (Gilley, Ribchester et al. 2017), and maintained on a C57BL/6 background.

Sarm1<sup>em1.1Tftc</sup> and isogenic Sarm1<sup>wt</sup> littermate controls were generated using CRISPR-Cas9 technology and provided by R. Sugisawa.

Thy1-YFP transgenic mice (B6.Cg-Tg(Thy1-YFP)16Jrs/J, JAX #003709) expressing YFP in subsets of projection neurons were used for imaging axonal architecture.

Both male and female animals were used in all experiments, with the exception of NSG mice used in the PDX model experiment, which were all female.

#### 2.1.2 Tumour induction

Somatic model: *De novo* tumours were generated by intracerebroventricular injection of piggyBac/piggyBase plasmids encoding CRISPR/Cas9 components and targeting Nf1, Pten, and Trp53 ("npp"). Tumour induction was achieved using a combination of piggyBase (hGFAP<sub>MIN</sub>-SpCas9-T2A-PBase, 1 mg/ml) and piggyBac vector (U6-Nf1,Pten,Trp53-EF1a-tdTomato, 0.564 mg/ml), mixed at a molar ratio of 1:1. 0.1% Fast Green dye (Sigma, F7258) was added to the plasmid mix to aid visualisation of the injection.

Postnatal day 2 (P2) pups were immobilised under isoflurane anaesthesia (3% in  $O_2$ ) whilst their temperature was maintained on a heat pad. Intraventricular injections (right lateral ventricle) were performed using a Femtojet 4i microinjector (Eppendorf, 5247000030) attached to glass capillaries (Cat number GC100F- 10) pulled on a Sutter electrode puller. Each pup received approximately 1  $\mu$ L of plasmid cocktail. Electroporation was carried out immediately following injection by placing platinum tweezer electrodes (positive electrode on the right-hand side of the pup) and delivering

5 square pulses at 100 V for 50 ms at 850 ms intervals from a BTX Gemini Twin Wave Electroporators.

Following injection and electroporation, pups were returned to the nest and monitored closely. Injection success was confirmed by the presence of fast green dye at the time of injection, and tdTomato expression in harvested brains at early timepoints. All procedures were performed by experienced staff (M. Clements, H. Simpson Ragdale)M. Clements et al. 2024.

PDX model: Orthotopic xenografts were established in NSG mice by stereotactic injection of patient-derived glioblastoma cell lines (Pollard et al. 2009). Cell lines were obtained from the CRUK glioma cellular genetics resource (GCGR, in preparation, Morrison et al.). All procedures were performed by experienced staff (M. Clements, M. Woodberry, and H. Simpson Ragdale).

### 2.1.3 Animal monitoring

Animals were monitored daily for general health and signs of neurological deterioration. Body weight was recorded weekly. Pre-defined humane endpoints included:

15% weight loss

Intermittent abnormal respiratory pattern

Seizures

Lethargy, hunched posture, or loss of body condition

Ocular/nasal discharge

Persistent motor or behavioural abnormalities

Animals reaching endpoints were euthanised using cervical dislocation (for tissue harvesting) or transcardial perfusion with PBS and 4% PFA under terminal anaesthesia (for immunohistochemistry).

#### 2.1.4 Animal behavioural assessment

To evaluate the functional consequences of tumour progression and *Sarm1* deletion, two complementary behavioural paradigms were employed: the Neuroscore for motor dysfunction and the novel object recognition (NOR) test for cognitive performance. All behavioural experiments were conducted during the light phase of the housing cycle in a dedicated behavioural testing suite, with animals habituated to the testing environment prior to assessment. All testing was performed blinded to genotype, over three consecutive days to increase the robustness of the results and account for variability.

**Neuroscore motor testing:** Motor function was assessed using a composite Neuroscore, a validated scale for detecting progressive neurological deterioration in mouse models of neurodegeneration and glioma (Guyenet et al. 2010). The test battery included four components:

Ledge test: Mice were placed on the edge of the home cage, and their ability to walk along the narrow ledge and descend into the cage was scored:

- 0 = Confident walk and controlled descent
- 1 = Occasional wobbles or slips
- 2 = Frequent slips or hesitancy, with partial failure to descend
- 3 = Inability to balance or descend

Hindlimb clasping: Mice were suspended gently by the tail for 10 seconds, and

the position of their hindlimbs was evaluated:

- 0 = Hindlimbs consistently splayed outward
- 1 = Mild retraction toward the abdomen
- 2 = Persistent retraction for > 50
- 3 = Strong clasping of hindlimbs against the body

Gait analysis: Mice were observed walking freely in an open area:

- 0 = Normal gait
- 1 = Mild gait abnormality or tremor
- 2 = Obvious gait abnormality, raised pelvis or pronounced tremor
- 3 = Marked motor dysfunction, irregular or stuttering movement

Kyphosis: Spinal posture during movement was evaluated:

- 0 = Normal posture
- 1 = Transient curvature
- 2 = Persistent mild kyphosis
- 3 = Severe and continuous kyphosis

Each component was scored from 0–3, with a total possible score of 12, where higher scores indicated greater motor impairment. Mice were tested once daily for three consecutive days at both early (8 weeks post-tumour induction) and advanced disease stages (typically 2 weeks prior to humane endpoint - at this stage, animals were tested weekly, and the time-point matching 2 weeks prior to terminal disease was selected for analysis). For each animal, the average score across the three days was used for final analysis.

**Novel Object Recognition (NOR) task:** The NOR test was used to assess recognition memory and exploratory behaviour, adapted from the standard paradigm described

by Ennaceur and Delacour (Ennaceur et al. 1988). The test took place in a  $30 \text{ cm} \times 30 \text{ cm} \times 30 \text{ cm} \times 30 \text{ cm}$  red acrylic arena, cleaned with 70% ethanol between trials to eliminate olfactory cues. Mice underwent the following three stages per day, over three testing days:

Habituation phase (Day 0): Mice were individually placed in the empty arena for 5 minutes to familiarise them with the testing environment.

Familiarisation phase: On each test day, mice were placed in the arena containing two identical objects (e.g., plastic blocks and foil-wrapped Eppendorf tubes) for 10 minutes. Object placement (left vs right) was randomised between animals.

Test phase: one of the familiar objects was replaced with a novel object of similar size and material but different shape and texture. Mice were returned to the arena for 10 minutes, and the time spent exploring each object was recorded.

Exploration was defined as sniffing or directing the nose toward an object at a distance of  $\leq 1$  cm. Climbing or resting on the object was not counted as exploration. To minimise learning bias and novelty fatigue, a different object pair was used each day of testing, with careful control for visual and tactile differences.

The percentage of time spent exploring the novel object was recorded as the result.

# 2.1.5 Microglial depletion

To deplete microglia, mice were fed a custom rodent diet containing the CSF1R inhibitor PLX5622 (Product number D19101002S AIN-76A), formulated as a rodent diet with 1,200 ppm PLX5622 and a pink dye indicator. Control animals received a matched AIN-76A diet lacking the inhibitor (Product number D10001AIN-76A, green dye).

Diets were provided ad libitum for 4 weeks, starting at 8 weeks after tumour induction and continuing through to 12 weeks. Animals were then returned to standard chow, and tissue was collected at 14 weeks post-induction for analysis. This timing was selected to coincide with the period of peak tumour progression and allow assessment of microglial contribution to late-stage disease.

Mice were monitored daily for general health and weighed weekly throughout the dietary intervention.

Tissue was collected for histological analysis. The efficiency of the depletion was confirmed by Iba1 immunofluorescence staining in non-tumour-infiltrated brain regions.

#### 2.1.6 Tissue collection

For immunohistochemistry, mice were perfused with PBS and 4% PFA, followed by overnight fixation in PFA at 4°C and storage in PBS at 4°C. Brains were embedded in 3% agarose and sectioned coronally at 50µm using a vibratome (Leica VT1200S). For flow cytometry and scRNA-seq, mice were sacrificed via cervical dislocation, and brains were collected in ice-cold RPMI 1640 or HBSS for immediate processing.

# 2.2 In Vitro Work

#### 2.2.1 NSC isolation and culture

NSCs were isolated from the subventricular zone (SVZ). Dissected SVZ tissue was enzymatically dissociated using papain and DNAse (Worthington, LK003178) for 30 minutes at 37°C, and then quenched in ovomucoid inhibitor solution. Cells were cultured in neurosphere media and maintained at 37°C, 5% CO<sub>2</sub>. Neurospheres were

passaged or cryopreserved upon appearance (Conti et al. 2005).

#### 2.2.2 Generation of GSCs

NSCs were transferred to laminin-coated flasks and cultured under adherent conditions in GSC media (. Cells were transfected with the "npp" plasmid using FuGENE HD transfection reagent (Promega) to induce transformation.

#### 2.2.3 Cell culture media

The following compositions of cell culture media were used: Neurosphere media: DMEM F12 (Gibco, 11320-074), 15 mM HEPES (Gibco, 15630-056), 1000 U/ml penicillin-streptomycin (Merck, P0781), 10 ng/mL EGF (Biotechne, NBP2 35176), 10ng/ml FGF-2 (Biotechne, NBP2 35152), B27 without Vit A (1/50, Gibco, 12587-010).

GSC media: DMEM F12 (Gibco, 11320-074), 15 mM HEPES (Gibco, 15630-056), N2 (1/200), B27 (1/100) (Life Technologies), 1 mg/mL laminin (Merck L2020), 10 ng/mL EGF (Biotechne NBP2 35176), 10ng/ml FGF-2 (Biotechne NBP2 35152), 1x MEM NEAA (Fisher Scientific 12084947), 0.1 mM 2-mercaptoethanol (Fisher Scientific 31350010), 0.012% Bovine serum albumin (BSA) (ThermoFisher 15260-037), 0.2 g/L glucose (Merck G8769), 1000 U/ml penicillin-streptomycin (Merck P0781).

# 2.2.4 In Vitro functional assays

EdU cell cycle analysis: Cells were incubated with 10μM EdU for 2 hours, fixed in 4% PFA for 15 minutes at room temperature, permeabilised with 1% Triton X-100 for 15 minutes at room temperature, and labelled using the Click-iT EdU kit (AF647, Invitrogen). Cells were resuspended in DAPI(1/5000)/PBS and analysed using the BD Fortessa x20 cytometer.

**Migration assay:** Migration assays were performed using the Incucyte SX5. Cells were seeded into 96 well plates in serum-free media and migration tracked for 24 hours. Migration was manually quantified using *Manual Tracking* ImageJ plugin.

# 2.3 Histology and imaging

#### 2.3.1 Immunofluorescence

Free-floating brain sections were permeabilised and blocked overnight in 1% Triton-X100 and 10% donkey serum at 4°C. Primary antibodies were applied overnight at 4°C, followed by 2-hour incubation in secondary antibody (1/1000 concentration) with DAPI (1/10000 concentration). Sections were mounted using ProLong Gold Antifade (Invitrogen).

Antibodies: The following primary antibodies at specified concentrations were used for immunofluorescence in this thesis: rabbit anti-Ki67 (1:250; Abcam, ab16667); mouse anti-Ki67-BUV395 (1:100, Clone B56, BD 564071); goat anti-GFAP (1:1,000; Abcam, ab53554); rat anti-CD68 (1:500; Abcam, ab53444); rabbit anti-Iba1 (1:1,000; Wako, 019–19741); L0159), mouse anti-neurofilament H (1:1000 Enzo ENZ-ABS219-0100); mouse anti-myelin basic protein (1:1000 Covance SMI-99); mouse anti SMI32 (1:1000, Enzo, ENZ-ABS219-0010); chicken anti-GFP (1:1000, Abcam ab13970); rabbit anti-RFP (1:1000, ABIN129578); rabbit anti-TOMM20 (1:1000, ab186735); rabbit anti-laminin (1:500, Sigma, L9393); goat anti-CD31 (1:100, BioTechne, AF3628); and rat anti-PdgfrB (1:200, kind gift from I.Kim).

#### 2.3.2 Electron microscopy

Electron microscopy (EM) was performed in collaboration with Dr Ian White. Mice were perfused with EM grade 4% formaldehyde and immersion fixed overnight, embedded in 4% agarose, and sectioned on a vibrating microtome at 100µm thickness (1 mm/s speed, 0.80 mm amplitude). Sections were stained with DAPI (1:10000, 10 min at room temperature) and imaged using confocal microscopy to identify regions of interest (ROIs).

These regions were prepared for electron microscopy as follows. Sections were treated sequentially with formaldehyde: glutaraldehyde, osmium tetroxide: potassium ferricyanide, osmium tetroxide, thiocarbohydrazide, uranyl acetate and lead aspartate. They were then dehydrated through an ethanol series and embedded in Epoxy resin. Serial ultrathin sections (70nm) were taken using a diamond knife (Diatome) and an ultramicrotome (UC7, Leica) and collected on formvar coated slot grids. Sections were imaged on a scanning electron microscope (SEM) Pocratsky et al. 2023.

All EM analysis was conducted on  $\geq 50$  axons per bundle in  $\geq 3$  bundles (n=4). Degenerating axons were identified as those exhibiting any of the following features of axonal pathology: dark axoplasm, organelle accumulation, axonal swelling (watery degeneration), or vacuolisation. For quantitative analysis of demyelination, only axons with no obvious fixation artefacts, myelin decompaction or vacuolisation were analysedSaliani et al. 2017. The inner diameter, outer diameter, myelin thickness, and the corresponding g ratios of the myelinated axons were semiautomatically calculated using MyelTracer software programKaiser et al. 2021. Feret diameters were used for this quantification to account for the imperfect circularity of axons. This analysis was conducted in collaboration with Saketh Karamched.

#### 2.3.3 Image acquisition

Confocal imaging was performed using Zeiss LSM 880 (including high-resolution Airyscan), Zeiss LSM 900, and 3i spinning disk confocal microscopes.

#### 2.3.4 Image analysis

Quantitative and qualitative analyses of confocal images were performed using a combination of Imaris (v10.1.0, Oxford Instruments) and ImageJ/Fiji. For analysis of tumour cell distribution and proliferation, single z-plane images acquired using the 3i Spinning Disk confocal microscope were processed in Imaris. Spot detection was applied to the tdTomato (de novo tumours) or GFP (PDX tumours) channel to identify tumour cells, followed by filtering based on DAPI intensity (median or centre value) to refine nuclear segmentation. Tumour cells were further classified according Ki67 expression for proliferation analysis. Manual surface segmentation (drawing surfaces by hand) was used to delineate anatomical regions such as the striatum, subventricular zone (SVZ), and necrotic cores, with tumour cells in the SVZ and necrotic regions excluded from analysis. White matter bundles were segmented using the machine learning surface prediction tool by highlighting white matter areas as those that were MBP positive and grey matter areas as those free of MBP staining, and the algorithm was trained through repetitive corrections of the assigned white and grey matter areas until the performance was equivalent to what a manual segmentation would produce. White matter proportion of the striatum was then calculated as the proportion of tumour-infiltrated striatum occupied by white matter structures.

Fluorescence intensity measurements of axonal and glial markers were carried out in ImageJ on maximum intensity projections. Thy1-YFP and neurofilament

staining was analysed to assess axonal density, while Iba+ cell density and CD68 integrated density were used to quantify TAM cell responses. Fluorescence intensities were normalised to contralateral control regions. CD68 integrated density was measured following automated thresholding, with quantification performed using the *AnalyzeParticles* function.

To evaluate axon-tumour cell interactions, the spatial proximity of axonal varicosities to tumour cells was measured in single z-plane images. A total of 111 varicosities were individually selected and assigned to one of three categories based on their distance ( $<2~\mu m$  counting as proximity) from either a tumour cell body or tumour cell process. This analysis was done in collaboration with Saketh Karamched.

Vascular phenotypes were analysed using the *Vessel Analysis* plugin in ImageJ. MIP images were thresholded and converted to RGB format and inverted, to derive vessel parameters including CD31+ area, mean vessel diameter, and vascular length density. *Skeletonize3D* and *AnalyzeSkeleton* plugins were used to compute vessel branching. Co-localisation of CD31 with laminin or PDGFRB was assessed by applying thresholding to each channel, combining binary images using the Image Calculator's *AND* function, and computing percent overlap.

To create 3D reconstructions of images (Airyscan), z-stack confocal images were imported into Imaris and processed using the Surfaces tool for both tdTomato and GFP channels. Tumour and axonal structures were segmented, manually refined, and rendered for visualisation alongside the raw multichannel confocal stacks.

# 2.4 Flow cytometry

#### 2.4.1 Tissue dissociation and staining protocol

Tumour-bearing tissue was dissociated using Liberase TL(Roche, 05401020001) and DNAse(Sigma, D4263) at 37°C for 30 minutes, in RPMI (Sigma, R0883). After stopping the reaction with EDTA, myelin was removed using Myelin Removal Beads (130-096-722) and MACS sorting kit (Milteny Biotec). Cells were blocked with TruStain FcX (BioLegend, 101320), stained with surface antibodies, then fixed and permeabilised for intracellular staining.

A myeloid antibody panel was developed based on a previous panel used in the lab (Garcia-Diaz et al. 2023), which was optimised using spleen tissue. The panel consisted of the following antibodies used at indicated concentrations: rat anti-LY6G-BUV563 (1:100, Clone IA8, BD, 612921), rat anti-CD11b-BUV661 (1:400, Clone M1/70, BD, 612977), rat anti-MHC Class II-BB700 (1:800, Clone M5/114.15.2, BD, 746197), mouse anti-CD45-BUV805 (1:400, Clone 30-F11, BD, 748370), mouse anti-CD64-BV421 (1:100, Clone X54-5/7.1, Biolegend, 139309), mouse anti-CX3CR1-BV510 (1:400 Clone SA011f11, Biolegend 139309), rat anti-LY6C-BV605 (1:200, Clone AL-21, BD 563011), rat anti-CD19-BV650 (1:50, Clone ID3, BD 563235), hamster anti-CD11C-BV785 (1:100, Clone N418, Biolegend 117336), rat anti-CD49d-APC (1:200, Clone R1-2, Biolegend 103622), rat anti-F4/80-AF700 (1:100, Clone BM8, Biolegend 123130), mouse anti-Ki67-BUV395 (1:100, Clone B56, BD 564071), rat anti-CD3-BUV737 (1:300, Clone 17A2, BD564380), rat anti-CD206-AF488 (1:100, Clone C068C2, Biolegend 141710).

Cells were stained with surface antibodies and fixable viability dye eFluor780

(eBioscience, 65-0865-18) at a 1:1000 dilution for 20 minutes at 4°C. Following surface antibody staining, cells were permeabilised for 2 hours (Fixation/Permeabilisation kit (Invitrogen, eBioscience, 00-5523-00) at 4°C and stained with intracellular antibodies (anti-Ki67, anti-CD3 and anti-CD206) for a further 2 hours at 4°C. Additionally, compensation was done using ArC reactive and negative beads (Invitrogen, A10346 A and B) for viability dye compensation and UltraComp eBeads (Invitrogen, 01-2222-42) for all other fluorophores.

#### 2.4.2 Data acquisition and analysis

Flow cytometry was performed on BD FACSymphony and BD Fortessa x20 cytometers. Gating was conducted in FlowJo (v10.7.1). Live singlets were gated for all downstream analysis.

# 2.5 Transcriptomic profiling

# 2.5.1 Single-cell RNA sequencing: Sample preparation and library construction

Tissue from tdTomato+ tumour regions (located using Leica Stereo Microscope) was isolated and dissociated using papain as described above (see "NSC isolation and culture" section). Terminal npp tumours from 4 WT and 6 Sarm1<sup>-/-</sup> mice were used (equal numbers of males and females).scRNA-seq libraries were prepared using the Chromium Next GEM Chip G Kit (10x genomics; 1000127) by Imran Uddin, and sequenced on Nova Seq X Plus PE 150.

# 2.5.2 Single-cell RNA sequencing: data analysis

Data were analysed in collaboration with Gordon Beattie and conceptualised and conducted by Wenhao Tang. Reads were processed using CellRanger 7.0.1 and aligned to a custom mm10 reference including tdTomato. Datasets were first normalised using sctransform, and then integrated using Harmony (Hafemeister et al. 2019). Dimensionality reduction was carried out with PCA, followed by clustering with the Louvain algorithm (Blondel et al. 2008). Cells were first filtered to identify high-confidence tumour cells based on multiple criteria: tdTomato expression levels (UMI count  $\geq$  5), an euploidy prediction using copyKat (Gao et al. 2021), and tumour identity classification which was done using a supervised machine learning approach (random forest model) trained on published datasets (Ximerakis et al. 2019; Kalamakis et al. 2019; Yeo et al. 2022; Pombo Antunes et al. 2021). Cells expressing canonical immune markers (Ptprc and Cd68) were excluded. Non-tumour cells were identified by tdTomato negativity (UMI  $\leq$  2) and diploid status predicted using copyKat. Cell types were annotated based on canonical lineage markers and refined using gene set enrichment analysis (fgsea) (Korotkevich et al. 2016). Remaining unclassified cells were subjected to iterative clustering and classification via a random forest model trained on high-confidence cell annotations. TAMs were reclustered and annotated using marker sets from published datasets to distinguish microglial vs. monocyte-derived macrophage signatures (Kalamakis et al. 2019; Ximerakis et al. 2019). Differences in cell type proportions between genotypes were assessed by downsampling to equal cell numbers and applying a two-sample proportion test (prop. test in R). Differential expression analyses were conducted using the presto package (Korsunsky et al. 2019). Genes with p-values < 0.01 and high AUC values were selected and subjected to functional enrichment using the clusterProfiler R package (G. Yu et al. 2012). Ligand-receptor interactions were assessed using CellPhoneDB through the LIANA package (Dimitrov et al. 2022).

# 2.6 Statistical analysis

All statistical analyses were performed in GraphPad Prism 10 or R. Data are shown as mean  $\pm$ SD unless otherwise stated. All t tests were two-tailed. Significance thresholds were: \* p<0.05, \*\* p<0.01, \*\*\* p≤ 0.001. Tests used are specified in figure legends. Sample size was guided by existing literature and previous lab experience; no formal statistical method was used to predetermine sample size. scRNA-seq dataset visualisation was done using the ggplot2 package in R. Heatmaps were produced using ComplexHeatmap package (Z. Gu et al. 2016).

# Chapter 3

# Early glioblastoma lesions preferentially colonise white matter and cause axonal injury

## 3.1 Introduction

GBM is among the most aggressive and lethal forms of cancer, with patients commonly presenting late in the disease course when symptoms become aparent. Much of the current understanding of GBM biology is therefore derived from studying advanced disease, where tumours have already acquired complex cellular heterogeneity, widespread infiltration, and TME remodelling. In contrast, the earliest stages of gliomagenesis remain comparatively underexplored.

To overcome this limitation, this thesis employs a somatic, immunocompetent mouse model of GBM, referred to hereafter as the "npp" model (Garcia-Diaz et al. 2023; M. Clements et al. 2024). In this system, neural stem cells (NSCs) located within the subventricular zone (SVZ) are genetically transformed *in situ* via

CRISPR/Cas9-mediated inactivation of three key tumour suppressors — *Nf1*, *Pten*, and *Trp53* — a combination observed in human GBM (C. W. Brennan et al. 2013; Verhaak et al. 2010). The model incorporates a tdTomato fluorescent reporter, enabling direct visualisation and tracking of tumour cells over time (Figure 3.1).

The npp model uses a dual-vector piggyBac system to achieve efficient, cell type–specific somatic mutagenesis. One vector (piggyBase) encodes Cas9 under control of the human GFAP mini-promoter, thereby restricting Cas9 expression to GFAP-expressing cells in the SVZ (primarily NSCs and radial glia). The second vector (npp piggyBac) delivers three guide RNAs (gRNAs) targeting *Nf1*, *Pten*, and *Trp53*, along with a constitutively expressed tdTomato reporter under the EF1α promoter. The piggyBase and piggyBac vectors are injected together and electroporated into the lateral ventricle of neonatal mice (P2), discribed in more detail in the Methods chapter. These vectors enable stable integration and Cas9-mediated editing specifically in GFAP+ NSCs (Garcia-Diaz et al. 2023; M. Clements et al. 2024).

This approach offers several advantages. It avoids germline editing and instead models spontaneous somatic transformation and it ensures that transformation occurs in a relevant cell-of-origin (NSC) within the native brain environment. As a result, the npp model faithfully recapitulates key features of human GBM, including cellular heterogeneity, diffuse infiltration, and progressive microenvironmental remodelling (Garcia-Diaz et al. 2023; M. Clements et al. 2024). Crucially for this thesis, it also enables the study of early gliomagenesis in a controlled and trackable fashion.

This approach offers a tractable model to investigate the spatial, temporal, and phenotypic characteristics of early GBM development within the brain microenvironment. The experiments in this chapter leverage this system to build

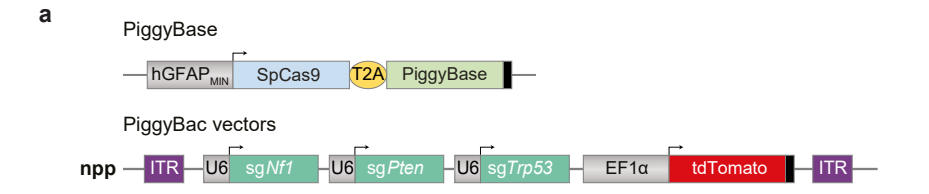


Figure 3.1. Schematic of the npp somatic GBM model.

a, Diagram illustrating the constructs used for in vivo electroporation. The top panel shows the piggyBase, while the bottom panel depicts the "npp" piggyBac construct carrying sgRNAs targeting *Nf1*, *Pten*, and *Trp53*, along with a tdTomato reporter for tumour cell labelling.

an understanding of early tumour cell behaviour, patterns of tissue colonisation, and the associated changes in the TME composition. These insights lay the foundation for subsequent exploration of the cellular and molecular mechanisms that govern tumour–brain interactions.

## 3.2 Results

# 3.2.1 Time-course analysis of glioblastoma growth reveals preferential early colonisation of white matter

The early spatial dynamics of glioblastoma growth were assessed through a longitudinal time-course analysis using the somatic "npp" mouse model. In this system, CRISPR/Cas9-mediated inactivation of *Nf1*, *Pten*, and *Trp53* in subventricular zone (SVZ) neural stem cells induces gliomagenesis, with tdTomato fluorescence permitting visualisation of tumour expansion.

Tumour-bearing brains were collected at defined timepoints following tumour induction: early ( $\leq$  8 weeks), intermediate (8–12 weeks), late (12–15 weeks), and terminal ( $\geq$  15 weeks, corresponding to the onset of clinical symptoms). At each

stage, the distribution of tdTomato-labelled tumour cells relative to white and grey matter compartments was analysed using immunofluorescence staining for myelin basic protein (MBP) to label WM and DAPI to label nuclei.

Initial qualitative assessment revealed a prominent localisation of tumour cells within white matter-rich structures, including the corpus callosum (CC) and striatal bundles. Grey matter regions such as the cortex and grey matter regions of the striatum exhibited relatively sparse tumour involvement at early stages. To quantitatively evaluate this spatial preference, the striatum was selected as a focus due to its consistent involvement throughout tumour progression and its clearly demarcated white and grey matter domains.

Co-staining for MBP demonstrated that tumour cells preferentially infiltrated MBP-positive white matter bundles in early lesions (Figure 3.2a). Quantification of tissue composition, based on machine learning approaches to define white matter bundles, indicated that white matter accounted for approximately 20% of the striatum during early stages (Figure 3.2b), which was similar to contralateral, normal, tumour-free striatal proportions. This proportion increased during intermediate and late stages, consistent with local expansion and deformation of white matter tracts by the growing tumour mass. However, a sharp decline in white matter fraction was observed at terminal stages, suggestive of advanced axonal degeneration and collapse of structural integrity of myelin sheets, with MBP staining no longer showing clear bundle pattern.

Mapping tumour cell distribution relative to white and grey matter confirmed a significant early-stage preference for white matter, with >60% of tdTomato<sup>+</sup> cells localising to MBP<sup>+</sup> regions (Figure 3.2c). This spatial bias diminished as disease

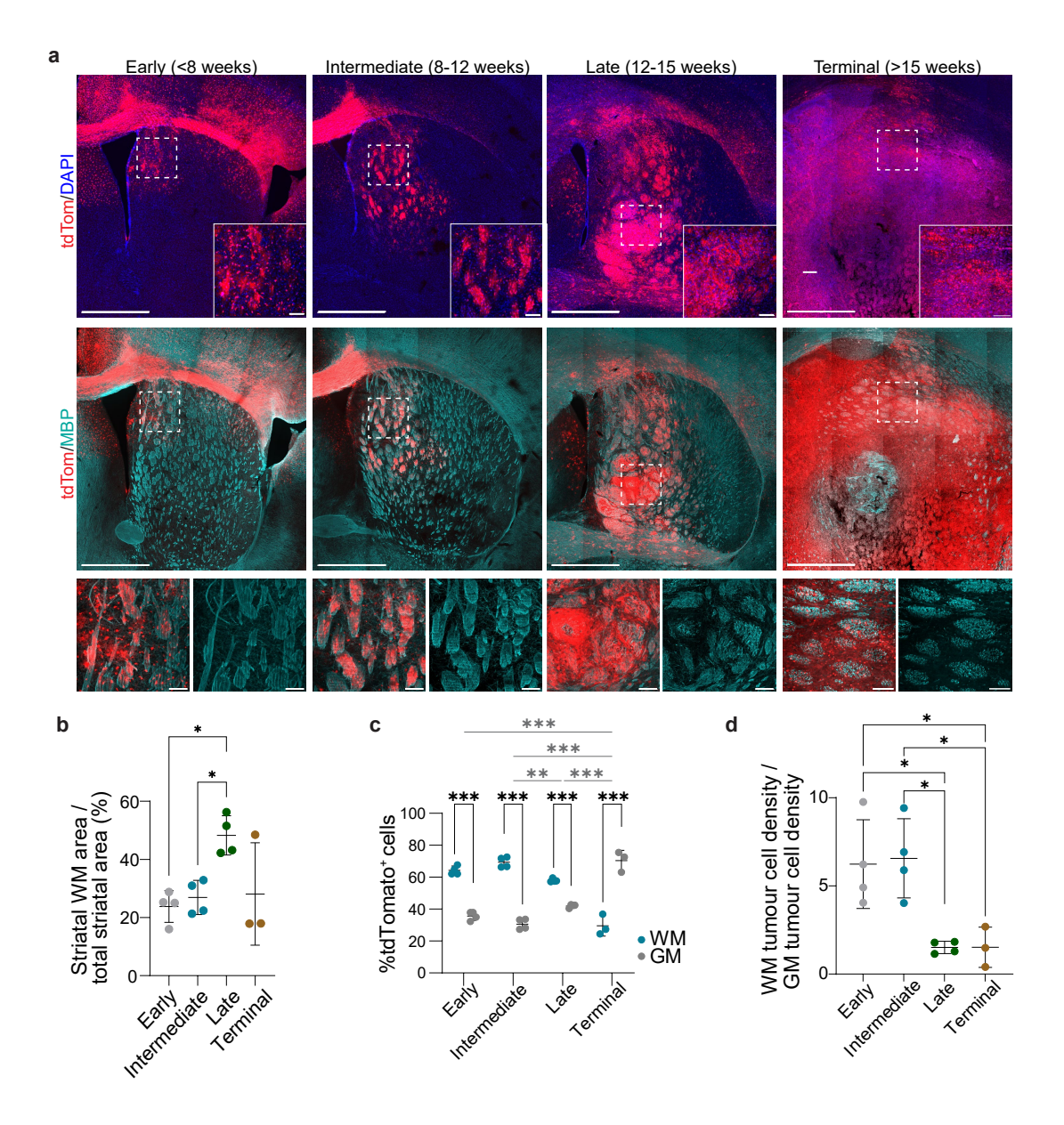


Figure 3.2. Glioblastoma cells preferentially occupy white matter regions in early disease stages.

a, Representative coronal brain sections showing tumour progression in npp mice at early ( $\leq$  8 weeks), intermediate (8–12 weeks), late (12–15 weeks), and terminal ( $\geq$  15 weeks) disease stages. White matter is identified by MBP (cyan), nuclei are stained with DAPI (blue), and tumour cells are labelled with tdTomato (red). Insets show magnified regions (dashed boxes). Scale bars: 1000µm (main), 100µm (insets). b, Quantification of MBP+ white matter area within the striatum across tumour stages. One-way ANOVA with Tukey's multiple comparisons. Early n=4, Intermediate n=4, Late n=4, Terminal n=3. c, Proportion of tdTomato+ tumour cells localised to white matter (WM, blue dots) or grey matter (GM, grey dots) in the striatum. Two-way ANOVA with Tukey's multiple comparisons. d, Ratio of tdTomato+ cell density in WM relative to GM across disease stages. One-way ANOVA with Tukey's multiple comparisons. n values as in (b).

advanced, with tumour cells increasingly occupying grey matter territories, and eventually infiltrating brain tissue indiscriminately at terminal stages (Figure 3.2a, c).

To account for dynamic changes in tissue architecture across stages, a relative density metric was calculated, comparing tumour cell density in white versus grey matter. Early-stage tumours exhibited a strong density skew towards white matter, which progressively equalised over time (Figure 3.2d), indicating loss of spatial confinement.

To determine whether white matter preference is a general feature of early gliomagenesis with human disease relevance, a panel of four patient-derived xenografts (PDXs) generated by Melanie Clements was analysed using matched immunofluorescence and spatial quantification.

PDX tumours demonstrated similar early-stage (stage with low disease burden and no obvious symptoms in animals) localisation patterns, with tumour cells preferentially occupying white matter regions over grey matter (Figure 3.3a). Quantification confirmed a higher proportion of tumour cells within white matter in early lesions, consistent across PDX models (Figure 3.3b). These findings suggest that early-stage white matter tropism represents a conserved feature of glioblastoma biology, rather than a model-specific artefact.

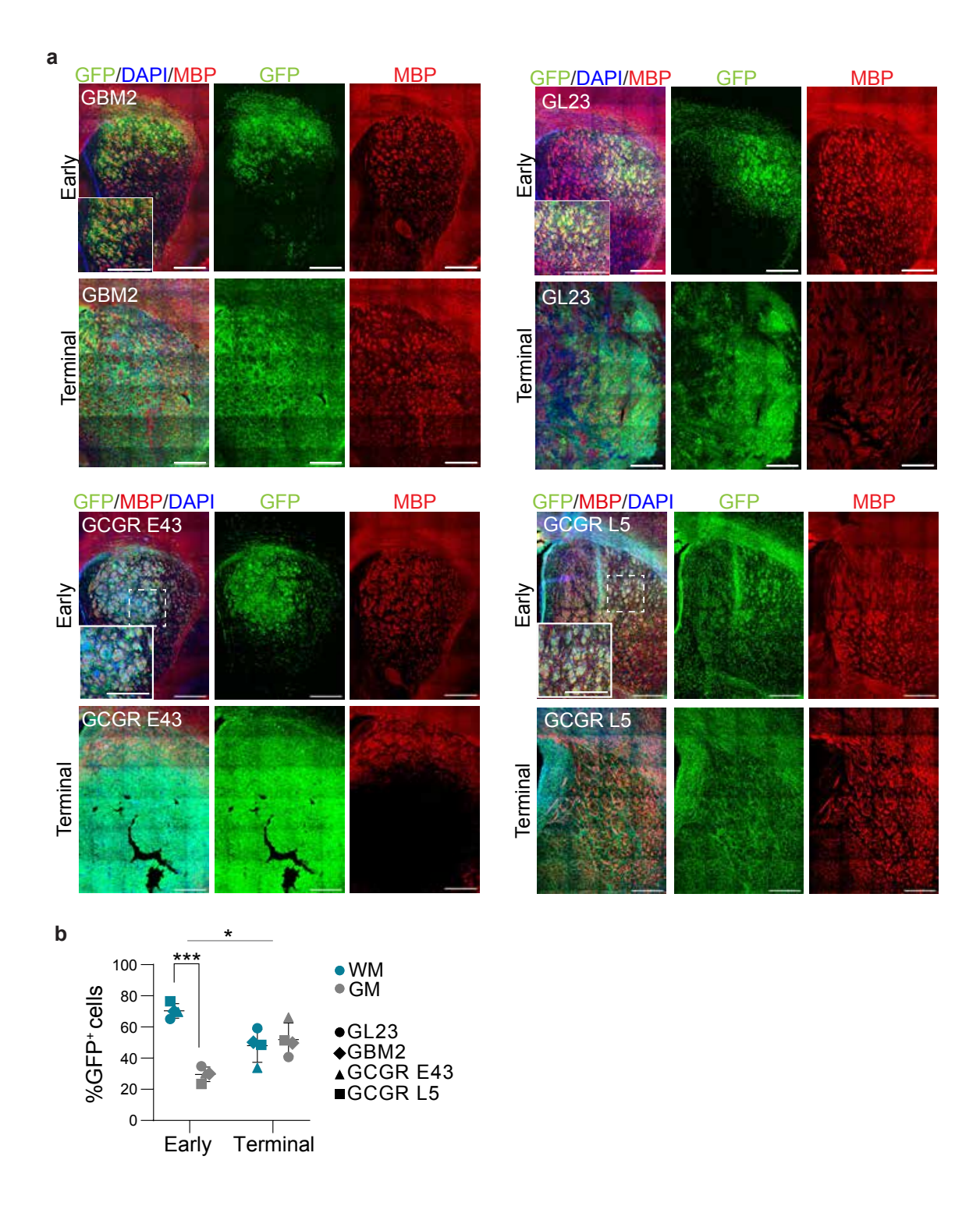


Figure 3.3. Early white matter tropism is preserved in PDX models.

a, Representative images of GFP-labelled PDX tumours (GBM2, GL23, GCGR-E43, GCGR-L5) at early and terminal disease stages. Insets show higher magnification of regions within dashed boxes. Scale bar =  $500\mu m$ . b, Proportion of GFP+ tumour cells in WM and GM of the striatum at early and terminal stages. Two-way ANOVA with Tukey's multiple comparisons; paired t-test for WM-GM distribution comparison. Early n=4, Terminal n=4.

#### 3.2.2 Glioblastoma

progression

from

indolent

# to rapidly growing disease occurs at the intermediate stage of

### tumour development

The proliferative dynamics of early-stage glioblastoma lesions were characterised by quantifying tumour cell proliferation across disease stages. Immunostaining for Ki67, a well-established marker of active cell cycle entry, was performed at early, intermediate, late, and terminal stages (Figure 3.4a).

At early and intermediate stages, a low proportion of tumour cells (approximately 1% of tdTomato<sup>+</sup> cells) expressed Ki67, indicating limited proliferative activity (Figure 3.4a, b). This finding is consistent with the indolent tumour behaviour observed in early lesions, despite substantial white matter infiltration.

A marked increase in Ki67 positivity was detected at the late and terminal stages, reaching levels of 15–20% (Figure 3.4b). This proliferative switch coincided temporally with the loss of white matter spatial restriction, as tumours expanded into grey matter regions and overall tumour burden increased (Figure 3.2a, c, d).

These data indicate that the growth pattern in early gliomagenesis consists of two stages: an initial indolent phase characterised by spatially constrained, low-proliferative tumour cells predominantly occupying white matter tracts, followed by a transition to a highly proliferative, invasive phenotype. The mechanisms underpinning this proliferative switch remain to be fully elucidated but may involve progressive remodelling of the tumour microenvironment, as explored in subsequent chapters.

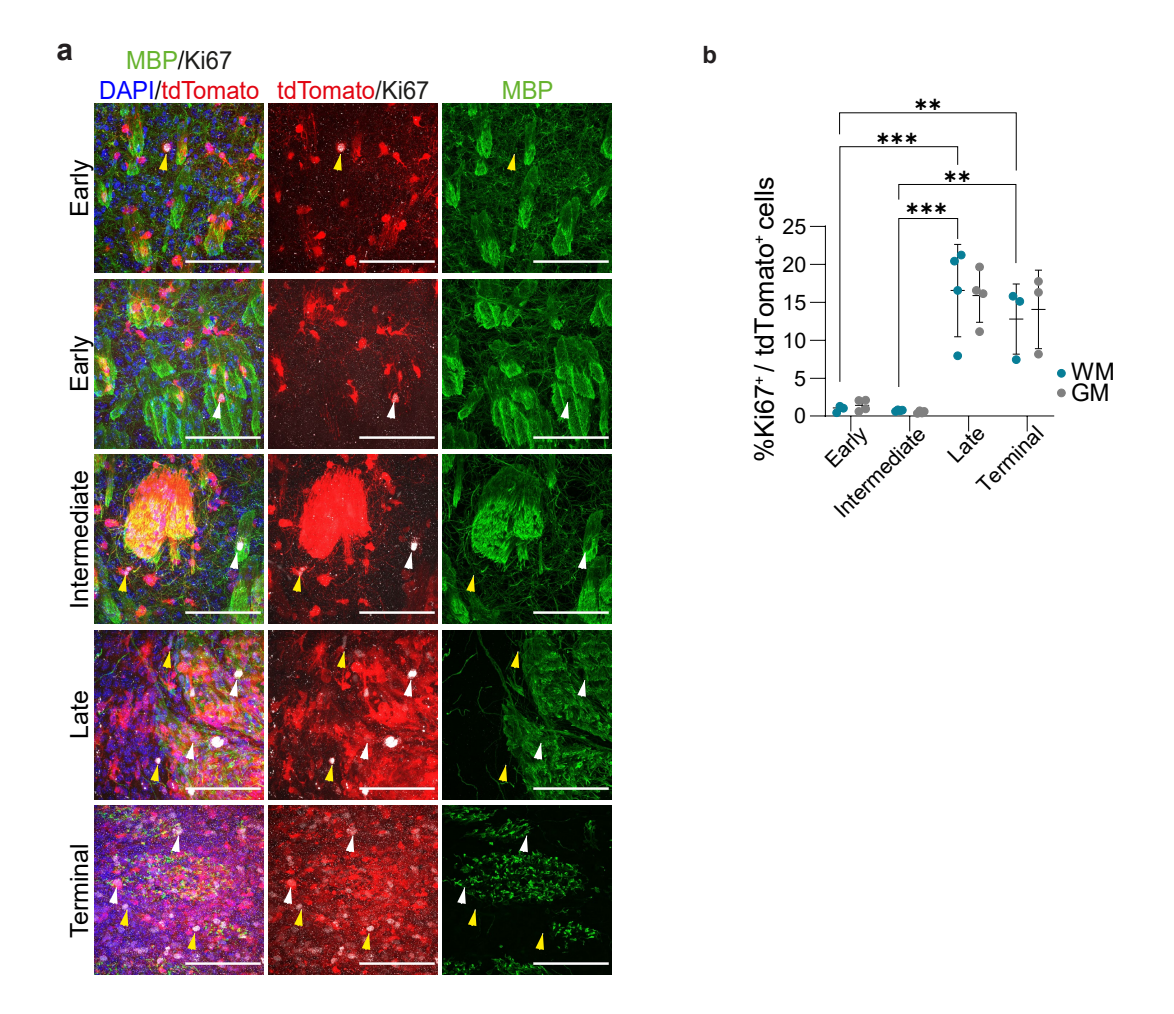


Figure 3.4. Glioblastoma lesion progression from low to high proliferation occurs at the intermediate stage of tumour development.

a, Images of tdTomato+ tumours stained for Ki67 (grey), MBP (green), and DAPI (blue) at indicated disease stages. Arrowheads denote Ki67+ tumour cells located within (white) or outside (yellow) white matter. Scale bar =  $100\mu m$ . b, Percentage of Ki67+/tdTomato+ cells in WM or GM. Two-way ANOVA with Tukey's multiple comparisons. Early n=4, Intermediate n=4, Late n=4, Terminal n=3.

# 3.2.3 Tumour growth triggers axonal injury and local neuroinflammation

Having established that glioblastoma (GBM) cells exhibit a marked preference for colonising white matter (WM) regions during early disease stages, before progressively expanding into grey matter (GM) as tumours become more proliferative. WM is highly enriched in myelinated axonal fibres and their associated glial support structures. Axons are known to be particularly vulnerable to mechanical, metabolic, and inflammatory insults due to their extreme polarity, dependency on long-distance transport, and high energetic demands (Beirowski 2022). Based on this knowledge, the potential for expansion of tumour cells to compromise axonal integrity at early stages of disease progression was systematically investigated.

Axonal integrity was assessed using Thy1-YFP reporter mice, in which projecting neurons express YFP under the Thy1 promoter, permitting visualisation of major axonal tracts in vivo (Feng et al. 2000). Npp tumours were induced in Thy1-YFP mice to allow direct evaluation of tumour–axon interactions. The striatum was selected as a region of interest due to its consistent involvement in tumour expansion and its abundance of discrete WM bundles.

At early stages of tumour development, YFP fluorescence within the tumour-bearing hemisphere was comparable to that of the contralateral, non-injected hemisphere, indicating preservation of axonal structure (Figure 3.5a). However, as tumours progressed to intermediate and late stages, a progressive reduction in YFP signal intensity was observed within striatal regions infiltrated by tumour cells. Quantification of mean fluorescence intensity (MFI), normalised to the contralateral

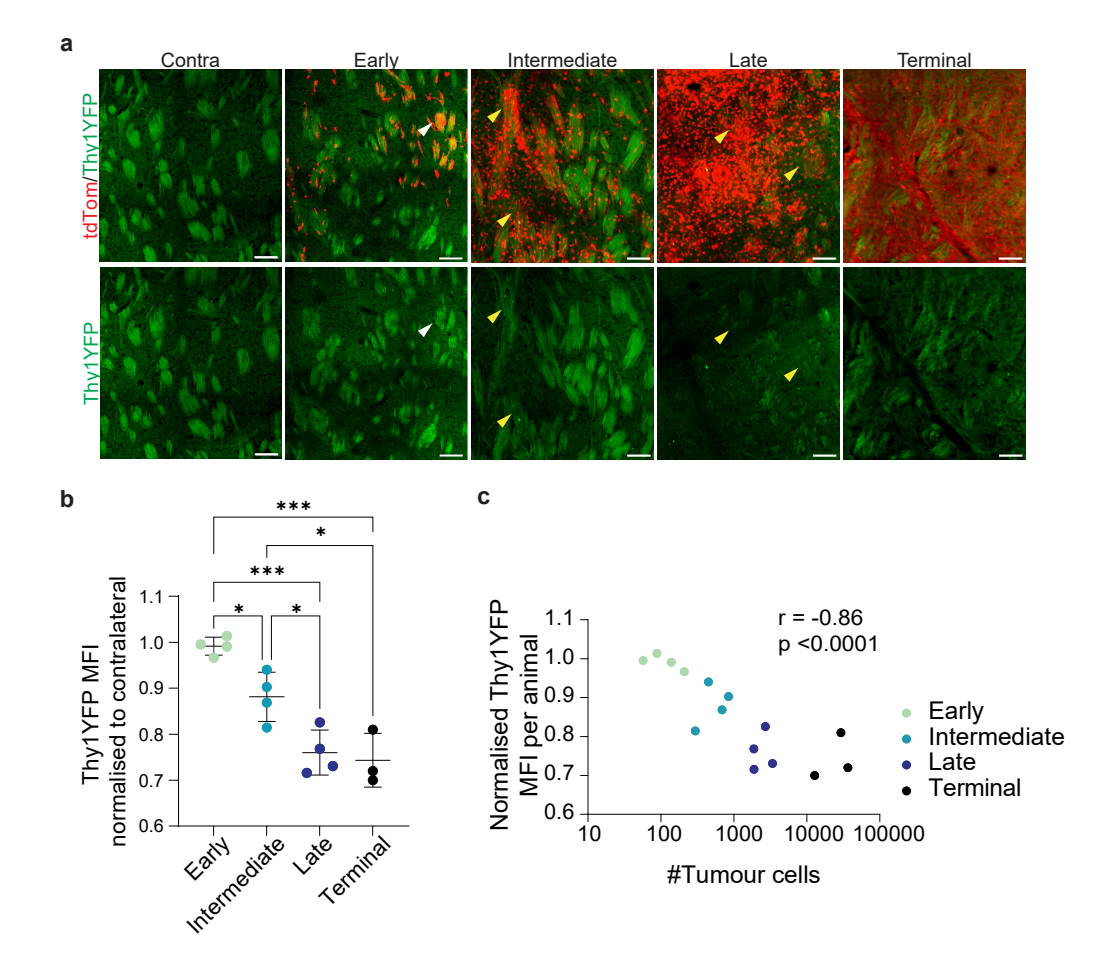


Figure 3.5. Loss of Thy1-YFP fluorescence reveals axonal loss over disease progression.

a, Representative images of striatal white matter in Thy1-YFP mice at different tumour stages. Arrowheads indicate examples of heavily (yellow) and minimally (white) infiltrated axon bundles. Scale bar =  $100\mu m$ . b, Quantification of YFP mean fluorescence intensity (MFI) in tumour-infiltrated striatum, normalised to contralateral control. One-way ANOVA with Tukey's multiple comparisons. Early n=4, Intermediate n=4, Late n=4, Terminal n=3. c, Correlation between normalised YFP MFI and tumour cell number in striatal WM at each timepoint. Pearson correlation. Each point represents one mouse.

hemisphere, revealed that axonal loss initiated at the intermediate stage and plateaued during late and terminal stages (Figure 3.5b). This plateau likely reflects the complex pathology of axonal degeneration, including the formation of axonal varicosities and beading, which can produce localised accumulations of YFP-labelled proteins that may partially obscure the extent of axonal loss on fluorescence-based measurements.

To examine whether axonal injury scaled with tumour burden, YFP MFI was correlated with tumour cell number in the striatum. A significant inverse correlation was observed (Figure 3.5c), supporting a model in which tumour expansion directly compromises axonal integrity.

In order to explore this relationship at higher spatial resolution, individual white matter bundles were analysed at the intermediate stage — a time point where axonal injury was detectable but tumour infiltration remained relatively confined. Tumour cell density and YFP MFI were measured for each bundle, and normalised to the corresponding region of the contralateral hemisphere to account for anatomical heterogeneity in YFP expression.

Even at this relatively early stage, a strong inverse correlation between tumour cell density and axonal Thy1-YFP signal was observed at the bundle level (Figure 3.6a,b). Importantly, loss of axonal integrity was evident even in bundles with only moderate tumour infiltration, suggesting that axonal degeneration is a highly sensitive local response to tumour growth, potentially preceding overt tissue destruction. This observation highlights the vulnerability of white matter tracts to early tumour–microenvironment interactions and suggests that axonal injury may serve as one of the earliest tissue-level consequences of gliomagenesis.

The biological significance of axonal loss extends beyond structural disruption, as

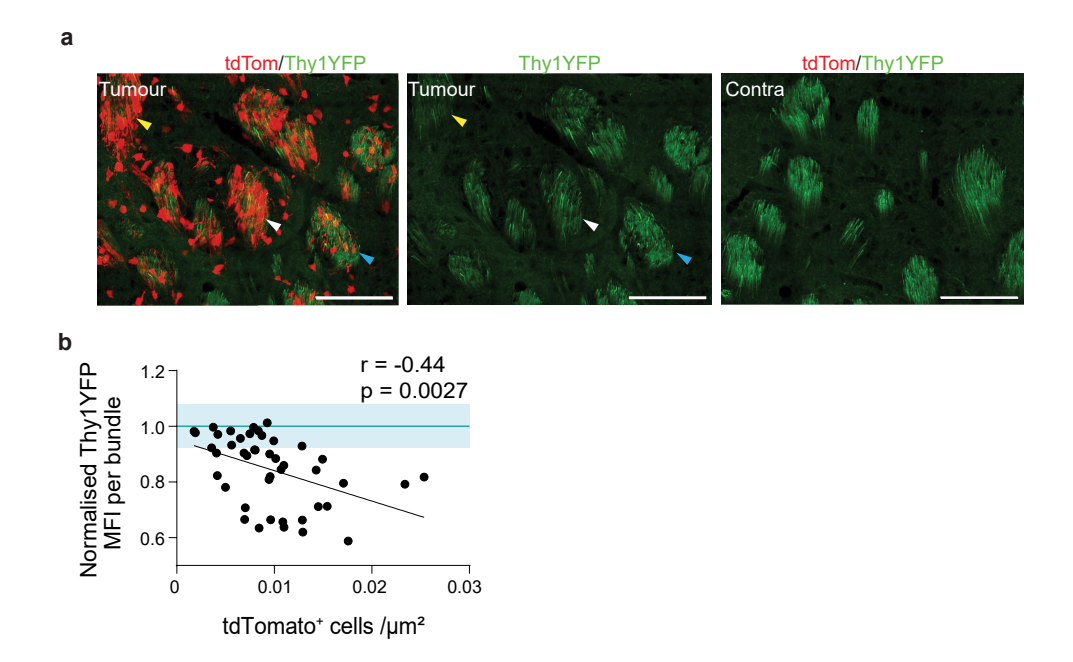


Figure 3.6. Tumour density inversely correlates with axonal integrity at intermediate stages.

a, Images of striatal white matter bundles at intermediate stage, showing tdTomato+tumour cells (red) and YFP+ axons (green). Arrowheads mark bundles with high (yellow), moderate (white), or low (blue) tumour burden. Scale bar =  $100\mu m$ . b, Plot of YFP MFI against tumour cell density per bundle. Contralateral means (turquoise line)  $\pm$  SD (blue band) shown for reference. Pearson correlation. n=6 mice.

axonal degeneration is a potent trigger of neuroinflammatory responses, as discussed in the Introduction. Axonal injury has been shown to activate resident microglia, promote astrocytic gliosis, and ultimately alter the immune landscape of the central nervous system (Beirowski 2022). Accordingly, the immune response associated with tumour progression was characterised across the disease time-course.

Flow cytometry was performed to profile immune cell infiltration during tumour development. A myeloid-focused marker panel, as detailed in the Methods section, was used to identify tumour-associated macrophages (TAMs), resident microglia, infiltrating monocyte-derived macrophages, and lymphocyte populations.

Representative gating strategies are shown in Figure 3.7a. Quantification of immune cell populations revealed a progressive increase in the proportion of CD45<sup>+</sup>

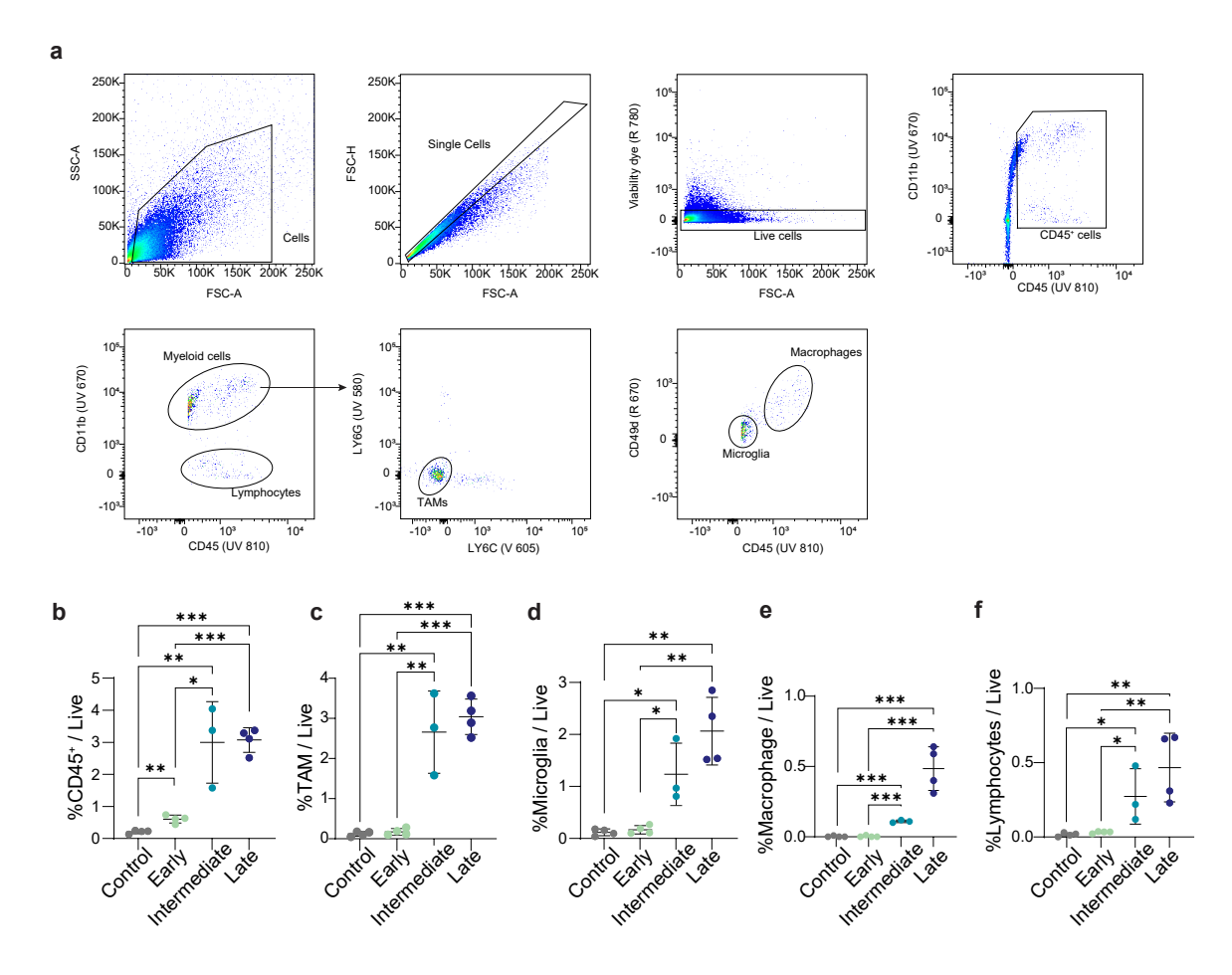


Figure 3.7. Time-course of immune infiltration using flow cytometry reveals progressive increase in immune cell accumulation within the tumour microenvironment as the disease advances.

a, Flow cytometry gating strategy used to isolate CD45+ cells and subtypes including TAMs, microglia, macrophages, and lymphocytes. b–f, Quantification of immune populations at control, early, intermediate, and late disease stages. Mean±SD. Multiple unpaired t-tests. n=4 for control, early, late; n=3 for intermediate.

immune cells within the tumour-bearing hemisphere over time (Figure 3.7b). This rise was modest during the early stages of tumour growth but became pronounced during the transition from the intermediate to late stages, coinciding with the timing of significant axonal loss.

Analysis of specific immune subsets indicated that resident microglia and TAMs accumulated earlier than peripheral macrophages or lymphocytes. Both microglia and TAMs increased in number from the intermediate stage onwards (Figure 3.7c,d),

whereas infiltrating macrophages, defined as CD45<sup>hi</sup> CD11b<sup>+</sup> Ly6G,C<sup>-</sup> CD49d<sup>hi</sup>, only became prominent during late disease (Figure 3.7e). The delayed appearance of peripheral macrophages is consistent with existing models proposing that breakdown of the blood-brain barrier (BBB) occurs late in GBM progression, thereby limiting early peripheral immune access.

In contrast, lymphocyte recruitment was detectable earlier than macrophage infiltration (Figure 3.7f), suggesting that mechanisms independent of BBB breakdown, such as local antigen presentation by activated microglia or astrocytes, may facilitate lymphocyte entry into the glioma microenvironment at intermediate stages.

To further characterise local glial responses, immunohistochemical analyses were conducted focusing on white matter bundles at intermediate stages of disease.

Astrocyte activation, assessed by GFAP immunofluorescence, was prominent within and around tumour-infiltrated white matter tracts (Figure 3.8a). Quantitative analysis demonstrated a proportional relationship between local tumour cell density and GFAP<sup>+</sup> astrocyte accumulation (Figure 3.8b), consistent with reactive astrocytosis being a direct consequence of tumour-induced tissue injury.

Similarly, TAM activation, assessed by CD68 staining and measurement of integrated density, exhibited a strong positive correlation with tumour burden (Figure 3.8c,d). Notably, both astrocytic and microglial activation were spatially confined to tumour-infiltrated white matter bundles, mirroring the distribution of axonal injury and suggesting that glioma-induced axonal disruption may be a primary driver of early glial responses.

Taken together, these data support a model in which early GBM expansion into white matter initiates axonal injury, which in turn triggers a localised

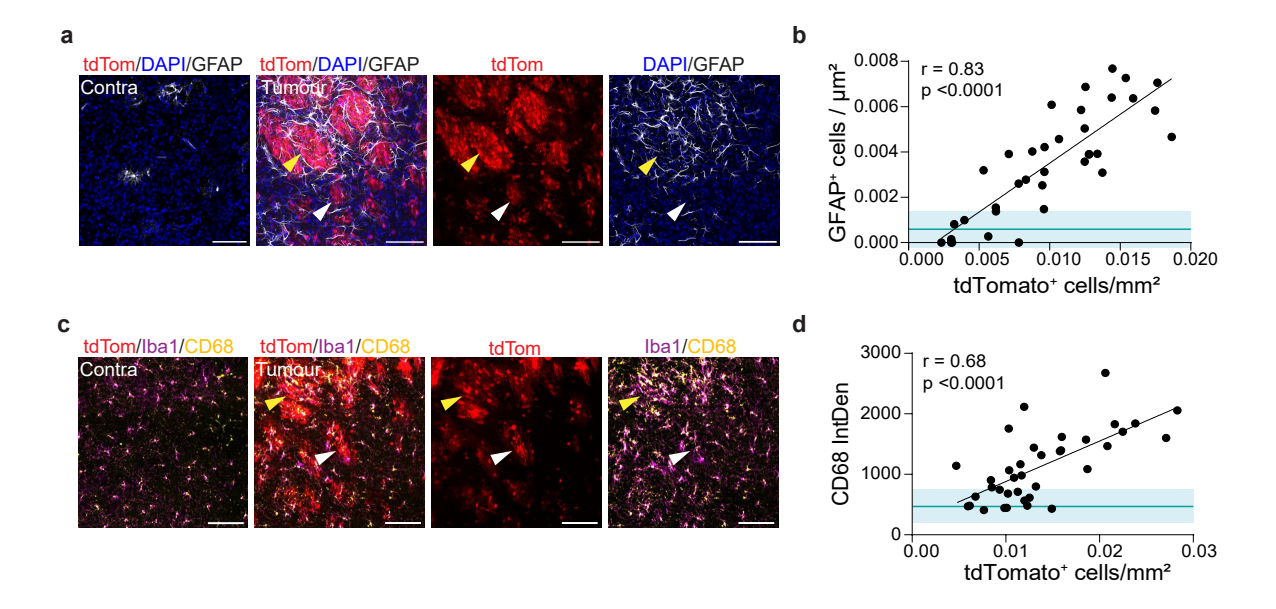


Figure 3.8. Reactive astrocytosis and microglial activation correlates with local tumour cell density.

a, Images showing GFAP+ astrocytes in tumour-infiltrated and contralateral striatal WM. Scale bar =  $100\mu m$ . b, GFAP+ astrocyte density plotted against tumour cell density. Each point represents a bundle.  $\geq 5$  bundles/mouse. Contralateral mean (turquoise line)  $\pm$  SD (blue band). Pearson R. n=6. c, Images of CD68+/Iba1+ microglia in tumour-involved and contralateral WM. Scale bar =  $100\mu m$ . d, CD68 integrated density (IntDen) per bundle as a function of tumour cell density. Contralateral baseline shown. Pearson R. n=4.

neuroinflammatory response characterised by reactive gliosis and gradual immune cell infiltration. These early changes may act to remodel the microenvironment in a manner that supports subsequent tumour proliferation, a hypothesis explored further in later chapters.

#### 3.3 Conclusions

The experiments presented in this chapter provide a detailed characterisation of the early dynamics of glioblastoma (GBM) development using a somatic, immunocompetent mouse model (npp), complemented by analysis of PDX models which strengthens the relevance of this finding to human disease. During the early,

indolent phase of tumour growth, GBM cells exhibited a strong spatial preference for white matter (WM) regions. This white matter tropism was observed consistently across models, suggesting that the affinity of early glioma cells for WM structures may represent a conserved feature of gliomagenesis rather than an artefact of a specific system.

At early stages, tumour cells displayed low proliferative activity, and the tumour microenvironment (TME) exhibited minimal immune cell infiltration, consistent with a relatively quiescent state. As disease progressed, this landscape changed markedly: tumour cells lost their spatial restriction to WM, proliferation rates increased, and broader tissue disruption, including pronounced axonal loss, became apparent.

Axonal injury emerged as a key pathological feature during this transition. Analysis using Thy1-YFP reporter mice demonstrated that loss of axonal integrity was detectable as early as the intermediate stage of disease and correlated with local tumour burden. Notably, axonal degeneration was observed even in areas with relatively modest tumour infiltration, indicating a high sensitivity of axons to glioma progression. This aligns with broader evidence that axons, particularly in myelinated WM tracts, are highly vulnerable to mechanical, metabolic, and inflammatory stressors (Beirowski 2022).

The onset of axonal injury was closely correlated a neuroinflammatory response. Flow cytometry and immunofluorescence analyses revealed that activation of resident glial populations, specifically TAMs and astrocytes, occurred at intermediate disease stages, when axonal loss was already prominent. This suggests that GBM-induced axonal injury may act as a driver of local TME activation, consistent with the known ability of axonal damage to trigger innate immune responses within the CNS (Bollaerts

et al. 2017; Mietto et al. 2015).

In contrast, the recruitment of peripheral immune cells, particularly infiltrating lymphocytes and macrophages, only became prominent during later stages. This temporal separation suggests that immune engagement in early gliomagenesis is dominated by resident CNS responses rather than by infiltration of peripheral cells which requires blood-brain barrier (BBB) disruption. This progression underscores the evolving nature of the GBM TME, shifting from a largely glia-driven local reaction to a more complex inflammatory environment involving peripheral immune cells.

Building on these findings, the next chapter investigates what role WD, a conserved program of axonal degeneration orchestrated by the protein SARM1, plays in GBM-associated axonal loss identified in this chapter.

# Chapter 4

# Axonal loss occurs via a programmed SARM1 dependent degeneration pathway

#### 4.1 Introduction

Axonal degeneration is a well-established pathological feature across many neurological diseases, including trauma, stroke, and neurodegeneration. In GBM, a tumour of the CNS, axonal integrity may be an important, yet understudied, determinant of disease progression. The previous chapter demonstrated that early GBM growth preferentially occurs within the WM, and that axonal loss emerges as a spatially correlated feature of early tumour expansion. However, the precise cellular and molecular mechanisms through which GBM cells induce axonal degeneration remain to be elucidated.

A large body of evidence in neurodegeneration research has demonstrated that axonal degeneration is orchestrated through active molecular mechanisms. One

such mechanism is Wallerian degeneration (WD), a regulated process of axon self-destruction triggered by injury which was described in the Introduction chapter of this thesis. Central to WD is the protein SARM1, which, when activated, initiates a cascade of metabolic and structural changes that lead to axonal breakdown. Genetic disruption of *Sarm1* in mouse models has been shown to robustly preserve axons following injury (Loreto et al. 2015; M. Ma, Toby A Ferguson et al. 2013a).

The potential involvement of SARM1 in GBM-associated axonal loss raises important conceptual and translational questions, including what mechanisms actually cause axonal injury occurs, whether axonal injury in GBM results in WD, and, if so, what the consequences of blocking this pathway are on tumour biology. This chapter aims to addrss these questions by firstly characterising the nature of the physical and spatial relationship between tumour cells and axons is, to determine whether axon disruption is an incidental or targeted phenomenon. Subsequently, the functional role of SARM1 is interrogated by using a *Sarm1*-deficient mouse model to assess whether genetic blockade of WD confers protection against axonal loss in GBM. Finally, the broader consequences of axonal preservation on tumour morphology, white matter architecture, and early disease dynamics are evaluated.

#### 4.2 Results

# 4.2.1 Axonal injury occurs in the presence of mechanical compression of axons by tumour cells

Previous analysis demonstrated that GBM cells preferentially colonise WM during early tumour development, with tumour expansion closely associated with loss of axonal integrity (Figure 3.2, 3.3). However, the mechanisms through which tumour cells interact with and damage axons remained unclear. To investigate this, the physical relationship between tumour cells and axonal fibres was examined using high-resolution confocal imaging of striatal bundles in npp tumour-bearing Thy1-YFP reporter mice. This approach enabled high-resolution visualisation of axons and their interactions with tdTomato<sup>+</sup> tumour cells.

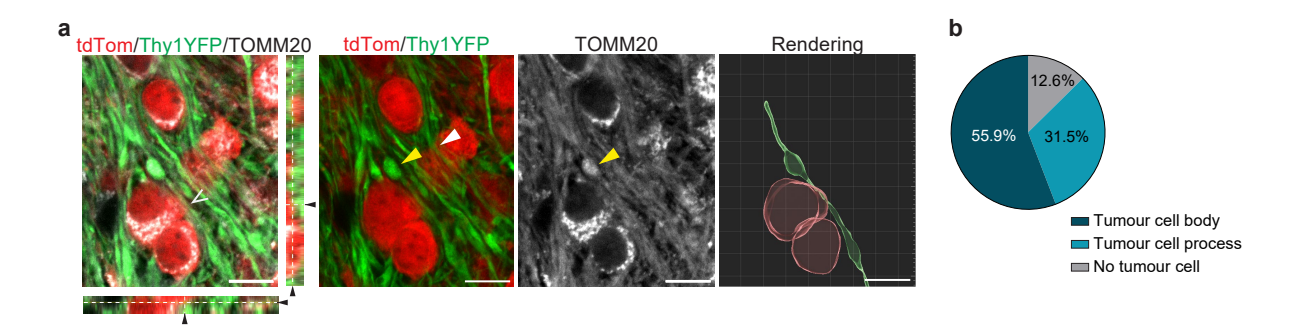


Figure 4.1. Mechanical compression of axons by tumour cells drives varicosity formation.

a, Representative super-resolution confocal images of tumour-involved striatal white matter bundles in Thy1YFP mice bearing intermediate npp tumours. Tissues were stained with TOMM20 (grey) to visualise mitochondria, tdTomato<sup>+</sup> tumour cells are shown in red, and axons (Thy1-YFP) in green. Yellow arrowhead indicates a mitochondria-filled axonal varicosity, a hallmark of physical injury; white arrowhead denotes a kinked axon. Side panels are orthogonal projections corresponding to the region marked by the open white arrowhead, highlighting direct tumour–axon contact. Scale bar =  $10\mu m$ . b, Pie chart quantifying the location of varicosities in tumour-infiltrated white matter. The majority of varicosities are within  $2\mu m$  of a tumour cell body or process. No varicosities were detected in contralateral white matter.

High-resolution confocal microscopy revealed that axons within tumour-infiltrated WM bundles frequently exhibited localised swellings, or varicosities, along their shafts (Figure 4.1a). Varicosities are well-established pathological features indicative of disrupted axonal transport and early axonal injury, often preceding full degeneration. In these regions, TOMM20 immunostaining demonstrated an aberrant accumulation of mitochondria within the varicosities, consistent with impaired organelle transport along the axons. Such transport disruptions are commonly associated with mechanical stress, cytoskeletal destabilisation, or energetic deficits, and represent a well-characterised mechanism underlying WD.

Importantly, analysis of the spatial relationship between axonal varicosities and tumour cells indicated that the majority of varicosities occurred within 2µm of a tumour cell body or process (Figure 4.1b). This suggests that local, direct mechanical interactions — rather than systemic metabolic or inflammatory effects — are likely one of the primary triggers for early axonal injury in this context. Orthogonal reconstructions further confirmed that tumour cells were often physically in contact with axons at or near the sites of varicosity formation (Figure 4.1a, right panel).

Interestingly, varicosities were not detected in the contralateral hemisphere, despite identical imaging and staining conditions. This suggests that the varicosities observed in tumour-infiltrated regions are not artefacts of tissue processing or intrinsic fragility of WM tracts, but rather represent a specific pathological response to tumour cell presence.

Several mechanisms could underlie the formation of these tumour-associated varicosities. Physical compression by expanding tumour cells is a likely contributor,

particularly given the confined anatomy of WM bundles, which may render axons particularly vulnerable to space-occupying lesions. Mechanical stress is known to impair axonal transport by disrupting microtubule structure and altering motor protein function, leading to organelle accumulation and swelling. Alternatively, biochemical factors secreted by tumour cells, such as proteases or reactive oxygen species, could contribute to cytoskeletal instability and varicosity formation. Further studies using tumour cell lines with different mechanical properties or secretory profiles would be required to disentangle these possibilities.

Overall, these findings suggest that direct tumour-axon interactions trigger early, localised axonal pathology that manifests as varicosity formation. This may represent the earliest detectable morphological manifestation of glioma-induced axonal stress, and could serve as an early marker of tumour invasion into WM regions.

### 4.2.2 Sarm1 deletion preserves axonal integrity in tumour regions

The observation that axons develop mitochondria-filled varicosities and undergo structural degradation in regions of glioblastoma (GBM) infiltration raised the possibility that axonal degeneration occurs through a programmed pathway rather than passive mechanical destruction. To determine whether the GBM-induced axonal loss proceeds via this mechanism, axonal integrity was assessed in tumour-bearing  $Sarm1^{-/-}$  mice, which lack SARM1 and are resistant to WD.

Intermediate-stage tumours were selected for analysis, corresponding to the period where axonal loss is first detectable in WT mice but before widespread tissue disruption confounds interpretation. Immunostaining for neurofilament (NF), a key cytoskeletal component of axons, was used to assess axonal preservation.

Quantification of NF mean fluorescence intensity (MFI) was performed across tumour-infiltrated striatal white matter bundles, normalised to corresponding contralateral regions to control for staining variability.

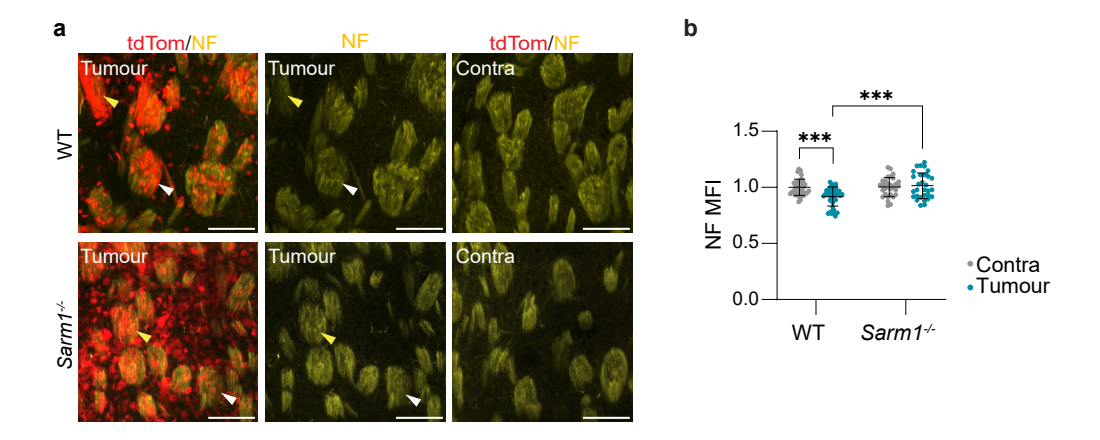


Figure 4.2. Sarm1 knockout preserves axonal integrity in tumour-infiltrated regions as measured by immunofluorescence.

a, Representative neurofilament (NF, yellow) staining of tumour-involved (Tumour) and contralateral (Contra) striatal white matter in WT and  $Sarm1^{-/-}$  mice bearing intermediate npp tumours. Moderately and heavily infiltrated bundles are marked with white and yellow arrowheads, respectively. Scale bar = 50µm. b, Quantification of NF mean fluorescence intensity (MFI) in individual white matter bundles. Two-way ANOVA with Tukey's multiple comparisons. WT,  $Sarm1^{-/-}$  n=3 animal, with a minimum of 5 bundles measured per animal.

In WT animals, tumour-infiltrated bundles within the striatum exhibited marked reductions in NF signal normalised to contralateral bundles, indicating axonal loss. In contrast,  $Sarm1^{-/-}$  animals retained near-normal levels NF fluorescence in these same regions, suggesting that genetic ablation of Sarm1 conferred substantial axonal protection (Figure 4.2a). Quantification confirmed this preservation, with significantly higher MFI in the striatum of  $Sarm1^{-/-}$  mice compared to WT controls (Figure 4.2b).

To complement these findings with ultrastructural detail, correlative light and electron microscopy (CLEM) was employed (Figure 4.3a). This approach enabled high-resolution visualisation of axonal morphology within tumour-infiltrated areas

previously mapped by confocal microscopy. This analysis was conducted on intermediate tumours, focusing on striatal bundles.

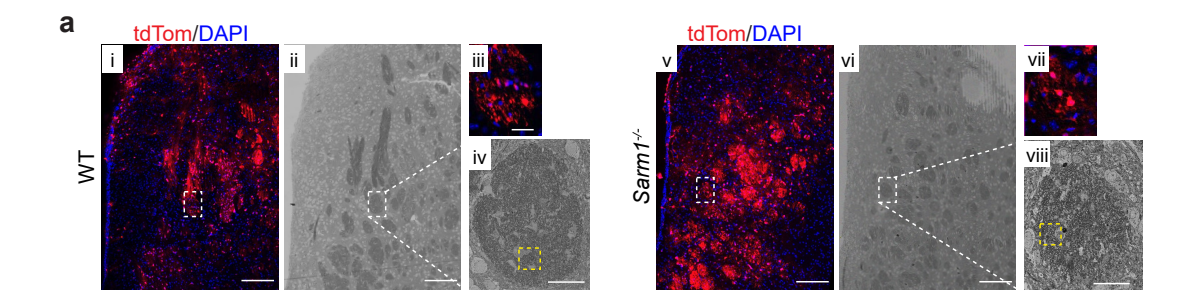


Figure 4.3. Correlative light and electron microscopy.

a, Correlative light and electron microscopy of intermediate npp tumours from WT (i–iv) and  $Sarm1^{-/-}$  (v–viii) mice at 10.5 weeks post-electroporation. i and v show low magnification confocal overviews (scale bar = 200 $\mu$ m); ii and vi show corresponding EM images. Dashed boxes denote regions enlarged in iii–iv and vii–viii, showing striatal white matter at high resolution. Scale bar = 50 $\mu$ m.

Electron micrographs of tumour-infiltrated white matter revealed characteristic features of Wallerian degeneration in WT mice, including axonal swelling, accumulation of vesicles and organelles, darkened axoplasm, and vacuolisation — all classical hallmarks of degenerating axons. These structural abnormalities were abundant in tumour-bearing regions of the striatum in WT animals, further supporting the presence of active axonal breakdown (Figure 4.4a). In contrast, such features were markedly less frequent in *Sarm1*<sup>-/-</sup> mice, indicating substantial protection from degeneration (Figure 4.4a).

Quantification of these ultrastructural changes confirmed that the number of degenerating axons was significantly reduced in *Sarm1*<sup>-/-</sup> animals relative to WT (Figure 4.4b). However, a small fraction of pathological axons was still observed in the knockout condition, suggesting that while *Sarm1* deletion delays or attenuates degeneration, it does not fully eliminate all injury-induced axonal loss.

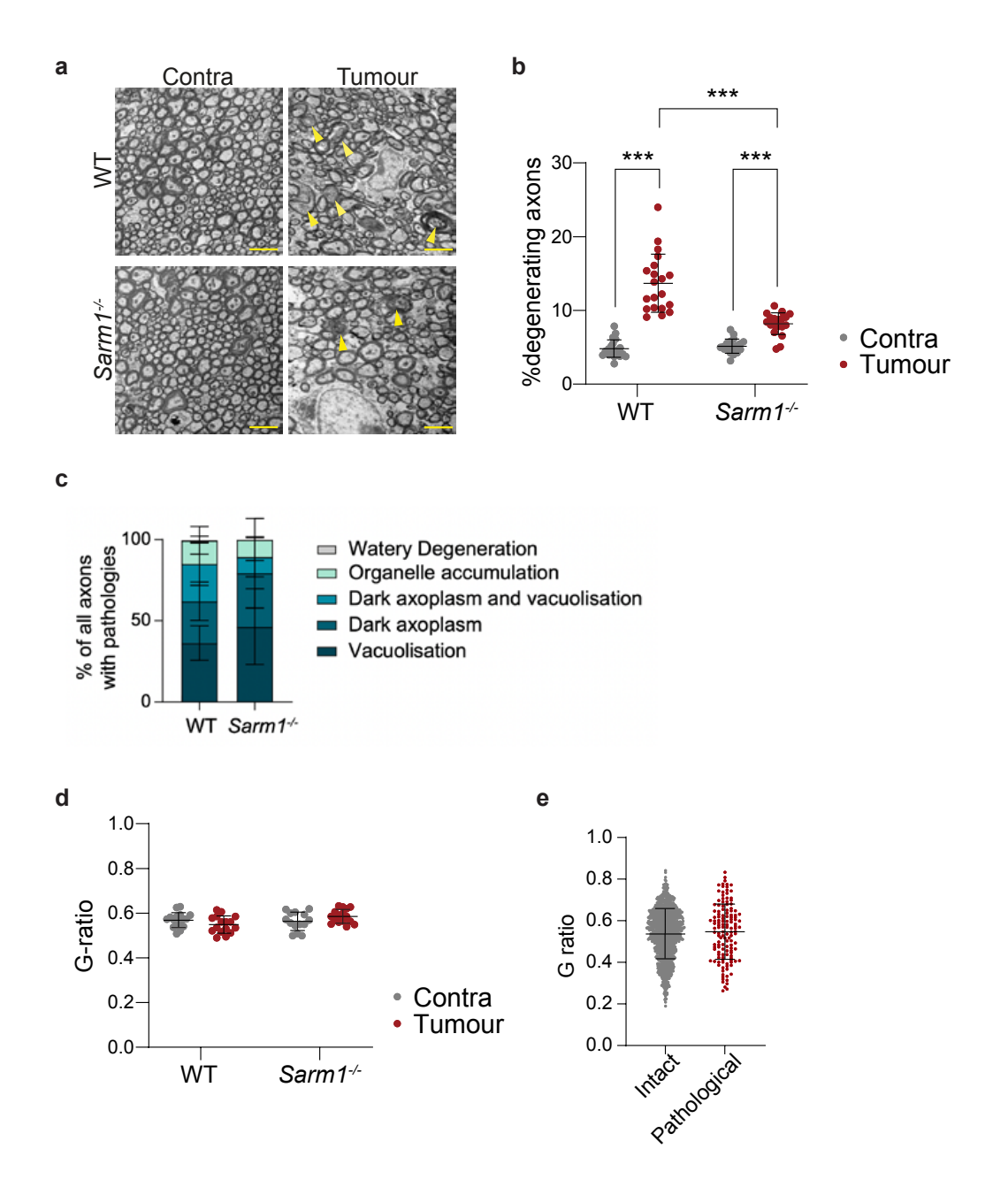


Figure 4.4. Quantitative EM shows reduced axonal degeneration without altered myelin.

a, Representative electron micrographs of tumour-involved and contralateral white matter bundles in WT and Sarm1-/- mice with intermediate npp tumours. Yellow arrows mark degenerating axons. Scale bar = 2.5µm. b, Quantification of degenerating axons as a percentage of total axons in tumour-infiltrated striatal bundles. Two-way ANOVA with Tukey's multiple comparisons. WT n=4,  $Sarm1^{-/-}$  n=4. c, Distribution of features of WD among pathological axons in WT and Sarm1<sup>-/-</sup> mice. The proportion of axons with individual features is represented. Features include vacuolisation, dark axoplasm, dark axoplasm with vacuolisation, organelle accumulation, and watery degeneration. Unpaired t test. WT, Sarm1-/- n=4 animals, with a minimum of 4 bundles quantified per animal. d, G-ratio analysis (axon diameter/total fibre diameter) comparing tumour-involved and contralateral striatal white matter. Two-way ANOVA with Tukey's multiple comparisons. WT n=4, Sarm1<sup>-/-</sup> n=4. e, G-ratio comparison between intact and pathological axons in tumour-infiltrated white matter from WT mice. Unpaired t test. WT, Sarm1-/- n=4 animals, with a minimum of 4 bundles quantified per animal. Each dot represents one axon, with a minimum of 30 axons quantified per bundle. Mean  $\pm$  SD. n=4.

To further characterise the nature of these residual degenerating axons, the ultrastructural features of pathological fibres were classified into five major categories: vacuolisation, dark axoplasm, dark axoplasm with vacuolisation, organelle accumulation, and watery degeneration (L. J. Brooks, M. P. Clements et al. 2021). The proportional distribution of these features did not significantly differ between WT and *Sarm1*<sup>-/-</sup> mice (Figure 4.4c), suggesting that although *Sarm1* deletion reduces the extent of degeneration, it does not qualitatively alter its morphological signatures when degeneration does occur.

To determine whether axonal degeneration was accompanied by loss of myelin, g-ratio analysis (the ratio of axon diameter to total fibre diameter) was performed on tumour-infiltrated and contralateral white matter. No significant differences were observed between hemispheres in either WT or Sarm1<sup>-/-</sup> mice (Figure 4.4d), indicating that demyelination was not a prominent feature of early tumour-induced injury. To further confirm that the preservation of g-ratios was not confounded by the inclusion of morphologically normal axons which are plentiful at this stage of tumour development, g-ratios were also compared between intact and degenerating axons within the same region. Again, no differences were detected (Figure 4.4e), suggesting that axonal degeneration in this context occurs in the absence of myelin loss.

These results collectively establish that GBM-induced axonal injury predominantly proceeds through an active WD pathway dependent on SARM1. Importantly, protection of axons by *Sarm1* deletion does not appear to be confounded by preservation of myelin, suggesting a direct neuroprotective effect on axons themselves. This mechanistic link between tumour presence and regulated axonal death raises the possibility that axonal degeneration is not merely a bystander

effect of tumour growth but may contribute to disease pathogenesis by modulating the tumour microenvironment.

# 4.2.3 Sarm1<sup>-/-</sup> tumours exhibit a diffuse tumour phenotype but retain intrinsic tumour cell behaviours

Having established that axonal degeneration proceeds via a SARM1-dependent pathway and can be blocked by *Sarm1* deletion, the impact of preserved axonal integrity on glioblastoma (GBM) growth patterns was next evaluated. Specifically, the overall morphology of terminal-stage tumours was compared between WT and *Sarm1*<sup>-/-</sup> animals to determine whether axonal protection influences tumour structure.

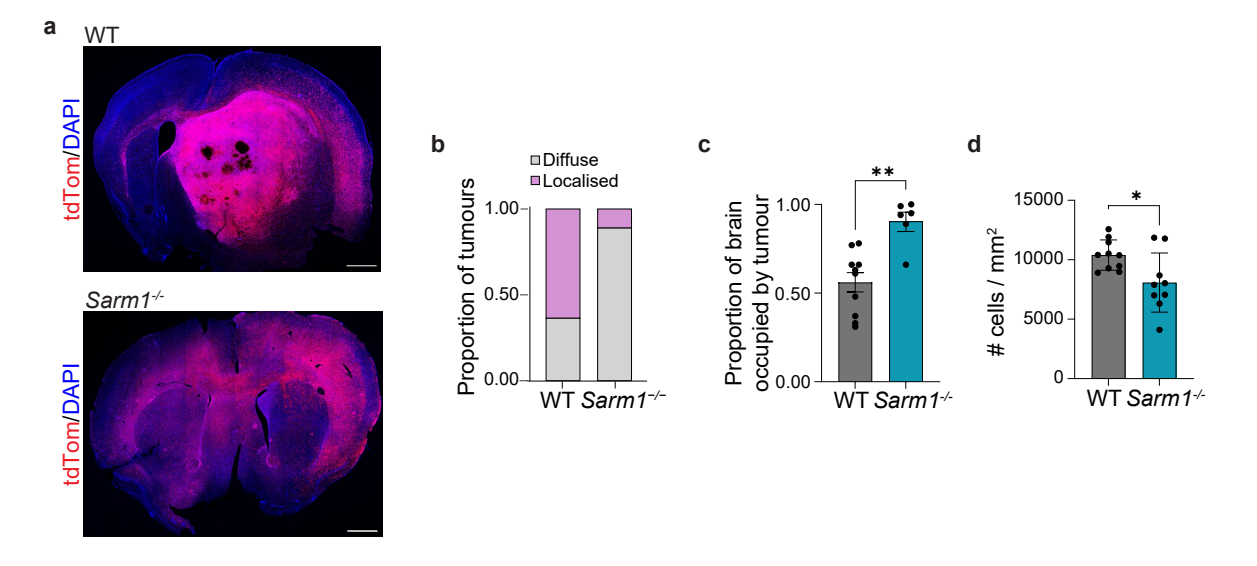


Figure 4.5. Terminal  $Sarm 1^{-/-}$  tumours exhibit diffuse morphology and lower cellular density.

a, Representative images of terminal npp tumours in WT and  $Sarm1^{-/-}$  mice. Scale bar = 1000µm. b, Classification of tumours as localised (with a defined bulk) or diffuse in WT and  $Sarm1^{-/-}$  mice. c, Quantification of total brain area occupied by tdTomato<sup>+</sup> tumour cells. Mean  $\pm$  SD. Unpaired t test. WT n=10,  $Sarm1^{-/-}$  n=6. d, Quantification of tumour cell density within confluent regions. Mean  $\pm$  SD. Unpaired t test. WT n=10,  $Sarm1^{-/-}$  n=9.

Striking differences in tumour architecture were observed upon gross examination of terminal npp tumours. While the majority of tumours in WT mice presented

as dense, localised masses often centred in the striatum or adjacent white matter, tumours in  $Sarm1^{-/-}$  mice appeared notably more diffuse, spreading across broader regions of the ipsilateral hemisphere without forming a compact bulk (Figure 4.5a). This qualitative impression was supported by blinded classification of tumours by experienced lab members, which revealed a significantly higher frequency of diffuse tumours in the  $Sarm1^{-/-}$  cohort compared to WT (Figure 4.5b).

To quantify these observations, the following metrics were assessed. First, the total area of brain tissue occupied by tdTomato<sup>+</sup> tumour cells was measured. Consistent with the more disseminated growth pattern,  $Sarm1^{-/-}$  tumours occupied a significantly greater area of the ipsilateral hemisphere than WT tumours (Figure 4.5c). Second, the local cellular density within confluent tumour regions was evaluated. Despite occupying a larger overall brain volume,  $Sarm1^{-/-}$  tumours exhibited a lower tumour cell density compared to WT (Figure 4.5d), indicating that the more diffuse phenotype is not driven by increased tumour mass per se, but rather by reduced compaction of tumour cells within a given area.

Together, these findings suggest that loss of SARM1 and consequent axonal preservation alters the organisational properties of GBM without necessarily increasing total tumour burden.

The observed changes in tumour morphology raised the possibility that intrinsic tumour cell behaviours, such as proliferation or migration, might be altered in *Sarm1*<sup>-/-</sup> tumours. To address this, adult NSCs isolated from WT and *Sarm1*<sup>-/-</sup> mice were transformed *in vitro* using the same CRISPR/Cas9-mediated npp plasmids and assessed for differences in proliferative and migratory capacities under standardised conditions.

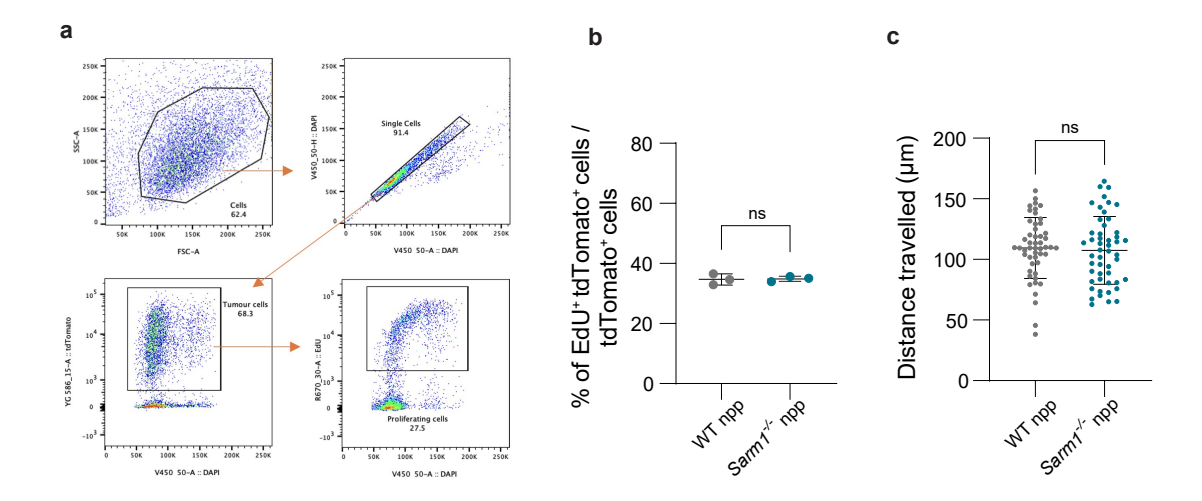


Figure 4.6. WT and  $Sarm 1^{-/-}$  tumour cells display similar proliferation and migration in vitro.

a, Gating strategy for EdU<sup>+</sup> tdTomato<sup>+</sup> cells in transformed WT and  $Sarm1^{-/-}$  tumour cells. b, Quantification of proliferating cells (EdU<sup>+</sup> tdTomato<sup>+</sup>) in vitro. Unpaired t test. WT n=3,  $Sarm1^{-/-}$ n=3. c, Quantification of tumour cell migration based on total distance travelled (µm) over 24 hours. WT and  $Sarm1^{-/-}$  n=50 cells.

Proliferation was quantified by EdU incorporation over a 2-hour pulse, followed by flow cytometric analysis of EdU<sup>+</sup> tdTomato<sup>+</sup> cells (representative gating strategy is shown in Figure 4.6a). No significant differences were observed in the percentage of proliferating cells between WT- and  $Sarm1^{-/-}$ -derived tumour cells (Figure 4.6b), suggesting that loss of Sarm1 does not intrinsically alter the ability of tumour cells to enter the cell cycle.

To assess migratory behaviour, time-lapse imaging was performed over 24 hours using the Incucyte platform, tracking the movement of individual tumour cells cultured on laminin-coated plates. Manual quantitative analysis of total distance travelled per cell revealed no significant differences between WT and Sarm1<sup>-/-</sup> tumour cells (Figure 4.6c), indicating that cell-intrinsic migratory capacity is similarly unaffected by Sarm1 loss.

Thus, neither proliferation nor migration appeared to be altered in vitro by

deletion of *Sarm1*. These findings imply that the diffuse morphology of *Sarm1*<sup>-/-</sup> tumours observed *in vivo* is unlikely to result from autonomous changes in tumour cell behaviour. Rather, it suggests that differences in the tumour microenvironment (TME), secondary to axonal preservation, may be responsible for shaping tumour spread and organisation.

Together, these findings indicate that the diffuse morphology of *Sarm1*<sup>-/-</sup> tumours arises not from altered cell-intrinsic properties. However, it is important to note that while *in vitro* assays provide a controlled system to assess basic cellular properties, they do not fully recapitulate the complexity of the brain microenvironment. Effects on invasion, tissue interaction, or response to extracellular cues might only manifest in the highly structured, dynamic environment of the brain parenchyma.

These considerations point toward the need for further dissection of the TME to understand how axonal integrity or its loss modulates tumour behaviour. This hypothesis is explored in the following chapter through single-cell transcriptomic profiling, aimed at elucidating the cellular and molecular consequences of SARM1-mediated axonal degeneration on the glioblastoma niche.

## 4.3 Conclusions

This chapter has explored the mechanisms underlying GBM-induced axonal degeneration, revealing that axonal injury within tumour-infiltrated WM regions occurs predominantly via the SARM1-dependent WD pathway. Through a combination of high-resolution imaging, immunohistochemistry, and ultrastructural analysis, it was demonstrated that early tumour expansion exerts mechanical stress on axons, leading to localised varicosity formation and subsequent axonal breakdown.

Genetic ablation of *Sarm1* preserved axonal integrity without affecting the associated myelin. Furthermore, preservation of axonal integrity was associated with a striking alteration in tumour morphology, with *Sarm1*<sup>-/-</sup> tumours displaying a more diffuse phenotype with less bulk formation. These changes occurred in the absence of detectable alterations in tumour cell-intrinsic proliferation or migration, further suggesting that it is the axon-TME interactions that play a key role in shaping tumour behaviour.

However, while axonal preservation clearly alters tumour architecture, the cellular and molecular mechanisms underlying these differences remain unresolved. In particular, it is not yet clear how axonal degeneration influences the composition, activation state, and function of the TME, including resident glial cells and infiltrating immune populations. Moreover, whether SARM1-dependent injury impacts tumour cell heterogeneity remains to be explored.

To tackle these outstanding questions, the next chapter applies single-cell RNA sequencing to systematically profile the cellular landscape of GBM tumours in the presence or absence of SARM1-mediated axonal degeneration. Through this approach, the broader consequences of neuroprotection on transcriptional changes in both tumour cells in the TME components can be dissected in finer molecular detail.

# Chapter 5

# Attenuation of axonal degeneration leads to development of less advanced tumours and confers a survival advantage

### 5.1 Introduction

In the previous chapters, it was demonstrated that GBM-associated axonal injury proceeds through a programmed WD pathway, mediated by SARM1 protein. Genetic ablation of *Sarm1* provided robust axonal protection *in vivo*, preserving white matter architecture in the context of tumour growth.

However, the implications of axonal protection for GBM biology and disease trajectory remain unclear. Axonal degeneration is known to initiate a cascade of secondary tissue responses, including neuroinflammation, microglial activation, and vascular remodelling, each of which may alter the tumour microenvironment (TME)

in ways that are permissive to malignant progression (J. T. Wang et al. 2024; Gaudet et al. 2011).

The experiments described in this chapter aimed to systematically investigate the consequences of attenuated axonal degeneration on tumour phenotype, TME composition, and disease course. By interrogating the consequences of blocking WD, this chapter seeks to determine the impact of axonal degeneration on tumour biology, with potential implications for therapeutic strategies that target not only the tumour cells themselves, but also the surrounding neural brain parenchyma.

# 5.2 Results

To explore how attenuation of axonal degeneration impacts tumour cell states, single-cell RNA sequencing (scRNA-seq) was performed on dissociated tumour-bearing hemispheres from WT and  $Sarm1^{-/-}$  mice at terminal disease stages (Table B.1. - B.5.). Following quality control and integration of datasets, tumour cells were identified based on tdTomato expression, aneuploidy, and transcriptional signature.

# 5.2.1 scRNA-seq reveals that Sarm1<sup>-/-</sup> tumour cells retain a more neurodevelopmental identity

Dimensionality reduction using Uniform Manifold Approximation and Projection (UMAP) revealed that tumour cells from both WT and *Sarm1*<sup>-/-</sup> mice occupied a common overarching landscape of transcriptional states (Figure 5.1a, b). These included neurodevelopmental states such as neural progenitor cell NPC-like, OPC-like, and AC-like (AC-like), alongside more injury-associated or MES-like states,

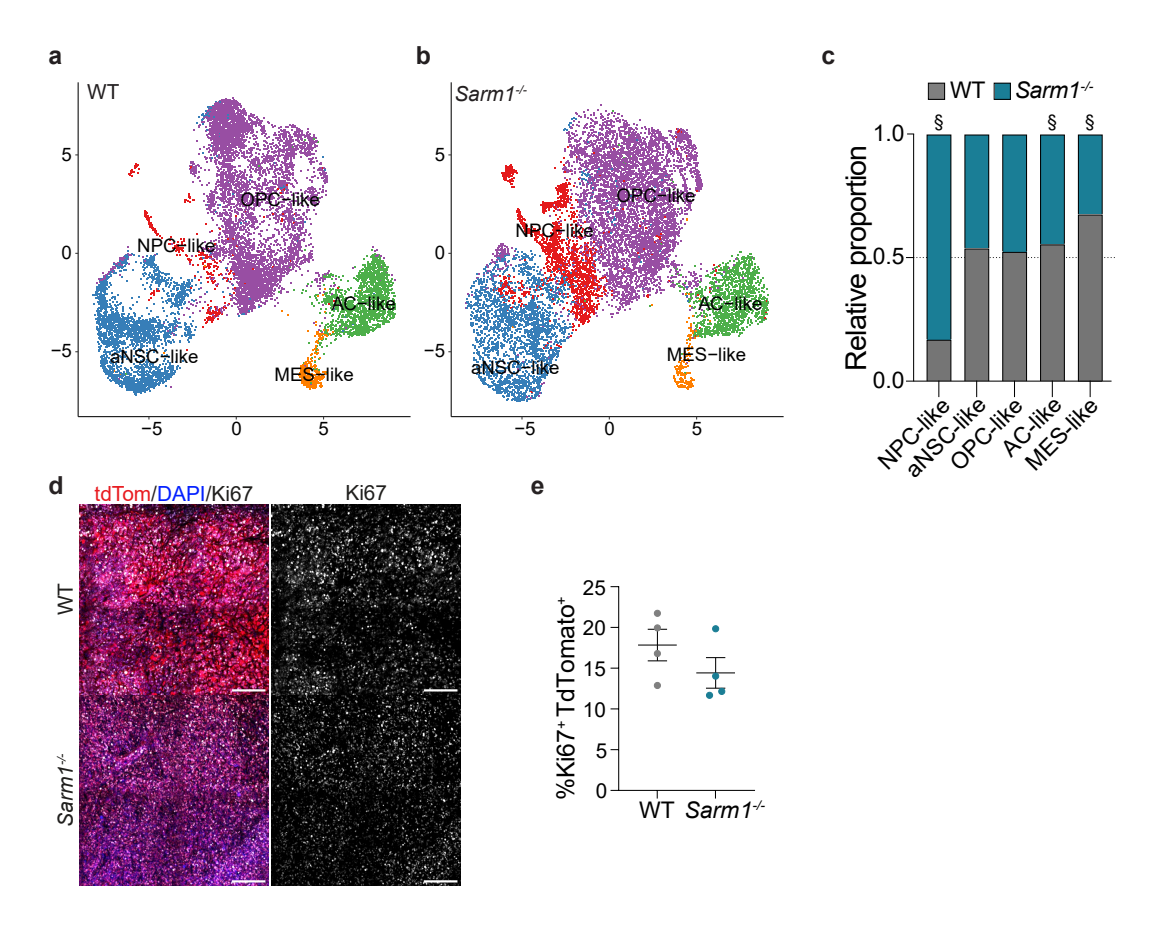


Figure 5.1. scRNA-seq shows reduced MES-like and increased NPC-like states in tumours generated in  $Sarm 1^{-/-}$  animals.

a, UMAP representation of scRNA-seq data from tdTomato+ tumour cells isolated from WT and  $Sarm1^{-/-}$  mice. Cell type labels were assigned using published signatures and marker genes: neural progenitor cell-like (NPC-like), oligodendrocyte progenitor cell-like (OPC-like), astrocyte-like (AC-like), mesenchymal-like (MES-like), and active neural stem cell-like (aNSC-like). Data were downsampled to equal numbers between genotypes. b, UMAP as in a for tumours generated in  $Sarm1^{-/-}$  animals. c, Proportion of tumour cell types in WT and tumours generated in  $Sarm1^{-/-}$  animals. n=12,054 cells downsampled per genotype. The dashed line at 0.5 indicates no change. Cell types were considered significantly different if Pearson's chi-squared test p<0.05 and relative difference >10%. d, Representative immunofluorescence images of terminal npp tumours stained for Ki67 (grey), tdTomato (red), and DAPI (blue). e, Quantification of Ki67+ tumour cells as a percentage of tdTomato+ cells. Unpaired t test. WT n=4,  $Sarm1^{-/-}$  n=4.

in line with established GBM transcriptional cell states (Neftel et al. 2019).

However, striking differences in the proportions of these states were observed between WT and tumours generated in  $Sarm1^{-/-}$  animals. tumours generated in  $Sarm1^{-/-}$  animals displayed a significant shift towards NPC-like states, while MES-like states were relatively depleted (Figure 5.1c, Table B.4.). This suggests that preventing axonal degeneration may hinder the transcriptional transition of tumour cells toward more advanced, injury-associated phenotypes (MES-like) (L. M. Richards et al. 2021).

Importantly, the proportion of proliferative tumour cells, captured by an aNSC-like cluster expressing cell cycle genes, was unchanged between genotypes. This was consistent with immunohistochemical analysis of Ki67 in terminal tumours, which revealed comparable rates of proliferation in WT and  $Sarm1^{-/-}$  animals (Figure 5.1d, e). These findings suggest that while the overall proliferative capacity of tumour cells remains intact in terminal tumours, the trajectory of transcriptional differentiation diverges in the absence of SARM1-mediated degeneration, favouring a more neurodevelopmental and less mesenchymal, injured state.

# 5.2.2 Sarm1 deletion dampens neuroinflammation and vascular remodelling in the tumour microenvironment

Axonal degeneration is a potent inducer of neuroinflammation, triggering local recruitment and activation of immune cells, as well as secondary changes to vascular structure and function. Given this, the next set of experiments focused on investigating whether preventing axonal degeneration via *Sarm1* deletion could reshape the TME in glioblastoma.

To address this, the scRNA-seq dataset from the previous section was used.

Following the exclusion of tumour cells, microenvironmental (non-tumour) cell populations were isolated and analysed separately. Unsupervised clustering revealed a diverse TME landscape comprising astrocytes, inflamed glia, oligodendrocyte precursor cells (OPCs), transient amplifying progenitors/neuroblasts (TAP/NB), endothelial cells (ECs), pericytes, tumour-associated macrophages (TAMs), monocytes, T cells, choroid plexus cells, and ependymal cells (Figure 5.2a).

In WT tumours, a greater proportion of endothelial cells (ECs) and inflamed glial populations were observed (Figure 5.2a, b, Table B.4.). This is suggestive of a more advanced and reactive TME with higher levels of angiogenesis and neuroinflammatory processes. In contrast, tumours generated in *Sarm1*<sup>-/-</sup> animals exhibited fewer of these cell types, suggesting that protection of axons dampened neuroinflammatory activation and vascular remodelling.

To more precisely characterise myeloid differences, the tumour-associated macrophage (TAM) compartment was extracted and re-clustered. Two distinct myeloid subsets emerged: a microglial-like cluster (cluster 1), expressing canonical microglial markers such as *P2ry12* and *Tmem119*, and a peripherally derived macrophage-like cluster (cluster 2) expressing genes such as *Spint2* and *Ccnd2* (Figure 5.2c–e). Quantification revealed a significant enrichment of peripheral macrophages within WT tumours, while tumours generated in *Sarm1*-/- animals exhibited a relative increase in resident microglia. This finding points to a reduced permeability of the blood–brain barrier (BBB) and diminished recruitment of circulating monocytes in *Sarm1*-deficient tumours, consistent with a less inflammatory and less advanced TME.

To investigate whether these cellular changes translated into altered intercellular communication, ligand-receptor (LR) analysis was performed using the LIANA

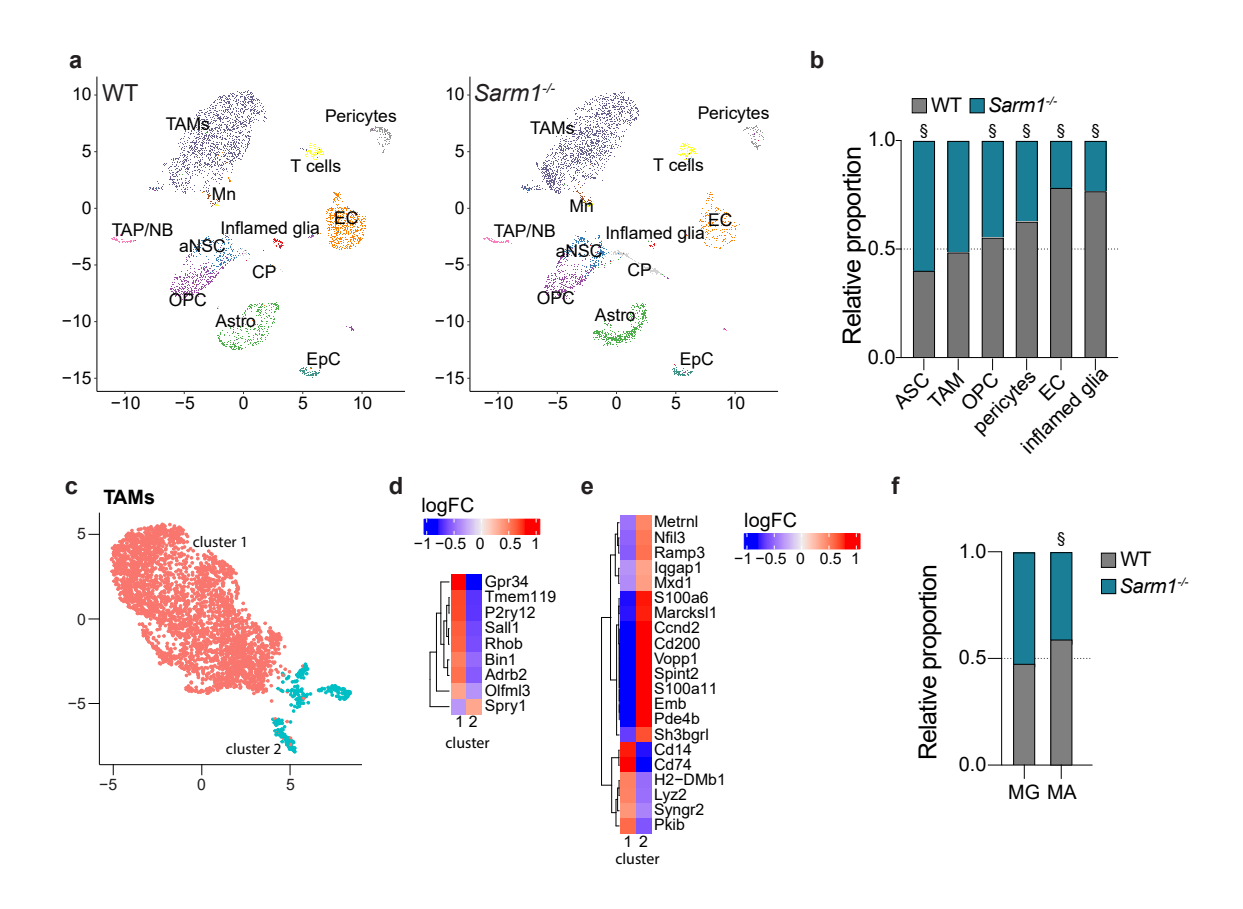


Figure 5.2. scRNA-seq reveals dampened inflammation and reduced angiogenic signatures in tumours generated in  $Sarm 1^{-/-}$  animals.

a, UMAP representation of scRNA-seq data from microenvironmental (non-tumour) cells isolated from WT and *Sarm1*<sup>-/-</sup> npp tumours. Cell types were annotated as choroid plexus cells (CP), astrocytes (Astro), inflamed glia, oligodendrocyte progenitor cells (OPCs), transient amplifying progenitors/neuroblasts (TAP/NB), active NSCs (aNSC), ependymal cells (EpC), endothelial cells (EC), pericytes, tumour-associated macrophages (TAMs), monocytes (Mn), and T cells. b, Proportion of microenvironmental cell types between WT and tumours generated in *Sarm1*<sup>-/-</sup> animals. n=4000 cells per genotype. The dashed line at 0.5 indicates no change. Cell types were considered significantly different if Pearson's chi-squared test p<0.05 and relative difference >10%. c, UMAP re-clustering of TAMs, identifying two clusters. d, Heatmaps of log fold-change (logFC) in expression of microglial and macrophage markers between the two TAM clusters. e, Proportional representation of microglia (MG) and macrophages (MA) in WT and tumours generated in *Sarm1*<sup>-/-</sup> animals.

framework (Dimitrov et al. 2022). Heatmap analysis revealed an overall reduction in LR pairings between TME and tumour cell compartments in tumours generated in *Sarm1*<sup>-/-</sup> animals compared to WT (Figure 5.3a, b, Table B.6, B.7). Closer inspection of selected LR pairs highlighted downregulation of several inflammationand angiogenesis-associated axes in the knockout condition (such as Apoe and Ptn; Figure 5.3c, d). Together, these findings suggest that axonal degeneration not only drives immune cell recruitment but also fuels inflammatory and angiogenic cross-talk between tumour and TME compartments.

To validate the scRNA-seq findings at the protein level, flow cytometry was performed on terminal tumours. In line with transcriptomic data, WT tumours exhibited a higher proportion of CD45<sup>+</sup> immune cells overall, with a specific enrichment of lymphocytes (CD45 high, CD11b low) and peripherally derived macrophages (CD49d high, CD45 high) (Figure 5.4a–e). Notably, microglial levels remained stable across genotypes, reinforcing the interpretation that the key difference lay in peripheral immune cell infiltration rather than changes in the resident brain immune landscape.

In parallel, immunohistochemical analysis of terminal tumour sections stained for Iba1 (a general mTAM marker) and CD68 (a lysosomal activation marker) was performed. Quantification revealed no significant difference in overall TAM density between genotypes (Figure 5.4g), but CD68 integrated density, reflecting the activation status of myeloid cells, was significantly reduced in tumours generated in *Sarm1*<sup>-/-</sup> animals (Figure 5.4h). This suggests that although TAM numbers were similar, their inflammatory activation was attenuated when axonal degeneration was prevented. These data collectively highlight that *Sarm1* deletion not only limits immune cell

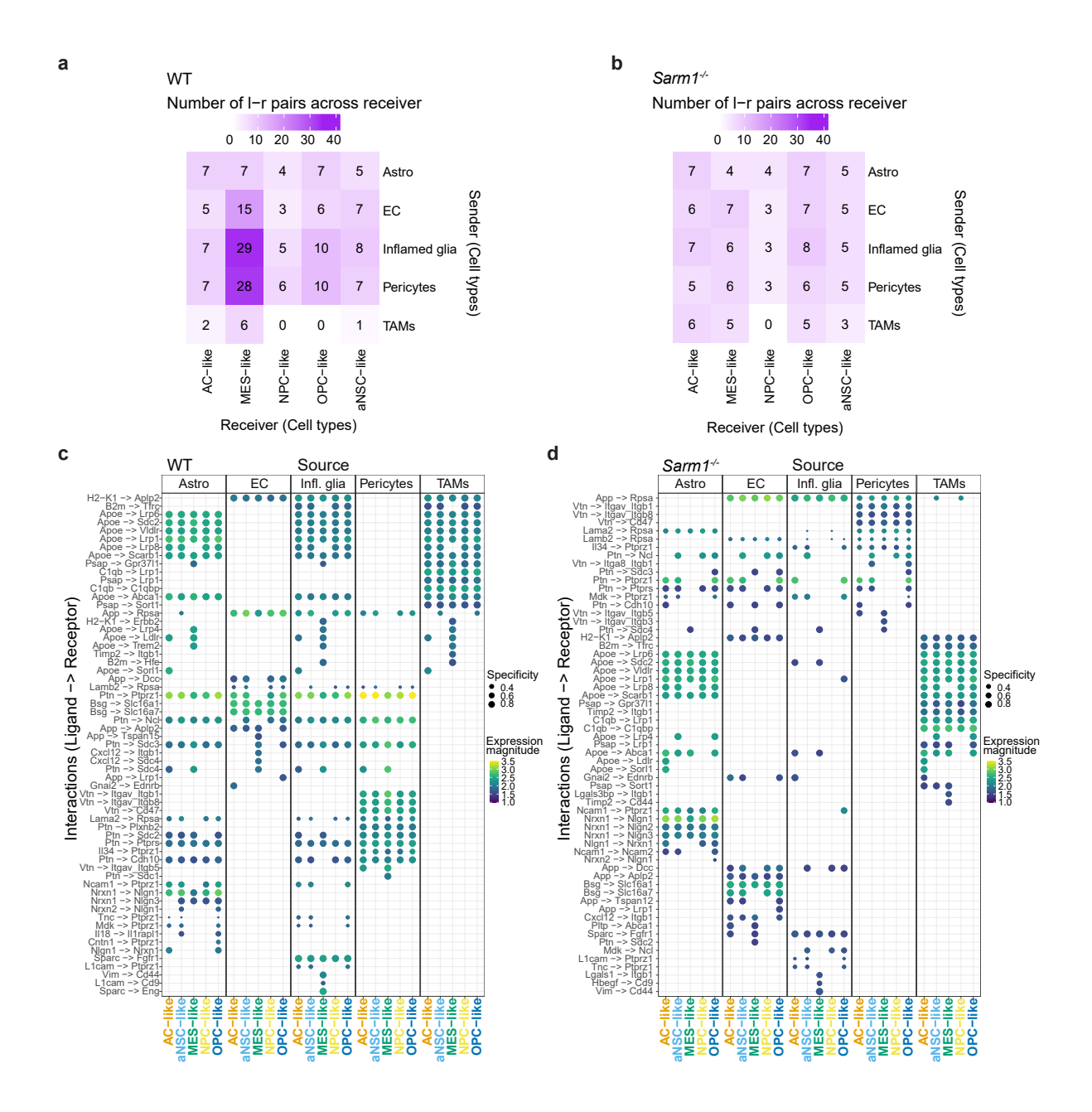


Figure 5.3. scRNA-seq reveals reduced signalling between the microenvironmental and tumour cell compartments in  $Sarm 1^{-/-}$  tumours.

a, LIANA ligand–receptor interaction analysis showing the number of significant interactions between microenvironmental (sender) and tumour (receiver) cells in WT tumours. b, As in a for tumours generated in  $Sarm1^{-/-}$  animals. c, Detailed LIANA plot in WT tumours displaying ligand–receptor pairs, with dot diameter representing the fraction of sender cells expressing the ligand and colour representing average ligand–receptor expression (lr.mean). d, As in c for tumours generated in  $Sarm1^{-/-}$  animals.

infiltration but also modulates the functional state of the TME towards a less reactive phenotype.

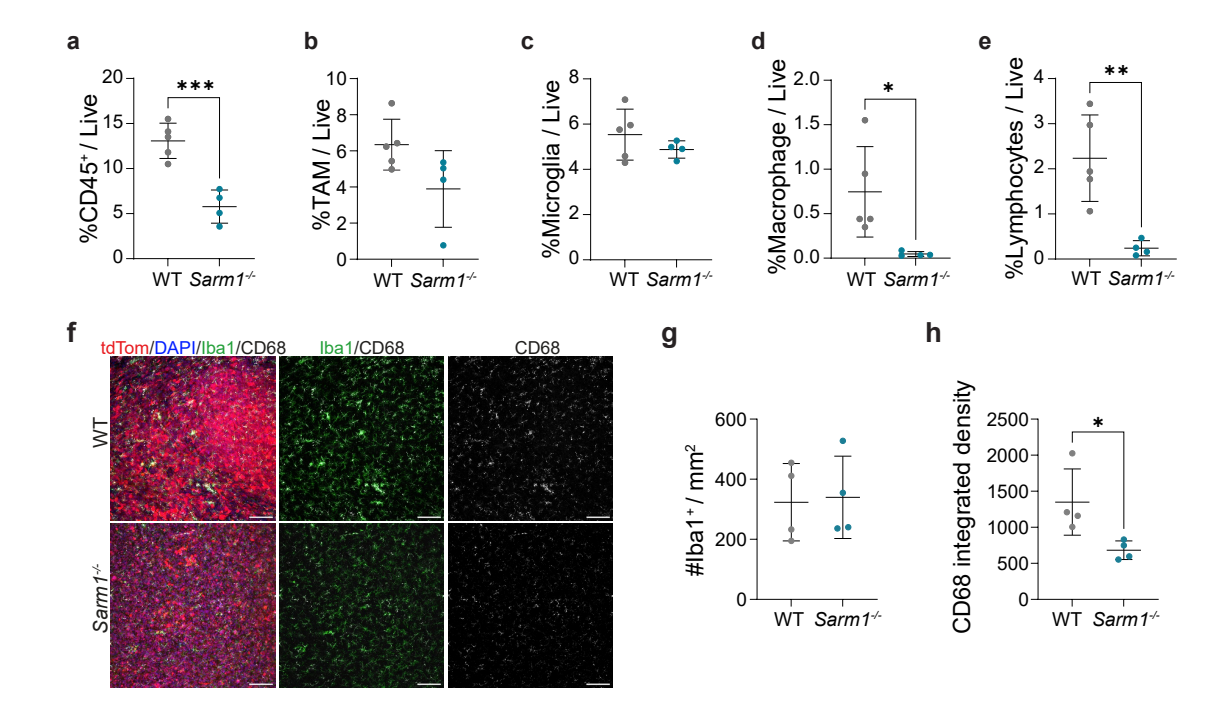


Figure 5.4. Flow cytometry and immunostaining confirm reduced immune cell infiltration and TAM activation in tumours generated in  $Sarm 1^{-/-}$  animals.

a–e, Flow cytometry analysis of immune cell populations in terminal WT and  $Sarm1^{-/-}$  npp tumours. Representative gating strategy is shown in Figure 3.7a. Mean±SD. Unpaired t tests. WT n=5,  $Sarm1^{-/-}$  n=5. f, Representative immunofluorescence images of terminal tumours stained for Iba1 (green), CD68 (grey), tdTomato (red), and DAPI (blue). g, Quantification of Iba1+ cell density per mm² tumour area. Unpaired t test. WT n=4,  $Sarm1^{-/-}$  n=4. h, Quantification of CD68 integrated density within tumours. Unpaired t test. WT n=4,  $Sarm1^{-/-}$  n=4.

To further investigate whether neuroinflammation actively contributes to tumour progression, rather than merely reflecting a downstream or correlative change, a targeted microglial depletion experiment was performed. If axonal degeneration promotes gliomagenesis in part by driving immune activation, then ablating microglia, the brain's resident immune cells, should suppress this axis and phenocopy aspects of the  $Sarm1^{-/-}$  condition.

To test this, a colony stimulating factor 1 receptor (CSF1R) inhibitor (PLX5622) was administered to tumour-bearing mice via chow to deplete microglia during tumour development. Effective depletion was confirmed by Iba1 immunostaining in tumour-contralateral, non-infiltrated brain regions, where microglia are normally abundant. PLX-treated animals, referred to as depleted in Figure 5.5, exhibited a significant reduction in Iba1<sup>+</sup> cells compared to controls, validating successful suppression of the microglial compartment (Figure 5.5a, b).

Following this confirmation, tumour burden and proliferation were assessed in PLX-treated and control mice. Immunofluorescent staining revealed that microglia-depleted animals developed smaller tumours (Figure 5.5c, d) with a significantly reduced proportion of proliferating cells (tdTomato<sup>+</sup>/Ki67<sup>+</sup>; Figure 5.5e, f). These findings indicate that the presence of microglia and the inflammatory signalling they sustain are important in supporting tumour growth.

Together, these results support a model in which axonal degeneration initiates an inflammatory cascade that potentiates tumour aggressiveness, and highlight microglia as key effectors of this axis.

Beyond inflammatory alterations, vascular remodelling is another hallmark of GBM progression, often linked to both hypoxia and inflammation. Given the increased endothelial representation in WT tumours observed by scRNA-seq, vascular architecture was assessed in more detail via immunofluorescent staining for CD31, a pan-endothelial marker.

Despite no significant differences in total vascular area or vessel density between WT and tumours generated in  $Sarm1^{-/-}$  animals (Figure 5.6b, c), important qualitative differences were observed. WT tumours exhibited larger mean vessel diameters and an

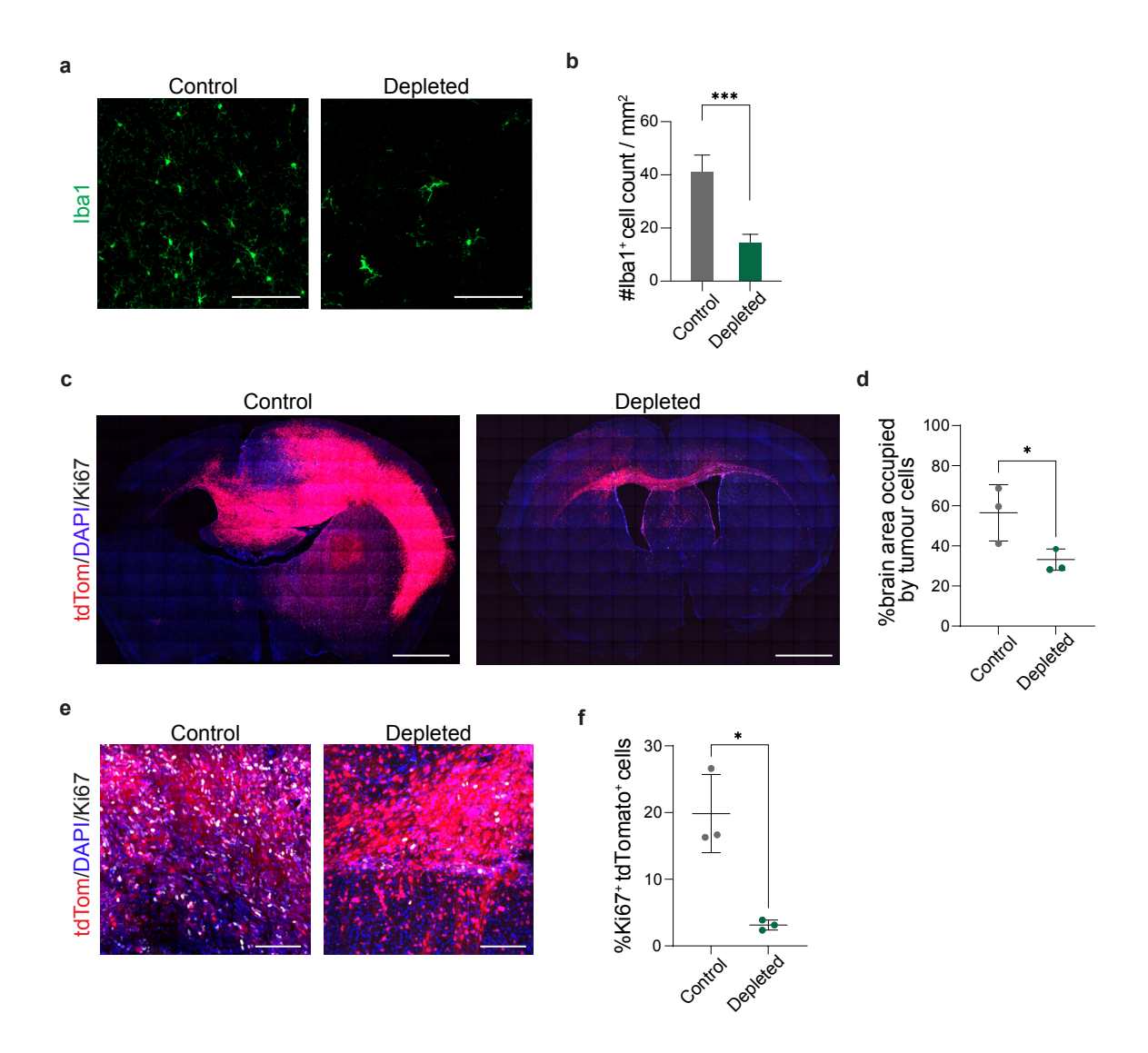


Figure 5.5. Microglial depletion via CSF1R inhibition reduces tumour size and proliferation.

a, Representative images of Iba1 immunofluorescence staining in control and PLX5622-treated brains. Images were taken from tumour-free, contralateral regions to confirm global depletion of microglia. Scale bar = 100µm. b, Quantification of Iba1<sup>+</sup> cell density in tumour-free regions. Five ROIs per mouse. Mean±SD. Unpaired t test. n=3. c, Representative images of terminal tumours in control and PLX-treated mice, showing tdTomato (red), Ki67 (grey), and DAPI (blue). Scale bar = 500µm. d, Quantification of tumour burden, calculated as the proportion of tdTomato<sup>+</sup> area over total brain area. Mean±SD. Unpaired t test. n=3. e, Higher magnification images of tdTomato<sup>+</sup> tumours stained for Ki67 (grey) in control and PLX-treated brains. f, Quantification of tumour cell proliferation, expressed as the percentage of tdTomato<sup>+</sup> cells that are Ki67<sup>+</sup>. Mean±SD. Unpaired t test. n=3.

increased number of vascular branching points (Figure 5.6d, e), indicative of aberrant angiogenesis — a phenomenon associated with aggressive tumour behaviour and poor prognosis (Saidi et al. 2008; Birner et al. 2003). In contrast, tumours generated in  $Sarm1^{-/-}$  animals maintained a more restrained vascular phenotype, with narrower and less tortuous vessels.

To assess the structural integrity of tumour vasculature, co-staining for laminin (basal lamina component) and platelet-derived growth factor receptor  $\beta$  (PDGFRB) (pericyte marker) was performed. No significant differences were detected in laminin coverage or pericyte association with blood vessels between genotypes (Figure 5.6g, i), suggesting that basic vessel structure remained preserved even as vessel morphology and complexity differed. These results indicate that SARM1-mediated axonal degeneration contributes specifically to vascular remodelling, rather than simply impairing vascular stability.

Together, these findings define a profound reprogramming of the tumour microenvironment following deletion of *Sarm1*. Tumours arising in the absence of SARM1-mediated axonal degeneration were characterised by a less inflammatory immune landscape, reduced infiltration of peripherally derived immune cells, diminished intercellular inflammatory signalling, and a less aberrant angiogenic profile. These results suggest that axonal injury is not merely a consequence of tumour progression, but an active upstream modulator of TME evolution, amplifying inflammation, vascular pathology, and ultimately driving disease advancement.

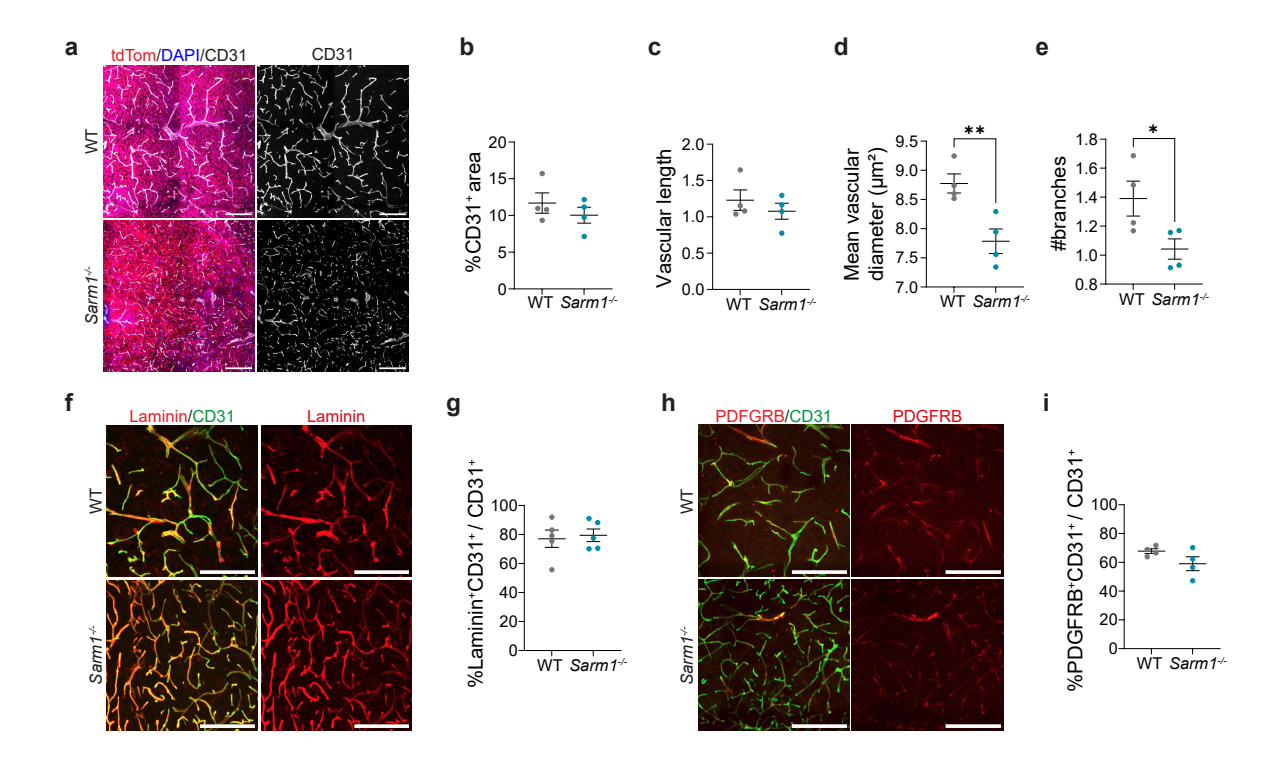


Figure 5.6. Vascular architecture analysis shows reduced vascular diameter and branching in tumours generated in  $Sarm 1^{-/-}$  animals.

a, Representative images of CD31 (grey) and tdTomato<sup>+</sup> tumour cells (red) in terminal WT and tumours generated in *Sarm1*<sup>-/-</sup> animals. DAPI (blue) stains nuclei. b–e, Quantification of vascular characteristics (CD31<sup>+</sup> area, vascular length, vessel diameter, and branching) in tumours. Unpaired t tests. WT n=4, *Sarm1*<sup>-/-</sup> n=4. f, Representative co-staining of laminin (red) and CD31 (green). g, Quantification of laminin coverage on CD31<sup>+</sup> vessels. h, Representative images of pericyte marker PDGFRB (red) and CD31 (green). i, Quantification of PDGFRB coverage on CD31<sup>+</sup> vessels. All vascular measurements: WT n=4, *Sarm1*<sup>-/-</sup> n=4.

# 5.2.3 Sarm1 deletion prolongs survival and preserves neurological function

The molecular and cellular differences observed in tumours generated in *Sarm1*<sup>-/-</sup> animals raise the critical question of whether the preservation of axonal integrity and reprogramming of the TME could translate into measurable clinical benefits. Therefore, the final part of the study assessed whether protection against axonal degeneration influenced survival outcomes and neurological function, two key

parameters of clinical relevance in glioblastoma.

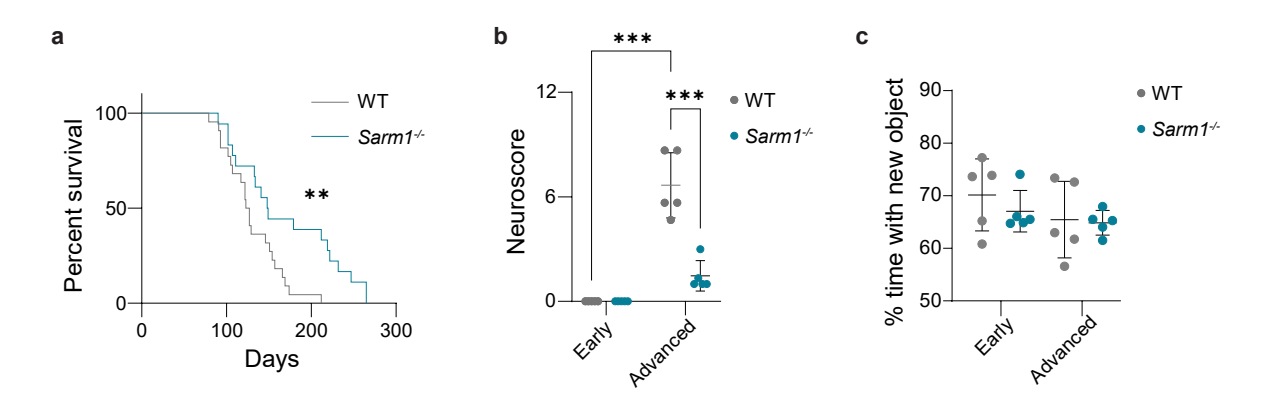


Figure 5.7. Survival analysis and behavioural testing indicate delayed disease progression  $Sarm 1^{-/-}$  tumours.

a, Kaplan–Meier survival curves comparing WT and  $Sarm1^{-/-}$  tumour-bearing mice. Median survival: WT=18 weeks,  $Sarm1^{-/-}$ =21 weeks. Log-rank test. WT n=22,  $Sarm1^{-/-}$  n=18. b, Neuroscore evaluation of motor function in WT and  $Sarm1^{-/-}$  mice at early (8 weeks) and advanced disease stages ( $\leq$  2 weeks before endpoint). Two-way ANOVA with Tukey's multiple comparisons. WT n=5,  $Sarm1^{-/-}$  n=5. c, Novel object recognition task evaluation, with % time spent with novel object shown in WT and  $Sarm1^{-/-}$  mice at early (8 weeks) and advanced disease stages ( $\leq$  2 weeks before endpoint). Two-way ANOVA with Tukey's multiple comparisons. WT n=5,  $Sarm1^{-/-}$  n=5.

To determine the impact on survival, longitudinal monitoring of tumour-bearing WT and  $Sarm1^{-/-}$  mice was conducted. Kaplan–Meier survival analysis revealed a significant extension in median overall survival in the  $Sarm1^{-/-}$  cohort compared to WT controls (median survival: WT = 18 weeks,  $Sarm1^{-/-}$  = 21 weeks; Figure 5.7a). This survival benefit was notable given that tumour proliferation rates, as measured by Ki67 staining, were not significantly different between genotypes, and that tumours in  $Sarm1^{-/-}$  mice appeared more spatially disseminated. These findings suggest that tumour burden alone was not the sole driver of clinical decline, and highlight the possibility that axonal integrity and tissue-level organisation play key roles in determining the functional deterioration associated with GBM progression.

To evaluate neurological function, motor performance was assessed using a

composite Neuroscore, an established scoring system that captures a range of motor deficits including gait disturbances, limb weakness, and generalised neurological decline. At early stages of tumourigenesis (8 weeks post tumour induction), when tumours are present but remain relatively indolent and are not expected to result in symptomatic disease, both WT and  $Sarm1^{-/-}$  mice demonstrated near-baseline performance, consistent with a pre-symptomatic phase of disease (mean scores near 0/12; Figure 5.7b). This indicated that early tumour growth did not yet translate into significant neurological impairment, irrespective of genotype.

However, striking differences emerged at later stages of disease progression. In the terminal phase (approximately two weeks prior to humane endpoints), WT animals exhibited marked motor deterioration (mean score 7/12), reflected in significant increases in Neuroscore values. In contrast,  $Sarm1^{-/-}$  mice retained near-baseline performance, with minimal neurological deficits detected even at advanced stages (Figure 5.7b). These results strongly suggest that preservation of axonal architecture in  $Sarm1^{-/-}$  mice mitigates functional deterioration typically associated with late-stage GBM, despite ongoing tumour growth.

Cognitive performance was also assessed using the novel object recognition task, a widely used behavioural paradigm for detecting changes in memory and recognition abilities. Both WT and *Sarm1*<sup>-/-</sup> mice performed similarly at both early and late disease stages, with no significant genotype-dependent differences detected (Figure 5.7c). The absence of cognitive decline in either group is likely attributable to the tumour localisation within the striatum in this model, a region predominantly associated with motor rather than cognitive functions. Moreover, it is possible that the NOR task alone may not capture more subtle cognitive impairments, highlighting a potential

limitation in sensitivity for detecting early cognitive deterioration in this setting.

Overall, these findings demonstrate that deletion of *Sarm1* confers not only a molecular and histopathological benefit but also a tangible improvement in functional outcomes, delaying the onset of motor dysfunction and prolonging survival. This underscores the broader clinical relevance of axonal protection strategies in glioblastoma and suggests that therapies targeting axonal degeneration pathways could provide meaningful benefits beyond tumour cell-intrinsic targeting alone.

To strengthen the conclusion that the phenotypic differences observed were attributable specifically to loss of *Sarm1* function rather than potential confounding genetic factors, tumours were additionally generated in an independently engineered CRISPR-based *Sarm1* knockout line (*Sarm1em1.1Tftc*). This model was selected in light of growing awareness that germline knockout strains created using traditional embryonic stem cell targeting approaches can carry "passenger mutations"—unintended genetic variations linked to the targeted allele—which may confound phenotypic interpretation (Uccellini et al. 2020). By contrast, CRISPR-based genome editing reduces the risk of such passenger effects and enables more rigorous attribution of phenotypes to the gene of interest.

In the CRISPR-generated *Sarm1*<sup>em1.1Tftc</sup> line, key features of the *Sarm1*-null phenotype were robustly recapitulated. Immunofluorescent analysis demonstrated a similarly more diffuse tumour architecture compared to background-matched WT controls, accompanied by reduced tumour cell density (Figure 5.8a, b). Furthermore, survival was significantly extended (Figure 5.8c) and motor function preserved at late stages of disease progression (Figure 5.8d), mirroring findings in the original *Sarm1*<sup>-/-</sup> strain.

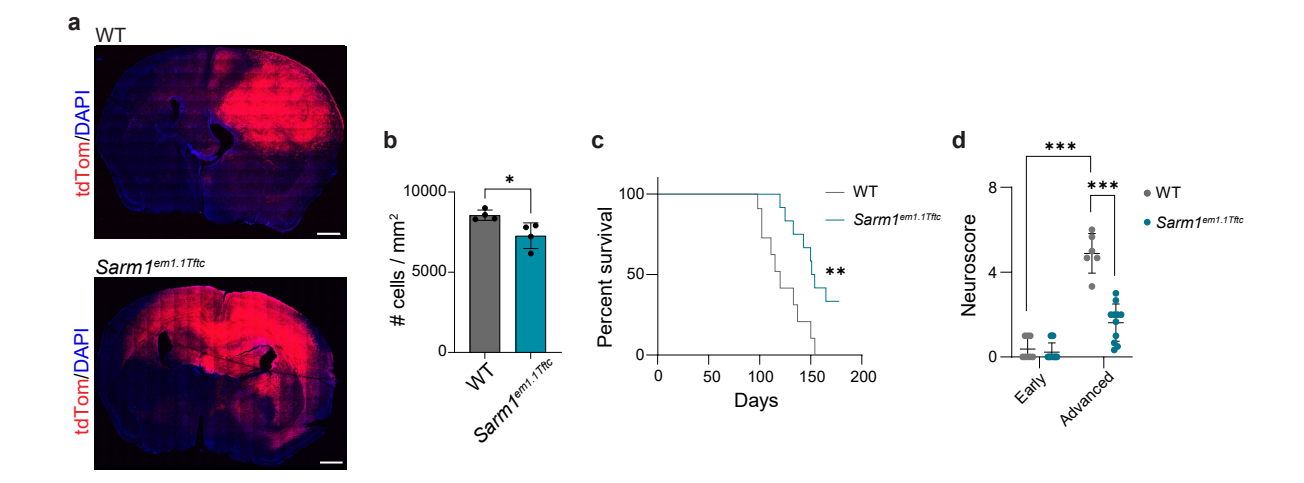


Figure 5.8. CRISPR-based Sarm1 knockout model independently validates Sarm1<sup>-/-</sup> phenoype.

a, Representative fluorescence images of npp tumours generated in  $Sarm1^{em1.1Tftc}$  and background-matched WT ( $Sarm1^{wt}$ ) mice. TdTomato<sup>+</sup> tumour cells shown in red; DAPI (blue) for nuclei. b, Quantification of tumour cell density (cells per mm²) in  $Sarm1^{em1.1Tftc}$  vs  $Sarm1^{wt}$  tumours. Unpaired t test. n=4 per genotype. c, Kaplan–Meier survival curves comparing  $Sarm1^{wt}$  and  $Sarm1^{em1.1Tftc}$  tumour-bearing mice. Median survival:  $Sarm1^{wt}$ =17 weeks,  $Sarm1^{em1.1Tftc}$ =22 weeks. Log-rank test.  $Sarm1^{wt}$  n=11,  $Sarm1^{em1.1Tftc}$  n=12. d, Neuroscore evaluation of motor function in  $Sarm1^{wt}$  and  $Sarm1^{em1.1Tftc}$  mice at early (8 weeks) and advanced ( $\leq$  2 weeks before endpoint) disease stages. Two-way ANOVA with Tukey's multiple comparisons.  $Sarm1^{wt}$  early n=8, advanced n=6;  $Sarm1^{em1.1Tftc}$  early n=13, advanced n=11.

Together, these results not only validate the effects of *Sarm1* deletion on GBM progression and neurological function but also provide additional confidence that these phenotypes reflect a true biological consequence of disrupting the WD pathway, rather than artefacts arising from background genetic variability.

### 5.3 Conclusions

The data presented in this chapter establish a multifaceted link between axonal integrity and GBM progression. Through genetic ablation of *Sarm1*, a central executioner of the WD pathway, it was demonstrated that preserving axonal architecture leads to alterations at the cellular, microenvironmental, and organism

level. Across tumour cell identity, TME composition, vascular phenotype, and clinical disease trajectory, attenuation of axonal degeneration consistently shifted disease features toward a less advanced, less malignant state.

At the terminal disease timepoint, tumours formed in *Sarm1*<sup>-/-</sup> mice retained a more neurodevelopmental transcriptional identity, with a striking reduction in mesenchymal (MES)-like states. MES-like tumour cells have previously been associated with injury response, therapeutic resistance, and poor prognosis, suggesting that their depletion reflects a less aggressive tumour phenotype (K. P. Bhat et al. 2013; Hara et al. 2021). Notably, these transcriptional shifts occurred in the absence of significant changes in tumour cell proliferation.

Beyond intrinsic tumour phenotype, Sarm1 deletion reprogrammed the TME at multiple levels. A dampened neuroinflammatory response was observed, including reduced infiltration of peripherally derived macrophages and a shift toward a microglia-dominated immune landscape. Importantly, while TAM numbers were comparable between genotypes, markers of TAM activation were markedly diminished in tumours generated in  $Sarm1^{-/-}$  animals, suggesting a less reactive and inflammatory TME. Vascular architecture was also altered, with reduced vessel diameter and branching complexity in tumours generated in  $Sarm1^{-/-}$  animals, features that are typically associated with less abnormal angiogenesis. These findings highlight that axonal degeneration reshapes the immune and vascular landscapes in ways that likely facilitate tumour progression.

To test whether neuroinflammation is not merely a correlate but a functional driver of tumour advancement, an additional experiment was performed in which microglia were pharmacologically depleted using a CSF1R inhibitor (PLX). This

intervention significantly reduced microglial numbers in non-tumour-infiltrated brain regions, validating the efficacy of this treatment. Strikingly, PLX-treated mice exhibited smaller tumours and reduced tumour cell proliferation, despite the absence of direct axonal intervention. These findings provide causal support for the hypothesis that injury-induced inflammation, particularly mediated by TAMs, acts downstream of axonal degeneration to foster a tumour-permissive environment. They further imply that targeting neuroinflammation alone, even without directly modulating axonal integrity, can partially recapitulate the tumour-suppressive effects observed in the *Sarm1*-/- background.

Furthermore, ligand–receptor analysis further revealed that deletion of *Sarm1* led to a global attenuation of tumour–TME crosstalk, reducing inflammatory and angiogenic signalling.

Critically, these molecular and histopathological changes translated into meaningful functional benefits. Preservation of neurological function, as assessed by motor performance, was significantly enhanced in  $Sarm1^{-/-}$  tumour-bearing mice, and overall survival was robustly prolonged. These benefits were observed even in the context of more spatially disseminated tumours, suggesting that maintenance of neural integrity, rather than tumour burden alone, plays a dominant role in determining clinical outcomes.

Replication of the key findings in an independently generated CRISPR-based *Sarm1* knockout line strengthened the validity of these conclusions, mitigating concerns regarding potential passenger mutations and genetic background effects inherent to traditional knockout models. This supports a robust interpretation that loss of SARM1 function, and the consequent preservation of axons, directly underlies

the observed phenotypic changes.

Collectively, these findings reposition axonal degeneration as a central, upstream event in GBM progression. Targeting axonal degeneration pathways such as WD thus offers a novel and complementary therapeutic axis in glioblastoma.

# Chapter 6

# Discussion and Future Perspectives

### 6.1 Introduction

Glioblastoma (GBM) remains one of the most lethal cancers, characterised by extensive invasiveness, resistance to therapy, and inevitable recurrence. Over the past decade, increasing attention has turned to the role of the neural microenvironment in shaping glioma biology, resulting in the emergence of the field of cancer neuroscience. While neuronal activity has been extensively proven to promote glioma growth (Venkatesh, Johung et al. 2015), this thesis explored a complementary and previously underappreciated aspect of neuronal biology: the impact of axonal injury and degeneration on tumour progression.

# 6.2 Summary of Results and Discussion

A key finding of this work is that glioma cells preferentially colonise WM in early disease, and that this spatial bias is conserved across both somatic and PDX mouse models. This observation lays the groundwork for addressing a key question regarding early gliomagenesis: although early tumour cells acquire mutations within

the subventricular zone (SVZ), they form tumours distally (Shepherd et al. 2019; Habib et al. 2022). Interestingly, human GBM has also been noted to primarily form within supratentorial, subcortical WM, further strengthening the relevance of this observation (Gaillard et al. 2008; Jun Wang et al. 2022). Until now, the factors driving this distal tumour formation have remained largely unknown. However, the data presented in this thesis suggests that WM represents a more permissive niche for early GBM expansion, offering unique neuroglial interactions that support survival.

Despite harbouring multiple oncogenic mutations, early tumour cells in the npp model remained relatively indolent throughout the early and intermediate stages of tumourigenesis, proliferating slowly and remaining spatially constrained within WM bundles. This latency mirrors clinical observations in GBM studies and suggests that WM may initially exert a tumour-suppressive or at least tumour-modulatory effect (Badve et al. 2015; Das et al. 2023). However, this thesis demonstrates that as tumour burden increases, axons within infiltrated WM regions become injured and start to degenerate, while GBM cells undergo a proliferative and transcriptional shift toward more aggressive states.

These findings offer direct experimental support for a two-stage model of glioblastoma pathogenesis. While the two-hit hypothesis of tumourigenesis has been around for decades and has grown to encompass both genomic and microenvironmental drivers, it hasn't been expanded into the GBM space before (Peters et al. 2024; Chernoff 2021). In this framework, gliomagenesis happens not as a single process, but as a temporally and spatially distinct sequence of events: starting with the acquisition of oncogenic mutations and culminating in a secondary phase of malignant transformation triggered by microenvironmental drivers (Figure 6.1).

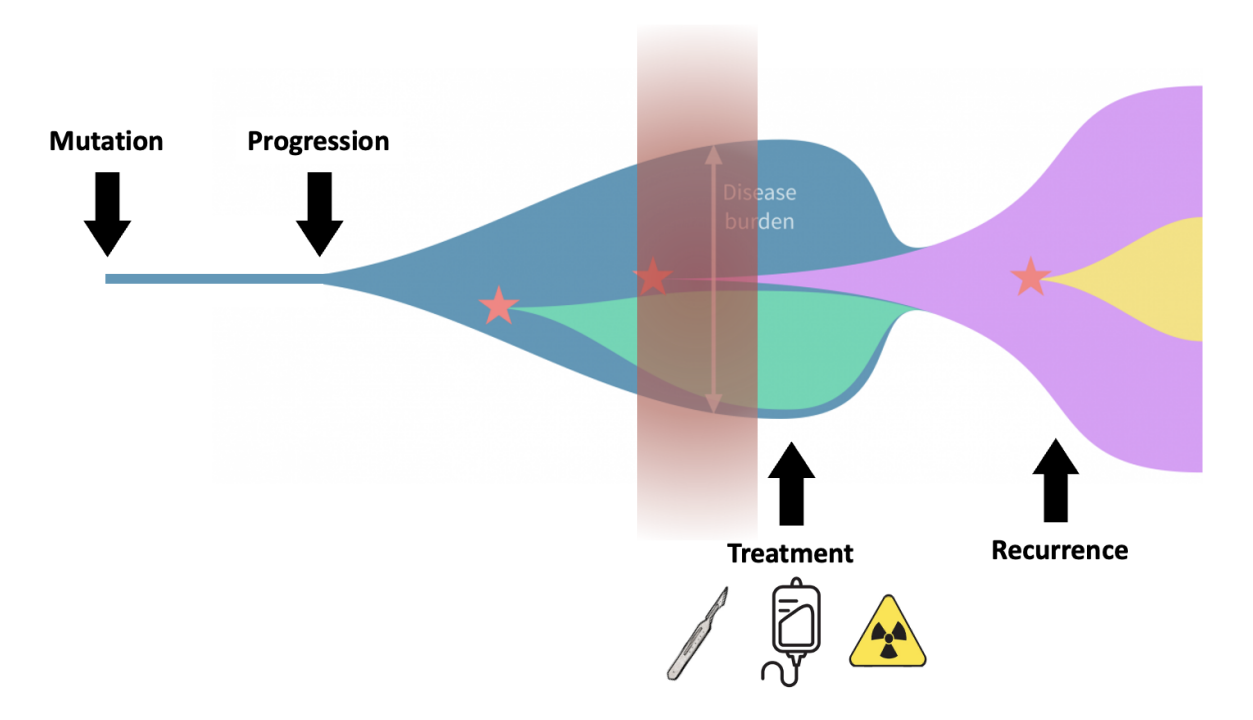


Figure 6.1. A two-stage model of glioblastoma.

A visual representation of the two-stage model of GBM development, with an initial mutation, followed by a driver which leads to a switch from indolent to rapidly growing disease. The colours represent clonal populations within the tumour, as a visual representation of heterogeneity and clonal expansion throughout GBM development. The red band signifies where GBM has traditionally been studied most, at the stage of clinical presentation and corresponding advanced disease. Treatment with resection, chemotherapy and radiotherapy, as well as disease recurrence, are also represented in this graphic. Adapted from Liuksiala 2023

The first stage of this two-hit hypothesis is marked by the acquisition of tumour-initiating mutations within a population of neural stem cells. These mutations, which often involve key tumour suppressors such as *TP53*, *PTEN*, and *NF1*, may occur within the SVZ, a known germinal niche with long-lived, mitotically active stem cells (Jurkowski et al. 2020). Importantly, this mutational priming alone is not sufficient to drive tumour formation.

In the second stage, tumour progression is initiated when these mutated progenitors encounter a permissive microenvironment. This occurs, as mentioned earlier, at distant anatomical sites — within WM tracts — where tumour cells

encounter specific extrinsic signals, including injury, inflammation, and altered glial architecture. These microenvironmental cues act as a secondary driver, promoting a shift toward malignant behaviour. The result is a transition in cellular identity, proliferation, and microenvironmental engagement, ultimately leading to clinically manifest GBM (Figure 6.1).

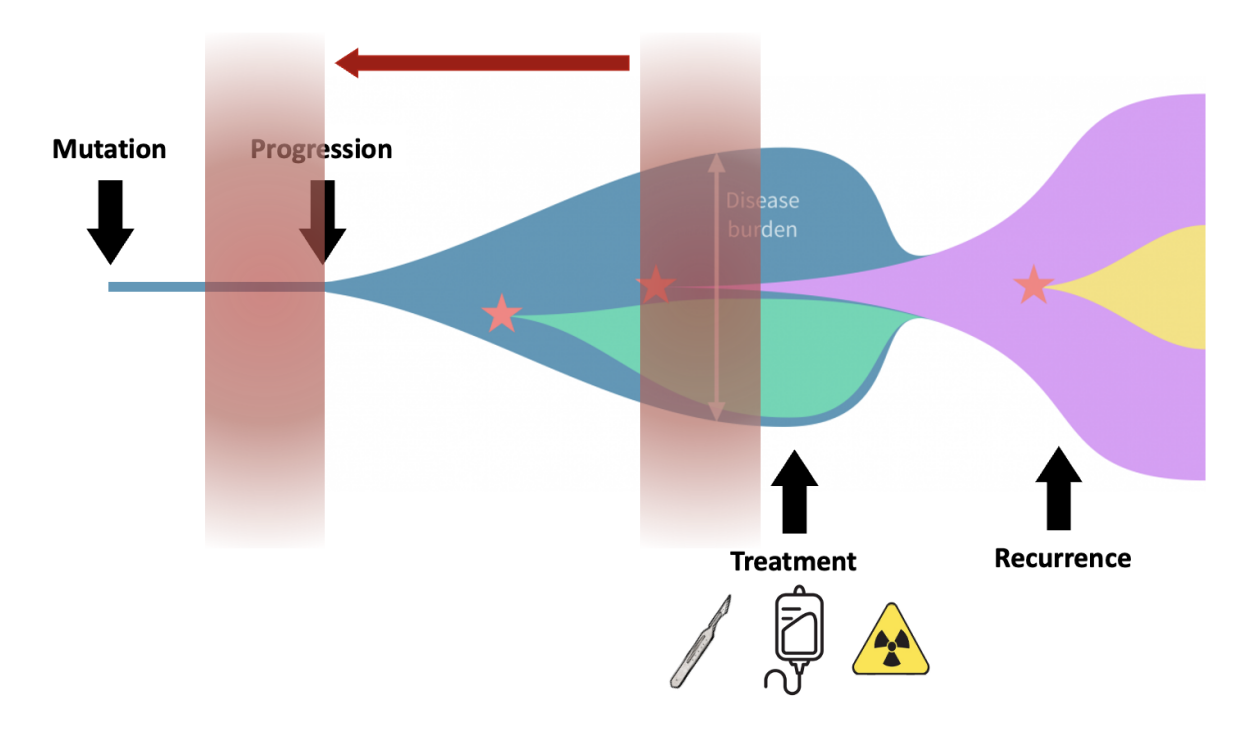


Figure 6.2. A shift towards studying early disease in the two-stage model of glioblastoma.

As in Figure 6.1, with a shift to studying early disease, represented with a red arrow and new red band.

This model aligns with broader paradigms in cancer biology that emphasise the role of the microenvironment as an active participant in tumour evolution (Brock et al. 2015). By recognising that malignant transformation is not merely the result of accumulating mutations, but also of spatio-temporally distinct environmental cues, the two-stage model offers a framework for identifying and targeting key vulnerabilities before full disease emergence.

The results in this thesis also explore what drivers in the permissive WM microenvironment trigger GBM progression, positioning axonal injury and subsequent degeneration as a key tractable driver of progression.

SARM1-dependent WD is identified as a key effector of early axonal degeneration and loss. Mechanistically, tumour cell proximity causes mechanical compression and transport blockages, initiating varicosity formation and downstream WD. These features, explored in detail using EM imaging, closely resemble models of trauma-induced axonopathy in neurodegenerative disease, reinforcing the pathological parallels between glioma invasion and neural trauma.

Deleting *Sarm1* substantially altered the course of the disease. Axonal preservation in *Sarm1*<sup>-/-</sup> mice reduced the progression of the TME toward angiogenic and neuroinflammatory states. Notably, tumours remained more neurodevelopmental, with reduced representation of MES-like states. These findings suggest that axonal degeneration acts as a molecular amplifier of malignancy, initiating local glial activation, vascular remodelling, and transcriptional reprogramming of tumour cells. These phenotypic differences also resulted in prolonged survival and improved neurological function, enhancing the translational relevance of this study.

However, several limitations warrant critical reflection.

First, the assessment of tumour cell-intrinsic properties was limited to *in vitro* proliferation and migration assays which showed no differences between WT and *Sarm1*<sup>-/-</sup> tumour cells. However, these conditions lack the complexity of the brain, where tumour cell behaviour is shaped by interactions with the TME. Orthotopic transplant experiments using reciprocal WT and *Sarm1*<sup>-/-</sup> backgrounds would have provided stronger evidence for or against cell-intrinsic effects. However, such

experiments were technically constrained in this model due to extracranial tumour growth following transplantation. Future work using alternative transplantation strategies or inducible *Sarm1* models may help circumvent this issue.

Second, the scRNA-seq analysis was performed on whole cells rather than nuclei, precluding the inclusion of mature neurons — the primary cell type affected by axonal degeneration. Consequently, it was not possible to directly characterise neuronal transcriptional responses to tumour growth or to dissect which neuronal subtypes are most vulnerable. Future studies using nuclear isolation could help bridge this gap and elucidate how tumour-induced axonal injury reprograms neurons themselves, and which injury related or regenerative signals these neurons release to reshape the TME.

Third, while deletion of *Sarm1* substantially protected axons, a subset of pathological axons persisted even in knockout mice. This observation suggests that SARM1-independent injury pathways are also likely to take place, particularly under conditions of high tumour burden or sustained mechanical stress. Candidate mechanisms may include calpain-mediated cytoskeletal breakdown, caspase activation, or oxidative stress. Additionally, the possibility that GBM cell-derived factors, such as extracellular vesicles, proteases, or inflammatory cytokines, may initiate or potentiate axonal injury remains to be explored. Distinguishing these possibilities can be done using further functional experiemnts such as *in vitro* cytokine release assays, caspase activity assays, and complementary genetic or pharmacological approaches.

Following on from this, while SARM1 was clearly shown to mediate axonal degeneration in this model, the downstream cellular effectors of WD remain undefined. Neuroinflammation was dampened in *Sarm1*<sup>-/-</sup> tumours, but the

specific contributions of astrocytes, microglia, and infiltrating macrophages were not disentangled. While astroglial reactivity was clearly reduced, whether this reflects a direct response to reduced axonal injury or is secondary to other TME alterations remains unknown. Similarly, although LIANA analysis revealed ECM and cytokine signals altered by *Sarm1*-/- status, higher-resolution profiling of glial subpopulations is needed to clarify which relationships may be of higher importance. Other TME responses downstream of axonal injury, such as fibrosis and tissue and neuronal regenerative signals, also remain to be explored further.

Of note, SARM1 is a Toll-like receptor adaptor protein and may therefore play a role in immune signalling. In fact, earlier studies suggested a role for SARM1 in innate immunity, particularly in regulating macrophage activation and cytokine production (Sugisawa et al. 2024; Gürtler et al. 2014). On the other hand, some recent studies have demonstrated minimal function of SARM1 in macrophages (Doran et al. 2021; Uccellini et al. 2020). In our model, we did not observe obvious immune defects attributable to *Sarm1* loss. However, this does not preclude a context-dependent role for SARM1 in modulating immune behaviour, particularly under inflammatory or injury conditions. Further immune classification with a focus on TAMs and their diverse subtypes that may play a varied and important role in shaping the TME and tumour cell fate, could help address this potential issue further. Furthermore, methods of selectively inhibiting SARM1 in neurons can be of use to address this issue - for example, a viral approach of neuron-speficic *Sarm1* inactivation is in use in the lab and has recapitulated the tumour phenotype found in *Sarm1*-/- mice.

Fourth, the context of axon-TME interactions is likely to be regionally specific.

WM axons differ from cortical ones in terms of diameter, myelination, metabolic

demand, and associated glial support (Karbowski 2007). While this study focused on striatal WM due to early tumour localisation to these regions, it is essential to consider that the axon-TME interactions may differ significantly between WM and cortical regions. Cortical axons, for example, exhibit distinct characteristics in terms of diameter, metabolic demands, and glial support compared to WM axons. These differences may influence the tumour's ability to invade and remodel surrounding tissue. Additionally, the regional heterogeneity of the TME, such as differences in astroglial populations and vascular architecture, could impact susceptibility to injury and tumour transformation. Investigating axonal injury responses in cortical regions and comparing them to WM responses will be crucial for understanding how different brain regions may uniquely contribute to glioblastoma progression.

Finally, although behavioural testing indicated preserved motor function and no differences in cognitive performance in  $Sarm1^{-/-}$  animals, the assessments were limited to composite Neuroscore and novel object recognition. More granular behavioural phenotyping, including motor coordination, anxiety, or learning paradigms, could uncover more subtle differences and help define which neuronal circuits are preserved or impaired in the presence or absence of axonal degeneration in this model. Furthermore, an exploration of seizure activity across genotypes could be informative, as epilepsy represents a significant burden on patient quality of life and may be altered when axonal integrity is preserved. Exploring these aspects in greater depth will help refine our understanding of the functional benefits of preserving axonal structure in the context of glioma progression.

### 6.3 Future Directions and Conclusion

Several promising avenues for future research emerge from this work. First, a key priority is the mechanistic dissection of WD downstream effectors to further the understanding of how axonal degeneration translates into glial activation, immune recruitment, and tumour cell reprogramming. This could be approached by functional experiments exploring the influence of cell-to-cell interactions on variables such as proliferation and motility, secretome analysis, as well as combining single nuclear transcriptomics, or through the use of conditional knockout models, such as astrocyteor microglia-specific deletion of inflammatory mediators. These varied approaches, taken together, should help resolve these signalling pathways.

Another important direction is the temporal and spatial profiling of tumour–microenvironment interactions. Spatial transcriptomics or *in situ* sequencing technologies could be leveraged to map how injury signals evolve and propagate within the tumour and surrounding brain tissue. Special attention should be given to the WM-GM interface, which may represent a key transition zone for tumour infiltration and progression.

The therapeutic modulation of axonal degeneration also presents a promising opportunity. Given the phenotypic benefits of *Sarm1* deletion observed in this study, testing pharmacological inhibitors of SARM1 in these tumour models would be a logical next step. Such interventions should ideally be evaluated in combination with current standard-of-care treatments to assess potential synergy and clinical relevance, and are worth exploring at different time-points to pinpoint the translational relevance of these treatments throughout the different stages of disease development. Specifically, it will be critical to evaluate whether blocking WD is beneficial only early

in gliomagenesis, or whether it also plays a role in controlling later disease or limiting recurrence after initial treatment.

The potential role of injury-induced relapse remains another underexplored area. Further work is needed to determine whether surgical, chemotherapeutic, or radiotherapeutic injuries similarly promote tumour evolution via WD. Animal models of post-treatment recurrence could first explore whether therapeutic injury is a driver of recurrence while simultaneously providing a platform to test whether inhibition of WD suppresses or delays relapse.

Additionally, the interplay between axonal injury, WD, and host brain state, particularly in the context of ageing, is likely to be significant. Given the increased neuroinflammatory tone in the ageing WM, it is plausible that WD exerts more pronounced effects in older brains (D. Raj et al. 2017; Hart et al. 2012). Comparative studies in young and aged mice could shed light on these potential context-specific dependencies.

Lastly, the ECM responses and fibrotic pathways activated downstream of WD merit further investigation. While this study identified ECM-related ligand–receptor signals using LIANA which differ between tumours in WT and  $Sarm1^{-/-}$  animals, more focused profiling of fibrotic and structural TME components is indicated. This line of inquiry could help identify downstream nodes within the injury response that are amenable to therapeutic intervention, even in cases where axonal degeneration cannot be completely prevented.

In conclusion, these findings position early-stage glioma as a tractable window for intervention — a phase in which modifying host–tumour interactions, particularly injury responses, may delay or even prevent malignant transformation. Ultimately, a

dual-focus approach - one that both limits tumour progression and protects the brain, preserving neurological function — may offer the most meaningful improvements in survival and quality of life for patients facing this devastating disease. By identifying early, modifiable drivers of gliomagenesis such as axonal injury, this work suggests that glioblastoma may be amenable not only to treatment but also to interception.

# Appendix A

# Data availability

Single-cell RNA sequencing data is available on GEO under the following accession code: GSE268298.

### Appendix B

# Extended data tables

Table B.1. Summary of patient-derived glioblastoma lines analysed in Figure 3.3.

Tumour subtypes were classified based on Neftel *et al.*Neftel et al. 2019 and Gangoso *et al.*Gangoso et al. 2021. Genetic alterations detected in each line are listed. Data originally generated by Melanie Clements.

Cell Line	Neftel	Gangoso	Mutations
GCGR_L5	AC-like	Non-MESImmune	EGFR; CDK6; MET; PTEN;
			MDM4
GL23	MES-like	Mixed	nd
GCGR_E43	NPC-like	Non-MESImmune	EGFR; CDK6; MET; PTEN;
			TP53; RB1; MDMA4; CDKN2C
GBM2	AC-like	Non-MESImmune	nd

Table B.2. Processing metrics for single-cell RNA-sequencing experiments.

Samples were processed with Cell Ranger 7.0.1. Metrics include sequencing saturation, mapping rates, Q30 scores, and UMI counts. Two wild-type (WT) and three  $Sarm1^{-/-}$  tumours were analysed. Data originally generated by Wenhao Tang.

Comp. In	Est.	Reads	Median	No.	Valid	Seq.	Q30	Q30	Q30	Mapped	Conf.	Conf.	Conf.	Conf.	Mapped	Mapped	Fraction	Genes	Median
Sample 1D	Cells	per Cell	Gen	Reads	Barcodes Sati	Saturation	Barcode	RNA Read L	UMI	Genome	Genome	Intergenic Ir	Intronic	Exonic	Transcriptome Ant	Antisense	Reads in Cells	Detected	UMIs/Cell
WB_1	23562	25072		590746529		0.552	0.973	0.965	0.979	0.971	0.954	0.027	0.205	0.722	0.852		0.926	26302	5846
WB_2	54569	22515		1228608935	0.895		0.972	0.956	0.978	0.950	0.934	0.035	0.297	0.602	0.755	0.139	0.935	27056	5862
SB_1	8129	29693	3955	241376562	0.977	0.405	096.0	0.918	0.931	0.963	0.943	0.027	0.163	0.753	0.848	0.063	0.941	24806	12554
SB_2	9716	22066		214397722	0.977		0.958	0.916	0.930	0.963	0.943	0.026	0.170	0.746	0.846	0.066	0.942	24892	10297
SB_3	6071	14843		90112196	0.979		0.981	0.933	0.973	0.954	0.926	0.037	0.225	0.664	0.797	0.088	0.847	24514	6942

#### Table B.3. Processing statistics for single-cell RNA sequencing data.

Table is available online at https://doi.org/10.5281/zenodo.15242891. If access is restricted, please contact zan.baronik.18@ucl.ac.uk. Metadata include curated cell annotations ("LABELS"), tdTomato UMI counts, CopyKat ploidy assignments, and predictions from external datasets (Antunes, Yeo, Ximerakis, and Kalamakis studiesPombo Antunes et al. 2021; Yeo et al. 2022; Ximerakis et al. 2019; Kalamakis et al. 2019). Data originally generated by Wenhao Tang.

Table B.4. Statistical testing of cell type proportions between WT and Sarm1<sup>-/-</sup> tumours.

Cell types were defined based on scRNA-seq data. Statistical comparisons were made using Pearson's chi-squared test. Tumour and microenvironment cell populations are indicated. Table originally generated by Wenhao Tang.

Cell Type	Significance Call	Genotype	Proportion	p-value	Туре
aNSC-like	ns	Sarm1 <sup>-/-</sup>	0.4602	6.81E-10	Tumour
OPC-like	ns	Sarm1 <sup>-/-</sup>	0.4736	4.37E-09	Tumour
AC-like	pval<0.01	Sarm1 <sup>-/-</sup>	0.4443	3.89E-238	Tumour
NPC-like	pval<0.01	Sarm1 <sup>-/-</sup>	0.8305	3.36E-09	Tumour
MES-like	pval<0.01	Sarm1 <sup>-/-</sup>	0.3224	2.02E-17	Tumour
aNSC-like	ns	WT	0.5398	6.81E-10	Tumour
OPC-like	ns	WT	0.5264	4.37E-09	Tumour
AC-like	pval<0.01	WT	0.5557	3.89E-238	Tumour
NPC-like	pval<0.01	WT	0.1695	3.36E-09	Tumour
MES-like	pval<0.01	WT	0.6776	2.02E-17	Tumour
Astro	pval<0.01	Sarm1 <sup>-/-</sup>	0.5983	1.47E-09	Microenvironment
TAMs	ns	Sarm1 <sup>-/-</sup>	0.5138	0.108	Microenvironment
OPC	pval<0.01	Sarm1 <sup>-/-</sup>	0.4446	7.71E-04	Microenvironment
Pericytes	pval<0.01	Sarm1 <sup>-/-</sup>	0.3713	9.72E-05	Microenvironment
Inflamed glia	pval<0.01	Sarm1 <sup>-/-</sup>	0.2319	1.46E-05	Microenvironment
EC	pval<0.01	Sarm1 <sup>-/-</sup>	0.2164	1.54E-61	Microenvironment
Astro	pval<0.01	WT	0.4017	1.47E-09	Microenvironment
TAMs	ns	WT	0.4862	0.108	Microenvironment
OPC	pval<0.01	WT	0.5554	7.71E-04	Microenvironment
Pericytes	pval<0.01	WT	0.6287	9.72E-05	Microenvironment
Inflamed glia	pval<0.01	WT	0.7681	1.46E-05	Microenvironment
EC	pval<0.01	WT	0.7836	1.54E-61	Microenvironment
MG	ns	Sarm1 <sup>-/-</sup>	0.5229	9.96E-03	Microenvironment
MAC	pval<0.01	Sarm1 <sup>-/-</sup>	0.4086	2.76E-03	Microenvironment
MG	ns	WT	0.4771	9.96E-03	Microenvironment
MAC	pval<0.01	WT	0.5914	2.76E-03	Microenvironment

Table B.5. Gene enrichment analysis of cell type markers in tumour and TME cells from WT and  $Sarm 1^{-/-}$ 

Supplementary Table B.5 is available online at https://doi.org/10.5281/zenodo.15242891. If access is restricted, please contact zan.baronik.18@ucl.ac.uk. Gene ontology enrichment analyses were performed on differentially expressed genes identified in tumour and TME cells, comparing WT and  $Sarm1^{-/-}$  tumours. Analyses conducted using the R package clusterProfiler. Data originally generated by Wenhao Tang.

. Table B.6. csRNA-seq.ligand-receptor analysis performed in R, including I-r pairs with significant p value.

pairs	Ptn_Ptprz1	Apoe_Lrp1	Ptn_Ptprz1	App_Rpsa	App_Rpsa	Apoe_Lrp1	Ptn_Ptprz1	Vtn_Itgav	Apoe_Lrp1	Ptn_Ptprz1	Ptn_Ncl	Ptn_Ptprz1	App_Rpsa	Ptn_Ptprz1							
pvalue	0.00	0.00	0.00	0.00	0.00	0.00	0.00	0.00	0.00	0.00	0.00	0.00	0.00	0.00	0.00	0.00	0.00	0.00	0.00	0.00	0.00
lr.mean	3.64	3.59	3.54	3.43	3.28	3.22	3.18	3.17	3.07	3.07	3.00	2.99	2.99	2.98	2.95	2.93	2.93	2.89	2.88	2.86	2.81
receptor.expr	3.37	3.27	3.18	2.95	3.37	3.27	3.18	2.43	1.02	2.95	3.56	3.56	0.85	3.37	1.37	0.74	3.27	1.88	3.18	3.28	2.43
ligand.expr	3.91	3.91	3.91	3.91	3.18	3.18	3.18	3.91	5.12	3.18	2.43	2.43	5.12	2.59	4.53	5.12	2.59	3.91	2.59	2.43	3.18
ligand.prop	0.92	0.92	0.92	0.92	0.95	0.95	0.95	0.92	1.00	0.95	0.92	0.92	1.00	0.82	96.0	1.00	0.82	0.92	0.82	0.92	0.95
receptor.prop	0.99	0.97	0.99	0.97	0.99	0.97	0.99	0.96	0.71	0.97	0.99	1.00	0.62	0.99	0.69	0.61	0.97	0.91	0.99	0.98	0.96
receptor	Ptprz1	Lrp1	Ptprz1	Rpsa	Rpsa	Lrp1	Ptprz1	Itgav	Lrp1	Ptprz1	Ncl	Ptprz1	Rpsa	Ptprz1							
ligand	Ptn	Apoe	Ptn	Арр	App	Apoe	Ptn	Vtn	Apoe	Ptn	Ptn	Ptn	Арр	Ptn							
target	OPC-like	AC-like	aNSC-like	NPC-like	OPC-like	AC-like	aNSC-like	MES-like	OPC-like	NPC-like	NPC-like	aNSC-like	AC-like	OPC-like	MES-like	aNSC-like	AC-like	NPC-like	aNSC-like	OPC-like	MES-like
source	pericytes	pericytes	pericytes	pericytes	ASC	ASC	ASC	pericytes	ASC	ASC	EC	EC	ASC	inflamed glia	pericytes	ASC	inflamed glia	pericytes	inflamed glia	EC	ASC

source	target	ligand	receptor	receptor.prop	ligand.prop	ligand.expr	receptor.expr	lr.mean	pvalue	pairs
pericytes	aNSC-like	Ptn	Ncl	0.91	0.92	3.91	1.69	2.80	0.00	Ptn_Ncl
pericytes	MES-like	Ptn	Sdc3	0.88	0.92	3.91	1.69	2.80	00.0	Ptn_Sdc3
EC	OPC-like	Ptn	Ptprz1	0.99	0.84	2.19	3.37	2.78	00.0	Ptn_Ptprz1
inflamed glia	NPC-like	Ptn	Ptprz1	0.97	0.82	2.59	2.95	2.77	0.00	Ptn_Ptprz1
pericytes	OPC-like	Ptn	Ncl	0.85	0.92	3.91	1.56	2.73	0.00	Ptn_Ncl
pericytes	MES-like	Vtn	Cd47	0.69	96.0	4.53	0.94	2.73	00.0	Vtn_Cd47
pericytes	MES-like	Vtn	Itgb8	0.63	96.0	4.53	0.93	2.73	0.00	Vtn_Itgb8
EC	AC-like	Ptn	Ptprz1	0.97	0.84	2.19	3.27	2.73	00.0	Ptn_Ptprz1
ASC	OPC-like	Nrxn1	Nlgn1	0.98	08.0	2.41	3.04	2.72	00.0	Nrxn1_Nlgn1
EC	aNSC-like	Ptn	Ptprz1	0.99	0.84	2.19	3.18	2.69	0.00	Ptn_Ptprz1
pericytes	MES-like	Ptn	Sdc4	0.70	0.92	3.91	1.45	2.68	00.0	Ptn_Sdc4
EC	AC-like	App	Rpsa	0.92	0.92	2.43	2.88	2.66	00.0	App_Rpsa
pericytes	MES-like	Ptn	Ncl	0.88	0.92	3.91	1.33	2.62	0.00	Ptn_Ncl
pericytes	AC-like	Ptn	Ncl	0.75	0.92	3.91	1.24	2.58	0.00	Ptn_Ncl
ASC	aNSC-like	Nrxn1	Nlgn1	0.96	08.0	2.41	2.73	2.57	0.00	Nrxn1_Nlgn1
EC	NPC-like	Ptn	Ptprz1	0.97	0.84	2.19	2.95	2.57	0.00	Ptn_Ptprz1
pericytes	OPC-like	Ptn	Sdc3	0.78	0.92	3.91	1.19	2.55	00.0	Ptn_Sdc3
ASC	NPC-like	Ptn	Ncl	0.91	6.95	3.18	1.88	2.53	0.00	Ptn_Ncl
ASC	NPC-like	Nrxn1	Nlgn1	0.96	08.0	2.41	2.62	2.52	0.00	Nrxn1_Nlgn1
inflamed glia	MES-like	Ptn	Ptprz1	0.96	0.82	2.59	2.43	2.51	0.00	Ptn_Ptprz1
TAM	OPC-like	C1qb	Lrp1	0.71	66:0	3.99	1.02	2.50	0.00	C1qb_Lrp1
ASC	AC-like	Nrxn1	Nlgn1	0.92	08.0	2.41	2.57	2.49	0.00	Nrxn1_Nlgn1

source	target	ligand	receptor	receptor.prop	ligand.prop	ligand.expr	receptor.expr	lr.mean	pvalue	pairs
inflamed glia	NPC-like	Арр	Rpsa	0.99	0.58	1.42	3.56	2.49	0.00	App_Rpsa
inflamed glia	aNSC-like	Арр	Rpsa	1.00	0.58	1.42	3.56	2.49	0.00	App_Rpsa
TAM	NPC-like	C1qb	C1qbp	0.64	66.0	3.99	0.95	2.47	0.00	C1qb_C1qbp
pericytes	MES-like	Ptn	Ptprs	0.81	0.92	3.91	1.00	2.45	0.00	Ptn_Ptprs
pericytes	OPC-like	Ptn	Ptprs	0.71	0.92	3.91	0.99	2.45	0.00	Ptn_Ptprs
TAM	MES-like	C1qb	C1qbp	0.74	66.0	3.99	0.89	2.44	0.00	C1qb_C1qbp
pericytes	aNSC-like	Ptn	Sdc3	0.72	0.92	3.91	0.97	2.44	0.00	Ptn_Sdc3
ASC	aNSC-like	Ptn	Ncl	0.91	0.95	3.18	1.69	2.44	0.00	Ptn_Ncl
ASC	MES-like	Ptn	Sdc3	0.88	0.95	3.18	1.69	2.43	00.0	Ptn_Sdc3
pericytes	NPC-like	Ptn	Ptprs	0.67	0.92	3.91	0.95	2.43	0.00	Ptn_Ptprs
TAM	OPC-like	Apoe	Lrp1	0.71	0.94	3.83	1.02	2.42	00.0	Apoe_Lrp1
TAM	AC-like	C1qb	Lrp1	0.62	66.0	3.99	0.85	2.42	0.00	C1qb_Lrp1
EC	MES-like	App	Rpsa	0.96	0.92	2.43	2.41	2.42	0.00	App_Rpsa
pericytes	aNSC-like	Ptn	Ptprs	0.72	0.92	3.91	0.93	2.42	0.00	Ptn_Ptprs
pericytes	OPC-like	1134	Ptprz1	0.99	0.61	1.46	3.37	2.41	0.00	Il34_Ptprz1
pericytes	NPC-like	Арр	Rpsa	0.99	0.55	1.23	3.56	2.40	0.00	App_Rpsa
pericytes	aNSC-like	Арр	Rpsa	1.00	0.55	1.23	3.56	2.39	0.00	App_Rpsa
TAM	OPC-like	C1qb	C1qbp	0.60	0.99	3.99	0.78	2.39	0.00	C1qb_C1qbp
pericytes	NPC-like	Ptn	Sdc3	0.62	0.92	3.91	0.86	2.38	0.00	Ptn_Sdc3
pericytes	AC-like	Ptn	Ptprs	0.63	0.92	3.91	0.84	2.38	0.00	Ptn_Ptprs
TAM	aNSC-like	C1qb	C1qbp	0.61	66.0	3.99	0.75	2.37	0.00	C1qb_C1qbp
ASC	OPC-like	Ptn	Ncl	0.85	0.95	3.18	1.56	2.37	0.00	Ptn_Ncl

source	target	ligand	receptor	receptor.prop	ligand.prop	ligand.expr	receptor.expr	lr.mean	pvalue	pairs
TAM	aNSC-like	C1qb	Lrp1	0.61	66.0	3.99	0.74	2.36	0.00	C1qb_Lrp1
pericytes	AC-like	1134	Ptprz1	0.97	0.61	1.46	3.27	2.36	0.00	1134_Ptprz1
TAM	AC-like	C1qb	C1qbp	0.56	66.0	3.99	0.72	2.36	0.00	C1qb_C1qbp
inflamed glia	OPC-like	Арр	Rpsa	0.98	0.58	1.42	3.28	2.35	0.00	App_Rpsa
pericytes	AC-like	Ptn	Sdc3	0.58	0.92	3.91	0.79	2.35	0.00	Ptn_Sdc3
pericytes	AC-like	Ptn	Cdh10	0.54	0.92	3.91	0.79	2.35	0.00	Ptn_Cdh10
pericytes	NPC-like	Lama2	Rpsa	0.99	0.48	1.13	3.56	2.34	0.00	Lama2_Rpsa
TAM	AC-like	Apoe	Lrp1	0.62	0.94	3.83	0.85	2.34	0.00	Apoe_Lrp1
pericytes	aNSC-like	Lama2	Rpsa	1.00	0.48	1.13	3.56	2.34	0.00	Lama2_Rpsa
pericytes	aNSC-like	1134	Ptprz1	66.0	0.61	1.46	3.18	2.32	0.00	1134_Ptprz1
ASC	MES-like	Ptn	Sdc4	0.70	0.95	3.18	1.45	2.32	0.00	Ptn_Sdc4
TAM	MES-like	Psap	Gpr3711	0.82	86.0	3.00	1.62	2.31	0.00	Psap_Gpr3711
TAM	aNSC-like	Apoe	Lrp1	0.61	0.94	3.83	0.74	2.29	0.00	Apoe_Lrp1
ASC	OPC-like	Ncam1	Ptprz1	0.99	0.59	1.20	3.37	2.28	0.00	Ncam1_Ptprz1
pericytes	OPC-like	App	Rpsa	0.98	0.55	1.23	3.28	2.26	0.00	App_Rpsa
inflamed glia	OPC-like	Apoe	Lrp1	0.71	0.86	3.50	1.02	2.26	0.00	Apoe_Lrp1
ASC	MES-like	Ptn	Ncl	0.88	0.95	3.18	1.33	2.26	0.00	Ptn_Ncl
inflamed glia	AC-like	H2-K1	Aplp2	0.76	0.91	3.33	1.18	2.25	0.00	H2-K1_Aplp2
inflamed glia	NPC-like	Ptn	Ncl	0.91	0.82	2.59	1.88	2.23	0.00	Ptn_Ncl
ASC	AC-like	Ncam1	Ptprz1	0.97	0.59	1.20	3.27	2.23	0.00	Ncam1_Ptprz1
ASC	AC-like	Ptn	Ncl	0.75	0.95	3.18	1.24	2.21	0.00	Ptn_Ncl
pericytes	OPC-like	Lama2	Rpsa	0.98	0.48	1.13	3.28	2.20	0.00	Lama2_Rpsa

source	target	ligand	receptor	receptor.prop	ligand.prop	ligand.expr	receptor.expr	lr.mean	pvalue	pairs
pericytes	NPC-like	1134	Ptprz1	0.97	0.61	1.46	2.95	2.20	0.00	Il34_Ptprz1
TAM	AC-like	H2-K1	Aplp2	0.76	86.0	3.22	1.18	2.20	00.0	H2-K1_Aplp2
ASC	aNSC-like	Ncam1	Ptprz1	66.0	0.59	1.20	3.18	2.19	0.00	Ncam1_Ptprz1
ASC	OPC-like	Ptn	Sdc3	0.78	0.95	3.18	1.19	2.18	0.00	Ptn_Sdc3
inflamed glia	MES-like	H2-K1	Aplp2	0.81	0.91	3.33	1.03	2.18	0.00	H2-K1_Aplp2
inflamed glia	AC-like	Apoe	Lrp1	0.62	0.86	3.50	0.85	2.17	0.00	Apoe_Lrp1
inflamed glia	AC-like	Арр	Rpsa	0.92	0.58	1.42	2.88	2.15	0.00	App_Rpsa
inflamed glia	OPC-like	Ncam1	Ptprz1	0.99	0.36	0.92	3.37	2.15	0.00	Ncam1_Ptprz1
inflamed glia	aNSC-like	Ptn	Ncl	0.91	0.82	2.59	1.69	2.14	0.00	Ptn_Ncl
inflamed glia	MES-like	Ptn	Sdc3	0.88	0.82	2.59	1.69	2.14	00.0	Ptn_Sdc3
inflamed glia	OPC-like	H2-K1	Aplp2	89.0	0.91	3.33	0.93	2.13	00.0	H2-K1_Aplp2
TAM	MES-like	H2-K1	Aplp2	0.81	86.0	3.22	1.03	2.13	00.0	H2-K1_Aplp2
inflamed glia	aNSC-like	H2-K1	Aplp2	0.71	0.91	3.33	0.92	2.12	0.00	H2-K1_Aplp2
inflamed glia	aNSC-like	Apoe	Lrp1	0.61	0.86	3.50	0.74	2.12	0.00	Apoe_Lrp1
inflamed glia	AC-like	Ncam1	Ptprz1	0.97	0.36	0.92	3.27	2.09	0.00	Ncam1_Ptprz1
ASC	MES-like	Ptn	Ptprs	0.81	0.95	3.18	1.00	2.09	0.00	Ptn_Ptprs
ASC	OPC-like	Ptn	Ptprs	0.71	0.95	3.18	0.99	2.08	0.00	Ptn_Ptprs
TAM	OPC-like	H2-K1	Aplp2	0.68	86.0	3.22	0.93	2.08	0.00	H2-K1_Aplp2
ASC	NPC-like	Ncam1	Ptprz1	0.97	0.59	1.20	2.95	2.07	0.00	Ncam1_Ptprz1
ASC	aNSC-like	Ptn	Sdc3	0.72	0.95	3.18	0.97	2.07	0.00	Ptn_Sdc3
TAM	aNSC-like	H2-K1	Aplp2	0.71	86.0	3.22	0.92	2.07	0.00	H2-K1_Aplp2
inflamed glia	OPC-like	Ptn	Ncl	0.85	0.82	2.59	1.56	2.07	0.00	Ptn_Ncl

source	target	ligand	receptor	receptor.prop	ligand.prop	ligand.expr	receptor.expr	lr.mean	pvalue	pairs
ASC	NPC-like	Ptn	Ptprs	0.67	0.95	3.18	0.95	2.07	0.00	Ptn_Ptprs
pericytes	AC-like	App	Rpsa	0.92	0.55	1.23	2.88	2.06	0.00	App_Rpsa
TAM	AC-like	Psap	Gpr3711	0.68	86.0	3.00	1.11	2.06	0.00	Psap_Gpr3711
ASC	aNSC-like	Ptn	Ptprs	0.72	0.95	3.18	0.93	2.05	0.00	Ptn_Ptprs
inflamed glia	aNSC-like	Ncam1	Ptprz1	66.0	0.36	0.92	3.18	2.05	0.00	Ncam1_Ptprz1
EC	AC-like	H2-K1	Aplp2	0.76	0.94	2.92	1.18	2.05	0.00	H2-K1_Aplp2
inflamed glia	NPC-like	H2-K1	Aplp2	0.58	0.91	3.33	0.77	2.05	0.00	H2-K1_Aplp2
EC	NPC-like	Ptn	Ncl	0.91	0.84	2.19	1.88	2.03	0.00	Ptn_Ncl
EC	OPC-like	App	Dcc	0.83	0.92	2.43	1.63	2.03	0.00	App_Dcc
inflamed glia	MES-like	Ptn	Sdc4	0.70	0.82	2.59	1.45	2.02	0.00	Ptn_Sdc4
ASC	NPC-like	Ptn	Sdc3	0.62	0.95	3.18	0.86	2.02	0.00	Ptn_Sdc3
ASC	AC-like	Ptn	Ptprs	0.63	0.95	3.18	0.84	2.01	0.00	Ptn_Ptprs
TAM	OPC-like	Psap	Lrp1	0.71	0.98	3.00	1.02	2.01	0.00	Psap_Lrp1
pericytes	AC-like	Lama2	Rpsa	0.92	0.48	1.13	2.88	2.00	0.00	Lama2_Rpsa
TAM	NPC-like	H2-K1	Aplp2	0.58	0.98	3.22	0.77	2.00	0.00	H2-K1_Aplp2
ASC	AC-like	Ptn	Sdc3	0.58	0.95	3.18	0.79	1.99	0.00	Ptn_Sdc3
ASC	AC-like	Ptn	Cdh10	0.54	0.95	3.18	0.79	1.98	0.00	Ptn_Cdh10
ASC	AC-like	Nlgn1	Nrxn1	0.91	0.62	1.34	2.63	1.98	0.00	Nlgn1_Nrxn1
EC	MES-like	H2-K1	Aplp2	0.81	0.94	2.92	1.03	1.97	0.00	H2-K1_Aplp2
EC	aNSC-like	App	Dcc	0.83	0.92	2.43	1.50	1.97	0.00	App_Dcc
inflamed glia	MES-like	Ptn	Ncl	0.88	0.82	2.59	1.33	1.96	0.00	Ptn_Ncl
pericytes	MES-like	1134	Ptprz1	0.96	0.61	1.46	2.43	1.95	0.00	1134_Ptprz1

source	target	ligand	receptor	receptor.prop	ligand.prop	ligand.expr	receptor.expr	lr.mean	pvalue	pairs
TAM	OPC-like	Psap	Gpr3711	0.62	86.0	3.00	0.89	1.94	0.00	Psap_Gpr3711
EC	NPC-like	Арр	Осс	0.79	0.92	2.43	1.45	1.94	0.00	App_Dcc
EC	aNSC-like	Ptn	Ncl	0.91	0.84	2.19	1.69	1.94	0.00	Ptn_Ncl
EC	MES-like	Ptn	Sdc3	0.88	0.84	2.19	1.69	1.94	0.00	Ptn_Sdc3
TAM	AC-like	Psap	Lrp1	0.62	86.0	3.00	0.85	1.93	0.00	Psap_Lrp1
EC	OPC-like	H2-K1	Aplp2	0.68	0.94	2.92	0.93	1.92	0.00	H2-K1_Aplp2
EC	aNSC-like	H2-K1	Aplp2	0.71	0.94	2.92	0.92	1.92	0.00	H2-K1_Aplp2
inflamed glia	AC-like	Ptn	Ncl	0.75	0.82	2.59	1.24	1.92	0.00	Ptn_Ncl
inflamed glia	OPC-like	Ptn	Sdc3	0.78	0.82	2.59	1.19	1.89	0.00	Ptn_Sdc3
EC	MES-like	Cxcl12	Itgb1	0.89	0.76	2.08	1.68	1.88	0.00	Cxcl12_Itgb1
ASC	MES-like	Psap	Gpr3711	0.82	0.83	2.13	1.62	1.87	0.00	Psap_Gpr3711
EC	OPC-like	Ptn	Ncl	0.85	0.84	2.19	1.56	1.87	0.00	Ptn_Ncl
TAM	aNSC-like	Psap	Lrp1	0.61	86.0	3.00	0.74	1.87	0.00	Psap_Lrp1
EC	NPC-like	H2-K1	Aplp2	0.58	0.94	2.92	0.77	1.84	0.00	H2-K1_Aplp2
EC	AC-like	Gnai2	Ednrb	0.75	0.89	2.36	1.30	1.83	0.00	Gnai2_Ednrb
EC	MES-like	Ptn	Sdc4	0.70	0.84	2.19	1.45	1.82	0.00	Ptn_Sdc4
EC	AC-like	Арр	Aplp2	0.76	0.92	2.43	1.18	1.81	0.00	App_Aplp2
inflamed glia	MES-like	Ptn	Ptprs	0.81	0.82	2.59	1.00	1.79	0.00	Ptn_Ptprs
TAM	MES-like	Timp2	Itgb1	68.0	0.85	1.90	1.68	1.79	0.00	Timp2_Itgb1
inflamed glia	OPC-like	Ptn	Ptprs	0.71	0.82	2.59	0.99	1.79	0.00	Ptn_Ptprs
inflamed glia	aNSC-like	Ptn	Sdc3	0.72	0.82	2.59	0.97	1.78	0.00	Ptn_Sdc3
inflamed glia	MES-like	Vim	Cd44	0.64	0.78	2.49	1.06	1.78	0.00	Vim_Cd44

source	target	ligand	receptor	receptor.prop	ligand.prop	ligand.expr	receptor.expr	lr.mean	pvalue	pairs
inflamed glia	NPC-like	Ptn	Ptprs	0.67	0.82	2.59	0.95	1.77	0.00	Ptn_Ptprs
pericytes	MES-like	Lama2	Rpsa	0.96	0.48	1.13	2.41	1.77	0.00	Lama2_Rpsa
EC	MES-like	Cxcl12	Sdc4	0.70	0.76	2.08	1.45	1.77	0.00	Cxcl12_Sdc4
inflamed glia	aNSC-like	Ptn	Ptprs	0.72	0.82	2.59	0.93	1.76	0.00	Ptn_Ptprs
EC	MES-like	Арр	Aplp2	0.81	0.92	2.43	1.03	1.73	0.00	App_Aplp2
inflamed glia	NPC-like	Ptn	Sdc3	0.62	0.82	2.59	0.86	1.72	0.00	Ptn_Sdc3
EC	OPC-like	Арр	Lrp1	0.71	0.92	2.43	1.02	1.72	0.00	App_Lrp1
inflamed glia	AC-like	Ptn	Ptprs	0.63	0.82	2.59	0.84	1.72	0.00	Ptn_Ptprs
inflamed glia	AC-like	Ptn	sdc3	0.58	0.82	2.59	0.79	1.69	0.00	Ptn_Sdc3
EC	OPC-like	Ptn	Sdc3	0.78	0.84	2.19	1.19	1.69	0.00	Ptn_Sdc3
inflamed glia	AC-like	Ptn	Cdh10	0.54	0.82	2.59	0.79	1.69	0.00	Ptn_Cdh10
EC	OPC-like	Арр	Aplp2	0.68	0.92	2.43	0.93	1.68	0.00	App_Aplp2
EC	aNSC-like	Арр	Aplp2	0.71	0.92	2.43	0.92	1.68	0.00	App_Aplp2
EC	AC-like	Арр	Dcc	0.55	0.92	2.43	0.90	1.66	0.00	App_Dcc
EC	AC-like	Арр	Lrp1	0.62	0.92	2.43	0.85	1.64	0.00	App_Lrp1
ASC	AC-like	Psap	Gpr3711	0.68	0.83	2.13	1.11	1.62	0.00	Psap_Gpr3711
EC	OPC-like	Fn1	Itga9	0.76	0.77	1.85	1.39	1.62	0.00	Fn1_Itga9
EC	MES-like	Fn1	Itgav	69.0	0.77	1.85	1.37	1.61	0.00	Fn1_Itgav
EC	NPC-like	Арр	Aplp2	0.58	0.92	2.43	0.77	1.60	0.00	App_Aplp2
EC	MES-like	Ptn	Ptprs	0.81	0.84	2.19	1.00	1.60	0.00	Ptn_Ptprs
EC	MES-like	App	Tspan15	09.0	0.92	2.43	0.75	1.59	0.00	App_Tspan15
EC	OPC-like	Ptn	Ptprs	0.71	0.84	2.19	0.99	1.59	0.00	Ptn_Ptprs

source	target	ligand	receptor	receptor.prop	ligand.prop	ligand.expr	receptor.expr	lr.mean	pvalue	pairs
EC	aNSC-like	App	Lrp1	0.61	0.92	2.43	0.74	1.59	0.00	App_Lrp1
EC	AC-like	Арр	Tspan12	0.58	0.92	2.43	0.74	1.58	0.00	App_Tspan12
EC	OPC-like	Apoe	Lrp1	0.71	0.84	2.15	1.02	1.58	0.00	Apoe_Lrp1
EC	aNSC-like	Gnai2	Igf1r	0.62	68.0	2.36	0.80	1.58	0.00	Gnai2_1gf1r
EC	aNSC-like	Ptn	Sdc3	0.72	0.84	2.19	0.97	1.58	0.00	Ptn_Sdc3
EC	aNSC-like	App	Tspan12	0.63	0.92	2.43	0.72	1.58	0.00	App_Tspan12
ASC	AC-like	Bcan	Nrcam	0.66	0.83	2.14	1.01	1.58	0.00	Bcan_Nrcam
ASC	OPC-like	Psap	Lrp1	0.71	0.83	2.13	1.02	1.57	0.00	Psap_Lrp1
EC	MES-like	Cxcl12	Itgav	0.69	0.76	2.08	1.07	1.57	0.00	Cxcl12_Itgav
EC	NPC-like	Ptn	Ptprs	0.67	0.84	2.19	0.95	1.57	0.00	Ptn_Ptprs
EC	NPC-like	Gnai2	Igf1r	0.57	68.0	2.36	0.77	1.56	0.00	Gnai2_lgf1r
EC	aNSC-like	Gnai2	Ednrb	0.62	68.0	2.36	0.76	1.56	0.00	Gnai2_Ednrb
EC	OPC-like	Gnai2	Ednrb	0.58	68.0	2.36	0.76	1.56	0.00	Gnai2_Ednrb
EC	aNSC-like	Ptn	Ptprs	0.72	0.84	2.19	0.93	1.56	0.00	Ptn_Ptprs
EC	OPC-like	Gnai2	lgf1r	0.55	0.89	2.36	0.73	1.55	0.00	Gnai2_lgf1r
EC	aNSC-like	Fn1	Itga9	0.76	0.77	1.85	1.25	1.55	0.00	Fn1_Itga9
TAM	MES-like	Lgals3bp	Itgb1	0.89	0.75	1.40	1.68	1.54	0.00	Lgals3bp_Itgb1
pericytes	MES-like	Mfge8	Itgav	69.0	62.0	1.99	1.07	1.53	0.00	Mfge8_Itgav
inflamed glia	MES-like	Timp2	Itgb1	0.89	0.52	1.37	1.68	1.53	0.00	Timp2_Itgb1
EC	NPC-like	Fn1	Itga9	69.0	0.77	1.85	1.21	1.53	0.00	Fn1_Itga9
inflamed glia	OPC-like	App	Dcc	0.83	0.58	1.42	1.63	1.52	0.00	App_Dcc
EC	AC-like	Ptn	Ptprs	0.63	0.84	2.19	0.84	1.52	0.00	Ptn_Ptprs

source	target	ligand	receptor	receptor.prop	ligand.prop	ligand.expr	receptor.expr	lr.mean	pvalue	pairs
ASC	OPC-like	Psap	Gpr3711	0.62	0.83	2.13	0.89	1.51	0.00	Psap_Gpr3711
EC	MES-like	Vim	Cd44	0.64	0.82	1.96	1.06	1.51	0.00	Vim_Cd44
EC	AC-like	Apoe	Lrp1	0.62	0.84	2.15	0.85	1.50	0.00	Apoe_Lrp1
ASC	AC-like	Psap	Lrp1	0.62	0.83	2.13	0.85	1.49	0.00	Psap_Lrp1
EC	AC-like	Ptn	Cdh10	0.54	0.84	2.19	0.79	1.49	0.00	Ptn_Cdh10
TAM	MES-like	Timp2	Cd44	0.64	0.85	1.90	1.06	1.48	0.00	Timp2_Cd44
inflamed glia	aNSC-like	Арр	Dcc	0.83	0.58	1.42	1.50	1.46	0.00	App_Dcc
TAM	AC-like	Gnai2	Ednrb	0.75	0.83	1.61	1.30	1.45	0.00	Gnai2_Ednrb
EC	MES-like	Fn1	Cd44	0.64	0.77	1.85	1.06	1.45	0.00	Fn1_Cd44
pericytes	MES-like	Psap	Gpr3711	0.82	0.55	1.28	1.62	1.45	0.00	Psap_Gpr3711
EC	aNSC-like	Apoe	Lrp1	0.61	0.84	2.15	0.74	1.44	0.00	Apoe_Lrp1
inflamed glia	MES-like	Psap	Gpr3711	0.82	0.47	1.26	1.62	1.44	0.00	Psap_Gpr3711
inflamed glia	NPC-like	Арр	Dcc	0.79	0.58	1.42	1.45	1.44	0.00	App_Dcc
EC	AC-like	Cxcl12	Itgb1	0.59	0.76	2.08	0.80	1.44	0.00	Cxcl12_Itgb1
inflamed glia	OPC-like	Pdgfa	Pdgfra	0.89	0.44	1.16	1.71	1.44	0.00	Pdgfa_Pdgfra
ASC	aNSC-like	Psap	Lrp1	0.61	0.83	2.13	0.74	1.44	0.00	Psap_Lrp1
EC	OPC-like	Cxcl12	Itgb1	0.61	0.76	2.08	0.79	1.43	0.00	Cxcl12_Itgb1
pericytes	OPC-like	Арр	Dcc	0.83	0.55	1.23	1.63	1.43	0.00	App_Dcc
EC	MES-like	Fn1	Itga4	0.33	0.77	1.85	1.00	1.42	0.00	Fn1_Itga4
inflamed glia	aNSC-like	Pdgfa	Pdgfra	0.90	0.44	1.16	1.68	1.42	0.00	Pdgfa_Pdgfra
EC	NPC-like	Cxcl12	Itgb1	0.56	0.76	2.08	0.74	1.41	0.00	Cxcl12_Itgb1
EC	MES-like	Psap	Gpr3711	0.82	0.62	1.17	1.62	1.39	0.00	Psap_Gpr3711

source	target	ligand	receptor	receptor.prop	ligand.prop	ligand.expr	receptor.expr	lr.mean	pvalue	pairs
ASC	OPC-like	Ncam1	Ncam2	0.82	65.0	1.20	1.59	1.39	0.00	Ncam1_Ncam2
EC	MES-like	Fn1	Itgb8	0.63	22.0	1.85	0.93	1.39	0.00	Fn1_Itgb8
inflamed glia	MES-like	Col3a1	Itga1	0.67	0.49	1.42	1.34	1.38	0.00	Col3a1_Itga1
pericytes	aNSC-like	Арр	Dcc	0.83	0.55	1.23	1.50	1.37	0.00	App_Dcc
inflamed glia	AC-like	Gnai2	Ednrb	0.75	0.58	1.43	1.30	1.37	0.00	Gnai2_Ednrb
TAM	AC-like	Timp2	Itgb1	0.59	0.85	1.90	0.80	1.35	0.00	Timp2_Itgb1
TAM	MES-like	Sirpa	Cd47	0.69	0.84	1.76	0.94	1.35	0.00	Sirpa_Cd47
TAM	OPC-like	Timp2	Itgb1	0.61	0.85	1.90	0.79	1.34	0.00	Timp2_Itgb1
pericytes	NPC-like	Арр	Dcc	0.79	0.55	1.23	1.45	1.34	0.00	App_Dcc
pericytes	AC-like	Gnai2	Ednrb	0.75	0.61	1.38	1.30	1.34	0.00	Gnai2_Ednrb
ASC	AC-like	Gnai2	Ednrb	0.75	0.64	1.37	1.30	1.34	0.00	Gnai2_Ednrb
inflamed glia	MES-like	Col1a2	Itga1	0.67	0.52	1.33	1.34	1.33	0.00	Colla2_Itga1
TAM	OPC-like	Serpine 2	Lrp1	0.71	0.83	1.65	1.02	1.33	0.00	Serpine 2_Lrp1
TAM	NPC-like	Timp2	Itgb1	0.56	0.85	1.90	0.74	1.32	0.00	Timp2_Itgb1
TAM	OPC-like	Hsp90b1	Lrp1	0.71	0.83	1.61	1.02	1.31	0.00	Hsp90b1_Lrp1
inflamed glia	MES-like	Col1a1	Itga1	0.67	0.44	1.26	1.34	1.30	0.00	Colla1_Itga1
inflamed glia	AC-like	Арр	Aplp2	0.76	85.0	1.42	1.18	1.30	0.00	App_Aplp2
inflamed glia	NPC-like	Pdgfa	Pdgfra	0.81	0.44	1.16	1.44	1.30	0.00	Pdgfa_Pdgfra
inflamed glia	MES-like	Lgals1	Itgb1	0.89	0.36	0.92	1.68	1.30	0.00	Lgals1_Itgb1
ASC	OPC-like	Serpine 2	Lrp1	0.71	0.72	1.56	1.02	1.29	0.00	Serpine 2_Lrp1
ASC	MES-like	Mfge8	Itgav	69.0	0.63	1.46	1.07	1.27	0.00	Mfge8_Itgav
ASC	aNSC-like	Ncam1	Ncam2	0.79	0.59	1.20	1.32	1.26	0.00	Ncam1_Ncam2

source	target	ligand	receptor	receptor.prop	ligand.prop	ligand.expr	receptor.expr	lr.mean	pvalue	pairs
inflamed glia	OPC-like	Ncam1	Ncam2	0.82	0.36	0.92	1.59	1.26	0.01	Ncam1_Ncam2
TAM	AC-like	Serpine 2	Lrp1	0.62	0.83	1.65	0.85	1.25	0.00	Serpine2_Lrp1
pericytes	MES-like	Col4a1	Itga1	0.67	0.50	1.14	1.34	1.24	0.00	Col4a1_Itga1
inflamed glia	MES-like	Col3a1	Itga2	0.42	0.49	1.42	1.05	1.23	0.00	Col3a1_Itga2
inflamed glia	MES-like	Col1a2	Itga9	0.39	0.52	1.33	1.14	1.23	0.00	Col1a2_Itga9
inflamed glia	MES-like	App	Aplp2	0.81	0.58	1.42	1.03	1.22	0.00	App_Aplp2
inflamed glia	OPC-like	Арр	Lrp1	0.71	0.58	1.42	1.02	1.22	0.00	App_Lrp1
inflamed glia	MES-like	Timp2	Cd44	0.64	0.52	1.37	1.06	1.22	0.00	Timp2_Cd44
EC	MES-like	Timp3	Cd44	0.64	0.67	1.37	1.06	1.21	0.00	Timp3_Cd44
inflamed glia	OPC-like	Col1a2	Itgb1	0.61	0.52	1.33	1.09	1.21	0.00	Col1a2_Itgb1
pericytes	AC-like	Арр	Aplp2	0.76	0.55	1.23	1.18	1.21	0.00	App_Aplp2
TAM	aNSC-like	Gnai2	lgf1r	0.62	0.83	1.61	0.80	1.20	0.00	Gnai2_lgf1r
inflamed glia	MES-like	Col1a1	Itga9	0.39	0.44	1.26	1.14	1.20	0.00	Collal_Itga9
pericytes	AC-like	Psap	Gpr37l1	0.68	0.55	1.28	1.11	1.19	0.00	Psap_Gpr3711
inflamed glia	MES-like	Col1a2	Cd44	0.64	0.52	1.33	1.06	1.19	0.00	Col1a2_Cd44
inflamed glia	MES-like	Col1a2	Itga2	0.42	0.52	1.33	1.05	1.19	0.00	Col1a2_Itga2
TAM	NPC-like	Gnai2	lgf1r	0.57	0.83	1.61	0.77	1.19	0.00	Gnai2_1gf1r
TAM	aNSC-like	Gnai2	Ednrb	0.62	0.83	1.61	0.76	1.19	0.00	Gnai2_Ednrb
TAM	OPC-like	Gnai2	Ednrb	0.58	0.83	1.61	0.76	1.18	0.00	Gnai2_Ednrb
pericytes	MES-like	Sdc2	Ptprj	0.71	0.56	1.23	1.14	1.18	0.00	Sdc2_Ptprj
ASC	AC-like	S100a1	Trpm3	0.51	69.0	1.50	0.86	1.18	0.00	S100a1_Trpm3
inflamed glia	OPC-like	App	Aplp2	0.68	0.58	1.42	0.93	1.18	0.00	App_Aplp2

source	target	ligand	receptor	receptor.prop	ligand.prop	ligand.expr	receptor.expr	lr.mean	pvalue	pairs
inflamed glia	OPC-like	Col1a1	Itgb1	0.61	0.44	1.26	1.09	1.18	0.00	Colla1_Itgb1
TAM	OPC-like	Gnai2	Igf1r	0.55	0.83	1.61	0.73	1.17	0.00	Gnai2_lgf1r
inflamed glia	aNSC-like	Арр	Aplp2	0.71	0.58	1.42	0.92	1.17	0.00	App_Aplp2
inflamed glia	MES-like	Col1a1	Cd44	0.64	0.44	1.26	1.06	1.16	0.00	Colla1_Cd44
inflamed glia	AC-like	Арр	Dcc	0.55	0.58	1.42	0.90	1.16	0.00	App_Dcc
inflamed glia	MES-like	Col1a1	Itga2	0.42	0.44	1.26	1.05	1.16	0.00	Colla1_Itga2
inflamed glia	NPC-like	Col1a2	Itgb1	0.56	0.52	1.33	0.98	1.15	0.00	Colla2_Itgb1
pericytes	OPC-like	Plat	Lrp1	0.71	0.56	1.29	1.02	1.15	0.00	Plat_Lrp1
inflamed glia	aNSC-like	Col1a2	Itgb1	0.58	0.52	1.33	0.97	1.15	0.00	Col1a2_Itgb1
pericytes	MES-like	Lama2	Dag1	0.78	0.48	1.13	1.16	1.15	0.00	Lama2_Dag1
EC	MES-like	Sorbs1	Itga1	0.67	99.0	1.29	1.00	1.14	0.00	Sorbs1_Itga1
pericytes	MES-like	Lamc1	Dag1	0.78	0.51	1.12	1.16	1.14	0.00	Lamc1_Dag1
inflamed glia	MES-like	Col5a2	Itga1	0.67	0.37	0.94	1.34	1.14	0.00	Col5a2_Itga1
EC	AC-like	Psap	Gpr3711	0.68	0.62	1.17	1.11	1.14	0.00	Psap_Gpr3711
pericytes	MES-like	Col4a1	Itga9	0.39	0.50	1.14	1.14	1.14	0.00	Col4a1_Itga9
ASC	MES-like	Vim	Cd44	0.64	0.51	1.22	1.06	1.14	0.00	Vim_Cd44
inflamed glia	AC-like	Арр	Lrp1	0.62	0.58	1.42	0.85	1.14	0.00	App_Lrp1
EC	MES-like	Col4a1	Itga1	0.67	0.54	0.93	1.34	1.14	0.00	Col4a1_Itga1
pericytes	MES-like	Lama2	Itga6	0.53	0.48	1.13	1.15	1.14	0.00	Lama2_Itga6
pericytes	MES-like	Lamc1	Itga6	0.53	0.51	1.12	1.15	1.14	0.00	Lamc1_Itga6
pericytes	MES-like	Lama2	Itga9	0.39	0.48	1.13	1.14	1.13	0.00	Lama2_Itga9
inflamed glia	MES-like	Col1a2	Itgb8	0.63	0.52	1.33	0.93	1.13	0.00	Col1a2_Itgb8

source	target	ligand	receptor	receptor.prop	ligand.prop	ligand.expr	receptor.expr	lr.mean	pvalue	pairs
pericytes	MES-like	Арр	Aplp2	0.81	0.55	1.23	1.03	1.13	0.00	App_Aplp2
pericytes	MES-like	Lamc1	Itga9	0.39	0.51	1.12	1.14	1.13	0.00	Lamc1_Itga9
pericytes	OPC-like	Арр	Lrp1	0.71	0.55	1.23	1.02	1.12	0.00	App_Lrp1
inflamed glia	MES-like	S100a4	Erbb3	0.60	0.53	1.41	0.83	1.12	0.00	S100a4_Erbb3
inflamed glia	NPC-like	Col1a1	Itgb1	0.56	0.44	1.26	0.98	1.12	0.00	Col1a1_Itgb1
inflamed glia	aNSC-like	Col1a1	Itgb1	0.58	0.44	1.26	0.97	1.12	0.00	Col1a1_Itgb1
EC	MES-like	Sema7a	Itga1	0.67	0.53	0.89	1.34	1.12	0.00	Sema7a_Itga1
pericytes	OPC-like	Col4a1	Itgb1	0.61	0.50	1.14	1.09	1.11	0.00	Col4a1_Itgb1
ASC	AC-like	Ncam1	Ptpra	0.71	0.59	1.20	1.02	1.11	0.00	Ncam1_Ptpra
pericytes	OPC-like	Lama2	Itgb1	0.61	0.48	1.13	1.09	1.11	0.00	Lama2_Itgb1
EC	OPC-like	Plat	Lrp1	0.71	0.62	1.20	1.02	1.11	0.00	Plat_Lrp1
pericytes	OPC-like	Lamc1	Itgb1	0.61	0.51	1.12	1.09	1.10	0.00	Lamc1_ltgb1
TAM	AC-like	Lgals3bp	Itgb1	0.59	0.75	1.40	0.80	1.10	0.00	Lgals3bp_Itgb1
pericytes	MES-like	Col4a1	Cd44	0.64	0.50	1.14	1.06	1.10	0.00	Col4a1_Cd44
inflamed glia	MES-like	Col1a1	Itgb8	0.63	0.44	1.26	0.93	1.10	0.00	Col1a1_Itgb8
inflamed glia	aNSC-like	Gnai2	Ednrb	0.62	0.58	1.43	0.76	1.10	0.00	Gnai2_Ednrb
pericytes	MES-like	Col4a1	Itga2	0.42	0.50	1.14	1.05	1.10	0.00	Col4a1_Itga2
inflamed glia	OPC-like	Gnai2	Ednrb	0.58	0.58	1.43	0.76	1.10	0.00	Gnai2_Ednrb
EC	MES-like	Pdgfb	Itgav	0.69	0.62	1.12	1.07	1.10	0.00	Pdgfb_Itgav
inflamed glia	NPC-like	App	Aplp2	0.58	0.58	1.42	0.77	1.10	0.00	App_Aplp2
TAM	OPC-like	Lgals3bp	Itgb1	0.61	0.75	1.40	0.79	1.09	0.00	Lgals3bp_Itgb1
pericytes	MES-like	Lama2	Cd44	0.64	0.48	1.13	1.06	1.09	0.00	Lama2_Cd44

source	target	ligand	receptor	receptor.prop	ligand.prop	ligand.expr	receptor.expr	lr.mean	pvalue	pairs
pericytes	MES-like	Lamc1	Cd44	0.64	0.51	1.12	1.06	1.09	0.00	Lamc1_Cd44
TAM	MES-like	Calr	Itgav	0.69	99:0	1.11	1.07	1.09	0.00	Calr_Itgav
pericytes	MES-like	Lama2	Itga2	0.42	0.48	1.13	1.05	1.09	0.00	Lama2_Itga2
pericytes	MES-like	Lamc1	Itga2	0.42	0.51	1.12	1.05	1.09	0.00	Lamc1_Itga2
inflamed glia	MES-like	Арр	Tspan15	0.60	0.58	1.42	0.75	1.09	0.00	App_Tspan15
ASC	aNSC-like	Gnai2	lgf1r	0.62	0.64	1.37	0.80	1.09	0.00	Gnai2_lgf1r
inflamed glia	AC-like	Timp2	Itgb1	0.59	0.52	1.37	0.80	1.09	0.00	Timp2_Itgb1
pericytes	OPC-like	Арр	Aplp2	0.68	0.55	1.23	0.93	1.08	0.00	App_Aplp2
inflamed glia	aNSC-like	Арр	Lrp1	0.61	0.58	1.42	0.74	1.08	0.00	App_Lrp1
inflamed glia	OPC-like	Timp2	Itgb1	0.61	0.52	1.37	0.79	1.08	0.00	Timp2_Itgb1
inflamed glia	AC-like	Арр	Tspan12	0.58	0.58	1.42	0.74	1.08	0.00	App_Tspan12
pericytes	aNSC-like	Арр	Aplp2	0.71	0.55	1.23	0.92	1.08	0.00	App_Aplp2
TAM	NPC-like	Lgals3bp	Itgb1	0.56	0.75	1.40	0.74	1.07	0.00	Lgals3bp_Itgb1
inflamed glia	aNSC-like	Арр	Tspan12	0.63	0.58	1.42	0.72	1.07	0.00	App_Tspan12
pericytes	MES-like	Timp3	Cd44	0.64	0.48	1.09	1.06	1.07	0.00	Timp3_Cd44
pericytes	aNSC-like	Gnai2	Ednrb	0.62	0.61	1.38	0.76	1.07	0.00	Gnai2_Ednrb
EC	OPC-like	Pdgfb	Lrp1	0.71	0.62	1.12	1.02	1.07	0.00	Pdgfb_Lrp1
pericytes	AC-like	Plat	Lrp1	0.62	0.56	1.29	0.85	1.07	0.00	Plat_Lrp1
pericytes	OPC-like	Gnai2	Ednrb	0.58	0.61	1.38	0.76	1.07	0.00	Gnai2_Ednrb
ASC	aNSC-like	Gnai2	Ednrb	0.62	0.64	1.37	0.76	1.07	0.00	Gnai2_Ednrb
ASC	aNSC-like	Ncam1	Cacnalc	0.67	0.59	1.20	0.94	1.07	0.00	Ncam1_Cacna1c
ASC	OPC-like	Gnai2	Ednrb	0.58	0.64	1.37	0.76	1.07	0.00	Gnai2_Ednrb

source	target	ligand	receptor	receptor.prop	ligand.prop	ligand.expr	receptor.expr	lr.mean	pvalue	pairs
TAM	OPC-like	Calr	Lrp1	0.71	99.0	1.11	1.02	1.06	0.00	Calr_Lrp1
pericytes	MES-like	Lama2	Itga1	0.67	0.48	1.13	1.00	1.06	0.00	Lama2_Itga1
pericytes	AC-like	Арр	Dcc	0.55	0.55	1.23	0.90	1.06	0.00	App_Dcc
pericytes	MES-like	Lamc1	Itga1	0.67	0.51	1.12	1.00	1.06	0.00	Lamc1_Itga1
inflamed glia	NPC-like	Timp2	Itgb1	0.56	0.52	1.37	0.74	1.06	0.00	Timp2_Itgb1
pericytes	NPC-like	Col4a1	Itgb1	0.56	0.50	1.14	0.98	1.06	0.00	Col4a1_Itgb1
pericytes	aNSC-like	Col4a1	Itgb1	0.58	0.50	1.14	0.97	1.06	0.00	Col4a1_Itgb1
pericytes	MES-like	Lama2	Itga7	0.31	0.48	1.13	0.98	1.06	0.00	Lama2_Itga7
pericytes	MES-like	Lamc1	Itga7	0.31	0.51	1.12	0.98	1.05	0.00	Lamc1_Itga7
ASC	OPC-like	Ncam1	Cacnalc	0.63	65.0	1.20	0.91	1.05	0.00	Ncam1_Cacna1c
pericytes	NPC-like	Lama2	Itgb1	0.56	0.48	1.13	0.98	1.05	0.00	Lama2_Itgb1
inflamed glia	MES-like	Timp3	Cd44	0.64	0.40	1.04	1.06	1.05	0.00	Timp3_Cd44
pericytes	aNSC-like	Lama2	Itgb1	0.58	0.48	1.13	0.97	1.05	0.00	Lama2_Itgb1
pericytes	NPC-like	Lamc1	Itgb1	0.56	0.51	1.12	0.98	1.05	0.00	Lamc1_Itgb1
pericytes	aNSC-like	Lamc1	Itgb1	0.58	0.51	1.12	0.97	1.05	0.00	Lamc1_Itgb1
pericytes	AC-like	Арр	Lrp1	0.62	0.55	1.23	0.85	1.04	0.00	App_Lrp1
EC	MES-like	Pkm	Cd44	0.64	0.59	1.03	1.06	1.04	0.00	Pkm_Cd44
pericytes	MES-like	Col4a1	Cd47	0.69	0.50	1.14	0.94	1.04	0.00	Col4a1_Cd47
pericytes	MES-like	Col4a1	Itgb8	0.63	0.50	1.14	0.93	1.04	0.00	Col4a1_Itgb8
EC	MES-like	Col4a1	Itga9	0.39	0.54	0.93	1.14	1.03	0.00	Col4a1_Itga9
pericytes	MES-like	Lama2	Itgb8	0.63	0.48	1.13	0.93	1.03	0.00	Lama2_Itgb8
pericytes	MES-like	Lamc1	Itgb8	0.63	0.51	1.12	0.93	1.03	0.00	Lamc1_Itgb8

source	target	ligand	receptor	receptor.prop	ligand.prop	ligand.expr	receptor.expr	lr.mean	pvalue	pairs
inflamed glia	AC-like	Col1a2	Itga9	0.44	0.52	1.33	0.72	1.03	00.0	Colla2_Itga9
EC	AC-like	Plat	Lrp1	0.62	0.62	1.20	0.85	1.02	00.0	Plat_Lrp1
pericytes	aNSC-like	Plat	Lrp1	0.61	0.56	1.29	0.74	1.01	0.00	Plat_Lrp1
EC	OPC-like	Col4a1	Itgb1	0.61	0.54	0.93	1.09	1.01	00.0	Col4a1_Itgb1
ASC	MES-like	Ncam1	Gfra1	0.58	0.59	1.20	0.82	1.01	0.00	Ncam1_Gfra1
ASC	MES-like	Timp3	Cd44	0.64	0.51	0.95	1.06	1.00	00.0	Timp3_Cd44
pericytes	NPC-like	Арр	Aplp2	0.58	0.55	1.23	0.77	1.00	0.00	App_Aplp2
inflamed glia	MES-like	Col5a2	Itga2	0.42	0.37	0.94	1.05	1.00	0.00	Col5a2_Itga2
pericytes	MES-like	Pkm	Cd44	0.64	0.46	0.94	1.06	1.00	0.00	Pkm_Cd44
EC	MES-like	Col4a1	Cd44	0.64	0.54	0.93	1.06	1.00	00.0	Col4a1_Cd44
inflamed glia	AC-like	Col1a1	Itga 9	0.44	0.44	1.26	0.72	66.0	00.0	Colla1_Itga9
EC	MES-like	Col4a1	Itga2	0.42	0.54	0.93	1.05	0.99	0.00	Col4a1_Itga2
pericytes	MES-like	Арр	Tspan15	09.0	0.55	1.23	0.75	66.0	0.00	App_Tspan15
EC	AC-like	Sptan1	Ptpra	0.71	0.57	0.96	1.02	0.99	0.00	Sptan1_Ptpra
TAM	MES-like	Pkm	Cd44	0.64	0.59	0.92	1.06	0.99	0.00	Pkm_Cd44
EC	AC-like	Pdgfb	Lrp1	0.62	0.62	1.12	0.85	0.99	0.00	Pdgfb_Lrp1
pericytes	aNSC-like	Арр	Lrp1	0.61	0.55	1.23	0.74	0.99	00.0	App_Lrp1
pericytes	AC-like	Арр	Tspan12	0.58	0.55	1.23	0.74	0.98	0.00	App_Tspan12
inflamed glia	AC-like	Pdgfa	Pdgfra	0.52	0.44	1.16	0.80	0.98	0.00	Pdgfa_Pdgfra
pericytes	aNSC-like	Арр	Tspan12	0.63	0.55	1.23	0.72	0.98	0.00	App_Tspan12
EC	aNSC-like	Plat	Lrp1	0.61	0.62	1.20	0.74	0.97	0.00	Plat_Lrp1
pericytes	MES-like	Vim	Cd44	0.64	0.36	0.87	1.06	96.0	0.00	Vim_Cd44

source	target	ligand	receptor	receptor.prop	ligand.prop	ligand.expr	receptor.expr	lr.mean	pvalue	pairs
EC	NPC-like	Col4a1	Itgb1	0.56	0.54	0.93	0.98	0.95	0.00	Col4a1_Itgb1
EC	aNSC-like	Col4a1	Itgb1	0.58	0.54	0.93	0.97	0.95	0.00	Col4a1_Itgb1
EC	MES-like	Col4a1	Cd47	0.69	0.54	0.93	0.94	0.93	0.00	Col4a1_Cd47
EC	MES-like	Col4a1	Itgb8	0.63	0.54	0.93	0.93	0.93	0.00	Col4a1_Itgb8
pericytes	AC-like	Col4a1	Itga9	0.44	0.50	1.14	0.72	0.93	0.00	Col4a1_Itga9
EC	aNSC-like	Pdgfb	Lrp1	0.61	0.62	1.12	0.74	0.93	0.00	Pdgfb_Lrp1
pericytes	AC-like	Lama2	Itga9	0.44	0.48	1.13	0.72	0.92	0.00	Lama2_Itga9
ASC	MES-like	Sirpa	Cd47	0.69	0.49	0.91	0.94	0.92	0.00	Sirpa_Cd47
pericytes	AC-like	Lamc1	Itga9	0.44	0.51	1.12	0.72	0.92	0.00	Lamc1_Itga9
EC	MES-like	Sptan1	Ptpra	0.76	0.57	0.96	0.86	0.91	0.00	Sptan1_Ptpra
EC	OPC-like	Sptan1	Ptpra	0.62	0.57	96.0	0.77	0.87	0.00	Sptan1_Ptpra
EC	aNSC-like	Sptan1	Ptpra	0.64	0.57	0.96	0.76	0.86	0.00	Sptan1_Ptpra
inflamed glia	AC-like	Lgals1	Itgb1	0.59	0.36	0.92	0.80	98.0	0.00	Lgals1_Itgb1
inflamed glia	OPC-like	Lgals1	Itgb1	0.61	0.36	0.92	0.79	0.85	0.00	Lgals1_Itgb1
inflamed glia	NPC-like	Lgals1	Itgb1	0.56	0.36	0.92	0.74	0.83	0.00	Lgals1_Itgb1
EC	AC-like	Col4a1	Itga9	0.44	0.54	0.93	0.72	0.83	0.00	Col4a1_Itga9

Output of the LIANA analysis performed in R, including I-r pairs with significant p-value.

noire	pairs	App_Rpsa	App_Rpsa	Apoe_Lrp1	C1qb_C1qbp	App_Rpsa	Ptn_Ptprz1	C1qb_C1qbp	C1qb_C1qbp	Ptn_Ptprz1	C1qb_C1qbp	App_Rpsa	Ptn_Ptprz1	Apoe_Lrp1	C1qb_C1qbp	Ptn_Ptprz1	Ptn_Ptprz1	Ptn_Ptprz1	Ptn_Ptprz1	Ptn_Ncl	C1qb_Lrp1	Ptn_Ptprz1
onlean	pvalue	0.00	0.00	00.0	00.0	0.00	0.00	0.00	0.00	0.00	0.00	0.00	0.00	00.0	0.00	0.00	00.0	00.0	00.0	00.0	0.00	0.00
lr moon	II.IIIcali	3.10	3.08	3.06	2.99	2.95	2.94	2.93	2.93	2.91	2.90	2.88	2.79	2.79	2.78	2.77	2.77	2.75	2.74	2.66	2.65	2.62
recentor ever	idva:ioidanai	3.86	3.81	0.68	1.37	3.55	3.07	1.24	1.24	3.02	1.18	3.41	2.77	0.68	0.94	3.07	3.07	3.02	3.02	2.52	0.68	2.77
liand over	ııganıd.expi	2.35	2.35	5.44	4.62	2.35	2.81	4.62	4.62	2.81	4.62	2.35	2.81	4.89	4.62	2.48	2.46	2.48	2.46	2.81	4.62	2.48
ligand pron	ngana.prop	0.87	0.87	1.00	66.0	0.87	0.86	66.0	0.99	0.86	66.0	0.87	0.86	0.94	66.0	0.85	09:0	0.85	09:0	98.0	66.0	0.85
rocentor neon	doid:ioidanai	1.00	0.99	0.59	0.87	0.99	0.98	0.88	0.78	0.97	0.77	0.99	0.98	0.59	0.77	0.98	0.98	0.97	0.97	0.99	0.59	0.98
rocontor	ioidanai	Rpsa	Rpsa	Lrp1	C1qbp	Rpsa	Ptprz1	C1qbp	C1qbp	Ptprz1	C1qbp	Rpsa	Ptprz1	Lrp1	C1qbp	Ptprz1	Ptprz1	Ptprz1	Ptprz1	Ncl	Lrp1	Ptprz1
ligand	ıığanın	Арр	Арр	Apoe	C1qb	App	Ptn	C1qb	C1qb	Ptn	C1qb	App	Ptn	Apoe	C1qb	Ptn	Ptn	Ptn	Ptn	Ptn	C1qb	Ptn
tanget	ıaığıı	aNSC-like	OPC-like	OPC-like	OPC-like	AC-like	OPC-like	aNSC-like	MES-like	AC-like	AC-like	MES-like	aNSC-like	OPC-like	NPC-like	OPC-like	OPC-like	AC-like	AC-like	aNSC-like	OPC-like	aNSC-like
9541109	sonnos	EC	EC	ASC	TAM	EC	ASC	TAM	TAM	ASC	TAM	EC	ASC	TAM	TAM	EC	pericytes	EC	pericytes	ASC	TAM	EC

source	target	ligand	receptor	receptor.prop	ligand.prop	ligand.expr	receptor.expr	lr.mean	pvalue	pairs
ASC	NPC-like	Ptn	Ncl	0.98	98.0	2.81	2.44	2.62	0.00	Ptn_Ncl
pericytes	aNSC-like	Ptn	Ptprz1	0.98	0.60	2.46	2.77	2.62	0.00	Ptn_Ptprz1
ASC	OPC-like	Ptn	Ncl	0.97	98.0	2.81	2.29	2.55	0.00	Ptn_Ncl
pericytes	NPC-like	Арр	Rpsa	1.00	0.49	1.08	3.96	2.52	0.00	App_Rpsa
ASC	MES-like	Ptn	Ptprz1	0.94	0.86	2.81	2.20	2.50	0.00	Ptn_Ptprz1
EC	aNSC-like	Ptn	Ncl	0.99	0.85	2.48	2.52	2.50	0.00	Ptn_Ncl
pericytes	aNSC-like	Ptn	Ncl	0.99	09.0	2.46	2.52	2.49	0.00	Ptn_Ncl
pericytes	aNSC-like	App	Rpsa	1.00	0.49	1.08	3.86	2.47	0.00	App_Rpsa
EC	NPC-like	Ptn	Ncl	0.98	0.85	2.48	2.44	2.46	0.00	Ptn_Ncl
pericytes	NPC-like	Ptn	Ncl	0.98	09.0	2.46	2.44	2.45	0.00	Ptn_Ncl
pericytes	OPC-like	Арр	Rpsa	0.99	0.49	1.08	3.81	2.45	0.00	App_Rpsa
inflamed glia	NPC-like	App	Rpsa	1.00	0.55	0.90	3.96	2.43	0.01	App_Rpsa
EC	OPC-like	Ptn	Ncl	0.97	0.85	2.48	2.29	2.38	0.00	Ptn_Ncl
pericytes	OPC-like	Ptn	Ncl	0.97	09.0	2.46	2.29	2.38	0.00	Ptn_Ncl
ASC	AC-like	Ptn	Ncl	0.91	0.86	2.81	1.89	2.35	0.00	Ptn_Nc1
pericytes	AC-like	Арр	Rpsa	0.99	0.49	1.08	3.55	2.32	0.00	App_Rpsa
TAM	MES-like	Timp2	Itgb1	0.87	0.90	2.71	1.71	2.21	0.00	Timp2_Itgb1
TAM	MES-like	Psap	Gpr3711	0.80	0.94	2.93	1.45	2.19	0.00	Psap_Gpr3711
inflamed glia	OPC-like	Mdk	Ptprz1	0.98	0.55	1.23	3.07	2.15	0.00	Mdk_Ptprz1
TAM	AC-like	Psap	Gpr3711	0.76	0.94	2.93	1.34	2.13	0.00	Psap_Gpr3711
inflamed glia	AC-like	Mdk	Ptprz1	0.97	0.55	1.23	3.02	2.12	0.00	Mdk_Ptprz1
TAM	OPC-like	Psap	Gpr3711	0.78	0.94	2.93	1.25	2.09	0.00	Psap_Gpr3711

source	target	ligand	receptor	receptor.prop	ligand.prop	ligand.expr	receptor.expr	lr.mean	pvalue	pairs
ASC	OPC-like	Ncam1	Ptprz1	0.98	0.47	1.09	3.07	2.08	0.00	Ncam1_Ptprz1
inflamed glia	OPC-like	Ncam1	Ptprz1	0.98	0.55	1.08	3.07	2.08	0.00	Ncam1_Ptprz1
ASC	AC-like	Ncam1	Ptprz1	0.97	0.47	1.09	3.02	2.05	00.0	Ncam1_Ptprz1
inflamed glia	AC-like	Ncam1	Ptprz1	0.97	0.55	1.08	3.02	2.05	0.00	Ncam1_Ptprz1
TAM	MES-like	H2-K1	Aplp2	0.78	0.91	2.88	1.23	2.05	0.00	H2-K1_Aplp2
EC	AC-like	Gnai2	Ednrb	0.83	98.0	2.38	1.68	2.03	00.0	Gnai2_Ednrb
TAM	AC-like	H2-K1	Aplp2	0.77	0.91	2.88	1.16	2.02	0.00	H2-K1_Aplp2
TAM	AC-like	Timp2	Itgb1	0.81	06.0	2.71	1.29	2.00	00.0	Timp2_Itgb1
inflamed glia	aNSC-like	Mdk	Ptprz1	0.98	0.55	1.23	2.77	2.00	0.00	Mdk_Ptprz1
TAM	OPC-like	Timp2	Itgb1	0.83	06.0	2.71	1.28	1.99	00.0	Timp2_Itgb1
pericytes	MES-like	Vtn	Itgav	0.36	02.0	2.81	1.06	1.94	00.0	Vtn_Itgav
TAM	aNSC-like	Timp2	Itgb1	0.84	06.0	2.71	1.15	1.93	00.0	Timp2_Itgb1
ASC	aNSC-like	Ncam1	Ptprz1	0.98	0.47	1.09	2.77	1.93	00.0	Ncam1_Ptprz1
inflamed glia	aNSC-like	Ncam1	Ptprz1	0.98	0.55	1.08	2.77	1.93	0.00	Ncam1_Ptprz1
EC	MES-like	Cxcl12	Itgb1	0.87	0.67	2.07	1.71	1.89	0.00	Cxcl12_Itgb1
EC	MES-like	H2-K1	Aplp2	0.78	68.0	2.56	1.23	1.89	0.00	H2-K1_Aplp2
inflamed glia	aNSC-like	Mdk	Ncl	66.0	9:22	1.23	2.52	1.87	00.0	Mdk_Nd
TAM	OPC-like	H2-K1	Aplp2	69.0	0.91	2.88	0.85	1.86	00.0	H2-K1_Aplp2
EC	AC-like	H2-K1	Aplp2	0.77	68.0	2.56	1.16	1.86	00.0	H2-K1_Aplp2
TAM	aNSC-like	Psap	Gpr3711	0.62	0.94	2.93	0.77	1.85	0.00	Psap_Gpr3711
inflamed glia	MES-like	Lgals1	Itgb1	0.87	0.73	1.98	1.71	1.85	0.00	Lgals1_Itgb1
TAM	aNSC-like	H2-K1	Aplp2	0.77	0.91	2.88	0.81	1.84	0.00	H2-K1_Aplp2

source	target	ligand	receptor	receptor.prop	ligand.prop	ligand.expr	receptor.expr	lr.mean	pvalue	pairs
ASC	OPC-like	Ptn	Ptprs	0.72	98.0	2.81	0.87	1.84	0.00	Ptn_Ptprs
inflamed glia	NPC-like	Mdk	Ncl	0.98	0.55	1.23	2.44	1.83	0.00	Mdk_Ncl
pericytes	AC-like	Vtn	Itgav	0.35	0.70	2.81	0.83	1.82	0.00	Vtn_Itgav
TAM	OPC-like	Psap	Lrp1	0.59	0.94	2.93	0.68	1.81	0.00	Psap_Lrp1
pericytes	MES-like	Vtn	Cd47	0.59	0.70	2.81	0.78	1.80	0.00	Vtn_Cd47
ASC	OPC-like	Ptn	Sdc3	0.65	98.0	2.81	0.77	1.79	0.00	Ptn_Sdc3
EC	MES-like	Арр	Aplp2	0.78	0.87	2.35	1.23	1.79	0.00	App_Aplp2
ASC	aNSC-like	Ptn	Ptprs	0.74	98.0	2.81	0.76	1.79	0.00	Ptn_Ptprs
ASC	MES-like	Ptn	Sdc4	0.52	98.0	2.81	0.75	1.78	0.00	Ptn_Sdc4
TAM	MES-like	Lgals3bp	Itgb1	0.87	0.77	1.82	1.71	1.77	0.00	Lgals3bp_Itgb1
ASC	AC-like	Ptn	Ptprs	0.58	0.86	2.81	0.72	1.77	0.00	Ptn_Ptprs
TAM	NPC-like	H2-K1	Aplp2	0.63	0.91	2.88	0.66	1.77	0.00	H2-K1_Aplp2
pericytes	OPC-like	Vtn	Itgav	0.19	0.70	2.81	0.72	1.77	0.00	Vtn_Itgav
inflamed glia	OPC-like	Mdk	Ncl	0.97	0.55	1.23	2.29	1.76	0.01	Mdk_Ncl
ASC	MES-like	Ptn	Sdc3	0.47	0.86	2.81	0.70	1.75	0.00	Ptn_Sdc3
EC	AC-like	Арр	Aplp2	0.77	0.87	2.35	1.16	1.75	0.00	App_Aplp2
inflamed glia	AC-like	Gnai2	Ednrb	0.83	0.82	1.77	1.68	1.72	0.00	Gnai2_Ednrb
EC	OPC-like	Gnai2	Ednrb	0.70	98.0	2.38	1.04	1.71	0.00	Gnai2_Ednrb
EC	OPC-like	H2-K1	Aplp2	69.0	68.0	2.56	0.85	1.70	0.00	H2-K1_Aplp2
EC	AC-like	Cxcl12	Itgb1	0.81	0.67	2.07	1.29	1.68	0.00	Cxcl12_Itgb1
EC	aNSC-like	H2-K1	Aplp2	0.77	0.89	2.56	0.81	1.68	0.00	H2-K1_Aplp2
EC	OPC-like	Ptn	Ptprs	0.72	0.85	2.48	0.87	1.68	0.00	Ptn_Ptprs

source	target	ligand	receptor	receptor.prop	ligand.prop	ligand.expr	receptor.expr	lr.mean	pvalue	pairs
EC	OPC-like	Cxcl12	Itgb1	0.83	0.67	2.07	1.28	1.68	0.00	Cxcl12_Itgb1
pericytes	OPC-like	Ptn	Ptprs	0.72	0.60	2.46	0.87	1.67	0.00	Ptn_Ptprs
TAM	AC-like	Gnai2	Ednrb	0.83	62.0	1.66	1.68	1.67	0.00	Gnai2_Ednrb
inflamed glia	MES-like	Timp2	Itgb1	0.87	0.64	1.57	1.71	1.64	0.00	Timp2_Itgb1
inflamed glia	AC-like	Lgals1	Itgb1	0.81	0.73	1.98	1.29	1.64	0.00	Lgals1_Itgb1
EC	aNSC-like	Gnai2	Ednrb	0.72	0.86	2.38	0.89	1.63	0.00	Gnai2_Ednrb
inflamed glia	OPC-like	Lgals1	Itgb1	0.83	0.73	1.98	1.28	1.63	0.00	Lgals1_Itgb1
EC	OPC-like	Ptn	Sdc3	0.65	0.85	2.48	0.77	1.63	0.00	Ptn_Sdc3
EC	aNSC-like	Ptn	Ptprs	0.74	0.85	2.48	0.76	1.62	0.00	Ptn_Ptprs
pericytes	OPC-like	Ptn	Sdc3	0.65	09.0	2.46	0.77	1.62	0.00	Ptn_Sdc3
EC	MES-like	Ptn	Sdc4	0.52	0.85	2.48	0.75	1.62	0.00	Ptn_Sdc4
EC	aNSC-like	Cxcl12	Itgb1	0.84	0.67	2.07	1.15	1.61	0.00	Cxcl12_Itgb1
pericytes	aNSC-like	Ptn	Ptprs	0.74	09.0	2.46	0.76	1.61	0.01	Ptn_Ptprs
pericytes	MES-like	Ptn	Sdc4	0.52	09:0	2.46	0.75	1.61	0.00	Ptn_Sdc4
EC	NPC-like	H2-K1	Aplp2	0.63	0.89	2.56	0.66	1.61	0.00	H2-K1_Aplp2
EC	AC-like	Ptn	Ptprs	0.58	0.85	2.48	0.72	1.60	0.00	Ptn_Ptprs
pericytes	MES-like	Lgals1	Itgb1	0.87	0.62	1.48	1.71	1.60	0.00	Lgals1_Itgb1
EC	OPC-like	App	Aplp2	0.69	0.87	2.35	0.85	1.60	0.00	App_Aplp2
EC	MES-like	Ptn	Sdc3	0.47	0.85	2.48	0.70	1.59	0.00	Ptn_Sdc3
pericytes	MES-like	Ptn	Sdc3	0.47	0.60	2.46	0.70	1.58	0.01	Ptn_Sdc3
EC	aNSC-like	App	Aplp2	0.77	0.87	2.35	0.81	1.58	0.00	App_Aplp2
inflamed glia	aNSC-like	Lgals1	Itgb1	0.84	0.73	1.98	1.15	1.57	0.00	Lgals1_Itgb1

source	target	ligand	receptor	receptor.prop	ligand.prop	ligand.expr	receptor.expr	lr.mean	pvalue	pairs
TAM	AC-like	Lgals3bp	Itgb1	0.81	0.77	1.82	1.29	1.56	0.00	Lgals3bp_Itgb1
EC	NPC-like	Gnai2	Ednrb	0.59	98.0	2.38	0.73	1.55	0.00	Gnai2_Ednrb
TAM	OPC-like	Lgals3bp	Itgb1	0.83	22.0	1.82	1.28	1.55	0.00	Lgals3bp_Itgb1
EC	AC-like	App	Tspan12	0.60	78.0	2.35	0.73	1.54	0.00	App_Tspan12
EC	OPC-like	App	Lrp1	0.59	0.87	2.35	0.68	1.52	0.00	App_Lrp1
EC	NPC-like	App	Aplp2	0.63	28.0	2.35	0.66	1.50	00.0	App_Aplp2
pericytes	AC-like	Gnai2	Ednrb	0.83	0.56	1.31	1.68	1.49	0.00	Gnai2_Ednrb
TAM	aNSC-like	Lgals3bp	Itgb1	0.84	22.0	1.82	1.15	1.49	00.0	Lgals3bp_Itgb1
EC	MES-like	Fn1	Itgav	0.36	0.73	1.80	1.06	1.43	0.00	Fn1_Itgav
inflamed glia	AC-like	Timp2	Itgb1	0.81	0.64	1.57	1.29	1.43	00.0	Timp2_Itgb1
ASC	MES-like	Psap	Gpr3711	0.80	95.0	1.41	1.45	1.43	00.0	Psap_Gpr3711
inflamed glia	OPC-like	Timp2	Itgb1	0.83	0.64	1.57	1.28	1.42	00.0	Timp2_Itgb1
EC	MES-like	Cxcl12	Sdc4	0.52	29.0	2.07	0.75	1.41	0.00	Cxcl12_Sdc4
inflamed glia	OPC-like	Gnai2	Ednrb	0.70	0.82	1.77	1.04	1.41	0.00	Gnai2_Ednrb
pericytes	AC-like	Lgals1	Itgb1	0.81	0.62	1.48	1.29	1.39	0.00	Lgals1_Itgb1
EC	MES-like	Col4a1	Itga1	0.65	0.58	1.34	1.43	1.38	0.00	Col4a1_Itga1
pericytes	OPC-like	Lgals1	Itgb1	0.83	0.62	1.48	1.28	1.38	00.0	Lgals1_Itgb1
EC	OPC-like	Apoe	Lrp1	0.59	82.0	2.07	0.68	1.37	00.0	Apoe_Lrp1
ASC	AC-like	Psap	Gpr3711	0.76	95.0	1.41	1.34	1.37	00.0	Psap_Gpr3711
inflamed glia	MES-like	Psap	Gpr3711	0.80	0.64	1.30	1.45	1.37	0.01	Psap_Gpr3711
EC	MES-like	Fn1	Itga4	0.12	0.73	1.80	0.92	1.36	0.00	Fn1_Itga4
inflamed glia	aNSC-like	Timp2	Itgb1	0.84	0.64	1.57	1.15	1.36	0.01	Timp2_Itgb1

source	target	ligand	receptor	receptor.prop	ligand.prop	ligand.expr	receptor.expr	lr.mean	pvalue	pairs
TAM	OPC-like	Gnai2	Ednrb	0.70	0.79	1.66	1.04	1.35	0.00	Gnai2_Ednrb
ASC	OPC-like	Psap	Gpr3711	0.78	0.56	1.41	1.25	1.33	0.00	Psap_Gpr3711
pericytes	aNSC-like	Lgals1	Itgb1	0.84	0.62	1.48	1.15	1.32	0.00	Lgals1_Itgb1
EC	AC-like	Fn1	Itgav	0.35	0.73	1.80	0.83	1.32	0.00	Fn1_Itgav
TAM	aNSC-like	Gnai2	Ednrb	0.72	0.79	1.66	0.89	1.27	0.00	Gnai2_Ednrb
EC	OPC-like	Fn1	Itgav	0.19	0.73	1.80	0.72	1.26	0.00	Fn1_Itgav
pericytes	MES-like	Col4a1	Itga1	0.65	0.42	1.09	1.43	1.26	0.00	Col4a1_Itga1
TAM	OPC-like	Hsp90b1	Lrp1	0.59	0.80	1.80	0.68	1.24	0.00	Hsp90b1_Lrp1
ASC	OPC-like	Serpine 2	Lrp1	0.59	89.0	1.77	0.68	1.23	0.00	Serpine 2_Lrp1
EC	MES-like	Col4a2	Itga1	0.65	0.50	1.01	1.43	1.22	0.00	Col4a2_Itga1
pericytes	MES-like	Psap	Gpr3711	0.80	0.45	0.95	1.45	1.20	0.00	Psap_Gpr3711
TAM	NPC-like	Gnai2	Ednrb	0.59	62.0	1.66	0.73	1.19	0.00	Gnai2_Ednrb
EC	MES-like	Psap	Gpr3711	0.80	0.46	0.91	1.45	1.18	0.00	Psap_Gpr3711
EC	MES-like	Col4a1	Itga 2	0.22	0.58	1.34	0.98	1.16	0.00	Col4a1_Itga2
pericytes	MES-like	Арр	Aplp2	0.78	0.49	1.08	1.23	1.15	0.00	App_Aplp2
pericytes	AC-like	Psap	Gpr3711	0.76	0.45	0.95	1.34	1.14	0.00	Psap_Gpr3711
EC	MES-like	Col4a1	Itga9	0.12	0.58	1.34	0.92	1.13	00.0	Col4a1_Itga9
EC	AC-like	Psap	Gpr3711	0.76	0.46	0.91	1.34	1.12	0.00	Psap_Gpr3711
TAM	OPC-like	Calr	Lrp1	0.59	0.73	1.56	0.68	1.12	0.00	Calr_Lrp1
pericytes	AC-like	Арр	Aplp2	0.77	0.49	1.08	1.16	1.12	0.00	App_Aplp2
pericytes	OPC-like	Psap	Gpr3711	0.78	0.45	0.95	1.25	1.10	0.01	Psap_Gpr3711
inflamed glia	MES-like	Mdk	Itga6	0.23	0.55	1.23	0.97	1.10	0.00	Mdk_Itga6

source	target	ligand	receptor	receptor.prop	ligand.prop	ligand.expr	receptor.expr	lr.mean	pvalue	pairs
ASC	aNSC-like	Psap	Gpr3711	0.62	0.56	1.41	0.77	1.09	0.00	Psap_Gpr3711
EC	OPC-like	Col4a1	Itga9	0.39	0.58	1.34	0.83	1.08	0.00	Col4a1_Itga9
EC	OPC-like	Psap	Gpr3711	0.78	0.46	0.91	1.25	1.08	0.00	Psap_Gpr3711
inflamed glia	MES-like	Mdk	Itga4	0.12	0.55	1.23	0.92	1.07	0.00	Mdk_Itga4
inflamed glia	MES-like	App	Aplp2	0.78	0.55	0.90	1.23	1.06	0.00	App_Aplp2
EC	MES-like	Col4a1	Cd47	0.59	0.58	1.34	0.78	1.06	0.00	Col4a1_Cd47
ASC	OPC-like	Psap	Lrp1	0.59	0.56	1.41	0.68	1.05	0.00	Psap_Lrp1
pericytes	MES-like	Col4a1	Itga 2	0.22	0.42	1.09	0.98	1.04	0.00	Col4a1_Itga2
EC	AC-like	Col4a1	Itga1	0.17	0.58	1.34	0.73	1.03	0.00	Col4a1_Itga1
inflamed glia	AC-like	App	Aplp2	0.77	0.55	0.90	1.16	1.03	0.01	App_Aplp2
ASC	AC-like	Ncam1	Ptpra	0.72	0.47	1.09	0.96	1.02	0.00	Ncam1_Ptpra
EC	aNSC-like	Col4a1	Itga9	0.34	0.58	1.34	0.70	1.02	0.00	Col4a1_Itga9
inflamed glia	OPC-like	Pdgfa	Pdgfra	0.77	0.45	0.93	1.11	1.02	0.00	Pdgfa_Pdgfra
inflamed glia	AC-like	Ncam1	Ptpra	0.72	0.55	1.08	0.96	1.02	0.00	Ncam1_Ptpra
inflamed glia	AC-like	Mdk	Itga6	0.25	0.55	1.23	0.79	1.01	0.00	Mdk_1tga6
pericytes	MES-like	Col4a1	Itga9	0.12	0.42	1.09	0.92	1.00	0.00	Col4a1_Itga9
inflamed glia	OPC-like	Mdk	Sdc3	0.65	0.55	1.23	0.77	1.00	0.00	Mdk_Sdc3
EC	MES-like	Col4a2	Itga2	0.22	0.50	1.01	0.98	1.00	0.00	Col4a2_Itga2
inflamed glia	MES-like	Mdk	Sdc4	0.52	0.55	1.23	0.75	0.99	0.00	Mdk_Sdc4
EC	MES-like	Col4a2	Itga9	0.12	0.50	1.01	0.92	96.0	0.00	Col4a2_Itga9
inflamed glia	MES-like	Mdk	Sdc3	0.47	0.55	1.23	0.70	96.0	0.01	Mdk_Sdc3
pericytes	OPC-like	App	Aplp2	0.69	0.49	1.08	0.85	96.0	0.00	App_Aplp2

source	target	ligand	receptor	receptor.prop	ligand.prop	ligand.expr	receptor.expr	lr.mean	pvalue	pairs
inflamed glia	aNSC-like	Pdgfa	Pdgfra	0.80	0.45	0.93	0.99	96.0	0.00	Pdgfa_Pdgfra
pericytes	OPC-like	Col4a1	Itga9	0.39	0.42	1.09	0.83	0.96	0.00	Col4a1_Itga9
inflamed glia	OPC-like	Mdk	Lrp1	0.59	0.55	1.23	0.68	0.95	0.01	Mdk_Lrp1
pericytes	aNSC-like	App	Aplp2	0.77	0.49	1.08	0.81	0.94	0.00	App_Aplp2
pericytes	MES-like	Col4a1	Cd47	0.59	0.42	1.09	0.78	0.94	0.00	Col4a1_Cd47
inflamed glia	MES-like	Cxcl10	Sdc4	0.52	0.27	1.12	0.75	0.94	0.00	Cxcl10_Sdc4
EC	OPC-like	Col4a2	Itga9	0.39	0.50	1.01	0.83	0.92	0.00	Col4a2_Itga9
EC	AC-like	Sptan1	Ptpra	0.72	0.45	0.88	0.96	0.92	0.00	Sptan1_Ptpra
pericytes	AC-like	Col4a1	Itga1	0.17	0.42	1.09	0.73	0.91	0.00	Col4a1_Itga1
TAM	MES-like	Sirpa	Cd47	0.59	0.60	1.02	0.78	0.90	0.00	Sirpa_Cd47
pericytes	AC-like	App	Tspan12	0.60	0.49	1.08	0.73	0.90	0.00	App_Tspan12
pericytes	aNSC-like	Col4a1	Itga9	0.34	0.42	1.09	0.70	0.90	0.00	Col4a1_Itga9
pericytes	OPC-like	Арр	Lrp1	0.59	0.49	1.08	0.68	0.88	0.00	App_Lrp1
EC	AC-like	Col4a2	Itga1	0.17	0.50	1.01	0.73	0.87	0.00	Col4a2_Itga1
pericytes	NPC-like	App	Aplp2	0.63	0.49	1.08	0.66	0.87	0.00	App_Aplp2
EC	aNSC-like	Col4a2	Itga9	0.34	0.50	1.01	0.70	0.86	0.00	Col4a2_Itga9
TAM	MES-like	Ccl5	Sdc4	0.52	0.37	96.0	0.75	0.86	0.00	Ccl5_Sdc4
inflamed glia	NPC-like	Pdgfa	Pdgfra	0.60	0.45	0.93	0.73	0.83	0.00	Pdgfa_Pdgfra
inflamed glia	MES-like	Cc15	Sdc4	0.52	0.27	0.87	0.75	0.81	0.00	Ccl5_Sdc4

## Appendix C

## Colophon

This document was set in the Times Roman typeface using LaTeX and BibTeX, composed with a text editor. The figures were generated using Adobe Illustrator software and Biorender. ChatGPT-40 was used for support with document structure and formatting.

## **Bibliography**

- Addington, Caroline P, Adam Roussas, Dipankar Dutta and Sarah E Stabenfeldt (2015). 'Endogenous repair signaling after brain injury and complementary bioengineering approaches to enhance neural regeneration: Supplementary issue: Stem cell biology'. In: *Biomarker insights* 10, BMI–S20062.
- Agnihotri, Sameer and Gelareh Zadeh (2015). 'Metabolic reprogramming in glioblastoma: the influence of cancer metabolism on epigenetics and unanswered questions'. In: *Neuro-oncology* 18.2, pp. 160–172.
- Albulescu, Radu, Elena Codrici, Ionela Daniela Popescu, Simona Mihai, Laura Georgiana Necula, Daniel Petrescu, Mihaela Teodoru and Cristiana Pistol Tanase (2013). 'Cytokine patterns in brain tumour progression'. In: *Mediators of inflammation* 2013.1, p. 979748.
- Alcantara Llaguno, Sheila R and Luis F Parada (2016). 'Cell of origin of glioma: biological and clinical implications'. In: *British journal of cancer* 115.12, pp. 1445–1450.
- Aldape, Kenneth, Gelareh Zadeh, Sheila Mansouri, Guido Reifenberger and Andreas von Deimling (2015). 'Glioblastoma: pathology, molecular mechanisms and markers'. In: *Acta neuropathologica* 129, pp. 829–848.

- Alexandris, Athanasios S, Jiwon Ryu, Labchan Rajbhandari, Robert Harlan, James McKenney, Yiqing Wang, Susan Aja, David Graham, Arun Venkatesan and Vassilis E Koliatsos (2022). 'Protective effects of NAMPT or MAPK inhibitors and NaR on Wallerian degeneration of mammalian axons'. In: *Neurobiology of disease* 171, p. 105808.
- Ali, Md Yousuf, Claudia R Oliva, Abu Shadat M Noman, Bryan G Allen, Prabhat C Goswami, Yousef Zakharia, Varun Monga, Douglas R Spitz, John M Buatti and Corinne E Griguer (2020). 'Radioresistance in Glioblastoma and the Development of Radiosensitizers'. In: *Cancers* 12.9, p. 2511.
- Alvarez, Susana, Mihai Moldovan and Christian Krarup (2008). 'Acute energy restriction triggers Wallerian degeneration in mouse'. In: *Experimental neurology* 212.1, pp. 166–178.
- An, Joseph, Emily Freeman, Ian J Stewart and Michael Dore (2024). 'Association of traumatic brain injury and glioblastoma multiforme: a case series'. In: *Military Medicine* 189.1-2, e391–e395.
- Andersen, Rikke Sick, Atul Anand, Dylan Scott Lykke Harwood and Bjarne Winther Kristensen (2021). 'Tumor-associated microglia and macrophages in the glioblastoma microenvironment and their implications for therapy'. In: *Cancers* 13.17, p. 4255.
- Anderson, Mark A, Yan Ao and Michael V Sofroniew (2014). 'Heterogeneity of reactive astrocytes'. In: *Neuroscience letters* 565, pp. 23–29.
- Anderson, Mark A, Joshua E Burda, Yilong Ren, Yan Ao, Timothy M O'Shea, Riki Kawaguchi, Giovanni Coppola, Baljit S Khakh, Timothy J Deming and Michael

- V Sofroniew (2016). 'Astrocyte scar formation aids central nervous system axon regeneration'. In: *Nature* 532.7598, pp. 195–200.
- Apte, Rajendra S, Daniel S Chen and Napoleone Ferrara (2019). 'VEGF in signaling and disease: beyond discovery and development'. In: *Cell* 176.6, pp. 1248–1264.
- Armstrong, Terri S., Robin Grant, Mark R. Gilbert, Jong Woo Lee and Andrew D. Norden (Nov. 2015). 'Epilepsy in glioma patients: mechanisms, management, and impact of anticonvulsant therapy'. In: *Neuro-Oncology* 18.6, pp. 779–789. ISSN: 1522-8517. DOI: 10.1093/neuonc/nov269. eprint: https://academic.oup.com/neuro-oncology/article-pdf/18/6/779/11281251/nov269.pdf. URL: https://doi.org/10.1093/neuonc/nov269.
- Aziz, Peer Asad, Salma Farrukh Memon, Mubarak Hussain, A Rauf Memon, Kiran Abbas, Shurjeel Uddin Qazi, Riaz AR Memon, Kanwal Ali Qambrani, Osama Taj, Shamas Ghazanfar et al. (2023). 'Supratotal Resection: An Emerging Concept of Glioblastoma Multiforme Surgery—Systematic Review And Meta-Analysis'. In: World Neurosurgery 179, e46–e55.
- Badve, Chaitra and Andrew E Sloan (2015). Modeling the growth dynamics of glioblastoma using magnetic resonance imaging.
- Bagley, Stephen J, Arati S Desai, Gerald P Linette, Carl H June and Donald M O'Rourke (2018). 'CAR T-cell therapy for glioblastoma: recent clinical advances and future challenges'. In: *Neuro-oncology* 20.11, pp. 1429–1438.
- Bao, Shideng, Qiulian Wu, Roger E McLendon, Yueling Hao, Qing Shi, Anita B Hjelmeland, Mark W Dewhirst, Darell D Bigner and Jeremy N Rich (2006). 'Glioma stem cells promote radioresistance by preferential activation of the DNA damage response'. In: *nature* 444.7120, pp. 756–760.

- Bazzoni, Riccardo and Angela Bentivegna (2019). 'Role of notch signaling pathway in glioblastoma pathogenesis'. In: *Cancers* 11.3, p. 292.
- Beier, Dagmar, Peter Hau, Martin Proescholdt, Annette Lohmeier, Jörg Wischhusen, Peter J Oefner, Ludwig Aigner, Alexander Brawanski, Ulrich Bogdahn and Christoph P Beier (2007). 'CD133+ and CD133- glioblastoma-derived cancer stem cells show differential growth characteristics and molecular profiles'. In: *Cancer research* 67.9, pp. 4010–4015.
- Beirowski, Bogdan (2022). 'Emerging evidence for compromised axonal bioenergetics and axoglial metabolic coupling as drivers of neurodegeneration'. In: *Neurobiology of disease* 170, p. 105751.
- Bellail, Anita C, Stephen B Hunter, Daniel J Brat, Chalet Tan and Erwin G Van Meir (2004). 'Microregional extracellular matrix heterogeneity in brain modulates glioma cell invasion'. In: *The international journal of biochemistry & cell biology* 36.6, pp. 1046–1069.
- Berger, Felicitas, Corinna Lau, Mathias Dahlmann and Mathias Ziegler (2005). 
  'Subcellular compartmentation and differential catalytic properties of the three human nicotinamide mononucleotide adenylyltransferase isoforms'. In: *Journal of Biological Chemistry* 280.43, pp. 36334–36341.
- Bergo, E., G. Lombardi, I. Guglieri, E. Capovilla, A. Pambuku and V. Zagone (2019). 'Neurocognitive functions and health-related quality of life in glioblastoma patients: a concise review of the literature'. In: *Eur J Cancer Care (Engl)* 28.1, e12410. ISSN: 0961-5423. DOI: 10.1111/ecc.12410.

- Bernard-Arnoux, F, M Lamure, F Ducray, Gilles Aulagner, J Honnorat and Xavier Armoiry (2016). 'The cost-effectiveness of tumor-treating fields therapy in patients with newly diagnosed glioblastoma'. In: *Neuro-oncology* 18.8, pp. 1129–1136.
- Bernstock, Joshua D, Sam E Gary, Neil Klinger, Pablo A Valdes, Walid Ibn Essayed, Hannah E Olsen, Gustavo Chagoya, Galal Elsayed, Daisuke Yamashita, Patrick Schuss et al. (2022). 'Standard clinical approaches and emerging modalities for glioblastoma imaging'. In: *Neuro-Oncology Advances* 4.1, vdac080.
- Bhat, Gh Rasool, Itty Sethi, Hana Q Sadida, Bilal Rah, Rashid Mir, Naseh Algehainy, Ibrahim Altedlawi Albalawi, Tariq Masoodi, Gowtham Kumar Subbaraj, Farrukh Jamal et al. (2024). 'Cancer cell plasticity: from cellular, molecular, and genetic mechanisms to tumor heterogeneity and drug resistance'. In: *Cancer and Metastasis Reviews* 43.1, pp. 197–228.
- Bhat, Krishna PL, Veerakumar Balasubramaniyan, Brian Vaillant, Ravesanker Ezhilarasan, Karlijn Hummelink, Faith Hollingsworth, Khalida Wani, Lindsey Heathcock, Johanna D James, Lindsey D Goodman et al. (2013). 'Mesenchymal differentiation mediated by NF-κB promotes radiation resistance in glioblastoma'. In: *Cancer cell* 24.3, pp. 331–346.
- Binabaj, Maryam Moradi, Afsane Bahrami, Soodabeh ShahidSales, Marjan Joodi, Mona Joudi Mashhad, Seyed Mahdi Hassanian, Kazem Anvari and Amir Avan (2018). 'The prognostic value of MGMT promoter methylation in glioblastoma: a meta-analysis of clinical trials'. In: *Journal of cellular physiology* 233.1, pp. 378–386.
- Birner, Peter, Maria Piribauer, Ingeborg Fischer, Brigitte Gatterbauer, Christine Marosi, Peter F Ambros, Inge M Ambros, Markus Bredel, Georg Oberhuber, Karl Rössler et al. (2003). 'Vascular patterns in glioblastoma influence clinical outcome

- and associate with variable expression of angiogenic proteins: evidence for distinct angiogenic subtypes'. In: *Brain pathology* 13.2, pp. 133–143.
- Blondel, Vincent D, Jean-Loup Guillaume, Renaud Lambiotte and Etienne Lefebvre (2008). 'Fast unfolding of communities in large networks'. In: *Journal of statistical mechanics: theory and experiment* 2008.10, P10008.
- Bollaerts, Ilse, Jessie Van Houcke, Lien Andries, Lies De Groef and Lieve Moons (2017). 'Neuroinflammation as fuel for axonal regeneration in the injured vertebrate central nervous system'. In: *Mediators of inflammation* 2017.1, p. 9478542.
- Braganza, M. Z., C. M. Kitahara, A. Berrington de González, P. D. Inskip, K. J. Johnson and P. Rajaraman (2012). 'Ionizing radiation and the risk of brain and central nervous system tumors: a systematic review'. In: *Neuro Oncol* 14.11, pp. 1316–24. ISSN: 1522-8517 (Print) 1522-8517. DOI: 10.1093/neuonc/nos208.
- Braganza, M. Z., P. Rajaraman, Y. Park, P. D. Inskip, N. D. Freedman, A. R. Hollenbeck, A. Berrington de González and C. M. Kitahara (2014). 'Cigarette smoking, alcohol intake, and risk of glioma in the NIH-AARP Diet and Health Study'. In: *British Journal of Cancer* 110.1, pp. 242–248. ISSN: 1532-1827. DOI: 10.1038/bjc.2013.611. URL: https://doi.org/10.1038/bjc.2013.611.
- Brennan, Cameron W, Roel GW Verhaak, Aaron McKenna, Benito Campos, Houtan Noushmehr, Sofie R Salama, Siyuan Zheng, Debyani Chakravarty, J Zachary Sanborn, Samuel H Berman et al. (2013). 'The somatic genomic landscape of glioblastoma'. In: *cell* 155.2, pp. 462–477.
- Brock, Amy, Silva Krause and Donald E Ingber (2015). 'Control of cancer formation by intrinsic genetic noise and microenvironmental cues'. In: *Nature Reviews Cancer* 15.8, pp. 499–509.

- Brooks, Lucy J, Melanie P Clements, Jemima J Burden, Daniela Kocher, Luca Richards, Sara Castro Devesa, Leila Zakka, Megan Woodberry, Michael Ellis, Zane Jaunmuktane et al. (2021). 'The white matter is a pro-differentiative niche for glioblastoma'. In: *Nature communications* 12.1, p. 2184.
- Brooks, Lucy J, Holly Simpson Ragdale, Ciaran Scott Hill, Melanie Clements and Simona Parrinello (2022). 'Injury programs shape glioblastoma'. In: *Trends in Neurosciences* 45.11, pp. 865–876.
- Brooks, Michael D, Rajarshi Sengupta, Steven C Snyder and Joshua B Rubin (2013). 'Hitting them where they live: targeting the glioblastoma perivascular stem cell niche'. In: *Current pathobiology reports* 1, pp. 101–110.
- Brown, Christine E, Darya Alizadeh, Renate Starr, Lihong Weng, Jamie R Wagner, Araceli Naranjo, Julie R Ostberg, M Suzette Blanchard, Julie Kilpatrick, Jennifer Simpson et al. (2016). 'Regression of glioblastoma after chimeric antigen receptor T-cell therapy'. In: *New England Journal of Medicine* 375.26, pp. 2561–2569.
- Brown, Timothy J, Matthew C Brennan, Michael Li, Ephraim W Church, Nicholas J Brandmeir, Kevin L Rakszawski, Akshal S Patel, Elias B Rizk, Dima Suki, Raymond Sawaya et al. (2016). 'Association of the extent of resection with survival in glioblastoma: a systematic review and meta-analysis'. In: *JAMA oncology* 2.11, pp. 1460–1469.
- Buonfiglioli, Alice and Dolores Hambardzumyan (2021). 'Macrophages and microglia: the cerberus of glioblastoma'. In: *Acta neuropathologica communications* 9, pp. 1–21.
- Burda, Joshua E, Timothy M O'Shea, Yan Ao, Keshav B Suresh, Shinong Wang, Alexander M Bernstein, Ashu Chandra, Sandeep Deverasetty, Riki Kawaguchi, Jae

- H Kim et al. (2022). 'Divergent transcriptional regulation of astrocyte reactivity across disorders'. In: *Nature* 606.7914, pp. 557–564.
- Butenschoen, Vicki Marie, Anna Kelm, Bernhard Meyer and Sandro M Krieg (2019). 'Quality-adjusted life years in glioma patients: A systematic review on currently available data and the lack of evidence-based utilities'. In: *Journal of neuro-oncology* 144, pp. 1–9.
- Cahill, Kirk E, Ramin A Morshed and Bakhtiar Yamini (2015). 'Nuclear factor-κB in glioblastoma: insights into regulators and targeted therapy'. In: *Neuro-oncology* 18.3, pp. 329–339.
- Calabrese, Christopher, Helen Poppleton, Mehmet Kocak, Twala L Hogg, Christine Fuller, Blair Hamner, Eun Young Oh, M Waleed Gaber, David Finklestein, Meredith Allen et al. (2007). 'A perivascular niche for brain tumor stem cells'. In: *Cancer cell* 11.1, pp. 69–82.
- Campos, Benito, Lars Rønn Olsen, T Urup and HS Poulsen (2016). 'A comprehensive profile of recurrent glioblastoma'. In: *Oncogene* 35.45, pp. 5819–5825.
- Cedergren Weber, Gustav, Jonathan Timpka, Anna Rydelius, Johan Bengzon and Per Odin (2023). 'Tumoral parkinsonism—Parkinsonism secondary to brain tumors, paraneoplastic syndromes, intracranial malformations, or oncological intervention, and the effect of dopaminergic treatment'. In: *Brain and Behavior* 13.8, e3151.
- Chaichana, Kaisorn L, Scott L Parker, Alessandro Olivi and Alfredo Quiñones-Hinojosa (2009). 'Long-term seizure outcomes in adult patients undergoing primary resection of malignant brain astrocytomas'. In: *Journal of neurosurgery* 111.2, pp. 282–292.

- Chapman, Astrid G (2000). 'Glutamate and epilepsy'. In: *The Journal of nutrition* 130.4, 1043S–1045S.
- Chen, Andrew X, Robyn D Gartrell, Junfei Zhao, Pavan S Upadhyayula, Wenting Zhao, Jinzhou Yuan, Hanna E Minns, Athanassios Dovas, Jeffrey N Bruce, Anna Lasorella et al. (2021). 'Single-cell characterization of macrophages in glioblastoma reveals MARCO as a mesenchymal pro-tumor marker'. In: *Genome medicine* 13.1, p. 88.
- Chen, Kui, Hugo Andrade-Barazarte, Wenjia Liang, Qingyun Zhu, Haixing Guo, Yanxin Li, Haichun Li and Rongjun Qian (2022). 'Post-traumatic brain injury glioma: Characteristics, report of 2 cases report and literature review'. In: *Medicine* 101.52, e32477.
- Chen, Ruihuan, Merry C Nishimura, Stephanie M Bumbaca, Samir Kharbanda, William F Forrest, Ian M Kasman, Joan M Greve, Robert H Soriano, Laurie L Gilmour, Celina Sanchez Rivers et al. (2010). 'A hierarchy of self-renewing tumor-initiating cell types in glioblastoma'. In: *Cancer cell* 17.4, pp. 362–375.
- Chernoff, Jonathan (2021). 'The two-hit theory hits 50'. In: *Molecular biology of the cell* 32.22, rt1.
- Chkheidze, Rati, Jack Raisanen, Jeffrey Gagan, Timothy E Richardson, Marco C Pinho, Karuna Raj, Michael Achilleos, Chenelle Slepicka, Charles L White, Bret M Evers et al. (2021). 'Alterations in the RB pathway with inactivation of RB1 characterize glioblastomas with a primitive neuronal component'. In: *Journal of Neuropathology* & Experimental Neurology 80.12, pp. 1092–1098.
- Cieri, Maria Belen, Alejandro Villarreal, Dante Daniel Gomez-Cuautle, Ingrid Mailing and Alberto Javier Ramos (2023). 'Progression of reactive gliosis and astroglial

- phenotypic changes following stab wound-induced traumatic brain injury in mice'. In: *Journal of Neurochemistry* 167.2, pp. 183–203.
- Clements, Melanie, Holly Simpson Ragdale, Claudia Garcia-Diaz and Simona Parrinello (2024). 'Generation of immunocompetent somatic glioblastoma mouse models through in situ transformation of subventricular zone neural stem cells'.

  In: STAR protocols 5.1, p. 102928.
- Coleman, Michael P and Marc R Freeman (2010). 'Wallerian degeneration, wlds, and nmnat'. In: *Annual review of neuroscience* 33.1, pp. 245–267.
- Colopi, Ambra, Serena Fuda, Samuele Santi, Angelo Onorato, Valeriana Cesarini, Maurizio Salvati, Carmela Rita Balistreri, Susanna Dolci and Eugenia Guida (2023). 'Impact of age and gender on glioblastoma onset, progression, and management'. In: *Mechanisms of Ageing and Development* 211, p. 111801. ISSN: 0047-6374. DOI: https://doi.org/10.1016/j.mad.2023.111801. URL: https://www.sciencedirect.com/science/article/pii/S0047637423000271.
- Conti, Luciano, Steven M Pollard, Thorsten Gorba, Erika Reitano, Mauro Toselli, Gerardo Biella, Yirui Sun, Sveva Sanzone, Qi-Long Ying, Elena Cattaneo et al. (2005). 'Niche-independent symmetrical self-renewal of a mammalian tissue stem cell'. In: *PLoS biology* 3.9, e283.
- Coquerel, Bérénice, Florent Poyer, Frédéric Torossian, Virginie Dulong, Georges Bellon, Isabelle Dubus, Annie Reber and Jean-Pierre Vannier (2009). 'Elastin-derived peptides: matrikines critical for glioblastoma cell aggressiveness in a 3-D system'. In: *Glia* 57.16, pp. 1716–1726.
- Couturier, Charles P, Shamini Ayyadhury, Phuong U Le, Javad Nadaf, Jean Monlong, Gabriele Riva, Redouane Allache, Salma Baig, Xiaohua Yan, Mathieu Bourgey et

- al. (2020). 'Single-cell RNA-seq reveals that glioblastoma recapitulates a normal neurodevelopmental hierarchy'. In: *Nature communications* 11.1, p. 3406.
- Couturier, Charles P, Javad Nadaf, Zhaorong Li, Salma Baig, Gabriele Riva, Phuong Le, Daan J Kloosterman, Jean Monlong, Andriniaina Nkili Meyong, Redouane Allache et al. (2022). 'Glioblastoma scRNA-seq shows treatment-induced, immune-dependent increase in mesenchymal cancer cells and structural variants in distal neural stem cells'. In: *Neuro-oncology* 24.9, pp. 1494–1508.
- Cuddapah, Vishnu Anand, Stefanie Robel, Stacey Watkins and Harald Sontheimer (2014). 'A neurocentric perspective on glioma invasion'. In: *Nature Reviews Neuroscience* 15.7, pp. 455–465.
- Dadon-Nachum, Michal, Eldad Melamed and Daniel Offen (2011). 'The "dying-back" phenomenon of motor neurons in ALS'. In: *Journal of molecular neuroscience* 43, pp. 470–477.
- Das, Anisha, Shengxian Ding, Rongjie Liu and Chao Huang (2023). 'Quantifying the Growth of Glioblastoma Tumors Using Multimodal MRI Brain Images'. In: *Cancers* 15.14, p. 3614.
- De Silva, Manam Inushi, Brett W Stringer and Cedric Bardy (2023). 'Neuronal and tumourigenic boundaries of glioblastoma plasticity'. In: *Trends in cancer* 9.3, pp. 223–236.
- Dick, John E (2009). 'Looking ahead in cancer stem cell research'. In: *Nature biotechnology* 27.1, pp. 44–46.
- Díez Valle, Ricardo, Constantinos G Hadjipanayis and Walter Stummer (2019). 'Established and emerging uses of 5-ALA in the brain: an overview'. In: *Journal of Neuro-oncology* 141, pp. 487–494.

- Dimitrov, Daniel, Dénes Türei, Martin Garrido-Rodriguez, Paul L Burmedi, James S Nagai, Charlotte Boys, Ricardo O Ramirez Flores, Hyojin Kim, Bence Szalai, Ivan G Costa et al. (2022). 'Comparison of methods and resources for cell-cell communication inference from single-cell RNA-Seq data'. In: *Nature communications* 13.1, p. 3224.
- Dipro, S., F. Al-Otaibi, A. Alzahrani, A. Ulhaq and E. Al Shail (2012). 'Turcot syndrome: a synchronous clinical presentation of glioblastoma multiforme and adenocarcinoma of the colon'. In: *Case Rep Oncol Med* 2012, p. 720273. ISSN: 2090-6706 (Print). DOI: 10.1155/2012/720273.
- Dirkse, Anne, Anna Golebiewska, Thomas Buder, Petr V Nazarov, Arnaud Muller, Suresh Poovathingal, Nicolaas HC Brons, Sonia Leite, Nicolas Sauvageot, Dzjemma Sarkisjan et al. (2019). 'Stem cell-associated heterogeneity in Glioblastoma results from intrinsic tumor plasticity shaped by the microenvironment'. In: *Nature communications* 10.1, p. 1787.
- Donat, Cornelius K, Gregory Scott, Steve M Gentleman and Magdalena Sastre (2017). 'Microglial activation in traumatic brain injury'. In: *Frontiers in aging neuroscience* 9, p. 208.
- Dong, Minhai, Xiaolin Zhang, Peng Peng, Zirong Chen, Yang Zhang, Lijun Wan, Wang Xiang, Guohao Liu, Yang Guo, Qungen Xiao et al. (2024). 'Hypoxia-induced TREM1 promotes mesenchymal-like states of glioma stem cells via alternatively activating tumor-associated macrophages'. In: *Cancer Letters* 590, p. 216801.
- Doran, Ciara G, Ryoichi Sugisawa, Michael Carty, Fiona Roche, Claire Fergus, Karsten Hokamp, Vincent P Kelly and Andrew G Bowie (2021). 'CRISPR/Cas9-mediated SARM1 knockout and epitope-tagged mice reveal that SARM1 does not regulate

- nuclear transcription, but is expressed in macrophages'. In: *Journal of Biological Chemistry* 297.6.
- Dorrier, Cayce E, Hannah E Jones, Lucija Pintarić, Julie A Siegenthaler and Richard Daneman (2022). 'Emerging roles for CNS fibroblasts in health, injury and disease'. In: *Nature Reviews Neuroscience* 23.1, pp. 23–34.
- Drucker, Kristen L, Robert B Jenkins and Daniel Schramek (2025). 'Switching Drivers: Epigenetic Rewiring to Genetic Progression in Glioma'. In: *Cancer Research* 85.5, pp. 836–837.
- Ellis, Hayley P, Mark Greenslade, Ben Powell, Inmaculada Spiteri, Andrea Sottoriva and Kathreena M Kurian (2015). 'Current challenges in glioblastoma: intratumour heterogeneity, residual disease, and models to predict disease recurrence'. In: Frontiers in oncology 5, p. 251.
- Elsayed, Heba, Alessandro Faroni, Mohammad R. Ashraf, Judith Osuji, Lydia Wunderley, Ling Zhang, Hesham Elsobky, Mohamed Mansour, Ashraf S. Zidan and Adam J. Reid (2020). 'Development and Characterisation of an in vitro Model of Wallerian Degeneration'. In: Frontiers in Bioengineering and Biotechnology Volume 8 2020. ISSN: 2296-4185. DOI: 10.3389/fbioe.2020.00784. URL: https://www.frontiersin.org/journals/bioengineering-and-biotechnology/articles/10.3389/fbioe.2020.00784.
- Ennaceur, Abdelkader and Jean Delacour (1988). 'A new one-trial test for neurobiological studies of memory in rats. 1: Behavioral data'. In: *Behavioural brain research* 31.1, pp. 47–59.
- Essuman, Kow, Daniel W Summers, Yo Sasaki, Xianrong Mao, Aaron DiAntonio and Jeffrey Milbrandt (2017). 'The SARM1 toll/interleukin-1 receptor domain

- possesses intrinsic NAD+ cleavage activity that promotes pathological axonal degeneration'. In: *Neuron* 93.6, pp. 1334–1343.
- Everhard, Sibille, Jörg Tost, Hafida El Abdalaoui, Emmanuelle Crinière, Florence Busato, Yannick Marie, Ivo G Gut, Marc Sanson, Karima Mokhtari, Florence Laigle-Donadey et al. (2009). 'Identification of regions correlating MGMT promoter methylation and gene expression in glioblastomas'. In: *Neuro-oncology* 11.4, pp. 348–356.
- Feng, Guoping, Rebecca H Mellor, Michael Bernstein, Cynthia Keller-Peck, Quyen T Nguyen, Mia Wallace, Jeanne M Nerbonne, Jeff W Lichtman and Joshua R Sanes (2000). 'Imaging neuronal subsets in transgenic mice expressing multiple spectral variants of GFP'. In: *Neuron* 28.1, pp. 41–51.
- Fernandes, Catarina, Andreia Costa, Lígia Osório, Rita Costa Lago, Paulo Linhares, Bruno Carvalho and Cláudia Caeiro (2017). 'Current standards of care in glioblastoma therapy'. In: *Exon Publications*, pp. 197–241.
- Fernandez-Castaneda, Anthony and Alban Gaultier (2016). 'Adult oligodendrocyte progenitor cells–multifaceted regulators of the CNS in health and disease'. In: *Brain, behavior, and immunity* 57, pp. 1–7.
- Figley, Matthew D, Weixi Gu, Jeffrey D Nanson, Yun Shi, Yo Sasaki, Katie Cunnea, Alpeshkumar K Malde, Xinying Jia, Zhenyao Luo, Forhad K Saikot et al. (2021). 'SARM1 is a metabolic sensor activated by an increased NMN/NAD+ ratio to trigger axon degeneration'. In: *Neuron* 109.7, pp. 1118–1136.
- Filppu, Pauliina, Jayendrakishore Tanjore Ramanathan, Kirsi J Granberg, Erika Gucciardo, Hannu Haapasalo, Kaisa Lehti, Matti Nykter, Vadim Le Joncour and Pirjo Laakkonen (2021). 'CD109-GP130 interaction drives glioblastoma stem

- cell plasticity and chemoresistance through STAT3 activity'. In: *JCI insight* 6.9, e141486.
- Finn, J. T., M. Weil, F. Archer, R. Siman, A. Srinivasan and M. C. Raff (2000). 'Evidence that Wallerian degeneration and localized axon degeneration induced by local neurotrophin deprivation do not involve caspases'. In: *J Neurosci* 20.4, pp. 1333–41. ISSN: 0270-6474 (Print) 0270-6474. DOI: 10.1523/jneurosci.20-04-01333.2000.
- Francis, Joshua M, Cheng-Zhong Zhang, Cecile L Maire, Joonil Jung, Veronica E Manzo, Viktor A Adalsteinsson, Heather Homer, Sam Haidar, Brendan Blumenstiel, Chandra Sekhar Pedamallu et al. (2014). 'EGFR variant heterogeneity in glioblastoma resolved through single-nucleus sequencing'. In: *Cancer discovery* 4.8, pp. 956–971.
- Friedmann-Morvinski, Dinorah, Eric A Bushong, Eugene Ke, Yasushi Soda, Tomotoshi Marumoto, Oded Singer, Mark H Ellisman and Inder M Verma (2012). 'Dedifferentiation of neurons and astrocytes by oncogenes can induce gliomas in mice'. In: *Science* 338.6110, pp. 1080–1084.
- Fueyo, Juan, Candelaria Gomez-Manzano, Ramon Alemany, Polly SY Lee, Timothy J McDonnell, Paraskevi Mitlianga, Yue-Xi Shi, VA Levin, WK Yung and Athanassios P Kyritsis (2000). 'A mutant oncolytic adenovirus targeting the Rb pathway produces anti-glioma effect in vivo'. In: *Oncogene* 19.1, pp. 2–12.
- Gaillard, Frank, Paul Ryan and Lam Le (Nov. 2008). 'Glioblastoma, IDH-wildtype'. en. In: *Radiopaedia.org*. Radiopaedia.org.
- Galvao, Rui Pedro, Anita Kasina, Robert S McNeill, Jordan E Harbin, Oded Foreman, Roel GW Verhaak, Akiko Nishiyama, C Ryan Miller and Hui Zong (2014).

'Transformation of quiescent adult oligodendrocyte precursor cells into malignant glioma through a multistep reactivation process'. In: *Proceedings of the National Academy of Sciences* 111.40, E4214–E4223.

## Gangoso,

Ester, Benjamin Southgate, Leanne Bradley, Stefanie Rus, Felipe Galvez-Cancino, Niamh McGivern, Esra Güç, Chantriolnt-Andreas Kapourani, Adam Byron, Kirsty M Ferguson et al. (2021). 'Glioblastomas acquire myeloid-affiliated transcriptional programs via epigenetic immunoediting to elicit immune evasion'. In: *Cell* 184.9, pp. 2454–2470.

- Gao, Ruli, Shanshan Bai, Ying C Henderson, Yiyun Lin, Aislyn Schalck, Yun Yan, Tapsi Kumar, Min Hu, Emi Sei, Alexander Davis et al. (2021). 'Delineating copy number and clonal substructure in human tumors from single-cell transcriptomes'. In: *Nature biotechnology* 39.5, pp. 599–608.
- Garcia-Diaz, Claudia, Anni Pöysti, Elisabetta Mereu, Melanie P Clements, Lucy J Brooks, Felipe Galvez-Cancino, Simon P Castillo, Wenhao Tang, Gordon Beattie, Lilas Courtot et al. (2023). 'Glioblastoma cell fate is differentially regulated by the microenvironments of the tumor bulk and infiltrative margin'. In: *Cell Reports* 42.5.
- Garten, Antje, Susanne Schuster, Melanie Penke, Theresa Gorski, Tommaso De Giorgis and Wieland Kiess (2015). 'Physiological and pathophysiological roles of NAMPT and NAD metabolism'. In: *Nature Reviews Endocrinology* 11.9, pp. 535–546.
- Gaudet, Andrew D, Phillip G Popovich and Matt S Ramer (2011). 'Wallerian degeneration: gaining perspective on inflammatory events after peripheral nerve injury'. In: *Journal of neuroinflammation* 8, pp. 1–13.

- Gerstner, Elizabeth R, A Gregory Sorensen, Rakesh K Jain and Tracy T Batchelor (2009). 'Anti-vascular endothelial growth factor therapy for malignant glioma'.

  In: Current neurology and neuroscience reports 9.3, pp. 254–262.
- Ghosh, Mitrajit, Anna M Lenkiewicz and Bozena Kaminska (2022). 'The interplay of tumor vessels and immune cells affects immunotherapy of glioblastoma'. In: *Biomedicines* 10.9, p. 2292.
- Gil-Perotín, Sara, María Duran-Moreno, Arantxa Cebrián-Silla, Mónica Ramírez, Paula García-Belda and José Manuel García-Verdugo (2013). 'Adult neural stem cells from the subventricular zone: a review of the neurosphere assay'. In: *The Anatomical Record* 296.9, pp. 1435–1452.
- Gilley, Jonathan and Michael P Coleman (2010). 'Endogenous Nmnat2 is an essential survival factor for maintenance of healthy axons'. In: *PLoS biology* 8.1, e1000300.
- Gilley, Jonathan, Richard R Ribchester and Michael P Coleman (2017). 'Sarm1 deletion, but not WldS, confers lifelong rescue in a mouse model of severe axonopathy'. In: *Cell reports* 21.1, pp. 10–16.
- Giovannoni, Federico and Francisco J Quintana (2020). 'The role of astrocytes in CNS inflammation'. In: *Trends in immunology* 41.9, pp. 805–819.
- Golán-Cancela, Irene and Laia Caja (2024). 'The TGF-β family in glioblastoma'. In:

  International Journal of Molecular Sciences 25.2, p. 1067.
- Goldner, Ron and Avraham Yaron (2017). 'TIR axons apart: unpredicted NADase controls axonal degeneration'. In: *Neuron* 93.6, pp. 1239–1241.
- Grech, N., T. Dalli, S. Mizzi, L. Meilak, N. Calleja and A. Zrinzo (2020). 'Rising Incidence of Glioblastoma Multiforme in a Well-Defined Population'. In: *Cureus* 12.5, e8195. ISSN: 2168-8184 (Print) 2168-8184. DOI: 10.7759/cureus.8195.

- Groot, John de and Harald Sontheimer (2011). 'Glutamate and the biology of gliomas'.

  In: *Glia* 59.8, pp. 1181–1189.
- Gu, Zuguang, Roland Eils and Matthias Schlesner (2016). 'Complex heatmaps reveal patterns and correlations in multidimensional genomic data'. In: *Bioinformatics* 32.18, pp. 2847–2849.
- Guo, X., L. Gu, Y. Li, Z. Zheng, W. Chen, Y. Wang, Y. Wang, H. Xing, Y. Shi, D. Liu, T. Yang, Y. Xia, J. Li, J. Wu, K. Zhang, T. Liang, H. Wang, Q. Liu, S. Jin, T. Qu, S. Guo, H. Li, Y. Wang and W. Ma (2023). 'Histological and molecular glioblastoma, IDH-wildtype: a real-world landscape using the 2021 WHO classification of central nervous system tumors'. In: *Front Oncol* 13, p. 1200815. ISSN: 2234-943X (Print) 2234-943x. DOI: 10.3389/fonc.2023.1200815.
- Gürtler, Claudia, Michael Carty, Jay Kearney, Stefan A Schattgen, Aihao Ding, Katherine A Fitzgerald and Andrew G Bowie (2014). 'SARM regulates CCL5 production in macrophages by promoting the recruitment of transcription factors and RNA polymerase II to the Ccl5 promoter'. In: *The Journal of Immunology* 192.10, pp. 4821–4832.
- Guyenet, Stephan J, Stephanie A Furrer, Vincent M Damian, Travis D Baughan, Albert R La Spada and Gwenn A Garden (2010). 'A simple composite phenotype scoring system for evaluating mouse models of cerebellar ataxia'. In: *Journal of visualized experiments: JoVE* 39, p. 1787.
- Guyon, Joris, Candice Chapouly, Laetitia Andrique, Andreas Bikfalvi and Thomas Daubon (2021). 'The normal and brain tumor vasculature: morphological and functional characteristics and therapeutic targeting'. In: *Frontiers in Physiology* 12, p. 622615.

- Habib, Ahmed, Meagan Hoppe, Jamison Beiriger, Chowdari V Kodavali, Lincoln Edwards and Pascal O Zinn (2022). 'Glioblastoma Cell of Origin'. In: *Stem Cell Reviews and Reports*, pp. 1–3.
- Hafemeister, Christoph and Rahul Satija (2019). 'Normalization and variance stabilization of single-cell RNA-seq data using regularized negative binomial regression'. In: *Genome biology* 20.1, p. 296.
- Hagemann, Carsten, Jelena Anacker, Ralf-Ingo Ernestus and Giles H Vince (2012).

  'A complete compilation of matrix metalloproteinase expression in human malignant gliomas'. In: *World journal of clinical oncology* 3.5, p. 67.
- Hamad, Azzam, Gaukhar M Yusubalieva, Vladimir P Baklaushev, Peter M Chumakov and Anastasiya V Lipatova (2023). 'Recent developments in glioblastoma therapy: oncolytic viruses and emerging future strategies'. In: *Viruses* 15.2, p. 547.
- Hamed, Akram A, Kui Hua, Quang M Trinh, Benjamin D Simons, John C Marioni, Lincoln D Stein and Peter B Dirks (2025). 'Gliomagenesis mimics an injury response orchestrated by neural crest-like cells'. In: *Nature*, pp. 1–11.
- Hara, Toshiro, Rony Chanoch-Myers, Nathan D Mathewson, Chad Myskiw, Lyla Atta, Lillian Bussema, Stephen W Eichhorn, Alissa C Greenwald, Gabriela S Kinker, Christopher Rodman et al. (2021). 'Interactions between cancer cells and immune cells drive transitions to mesenchymal-like states in glioblastoma'. In: *Cancer cell* 39.6, pp. 779–792.
- Hart, Adam D, Andreas Wyttenbach, V Hugh Perry and Jessica L Teeling (2012). 'Age related changes in microglial phenotype vary between CNS regions: grey versus white matter differences'. In: *Brain, behavior, and immunity* 26.5, pp. 754–765.

- Henrik Heiland, Dieter, Vidhya M Ravi, Simon P Behringer, Jan Hendrik Frenking, Julian Wurm, Kevin Joseph, Nicklas WC Garrelfs, Jakob Strähle, Sabrina Heynckes, Jürgen Grauvogel et al. (2019). 'Tumor-associated reactive astrocytes aid the evolution of immunosuppressive environment in glioblastoma'. In: *Nature communications* 10.1, p. 2541.
- Henssen, Dylan, Frederick Meijer, Frederik A Verburg and Marion Smits (2023). 'Challenges and opportunities for advanced neuroimaging of glioblastoma'. In: The British Journal of Radiology 96.1141, p. 20211232.
- Hira, Vashendriya VV, Diana A Aderetti and Cornelis JF van Noorden (2018). 'Glioma stem cell niches in human glioblastoma are periarteriolar'. In: *Journal of Histochemistry & Cytochemistry* 66.5, pp. 349–358.
- Hu, Xiaoming, Peiying Li, Yanling Guo, Haiying Wang, Rehana K Leak, Songela Chen, Yanqin Gao and Jun Chen (2012). 'Microglia/macrophage polarization dynamics reveal novel mechanism of injury expansion after focal cerebral ischemia'. In: *Stroke* 43.11, pp. 3063–3070.
- Huebner, Eric A and Stephen M Strittmatter (2009). 'Axon regeneration in the peripheral and central nervous systems'. In: *Cell biology of the axon*, pp. 305–360.
- Hur, Eun-Mi, Feng-Quan Zhou et al. (2012). 'Growing the growth cone: remodeling the cytoskeleton to promote axon regeneration'. In: *Trends in neurosciences* 35.3, pp. 164–174.
- Ignatova, Tatyana N, Valery G Kukekov, Eric D Laywell, Oleg N Suslov, Frank D Vrionis and Dennis A Steindler (2002). 'Human cortical glial tumors contain neural stem-like cells expressing astroglial and neuronal markers in vitro'. In: *Glia* 39.3, pp. 193–206.

- INTERPHONE, Study Group (May 2010). 'Brain tumour risk in relation to mobile telephone use: results of the INTERPHONE international case-control study'. In: International Journal of Epidemiology 39.3, pp. 675-694. ISSN: 0300-5771. DOI: 10. 1093/ije/dyq079. eprint: https://academic.oup.com/ije/article-pdf/39/3/675/14113072/dyq079.pdf. URL: https://doi.org/10.1093/ije/dyq079.
- Iyer, Karan, Shubham Saini, Suman Bhadra, Sohini Kulavi and Jaya Bandyopadhyay (2023). 'Precision medicine advancements in glioblastoma: A systematic review'.

  In: *Biomedicine* 13.2, p. 1.
- Jackson, Christina, John Choi, Adham M Khalafallah, Carrie Price, Chetan Bettegowda, Michael Lim, Gary Gallia, Jon Weingart, Henry Brem and Debraj Mukherjee (2020). 'A systematic review and meta-analysis of supratotal versus gross total resection for glioblastoma'. In: *Journal of neuro-oncology* 148, pp. 419–431.
- Jakola, Asgeir S, Lisa M Sagberg, Sasha Gulati and Ole Solheim (2015). 'Perioperative quality of life in functionally dependent glioblastoma patients: a prospective study'. In: *British journal of neurosurgery* 29.6, pp. 843–849.
- Jang, Hyun Ji and Jong-Whi Park (2025). 'Microenvironmental Drivers of Glioma Progression'. In: *International Journal of Molecular Sciences* 26.5, p. 2108.
- Jiang, Yang, Sheng Han, Wen Cheng, Zixun Wang and Anhua Wu (2017).

  'NFAT1-regulated IL6 signalling contributes to aggressive phenotypes of glioma'.

  In: Cell Communication and Signaling 15, pp. 1–11.
- John Lin, Chia-Ching, Kwanha Yu, Asante Hatcher, Teng-Wei Huang, Hyun Kyoung Lee, Jeffrey Carlson, Matthew C Weston, Fengju Chen, Yiqun Zhang, Wenyi Zhu et al. (2017). 'Identification of diverse astrocyte populations and their malignant analogs'. In: *Nature neuroscience* 20.3, pp. 396–405.

- Joosten, Elbert AJ, Sipke Dijkstra, Gary A Brook, Henk Veldman and Peter R Bär (2000). 'Collagen IV deposits do not prevent regrowing axons from penetrating the lesion site in spinal cord injury'. In: *Journal of neuroscience research* 62.5, pp. 686–691.
- Jurga, AM, M Paleczna and KZ Kuter (2020). Overview of general and discriminating markers of differential microglia phenotypes. Front Cell Neurosci 14: 198.
- Jurkowski, Michal P, Luis Bettio, Emma K. Woo, Anna Patten, Suk-Yu Yau and Joana Gil-Mohapel (2020). 'Beyond the hippocampus and the SVZ: adult neurogenesis throughout the brain'. In: *Frontiers in cellular neuroscience* 14, p. 576444.
- Kaiser, Tobias, Harrison Mitchell Allen, Ohyoon Kwon, Boaz Barak, Jing Wang, Zhigang He, Minqing Jiang and Guoping Feng (2021). 'MyelTracer: a semi-automated software for myelin g-ratio quantification'. In: *eneuro* 8.4.
- Kalamakis, Georgios, Daniel Brüne, Srikanth Ravichandran, Jan Bolz, Wenqiang Fan, Frederik Ziebell, Thomas Stiehl, Francisco Catalá-Martinez, Janina Kupke, Sheng Zhao et al. (2019). 'Quiescence modulates stem cell maintenance and regenerative capacity in the aging brain'. In: *Cell* 176.6, pp. 1407–1419.
- Kalogeris, Theodore, Christopher P Baines, Maike Krenz and Ronald J Korthuis (2012). 'Cell biology of ischemia/reperfusion injury'. In: *International review of cell and molecular biology* 298, pp. 229–317.
- Kamiguchi, Hiroyuki, Ryuzo Shiobara and Shigeo Toya (1996). 'Accidentally detected brain tumors: clinical analysis of a series of 110 patients'. In: *Clinical neurology and neurosurgery* 98.2, pp. 171–175.
- Kanderi, Tejaswi, Sunil Munakomi and Vikas Gupta (2024). 'Glioblastoma multiforme'. In: *StatPearls [Internet]*. StatPearls Publishing.

- Kaplan-Arabaci, Oykum, Alperen Acari, Pinar Ciftci and Devrim Gozuacik (2022). 'Glutamate scavenging as a neuroreparative strategy in ischemic stroke'. In: Frontiers in Pharmacology 13, p. 866738.
- Karbowski, Jan (2007). 'Global and regional brain metabolic scaling and its functional consequences'. In: *BMC biology* 5, pp. 1–11.
- Katz, Amanda M, Nduka M Amankulor, Ken Pitter, Karim Helmy, Massimo Squatrito and Eric C Holland (2012). 'Astrocyte-specific expression patterns associated with the PDGF-induced glioma microenvironment'. In: *PloS one* 7.2, e32453.
- Keu, Khun Visith, Timothy H Witney, Shahriar Yaghoubi, Jarrett Rosenberg, Anita Kurien, Rachel Magnusson, John Williams, Frezghi Habte, Jamie R Wagner, Stephen Forman et al. (2017). 'Reporter gene imaging of targeted T cell immunotherapy in recurrent glioma'. In: *Science translational medicine* 9.373, eaag2196.
- Khan, Fatima, Lizhi Pang, Madeline Dunterman, Maciej S Lesniak, Amy B Heimberger, Peiwen Chen et al. (2023). 'Macrophages and microglia in glioblastoma: heterogeneity, plasticity, and therapy'. In: *The Journal of clinical investigation* 133.1.
- Khanna, Kum Kum and Stephen P Jackson (2001). 'DNA double-strand breaks: signaling, repair and the cancer connection'. In: *Nature genetics* 27.3, pp. 247–254.
- Kiesel, Barbara, Lisa I Wadiura, Mario Mischkulnig, Jessica Makolli, Veronika Sperl, Martin Borkovec, Julia Freund, Alexandra Lang, Matthias Millesi, Anna S Berghoff et al. (2021). 'Efficacy, outcome, and safety of elderly patients with glioblastoma in the 5-ALA era: single center experience of more than 10 years'. In: *Cancers* 13.23, p. 6119.

- Kim, Jun-Kyum, Xiong Jin, Young-Woo Sohn, Xun Jin, Hee-Young Jeon, Eun-Jung Kim, Seok Won Ham, Hye-Min Jeon, So-Young Chang, Se-Yeong Oh et al. (2014). 'Tumoral RANKL activates astrocytes that promote glioma cell invasion through cytokine signaling'. In: *Cancer letters* 353.2, pp. 194–200.
- Kitange, Gaspar J, Brett L Carlson, Mark A Schroeder, Patrick T Grogan, Jeff D Lamont, Paul A Decker, Wenting Wu, C David James and Jann N Sarkaria (2009). 'Induction of MGMT expression is associated with temozolomide resistance in glioblastoma xenografts'. In: *Neuro-oncology* 11.3, pp. 281–291.
- Korotkevich, Gennady, Vladimir Sukhov, Nikolay Budin, Boris Shpak, Maxim N Artyomov and Alexey Sergushichev (2016). 'Fast gene set enrichment analysis'. In: *biorxiv*, p. 060012.
- Korsunsky, Ilya, Aparna Nathan, Nghia Millard and Soumya Raychaudhuri (2019). 'Presto scales Wilcoxon and auROC analyses to millions of observations'. In: BioRxiv, p. 653253.
- Koul, Dimpy, Yasunari Takada, Ruijun Shen, Bharat B Aggarwal and WK Alfred Yung (2006). 'PTEN enhances TNF-induced apoptosis through modulation of nuclear factor-κB signaling pathway in human glioma cells'. In: *Biochemical and biophysical research communications* 350.2, pp. 463–471.
- Krauss, R, T Bosanac, TM Engber, R Devraj and R Hughes (2019). 'Small molecule inhibitors of SARM1 prevent axonal degeneration in vitro and in vivo'. In: Poster Presented at Society for Neuroscience Annual Meeting Planner (Chicago, IL: Society for Neuroscience). Available online at: https://www.abstractsonline.com/pp8. Vol. 7883.
- Krusche, Benjamin, Cristina Ottone, Melanie P Clements, Ewan R Johnstone, Katrin Goetsch, Huang Lieven, Silvia G Mota, Poonam Singh, Sanjay Khadayate, Azhaar

- Ashraf et al. (2016). 'EphrinB2 drives perivascular invasion and proliferation of glioblastoma stem-like cells'. In: *Elife* 5, e14845.
- Kwon, Chang-Hyuk, Dawen Zhao, Jian Chen, Sheila Alcantara, Yanjiao Li, Dennis K Burns, Ralph P Mason, Eva Y-HP Lee, Hong Wu and Luis F Parada (2008). 'Pten haploinsufficiency accelerates formation of high-grade astrocytomas'. In: *Cancer research* 68.9, pp. 3286–3294.
- Lafrenaye, Audrey D (2016). 'Physical interactions between activated microglia and injured axons: do all contacts lead to phagocytosis?' In: *Neural Regeneration Research* 11.4, pp. 538–540.
- Lapidot, Tsvee, Christian Sirard, Josef Vormoor, Barbara Murdoch, Trang Hoang, Julio Caceres-Cortes, Mark Minden, Bruce Paterson, Michael A Caligiuri and John E Dick (1994). 'A cell initiating human acute myeloid leukaemia after transplantation into SCID mice'. In: *nature* 367.6464, pp. 645–648.
- Lathia, Justin D, Stephen C Mack, Erin E Mulkearns-Hubert, Claudia LL Valentim and Jeremy N Rich (2015). 'Cancer stem cells in glioblastoma'. In: *Genes & development* 29.12, pp. 1203–1217.
- Le, Duc M, Arnaud Besson, Darrin K Fogg, Kyu-Sil Choi, David M Waisman, Cynthia G Goodyer, Barry Rewcastle and V Wee Yong (2003). 'Exploitation of astrocytes by glioma cells to facilitate invasiveness: a mechanism involving matrix metalloproteinase-2 and the urokinase-type plasminogen activator–plasmin cascade'. In: *Journal of Neuroscience* 23.10, pp. 4034–4043.
- Lee, Jeongwu, Svetlana Kotliarova, Yuri Kotliarov, Aiguo Li, Qin Su, Nicholas M Donin, Sandra Pastorino, Benjamin W Purow, Neil Christopher, Wei Zhang et al. (2006). 'Tumor stem cells derived from glioblastomas cultured in bFGF and

- EGF more closely mirror the phenotype and genotype of primary tumors than do serum-cultured cell lines'. In: *Cancer cell* 9.5, pp. 391–403.
- Lee, Joo Ho, Jeong Eun Lee, Jee Ye Kahng, Se Hoon Kim, Jun Sung Park, Seon Jin Yoon, Ji-Yong Um, Woo Kyeong Kim, June-Koo Lee, Junseong Park et al. (2018). 'Human glioblastoma arises from subventricular zone cells with low-level driver mutations'. In: *Nature* 560.7717, pp. 243–247.
- Leeuw, Charles N de and Michael A Vogelbaum (2019). 'Supratotal resection in glioma: a systematic review'. In: *Neuro-oncology* 21.2, pp. 179–188.
- Li, Qingyun and Ben A Barres (2018). 'Microglia and macrophages in brain homeostasis and disease'. In: *Nature Reviews Immunology* 18.4, pp. 225–242.
- Li, Ronghui, Gang Li, Lin Deng, Qinglin Liu, Jun Dai, Jie Shen and Jian Zhang (2010). 'IL-6 augments the invasiveness of U87MG human glioblastoma multiforme cells via up-regulation of MMP-2 and fascin-1'. In: *Oncology reports* 23.6, pp. 1553–1559.
- Li, Ziyu, Shuisheng Yu, Xuyang Hu, Yiteng Li, Xingyu You, Dasheng Tian, Li Cheng, Meige Zheng and Juehua Jing (2021). 'Fibrotic scar after spinal cord injury: crosstalk with other cells, cellular origin, function, and mechanism'. In: *Frontiers in cellular neuroscience* 15, p. 720938.
- Liddelow, Shane A, Kevin A Guttenplan, Laura E Clarke, Frederick C Bennett, Christopher J Bohlen, Lucas Schirmer, Mariko L Bennett, Alexandra E Münch, Won-Suk Chung, Todd C Peterson et al. (2017). 'Neurotoxic reactive astrocytes are induced by activated microglia'. In: *Nature* 541.7638, pp. 481–487.

- Lindberg, Nanna, Marianne Kastemar, T Olofsson, Anja Smits and Lene Uhrbom (2009). 'Oligodendrocyte progenitor cells can act as cell of origin for experimental glioma'. In: *Oncogene* 28.23, pp. 2266–2275.
- Lipková, Jana, Bjoern Menze, Benedikt Wiestler, Petros Koumoutsakos and John S Lowengrub (2022). 'Modelling glioma progression, mass effect and intracranial pressure in patient anatomy'. In: *Journal of the Royal Society Interface* 19.188, p. 20210922.
- Liu, Chong, Jonathan C Sage, Michael R Miller, Roel GW Verhaak, Simon Hippenmeyer, Hannes Vogel, Oded Foreman, Roderick T Bronson, Akiko Nishiyama, Liqun Luo et al. (2011). 'Mosaic analysis with double markers reveals tumor cell of origin in glioma'. In: *Cell* 146.2, pp. 209–221.
- Liuksiala, Thomas (July 2023). *Clonal Evolutionary Analysis of Cancer*. URL: https://geneviatechnologies.com/blog/clonal-evolutionary-analysis-of-cancer/.
- Loreto, Andrea, Michele Di Stefano, Martin Gering and Laura Conforti (2015). 'Wallerian degeneration is executed by an NMN-SARM1-dependent late Ca2+ influx but only modestly influenced by mitochondria'. In: *Cell reports* 13.11, pp. 2539–2552.
- Louis, D. N., A. Perry, P. Wesseling, D. J. Brat, I. A. Cree, D. Figarella-Branger, C. Hawkins, H. K. Ng, S. M. Pfister, G. Reifenberger, R. Soffietti, A. von Deimling and D. W. Ellison (2021). 'The 2021 WHO Classification of Tumors of the Central Nervous System: a summary'. In: *Neuro Oncol* 23.8, pp. 1231–1251. ISSN: 1522-8517 (Print) 1522-8517. DOI: 10.1093/neuonc/noab106.

- Luo, Liqun and Dennis DM O'Leary (2005). 'Axon retraction and degeneration in development and disease'. In: *Annu. Rev. Neurosci.* 28.1, pp. 127–156.
- Ma, Jiacheng, Sunil Goodwani, Paul J Acton, Virginie Buggia-Prevot, Shelli R Kesler, Imran Jamal, Iteeben D Mahant, Zhen Liu, Faika Mseeh, Bruce L Roth et al. (2021). 'Inhibition of dual leucine zipper kinase prevents chemotherapy-induced peripheral neuropathy and cognitive impairments'. In: *Pain* 162.10, pp. 2599–2612.
- Ma, Marek, Toby A Ferguson, Kathleen M Schoch, Jian Li, Yaping Qian, Frances S Shofer, Kathryn E Saatman and Robert W Neumar (2013a). 'Calpains mediate axonal cytoskeleton disintegration during Wallerian degeneration'. In:

  Neurobiology of disease 56, pp. 34–46.
- (2013b). 'Calpains mediate axonal cytoskeleton disintegration during Wallerian degeneration'. In: Neurobiology of Disease 56, pp. 34–46. ISSN: 0969-9961. DOI: https://doi.org/10.1016/j.nbd.2013.03.009. URL: https://www.sciencedirect.com/science/article/pii/S0969996113000971.
- Ma, Ruichong, Laurent J Livermore, Louis Taylor, Jake Laycock, Sarah Williams, Olaf Ansorge, Claire Vallance and Puneet Plaha (2024). 'Endoscopic 5-Aminolevulinic Acid–Induced Fluorescence-Guided Intraparenchymal Brain Tumor Resection—Can the Endoscope Detect More Fluorescence Than the Microscope?' In: World Neurosurgery 185, e1268–e1279.
- Magnusson, Jens P, Christian Göritz, Jemal Tatarishvili, David O Dias, Emma MK Smith, Olle Lindvall, Zaal Kokaia and Jonas Frisén (2014). 'A latent neurogenic program in astrocytes regulated by Notch signaling in the mouse'. In: *Science* 346.6206, pp. 237–241.

- Mathur, T and S Mathur (2014). 'A case of glioblastoma multiforme masquerading a s rapidly progressive dementia'. In: *Brain Disord Ther* 3.113, p. 2.
- McGuinness, Helen Y, Weixi Gu, Yun Shi, Bostjan Kobe and Thomas Ve (2024). 'Sarm1-dependent axon degeneration: Nucleotide signaling, neurodegenerative disorders, toxicity, and therapeutic opportunities'. In: *The Neuroscientist* 30.4, pp. 473–492.
- McKinnon, Chris, Meera Nandhabalan, Scott A Murray and Puneet Plaha (2021). 
  'Glioblastoma: clinical presentation, diagnosis, and management'. In: *BMJ* 374.

  DOI: 10.1136/bmj.n1560.eprint: https://www.bmj.com/content/374/bmj.

  n1560.full.pdf.url: https://www.bmj.com/content/374/bmj.n1560.
- Mesfin, Fassil B, Nishant Gupta, RS Taylor et al. (2017). 'Diffuse axonal injury'. In.
- Mietto, Bruno Siqueira, Klauss Mostacada and Ana Maria Blanco Martinez (2015). 'Neurotrauma and inflammation: CNS and PNS responses'. In: *Mediators of inflammation* 2015.1, p. 251204.
- Milde, Stefan, Jonathan Gilley and Michael P Coleman (2013). 'Axonal trafficking of NMNAT2 and its roles in axon growth and survival in vivo'. In: *Bioarchitecture* 3.5, pp. 133–140.
- Mohiuddin, Enaya and Hiroaki Wakimoto (2021). 'Extracellular matrix in glioblastoma: opportunities for emerging therapeutic approaches'. In: *American journal of cancer research* 11.8, p. 3742.
- Mosteiro, Alejandra, Leire Pedrosa, Abel Ferrés, Diouldé Diao, Àngels Sierra and José Juan González (2022). 'The vascular microenvironment in glioblastoma: a comprehensive review'. In: *Biomedicines* 10.6, p. 1285.

- Nagarajan, Raman P and Joseph F Costello (2009). 'Epigenetic mechanisms in glioblastoma multiforme'. In: *Seminars in cancer biology*. Vol. 19. 3. Elsevier, pp. 188–197.
- Neftel, Cyril, Julie Laffy, Mariella G Filbin, Toshiro Hara, Marni E Shore, Gilbert J Rahme, Alyssa R Richman, Dana Silverbush, McKenzie L Shaw, Christine M Hebert et al. (2019). 'An integrative model of cellular states, plasticity, and genetics for glioblastoma'. In: *Cell* 178.4, pp. 835–849.
- Neukomm, Lukas J, Thomas C Burdett, Andrew M Seeds, Stefanie Hampel, Jaeda C Coutinho-Budd, Jonathan E Farley, Jack Wong, Yonca B Karadeniz, Jeannette M Osterloh, Amy E Sheehan et al. (2017). 'Axon death pathways converge on axundead to promote functional and structural axon disassembly'. In: *Neuron* 95.1, pp. 78–91.
- Nikić, Ivana, Doron Merkler, Catherine Sorbara, Mary Brinkoetter, Mario Kreutzfeldt, Florence M Bareyre, Wolfgang Brück, Derron Bishop, Thomas Misgeld and Martin Kerschensteiner (2011). 'A reversible form of axon damage in experimental autoimmune encephalomyelitis and multiple sclerosis'. In: *Nature medicine* 17.4, pp. 495–499.
- Ohmura, Kazufumi, Hiroyuki Tomita and Akira Hara (2023). 'Peritumoral edema in gliomas: a review of mechanisms and management'. In: *Biomedicines* 11.10, p. 2731.
- Ohnishi, Takanori, Shoju Hiraga, Shuichi Izumoto, Hirotaka Matsumura, Yonehiro Kanemura, Norio Arita and Toru Hayakawa (1998). 'Role of fibronectin-stimulated tumor cell migration in glioma invasion in vivo: clinical

- significance of fibronectin and fibronectin receptor expressed in human glioma tissues'. In: *Clinical & experimental metastasis* 16, pp. 729–741.
- Ooi, Yinn Cher, Patrick Tran, Nolan Ung, Kimberly Thill, Andy Trang, Brendan M Fong, Daniel T Nagasawa, Michael Lim and Isaac Yang (2014). 'The role of regulatory T-cells in glioma immunology'. In: Clinical neurology and neurosurgery 119, pp. 125–132.
- Osswald, Matthias, Erik Jung, Felix Sahm, Gergely Solecki, Varun Venkataramani, Jonas Blaes, Sophie Weil, Heinz Horstmann, Benedikt Wiestler, Mustafa Syed et al. (2015). 'Brain tumour cells interconnect to a functional and resistant network'. In: *Nature* 528.7580, pp. 93–98.
- Ostrom, Quinn T, Mackenzie Price, Corey Neff, Gino Cioffi, Kristin A Waite, Carol Kruchko and Jill S Barnholtz-Sloan (Oct. 2023). 'CBTRUS Statistical Report: Primary Brain and Other Central Nervous System Tumors Diagnosed in the United States in 2016—2020'. In: Neuro-Oncology 25.Supplement4, pp. iv1—iv99. ISSN: 1522-8517. DOI: 10.1093/neuonc/noad149.eprint: https://academic.oup.com/neuro-oncology/article-pdf/25/Supplement\\_4/iv1/51862844/noad149.pdf. URL: https://doi.org/10.1093/neuonc/noad149.
- Ouchi, Rie, Sachiko Okabe, Toshiro Migita, Ichiro Nakano and Hiroyuki Seimiya (2016). 'Senescence from glioma stem cell differentiation promotes tumor growth'.

  In: Biochemical and biophysical research communications 470.2, pp. 275–281.
- Parsons, Michael W and Jörg Dietrich (2021). 'Assessment and Management of Cognitive Symptoms in Patients With Brain Tumors.' In: American Society of Clinical Oncology Educational book. American Society of Clinical Oncology. Annual Meeting. Vol. 41, e90–e99.

- Patel, Anoop P, Itay Tirosh, John J Trombetta, Alex K Shalek, Shawn M Gillespie, Hiroaki Wakimoto, Daniel P Cahill, Brian V Nahed, William T Curry, Robert L Martuza et al. (2014). 'Single-cell RNA-seq highlights intratumoral heterogeneity in primary glioblastoma'. In: *Science* 344.6190, pp. 1396–1401.
- Patel, Snahel, Frederick Cohen, Brian J Dean, Kelly De La Torre, Gauri Deshmukh, Anthony A Estrada, Arundhati Sengupta Ghosh, Paul Gibbons, Amy Gustafson, Malcolm P Huestis et al. (2015). 'Discovery of dual leucine zipper kinase (DLK, MAP3K12) inhibitors with activity in neurodegeneration models'. In: *Journal of medicinal chemistry* 58.1, pp. 401–418.
- Pearce, M. S., J. A. Salotti, M. P. Little, K. McHugh, C. Lee, K. P. Kim, N. L. Howe, C. M. Ronckers, P. Rajaraman, A. W. Sir Craft, L. Parker and A. Berrington de González (2012). 'Radiation exposure from CT scans in childhood and subsequent risk of leukaemia and brain tumours: a retrospective cohort study'. In: *Lancet* 380.9840, pp. 499–505. ISSN: 0140-6736 (Print) 0140-6736. DOI: 10.1016/s0140-6736(12) 60815-0.
- Peng, Chenghao, Zhengxin Chen, Shuai Wang, Hong-Wei Wang, Wenjin Qiu, Lin Zhao, Ran Xu, Hui Luo, Yuanyuan Chen, Dan Chen et al. (2016). 'The error-prone DNA polymerase  $\kappa$  promotes temozolomide resistance in glioblastoma through Rad17-dependent activation of ATR-Chk1 signaling'. In: *Cancer research* 76.8, pp. 2340–2353.

Peters, Luriano,
Avanthika Venkatachalam and Yinon Ben-Neriah (2024). 'Tissue-predisposition to cancer driver mutations'. In: *Cells* 13.2, p. 106.

- Pfenninger, Cosima V, Teona Roschupkina, Falk Hertwig, Denise Kottwitz, Elisabet Englund, Johan Bengzon, Sten Eirik Jacobsen and Ulrike A Nuber (2007). 'CD133 is not present on neurogenic astrocytes in the adult subventricular zone, but on embryonic neural stem cells, ependymal cells, and glioblastoma cells'. In: *Cancer research* 67.12, pp. 5727–5736.
- Pocratsky, Amanda M, Filipe Nascimento, M Görkem Özyurt, Ian J White, Roisin Sullivan, Benjamin J O'Callaghan, Calvin C Smith, Sunaina Surana, Marco Beato and Robert M Brownstone (2023). 'Pathophysiology of Dyt1-Tor1a dystonia in mice is mediated by spinal neural circuit dysfunction'. In: *Science translational medicine* 15.694, eadg3904.
- Pollard, Steven M, Koichi Yoshikawa, Ian D Clarke, Davide Danovi, Stefan Stricker, Roslin Russell, Jane Bayani, Renee Head, Marco Lee, Mark Bernstein et al. (2009). 'Glioma stem cell lines expanded in adherent culture have tumor-specific phenotypes and are suitable for chemical and genetic screens'. In: *Cell stem cell* 4.6, pp. 568–580.
- Pombo Antunes, Ana Rita, Isabelle Scheyltjens, Francesca Lodi, Julie Messiaen, Asier Antoranz, Johnny Duerinck, Daliya Kancheva, Liesbet Martens, Karen De Vlaminck, Hannah Van Hove et al. (2021). 'Single-cell profiling of myeloid cells in glioblastoma across species and disease stage reveals macrophage competition and specialization'. In: *Nature neuroscience* 24.4, pp. 595–610.
- Pouyan, Ashkan, Masoud Ghorbanlo, Masoud Eslami, Majid Jahanshahi, Ehsan Ziaei, Ali Salami, Khatere Mokhtari, Koorosh Shahpasand, Najma Farahani, Tohid Emami Meybodi et al. (2025). 'Glioblastoma multiforme: insights into

- pathogenesis, key signaling pathways, and therapeutic strategies'. In: *Molecular Cancer* 24.1, p. 58.
- Preusser, Matthias, Michael Lim, David A Hafler, David A Reardon and John H Sampson (2015). 'Prospects of immune checkpoint modulators in the treatment of glioblastoma'. In: *Nature Reviews Neurology* 11.9, pp. 504–514.
- Qazi, MA, P Vora, C Venugopal, SS Sidhu, J Moffat, C Swanton and SK Singh (2017). 'Intratumoral heterogeneity: pathways to treatment resistance and relapse in human glioblastoma'. In: *Annals of Oncology* 28.7, pp. 1448–1456.
- Raj, Divya, Zhuoran Yin, Marjolein Breur, Janine Doorduin, Inge R Holtman, Marta Olah, Ietje J Mantingh-Otter, Debby Van Dam, Peter P De Deyn, Wilfred den Dunnen et al. (2017). 'Increased white matter inflammation in aging-and Alzheimer's disease brain'. In: *Frontiers in molecular neuroscience* 10, p. 206.
- Ramírez-Expósito, María Jesús and José M Martínez-Martos (2019). 'The delicate equilibrium between oxidants and antioxidants in brain glioma'. In: *Current neuropharmacology* 17.4, pp. 342–351.
- Rath, Barbara H, Joshlean M Fair, Muhammad Jamal, Kevin Camphausen and Philip J Tofilon (2013). 'Astrocytes enhance the invasion potential of glioblastoma stem-like cells'. In: *PloS one* 8.1, e54752.
- Ravi, Vidhya M, Paulina Will, Jan Kueckelhaus, Na Sun, Kevin Joseph, Henrike Salié, Lea Vollmer, Ugne Kuliesiute, Jasmin von Ehr, Jasim K Benotmane et al. (2022). 'Spatially resolved multi-omics deciphers bidirectional tumor-host interdependence in glioblastoma'. In: *Cancer cell* 40.6, pp. 639–655.
- Raychaudhuri, Baisakhi, Patricia Rayman, Joanna Ireland, Jennifer Ko, Brian Rini, Ernest C Borden, Jorge Garcia, Michael A Vogelbaum and James Finke (2011).

- 'Myeloid-derived suppressor cell accumulation and function in patients with newly diagnosed glioblastoma'. In: *Neuro-oncology* 13.6, pp. 591–599.
- Regli, LKP, SMH Huijs, RCOS Pasmans, C Leue, JB Dijkstra, DBP Eekers, KE Hovinga, MHME Anten, A Hoeben and MPG Broen (2023). 'Incidence of clinically relevant psychiatric symptoms during glioblastoma treatment: an exploratory study'. In: *Journal of Neuro-Oncology* 163.1, pp. 185–194.
- Reichert, Fanny and Shlomo Rotshenker (1996). 'Deficient activation of microglia during optic nerve degeneration'. In: *Journal of neuroimmunology* 70.2, pp. 153–161.
- Richards, Laura M, Owen KN Whitley, Graham MacLeod, Florence MG Cavalli, Fiona J Coutinho, Julia E Jaramillo, Nataliia Svergun, Mazdak Riverin, Danielle C Croucher, Michelle Kushida et al. (2021). 'Gradient of developmental and injury response transcriptional states defines functional vulnerabilities underpinning glioblastoma heterogeneity'. In: *Nature Cancer* 2.2, pp. 157–173.
- Risling, M, K Fried, H Lindå, T Carlstedt and S Cullheim (1993). 'Regrowth of motor axons following spinal cord lesions: distribution of laminin and collagen in the CNS scar tissue'. In: *Brain research bulletin* 30.3-4, pp. 405–414.
- Rominiyi, Ola, Aurelie Vanderlinden, Susan Jane Clenton, Caroline Bridgewater, Yahia Al-Tamimi and Spencer James Collis (2021). 'Tumour treating fields therapy for glioblastoma: current advances and future directions'. In: *British journal of cancer* 124.4, pp. 697–709.
- Sa, Jason K, Nakho Chang, Hye Won Lee, Hee Jin Cho, Michele Ceccarelli, Luigi Cerulo, Jinlong Yin, Sung Soo Kim, Francesca P Caruso, Mijeong Lee et al. (2020).

- 'Transcriptional regulatory networks of tumor-associated macrophages that drive malignancy in mesenchymal glioblastoma'. In: *Genome biology* 21, pp. 1–17.
- Safa, Ahmad R, Mohammad Reza Saadatzadeh, Aaron A Cohen-Gadol, Karen E Pollok and Khadijeh Bijangi-Vishehsaraei (2015). 'Glioblastoma stem cells (GSCs) epigenetic plasticity and interconversion between differentiated non-GSCs and GSCs'. In: *Genes & diseases* 2.2, pp. 152–163.
- Sagberg, Lisa Millgård, Daniel Høyer Iversen, Even Hovig Fyllingen, Asgeir Store Jakola, Ingerid Reinertsen and Ole Solheim (2019). 'Brain atlas for assessing the impact of tumor location on perioperative quality of life in patients with high-grade glioma: A prospective population-based cohort study'. In: *NeuroImage: Clinical* 21, p. 101658.
- Saggu, Sarabjit K, Hiren P Chotaliya, Peter C Blumbergs and Robert J Casson (2010). 'Wallerian-like axonal degeneration in the optic nerve after excitotoxic retinal insult: an ultrastructural study'. In: *BMC neuroscience* 11, pp. 1–14.
- Saidi, Ahlame, Sophie Javerzat, Akeila Bellahcene, John De Vos, Lorenzo Bello, Vincent Castronovo, Manuel Deprez, Hugues Loiseau, Andreas Bikfalvi and Martin Hagedorn (2008). 'Experimental anti-angiogenesis causes upregulation of genes associated with poor survival in glioblastoma'. In: *International journal of cancer* 122.10, pp. 2187–2198.
- Saliani, Ariane, Blanche Perraud, Tanguy Duval, Nikola Stikov, Serge Rossignol and Julien Cohen-Adad (2017). 'Axon and myelin morphology in animal and human spinal cord'. In: *Frontiers in neuroanatomy* 11, p. 129.
- Sanson, Marc, Yannick Marie, Sophie Paris, Ahmed Idbaih, Julien Laffaire, François Ducray, Soufiane El Hallani, Blandine Boisselier, Karima Mokhtari, Khe

- Hoang-Xuan and Jean-Yves Delattre (2009). 'Isocitrate Dehydrogenase 1 Codon 132 Mutation Is an Important Prognostic Biomarker in Gliomas'. In: *Journal of Clinical Oncology* 27.25. PMID: 19636000, pp. 4150–4154. DOI: 10.1200/JC0.2009.21.9832. eprint: https://ascopubs.org/doi/pdf/10.1200/JC0.2009.21.9832. URL: https://ascopubs.org/doi/abs/10.1200/JC0.2009.21.9832.
- Sawamiphak, Suphansa, Sascha Seidel, Clara L Essmann, George A Wilkinson, Mara E Pitulescu, Till Acker and Amparo Acker-Palmer (2010). 'Ephrin-B2 regulates VEGFR2 function in developmental and tumour angiogenesis'. In: *Nature* 465.7297, pp. 487–491.
- Schuldiner, Oren and Avraham Yaron (2015). 'Mechanisms of developmental neurite pruning'. In: *Cellular and Molecular Life Sciences* 72, pp. 101–119.
- Seano, Giorgio, Hadi T Nia, Kyrre E Emblem, Meenal Datta, Jun Ren, Shanmugarajan Krishnan, Jonas Kloepper, Marco C Pinho, William W Ho, Mitrajit Ghosh et al. (2019). 'Solid stress in brain tumours causes neuronal loss and neurological dysfunction and can be reversed by lithium'. In: *Nature biomedical engineering* 3.3, pp. 230–245.
- Serres, E, F Debarbieux, F Stanchi, L Maggiorella, D Grall, L Turchi, F Burel-Vandenbos, D Figarella-Branger, T Virolle, G Rougon et al. (2014). 'Fibronectin expression in glioblastomas promotes cell cohesion, collective invasion of basement membrane in vitro and orthotopic tumor growth in mice'. In: *Oncogene* 33.26, pp. 3451–3462.
- Seystahl, Katharina, Wolfgang Wick and Michael Weller (2016). 'Therapeutic options in recurrent glioblastoma—An update'. In: *Critical reviews in oncology/hematology* 99, pp. 389–408.

- Shen, Hua, Krzysztof L Hyrc and Mark P Goldberg (2013). 'Maintaining energy homeostasis is an essential component of WldS-mediated axon protection'. In: *Neurobiology of disease* 59, pp. 69–79.
- Shepherd, STC, K Litchfield and S Turajlic (2019). 'Searching for the needle in the haystack: deconvoluting the evolutionary dynamics of residual disease in human glioblastoma'. In: *Annals of Oncology* 30.3, pp. 355–357.
- Shi, Yun, Philip S Kerry, Jeffrey D Nanson, Todd Bosanac, Yo Sasaki, Raul Krauss, Forhad K Saikot, Sarah E Adams, Tamim Mosaiab, Veronika Masic et al. (2022). 'Structural basis of SARM1 activation, substrate recognition, and inhibition by small molecules'. In: *Molecular cell* 82.9, pp. 1643–1659.
- Simpson Ragdale, H., M. Clements, W. Tang, E. Deltcheva, C. Andreassi, A. G. Lai, W. H. Chang, M. Pandrea, I. Andrew, L. Game, I. Uddin, M. Ellis, T. Enver, A. Riccio, S. Marguerat and S. Parrinello (2023). 'Injury primes mutation-bearing astrocytes for dedifferentiation in later life'. In: *Curr Biol* 33.6, 1082–1098.e8. ISSN: 0960-9822 (Print) 0960-9822. DOI: 10.1016/j.cub.2023.02.013.
- Singh, Sheila K, Ian D Clarke, Mizuhiko Terasaki, Victoria E Bonn, Cynthia Hawkins, Jeremy Squire and Peter B Dirks (2003). 'Identification of a cancer stem cell in human brain tumors'. In: *Cancer research* 63.18, pp. 5821–5828.
- Singh, Sheila K, Cynthia Hawkins, Ian D Clarke, Jeremy A Squire, Jane Bayani, Takuichiro Hide, R Mark Henkelman, Michael D Cusimano and Peter B Dirks (2004). 'Identification of human brain tumour initiating cells'. In: *nature* 432.7015, pp. 396–401.
- Sivasankaran, Balasubramanian, Martin Degen, Anthony Ghaffari, Monika E Hegi, Marie-France Hamou, Mihai-Constantin S Ionescu, Christian Zweifel, Markus

- Tolnay, Morten Wasner, Susanne Mergenthaler et al. (2009). 'Tenascin-C is a novel RBPJ $\kappa$ -induced target gene for Notch signaling in gliomas'. In: *Cancer research* 69.2, pp. 458–465.
- Sloan, E. A., S. Hilz, R. Gupta, C. Cadwell, B. Ramani, J. Hofmann, C. N. Kline, A. Banerjee, A. Reddy, N. A. Oberheim Bush, S. Chang, S. Braunstein, E. F. Chang, C. Raffel, N. Gupta, P. P. Sun, J. Y. H. Kim, G. Moes, E. Alva, R. Li, C. S. Bruggers, M. Alashari, C. Wetmore, S. Garg, M. Dishop, J. Van Ziffle, C. Onodera, P. Devine, J. P. Grenert, J. C. Lee, J. J. Phillips, M. Pekmezci, T. Tihan, A. W. Bollen, M. S. Berger, J. F. Costello, A. Perry and D. A. Solomon (2020). 'Gliomas arising in the setting of Li-Fraumeni syndrome stratify into two molecular subgroups with divergent clinicopathologic features'. In: *Acta Neuropathol* 139.5, pp. 953–957.
  ISSN: 0001-6322 (Print) 0001-6322. DOI: 10.1007/s00401-020-02144-8.
- Smirniotopoulos, JG and FM Murphy (1992). 'The phakomatoses'. In: *AJNR: American Journal of Neuroradiology* 13.2, p. 725.
- Sobstyl, Michał, Ewa Nagańska, Piotr Glinka, Teresa Wierzba-Bobrowicz, Albert Acewicz and Aleksandra Kuls-Oszmaniec (2023). 'Large haemorrhage within glioblastoma mimicking haemorrhagic stroke and coexistance of meningioma: a case of collision tumours'. In: *Folia Neuropathologica* 61.4, pp. 433–441.
- Sofroniew, Michael V (2009). 'Molecular dissection of reactive astrogliosis and glial scar formation'. In: *Trends in neurosciences* 32.12, pp. 638–647.
- Solanki, Chirag, Divya Sadana, Arivazhagan Arimappamagan, KVLN Rao, Jamuna Rajeswaran, DK Subbakrishna, Vani Santosh and Paritosh Pandey (2017). 'Impairments in quality of life and cognitive functions in long-term survivors of glioblastoma'. In: *Journal of neurosciences in rural practice* 8.2, p. 228.

- Son, Myung Jin, Kevin Woolard, Do-Hyun Nam, Jeongwu Lee and Howard A Fine (2009). 'SSEA-1 is an enrichment marker for tumor-initiating cells in human glioblastoma'. In: *Cell stem cell* 4.5, pp. 440–452.
- Song, Mingxue, Kang Kang, Shuai Wang, Cuiqin Zhang, Xiulan Zhao and Fuyong Song (2024). 'Elevated intracellular Ca2+ functions downstream of mitodysfunction to induce Wallerian-like degeneration and necroptosis in organophosphorus-induced delayed neuropathy'. In: *Toxicology* 504, p. 153812.
- Sorbara, Catherine Diamante, Naomi Elizabeth Wagner, Anne Ladwig, Ivana Nikić, Doron Merkler, Tatjana Kleele, Petar Marinković, Ronald Naumann, Leanne Godinho, Florence Martine Bareyre et al. (2014). 'Pervasive axonal transport deficits in multiple sclerosis models'. In: *Neuron* 84.6, pp. 1183–1190.
- Sorribes, Inmaculada C, Matthew NJ Moore, Helen M Byrne and Harsh V Jain (2019). 'A biomechanical model of tumor-induced intracranial pressure and edema in brain tissue'. In: *Biophysical journal* 116.8, pp. 1560–1574.
- Sottoriva, Andrea, Inmaculada Spiteri, Sara GM Piccirillo, Anestis Touloumis, V Peter Collins, John C Marioni, Christina Curtis, Colin Watts and Simon Tavaré (2013). 'Intratumor heterogeneity in human glioblastoma reflects cancer evolutionary dynamics'. In: *Proceedings of the National Academy of Sciences* 110.10, pp. 4009–4014.
- Stensjøen, Anne Line, Erik Magnus Berntsen, Asgeir Store Jakola and Ole Solheim (2018). 'When did the glioblastoma start growing, and how much time can be gained from surgical resection? A model based on the pattern of glioblastoma growth in vivo'. In: *Clinical Neurology and Neurosurgery* 170, pp. 38–42.

- Stommel, Jayne M, Alec C Kimmelman, Haoqiang Ying, Roustem Nabioullin, Aditya H Ponugoti, Ruprecht Wiedemeyer, Alexander H Stegh, James E Bradner, Keith L Ligon, Cameron Brennan et al. (2007). 'Coactivation of receptor tyrosine kinases affects the response of tumor cells to targeted therapies'. In: *Science* 318.5848, pp. 287–290.
- Stummer, Walter, Alexander Novotny, Herbert Stepp, Claudia Goetz, Karl Bise and Hans Jürgen Reulen (2000). 'Fluorescence-guided resection of glioblastoma multiforme utilizing 5-ALA-induced porphyrins: a prospective study in 52 consecutive patients'. In: *Journal of neurosurgery* 93.6, pp. 1003–1013.
- Stupp, Roger, Warren P. Mason, Martin J. van den Bent, Michael Weller, Barbara Fisher, Martin J.B. Taphoorn, Karl Belanger, Alba A. Brandes, Christine Marosi, Ulrich Bogdahn, Jürgen Curschmann, Robert C. Janzer, Samuel K. Ludwin, Thierry Gorlia, Anouk Allgeier, Denis Lacombe, J. Gregory Cairncross, Elizabeth Eisenhauer and René O. Mirimanoff (2005). 'Radiotherapy plus Concomitant and Adjuvant Temozolomide for Glioblastoma'. In: *New England Journal of Medicine* 352.10, pp. 987–996. doi: 10.1056/NEJMoa043330. eprint: https://www.nejm.org/doi/full/10.1056/NEJMoa043330.
- Stupp, Roger, Sophie Taillibert, Andrew Kanner, William Read, David M Steinberg, Benoit Lhermitte, Steven Toms, Ahmed Idbaih, Manmeet S Ahluwalia, Karen Fink et al. (2017). 'Effect of tumor-treating fields plus maintenance temozolomide vs maintenance temozolomide alone on survival in patients with glioblastoma: a randomized clinical trial'. In: *Jama* 318.23, pp. 2306–2316.

- Sugisawa, Ryoichi, Katharine A Shanahan, Gavin M Davis, Gavin P Davey and Andrew G Bowie (2024). 'SARM1 regulates pro-inflammatory cytokine expression in human monocytes by NADase-dependent and-independent mechanisms'. In:

  \*Iscience 27.6.\*
- Sylaja, PN, M Goyal, T Watson and MD Hill (2007). 'Wallerian-like degeneration after ischemic stroke revealed by diffusion-weighted imaging'. In: *Canadian journal of neurological sciences* 34.2, pp. 243–244.
- Tebha, Sameer Saleem, Shahzeb Ali Memon, Qasim Mehmood, Dattatreya Mukherjee, Hodan Abdi and Ahmed Negida (2023). 'Glioblastoma management in low and middle-income countries; existing challenges and policy recommendations'. In: *Brain and Spine* 3, p. 101775.
- Tentori, Lucio and Grazia Graziani (2009). 'Recent approaches to improve the antitumor efficacy of temozolomide'. In: *Current medicinal chemistry* 16.2, pp. 245–257.
- Thaler, Paul B, Jian Yi Li, Yakov Isakov, Karen S Black, Michael Schulder and Alexis Demopoulos (2012). 'Normal or non-diagnostic neuroimaging studies prior to the detection of malignant primary brain tumors'. In: *Journal of Clinical Neuroscience* 19.3, pp. 411–414.
- Torrisi, Filippo, Cristiana Alberghina, Simona D'Aprile, Anna M. Pavone, Lucia Longhitano, Sebastiano Giallongo, Daniele Tibullo, Michelino Di Rosa, Agata Zappalà, Francesco P. Cammarata, Giorgio Russo, Massimo Ippolito, Giacomo Cuttone, Giovanni Li Volti, Nunzio Vicario and Rosalba Parenti (2022). 'The Hallmarks of Glioblastoma: Heterogeneity, Intercellular Crosstalk and Molecular Signature of Invasiveness and Progression'. In: *Biomedicines* 10.4. ISSN: 2227-9059.

- DOI: 10.3390/biomedicines10040806. URL: https://www.mdpi.com/2227-9059/10/4/806.
- Travis, Zachary D, Prativa Sherchan, William K Hayes and John H Zhang (2020). 'Surgically-induced brain injury: where are we now?' In: *Chinese Neurosurgical Journal* 6.01, pp. 45–55.
- Tyagi, Vineet, Jason Theobald, James Barger, Mark Bustoros, N Sumru Bayin, Aram S Modrek, Michael Kader, Erich G Anderer, Bernadine Donahue, Girish Fatterpekar et al. (2016). 'Traumatic brain injury and subsequent glioblastoma development: Review of the literature and case reports'. In: *Surgical neurology international* 7, p. 78.
- Uccellini, Melissa B, Susana V Bardina, Maria Teresa Sánchez-Aparicio, Kris M White, Ying-Ju Hou, Jean K Lim and Adolfo García-Sastre (2020). 'Passenger mutations confound phenotypes of SARM1-deficient mice'. In: *Cell reports* 31.1.
- Vasen, HFA, A Stormorken, FH Menko, FM Nagengast, JH Kleibeuker, G Griffioen, BG Taal, P Moller and JT Wijnen (2001). 'MSH2 mutation carriers are at higher risk of cancer than MLH1 mutation carriers: a study of hereditary nonpolyposis colorectal cancer families'. In: *Journal of Clinical Oncology* 19.20, pp. 4074–4080.
- Vehlow, Anne and Nils Cordes (2013). 'Invasion as target for therapy of glioblastoma multiforme'. In: *Biochimica et Biophysica Acta (BBA)-Reviews on Cancer* 1836.2, pp. 236–244.
- Venkataramani, Varun, Yvonne Yang, Marc Cicero Schubert, Ekin Reyhan, Svenja Kristin Tetzlaff, Niklas Wißmann, Michael Botz, Stella Judith Soyka, Carlo Antonio Beretta, Rangel Lyubomirov Pramatarov et al. (2022). 'Glioblastoma hijacks neuronal mechanisms for brain invasion'. In: *Cell* 185.16, pp. 2899–2917.

- Venkatesh, Humsa S, Tessa B Johung, Viola Caretti, Alyssa Noll, Yujie Tang, Surya Nagaraja, Erin M Gibson, Christopher W Mount, Jai Polepalli, Siddhartha S Mitra et al. (2015). 'Neuronal activity promotes glioma growth through neuroligin-3 secretion'. In: *Cell* 161.4, pp. 803–816.
- Venkatesh, Humsa S, Wade Morishita, Anna C Geraghty, Dana Silverbush, Shawn M Gillespie, Marlene Arzt, Lydia T Tam, Cedric Espenel, Anitha Ponnuswami, Lijun Ni et al. (2019). 'Electrical and synaptic integration of glioma into neural circuits'.

  In: *Nature* 573.7775, pp. 539–545.
- Verhaak, Roel GW, Katherine A Hoadley, Elizabeth Purdom, Victoria Wang, Yuan Qi, Matthew D Wilkerson, C Ryan Miller, Li Ding, Todd Golub, Jill P Mesirov et al. (2010). 'Integrated genomic analysis identifies clinically relevant subtypes of glioblastoma characterized by abnormalities in PDGFRA, IDH1, EGFR, and NF1'. In: *Cancer cell* 17.1, pp. 98–110.
- Verma, Manish, Britney N Lizama and Charleen T Chu (2022). 'Excitotoxicity, calcium and mitochondria: a triad in synaptic neurodegeneration'. In: *Translational neurodegeneration* 11.1, p. 3.
- Vial, Juan D. (Sept. 1958). 'The Early Changes in the Axoplasm during Wallerian Degeneration'. In: *The Journal of Biophysical and Biochemical Cytology* 4.5, pp. 551-556. ISSN: 0095-9901. DOI: 10.1083/jcb.4.5.551. eprint: https://rupress.org/jcb/article-pdf/4/5/551/1621611/551.pdf. URL: https://doi.org/10.1083/jcb.4.5.551.
- Walid, Mohammad Sami (2008). 'Prognostic factors for long-term survival after glioblastoma'. In: *The Permanente Journal* 12.4, p. 45.

- Wang, Guohua, Jia Zhang, Xiaoming Hu, Lili Zhang, Leilei Mao, Xiaoyan Jiang, Anthony Kian-Fong Liou, Rehana K Leak, Yanqin Gao and Jun Chen (2013). 'Microglia/macrophage polarization dynamics in white matter after traumatic brain injury'. In: *Journal of Cerebral Blood Flow & Metabolism* 33.12, pp. 1864–1874.
- Wang, Jack T, Andrew Song and Marion S Buckwalter (2024). 'Wallerian Axon Degeneration is Required for Chronic Neuroinflammation and Infarct-Induced Neurodegeneration'. In: *Stroke* 55.Suppl\_1, A73–A73.
- Wang, Jun, Liang Yi, Qing-mei Kang, Ji Zhou, Tian-qing Chen, Jean-philippe Hugnot and Shi-cang Yu (2022). 'Glioma invasion along white matter tracts: A dilemma for neurosurgeons'. In: *Cancer letters* 526, pp. 103–111.
- Wang, Qianghu, Baoli Hu, Xin Hu, Hoon Kim, Massimo Squatrito, Lisa Scarpace, Ana C DeCarvalho, Sali Lyu, Pengping Li, Yan Li et al. (2017). 'Tumor evolution of glioma-intrinsic gene expression subtypes associates with immunological changes in the microenvironment'. In: *Cancer cell* 32.1, pp. 42–56.
- Watson, Spencer S, Anoek Zomer, Nadine Fournier, Joao Lourenco, Manfredo Quadroni, Agnieszka Chryplewicz, Sina Nassiri, Pauline Aubel, Simona Avanthay, Davide Croci et al. (2024). 'Fibrotic response to anti-CSF-1R therapy potentiates glioblastoma recurrence'. In: *Cancer cell* 42.9, pp. 1507–1527.
- Watts, Colin and Nader Sanai (2016). 'Surgical approaches for the gliomas'. In: Handbook of clinical neurology 134, pp. 51–69.
- Webster, Henry deF. (Feb. 1962). 'TRANSIENT, FOCAL ACCUMULATION OF AXONAL MITOCHONDRIA DURING THE EARLY STAGES OF WALLERIAN DEGENERATION'. In: *Journal of Cell Biology* 12.2, pp. 361–383. ISSN: 0021-9525.

- DOI: 10.1083/jcb.12.2.361.eprint: https://rupress.org/jcb/article-pdf/12/2/361/1473515/361.pdf.URL: https://doi.org/10.1083/jcb.12.2.361.
- Wei, Ruolun, Jiasheng Zhou, Brandon Bui and Xianzhi Liu (2024). 'Glioma actively orchestrate a self-advantageous extracellular matrix to promote recurrence and progression'. In: *BMC cancer* 24.1, p. 974.
- Wei, Wei, Young Shik Shin, Min Xue, Tomoo Matsutani, Kenta Masui, Huijun Yang, Shiro Ikegami, Yuchao Gu, Ken Herrmann, Dazy Johnson et al. (2016). 'Single-cell phosphoproteomics resolves adaptive signaling dynamics and informs targeted combination therapy in glioblastoma'. In: *Cancer cell* 29.4, pp. 563–573.
- Winkler, Frank, Humsa S Venkatesh, Moran Amit, Tracy Batchelor, Ihsan Ekin Demir, Benjamin Deneen, David H Gutmann, Shawn Hervey-Jumper, Thomas Kuner, Donald Mabbott et al. (2023). 'Cancer neuroscience: State of the field, emerging directions'. In: *Cell* 186.8, pp. 1689–1707.
- Woroniecka, Karolina I, Kristen E Rhodin, Pakawat Chongsathidkiet, Kristin A Keith and Peter E Fecci (2018). 'T-cell dysfunction in glioblastoma: applying a new framework'. In: *Clinical Cancer Research* 24.16, pp. 3792–3802.
- Xie, X. P., M. Ganbold, J. Li, M. Lien, M. E. Chipman, T. Wang, C. D. Jayewickreme, A. M. Pedraza, T. Bale, V. Tabar, C. Brennan, D. Sun, R. Sharma and L. F. Parada (2024). 'Glioblastoma functional heterogeneity and enrichment of cancer stem cells with tumor recurrence'. In: *Neuron* 112.24, 4017–4032.e6. ISSN: 0896-6273 (Print) 0896-6273. DOI: 10.1016/j.neuron.2024.10.012.
- Ximerakis, Methodios, Scott L Lipnick, Brendan T Innes, Sean K Simmons, Xian Adiconis, Danielle Dionne, Brittany A Mayweather, Lan Nguyen, Zachary

- Niziolek, Ceren Ozek et al. (2019). 'Single-cell transcriptomic profiling of the aging mouse brain'. In: *Nature neuroscience* 22.10, pp. 1696–1708.
- Xu, Bo, Lei Tian, Jing Chen, Jing Wang, Rui Ma, Wenjuan Dong, Aimin Li, Jianying Zhang, E Antonio Chiocca, Balveen Kaur et al. (2021). 'An oncolytic virus expressing a full-length antibody enhances antitumor innate immune response to glioblastoma'. In: *Nature communications* 12.1, p. 5908.
- Xu, Shengchao, Lu Tang, Xizhe Li, Fan Fan and Zhixiong Liu (2020). 'Immunotherapy for glioma: current management and future application'. In: *Cancer letters* 476, pp. 1–12.
- Yaron, Avraham and Oren Schuldiner (2016). 'Common and divergent mechanisms in developmental neuronal remodeling and dying back neurodegeneration'. In: *Current Biology* 26.13, R628–R639.
- Ye, Zu-Cheng and Harald Sontheimer (1999). 'Glioma cells release excitotoxic concentrations of glutamate'. In: *Cancer research* 59.17, pp. 4383–4391.
- Yeo, Alan T, Shruti Rawal, Bethany Delcuze, Anthos Christofides, Agata Atayde, Laura Strauss, Leonora Balaj, Vaughn A Rogers, Erik J Uhlmann, Hemant Varma et al. (2022). 'Single-cell RNA sequencing reveals evolution of immune landscape during glioblastoma progression'. In: *Nature immunology* 23.6, pp. 971–984.
- Yoon, Seon-Jin, Jin-Kyoung Shim, Jong Hee Chang, Ju Hyung Moon, Tae-Hoon Roh, Kyoung Su Sung, Ji-Hyun Lee, Eui-Hyun Kim, Sun Ho Kim, Yong-Kil Hong et al. (2016). 'Tumor mesenchymal stem-like cell as a prognostic marker in primary glioblastoma'. In: *Stem Cells International* 2016.1, p. 6756983.

- Yu, Guangchuang, Li-Gen Wang, Yanyan Han and Qing-Yu He (2012). 'clusterProfiler: an R package for comparing biological themes among gene clusters'. In: *Omics: a journal of integrative biology* 16.5, pp. 284–287.
- Yuan, Jinzhou, Hanna Mendes Levitin, Veronique Frattini, Erin C Bush, Deborah M Boyett, Jorge Samanamud, Michele Ceccarelli, Athanassios Dovas, George Zanazzi, Peter Canoll et al. (2018). 'Single-cell transcriptome analysis of lineage diversity in high-grade glioma'. In: *Genome medicine* 10, pp. 1–15.
- Zhang, Yanlu, Michael Chopp, Zheng Gang Zhang, Yi Zhang, Li Zhang, Mei Lu, Talan Zhang, Stefan Winter, Edith Doppler, Hemma Brandstäetter et al. (2019). 'Cerebrolysin reduces astrogliosis and axonal injury and enhances neurogenesis in rats after closed head injury'. In: *Neurorehabilitation and neural repair* 33.1, pp. 15–26.
- Zhang, Ye and Ben A Barres (2010). 'Astrocyte heterogeneity: an underappreciated topic in neurobiology'. In: *Current opinion in neurobiology* 20.5, pp. 588–594.
- Zhang, Ying, Collin Dube, Myron Gibert Jr, Nichola Cruickshanks, Baomin Wang, Maeve Coughlan, Yanzhi Yang, Initha Setiady, Ciana Deveau, Karim Saoud et al. (2018). 'The p53 pathway in glioblastoma'. In: *Cancers* 10.9, p. 297.
- Zheng, H, H Ying, H Yan, AC Kimmelman, DJ Hiller, A-J Chen, SR Perry, G Tonon, GC Chu, Z Ding et al. (2008). 'Pten and p53 converge on c-Myc to control differentiation, self-renewal, and transformation of normal and neoplastic stem cells in glioblastoma'. In: *Cold Spring Harbor symposia on quantitative biology*. Vol. 73. Cold Spring Harbor Laboratory Press, pp. 427–437.
- Zhou, Tian, Yiming Zheng, Li Sun, Smaranda Ruxandra Badea, Yuanhu Jin, Yang Liu, Alyssa J Rolfe, Haitao Sun, Xi Wang, Zhijian Cheng et al. (2019). 'Microvascular

endothelial cells engulf myelin debris and promote macrophage recruitment and fibrosis after neural injury'. In: *Nature neuroscience* 22.3, pp. 421–435.

Zhu, Yuan, Frantz Guignard, Dawen Zhao, Li Liu, Dennis K Burns, Ralph P Mason, Albee Messing and Luis F Parada (2005). 'Early inactivation of p53 tumor suppressor gene cooperating with NF1 loss induces malignant astrocytoma'. In: *Cancer cell* 8.2, pp. 119–130.